Studies in Computational Intelligence 1068

Thi Dieu Linh Nguyen
Joan Lu *Editors*

Machine Learning and Mechanics Based Soft Computing Applications

Springer

Studies in Computational Intelligence

Volume 1068

Series Editor

Janusz Kacprzyk, Polish Academy of Sciences, Warsaw, Poland

The series “Studies in Computational Intelligence” (SCI) publishes new developments and advances in the various areas of computational intelligence—quickly and with a high quality. The intent is to cover the theory, applications, and design methods of computational intelligence, as embedded in the fields of engineering, computer science, physics and life sciences, as well as the methodologies behind them. The series contains monographs, lecture notes and edited volumes in computational intelligence spanning the areas of neural networks, connectionist systems, genetic algorithms, evolutionary computation, artificial intelligence, cellular automata, self-organizing systems, soft computing, fuzzy systems, and hybrid intelligent systems. Of particular value to both the contributors and the readership are the short publication timeframe and the world-wide distribution, which enable both wide and rapid dissemination of research output.

Indexed by SCOPUS, DBLP, WTI Frankfurt eG, zbMATH, SCImago.

All books published in the series are submitted for consideration in Web of Science.

Thi Dieu Linh Nguyen · Joan Lu
Editors

Machine Learning and Mechanics Based Soft Computing Applications

Springer

Editors
Thi Dieu Linh Nguyen
Hanoi University of Industry
Hanoi, Vietnam

Joan Lu
Department of Computer Science
University of Huddersfield
Huddersfield, UK

ISSN 1860-949X ISSN 1860-9503 (electronic)
Studies in Computational Intelligence
ISBN 978-981-19-6449-7 ISBN 978-981-19-6450-3 (eBook)
https://doi.org/10.1007/978-981-19-6450-3

Preface

In recent years, as some of the key drivers Industry 4.0, the enabling technologies including artificial intelligence, big data, cloud computing, Internet of Things, block chain, robotics, and digital twin have been widely attracting a lot of attention from researchers and practitioners. In addition, the development of soft computing techniques has enabled researchers to create more fidelity data-driven models and provide innovative solutions to real-world problems.

As we see today, the technologies are moving towards industry and society in the interdisciplinary mode to solve the societal problem; with this thought, this project is carried out and we believe that with collection of selected work by various author, this book helps many level people from academia to industry at different ways.

This book provides the latest research findings in the emerging technologies with special focus on soft computing intelligent techniques and applications in various fields of engineering, particularly smart eco-system including smart manufacturing and smart agriculture.

Starting from artificial intelligence to mechanics, robotics and how technology is helping in management is covered very selectively. We believe that the collection of these research works will be proved helping to give a support edge to many research problems.

The book is a comprehensive resource and will be beneficial for students, engineers, researchers, and practitioners who want to explore intelligent computing algorithms as well as harness different smart and cutting-edge technologies in solving current challenging engineering problems.

The book shares the highlights about the

6G discussion about futuristic approach
Artificial intelligence and management

Machine learnings and Industry 4.0
Mathematics and computational drives' applications
Mechanics and robotics applications
Soft computing applications

Hanoi, Vietnam — Thi Dieu Linh Nguyen
Huddersfield, UK — Joan Lu

Contents

Threshold Text Classification with Kullback–Leibler Divergence Approach

Hiep Xuan Huynh, Cang Anh Phan, Tu Cam Thi Tran, Hai Thanh Nguyen, and Dinh Quoc Truong

Abstract Text classification based on thresholds belongs to the supervised learning method which assigns text material to predefined classes or categories based on different thresholds with divergence approach. These categories are identified by a set of documents trained by an automated algorithm. This work presents an approach of text classification using an automatic keyword extraction algorithm based on the Kullback–Leibler divergence approach. The proposed method is evaluated on 2000 documents in Vietnamese, covering ten topics, collected from various e-journals and news portal Web sites including vietnamnet.vn, vnexpress.net, and so on to generate a completely new set of keywords. Such keywords, then, are leveraged to categorize the topic of new text documents. The obtained results verifying the practicality of our approach are feasible as well as outperform the state-of-the-art method.

Keywords Kullback–Leibler divergence approach · Threshold text classification · Vietnamese text documents

1 Introduction

Text classification based on threshold with multiple keywords is a fundamental problem of natural language processing where successful research process can save time for tasks including information summarization and search [1, 2]. The research results of text classification approaches have already been deploying in many applications which consist of the information retrieval, the text filtering, and the automatic news aggregator. Text documents can be automatically labeled (class/topic) based on different thresholds with divergence approach [3, 4]. Whichever method is deployed,

H. X. Huynh (✉) · H. T. Nguyen · D. Q. Truong
College of Information and Communication Technology, Can Tho University, Can Tho, Vietnam
e-mail: hxhiep@ctu.edu.vn

C. A. Phan · T. C. T. Tran
Vinh Long University of Technology Education, Vinh Long, Vietnam

T. D. L. Nguyen and J. Lu (eds.), *Machine Learning and Mechanics Based Soft Computing Applications*, Studies in Computational Intelligence 1068,
https://doi.org/10.1007/978-981-19-6450-3_2

previous approaches usually analyze the full-text content of the document to do classification tasks [4–6]. That means the process of the classification has to handle a large number of features. For that reason, we usually analyze the usefulness of a set of keywords to search for documents such as the books or the scientific articles, the news articles, or the magazines. This shows that the keywords can show up core content, key of the document [7], and so, they can be used as the topic of the document. Therefore, this study recommends that if we are able to identify a set of keywords that represent a specific topic based on the divergence approach, such keywords can be utilized to categorize new upcoming documents [8] with this method.

The text classification has been applied widely and also proposed in numerous studies. The authors in [9] proposed a two-stage framework including a network to identify the topics and utilize the learned knowledge when the learning did at the first stage to learn a sentiment classification model based on the context. Wang et al. in [10] presented two sets of parallel topic modeling processes, namely twin labeled LDA (TL-LDA). Threshold text classification using a vast of keywords has become popular, and this really helps save time for tasks of aggregating, searching, and managing data information [1, 2]. Text classification tasks were proposed in a vast of research which can be applied in numerous fields including searching, retrieving, and extracting information, automated news aggregator, and useful applications in electronic library. Documents are automatically labeled (class/topic) conducted from the extracted content or full-text content using a vast of thresholds [3]. For a variety of proposed methods, the authors usually consider documents' full-text content to perform text classification tasks [5, 6, 11–14]. This leads to the classification tasks have to process with a huge number of features while the authors often face the limitations of computation resources. As seen from many real applications, we frequently use a set of keywords to look for materials, scientific article, and etc. We can see that such keywords enable us to find the crux of the document and core content [7]. In this work, we propose a hypothesis that we are able to leverage such keywords to do classification tasks on the new coming documents based on a set of identified keywords which can represent a specific topic of the document. The issues including the variations among the thresholds with divergence approach are not observed carefully. Our study presents a new approach using keywords with different thresholds combined a divergence algorithm for text classification tasks. The motivation comes from the success of previous studies in the research area of automatic keyword extraction [3] and the research on the classification tasks using only the set of keywords based on various thresholds by divergence approach instead of the whole content.

2 Automatic Keyword Extraction Using Various Thresholds

2.1 Techniques for Word Segmentation

Natural language processing involves a lot of problems including machine translation, text summarization, and information extraction. To successfully resolve these challenging problems, word segmentation is important. Word segmentation aims to divide a string of written language into its component words (meaning words). As stated in [15, 16], a phrase is exhibited as a sequence including blank-separated syllables c1, c2, cn. For Vietnamese language, most of compound words include 2 syllables while the most frequent case of ambiguity composes of 3 consecutive syllables $c_i c_i + 1 c_i + 2$ where two segmentations $(c_i c_i + 1)(c_i + 2)$ and $(c_i)(c_i + 1 c_{i+2})$ can be correct, and this depends on the considered context. We noted that such type of ambiguity known as overlapping ambiguity whereas the string $c_i c_i + 1 c_i + 2$ is called as overlapping ambiguity string.

For illustrations in math, a phrase is illustrated as a linearly directed graph: $G = (T, E)$, where $T = \{t_0, t_1, \ldots, t_n, t_{n+1}\}$. Vertices of t_0 and t_{n+1} correspond to the beginning and the end vertex, respectively, while n vertices of $t_1, t_2, \ldots, t_n$ are aligned to n syllables of the phrase. We noted that there exists an arc [17] between t_i and t_j if the consecutive syllables $c_{i+1}, c_{i+2}, \ldots, c_j$ can compose a word, where all $i < j$.

2.2 Automatic Keyword Extraction

A sentence can include some or many words which can be separated by some stop mark such as ".", "?", or "!". Two words or terms in a sentence are determined to co-occur at the same time. Each sentence can be exhibited as a "basket." We skip grammatical requirement except and the word order while we extract sequences of words [18]. Frequency of a word can be obtained by counting the appearance of the word. For instance, Table 1 reveals the top 10 most frequent terms (denoted as G) [3] and shows the probabilities of occurrence which were normalized to the sum of them to be 1.

Table 1 Top ten frequent terms with the probability of occurrence, normalized so that the sum is to be 1

Frequent word	a	b	c	d	e	f	g	h	Total
Probability	0.408	0.127	0.089	0.089	0.078	0.072	0.070	0.066	1.000
Frequency	203	63	44	44	39	36	35	33	497

With a machine, b: computer, c: question, d: digital, e: answer, f: game, g: argument, h: make

2.3 The Method to Identify the Thresholds in a Text

Let denote S as the set of potential candidate keywords. We denote s as a word sequence, and the function ***sp(s)*** exhibits the ratio between the number of sentences containing words sequence and the total number of sentences in a text. Let say $S_{\min} \in (0, 1]$ denotes the minimum threshold while a word sequence s is named as the common threshold $S_{\min}$ in the case $sp(s) \geq S_{\min}$. The values of thresholds can be determined by initial some experiments with steps as follows:

- Step 1: **Preprocessing**, we extract words representing the content of the documents. We ignore words that include stop words as suggested in [19].
- Step 2: **Frequent terms selection**, all words generated in the first step are retained (the number of running terms, N_{Total}).
- Step 3: **Clustering terms**, we cluster a pair of terms whose Jensen–Shannon divergence is greater than the threshold. The formula of Jensen–Shannon divergence's is as follows [3]:

$$J(m_1, m_2) = \log 2 + \frac{1}{2} \sum_{m'C} \{h(P(m'|m_1) + P(m'|m_2) - h(P(m'm_1) - h(P(m'm_2)\} \quad (1)$$

With

$$h(x) = -x \log x,\ P(w'|w_1) = freq(w'|w_1)/\text{freq}(w_1)$$

A pair of terms whose mutual information is greater than the threshold (log2) is also clustered. Mutual information of m_1 and m_2 is illustrated in (2):

$$M(m_1, m_2) = \log \frac{P(m_1, m_2)}{P(m_1)P(m_2)} = \log \frac{N_{\text{total}} \text{freq}(m_1, m_2)}{\text{freq}(m_1)\text{freq}(m_2)} \quad (2)$$

Two terms belong to the same cluster in the case they are clustered using one of the two clustering algorithms. Let denote C as the obtained clusters, we have to some values as follows:

- Compute expected probability as follows: We count the number of the groups co-occurring with $c \varepsilon C$, exhibited as n_c to yield the expected probability $P_c = n_c/N_{\text{total}}$.
- Compute X'^2 value: For each group m, co-occurrence frequency with $c \varepsilon C$ is counted and defined as $\text{freg}(m_i, c)$. We count the total number of groups in the sentences consisting of m_i, defined as n_{mi}. Compute the X'^2 value with formula (3) [3].

$$X'^2(m_i) = \sum_{c \varepsilon C} \left\{ \frac{(\text{freq}(m_i, c) - n_{mi} p_c)^2}{n_{mi} p_c} \right\} - \max_{c \varepsilon C} \left\{ \frac{(\text{freq}(m_i, c) - n_{mi} p_c)^2}{n_{mi} p_c} \right\} \quad (3)$$

After the extraction process, we obtain the keywords with a given number of terms containing the largest X'^2 value.

3 Divergence Approach Using Kullback–Leibler Algorithm

3.1 Text Classification with Thresholds

Text classification algorithms usually compose of the elements as follows. A text set of $C = c_1, c_2, \ldots, c_m$, a set of topic item denoted as $M = m_1, m_2, \ldots m_n$, an evaluation matrix denoted as $R = (r_{\mathrm{jk}})$ where $j = 1 \ldots m$ and $k = 1 \ldots n$. Matrix R contains the text evaluation result s_j for a specific topic item m_k. Data of evaluation matrix R can be false (0) in the case the text s_j is not corresponded to the topic item w_k. Otherwise, it can be true (1) if text s_j has corresponded to been evaluated on the topic item w_k.

3.2 Divergence Approach with Kullback–Leibler Method

1. Computing the distance between words in a text

The similarity measurement computation is a statistic calculation to evaluate the similarity between two sets of samples. The similarity between two finite sample sets can be calculated as the size of the intersection of the sample sets divided by the size of the union such sample sets:

$$\text{similarity}(W, w) = \frac{(W \cap w)}{(W \cup w)} = \frac{|W \cap w|}{|W| + |w| - |W \cap w|} \tag{4}$$

In the formula (4), W $= \{w_{m1}, w_{m2}, \ldots, w_{mn}\}$ denotes a set of trained words corresponding to a specific topic (with $0 \leq$ similarity $(W, w) \leq 1$). In the case, if W and w are both empty, we consider the similarity $(W, w) = 1$.

The distance between the considered words can be representative to a topic and the words that represent the new text [Formula (5)]:

$$\text{Distance}(W, w) = 1 - \text{similarity}(W, w). \tag{5}$$

2. Divergence approach with the words in the text.

In this article, we are going to use **Kullback–Leibler** [20] divergence approach to classify the text with thresholds. For discrete probability distributions B and A identified on the same probability space, let say X, then the Kullback–Leibler divergence of A from B can be defined as follows.

$$K_{KB}(A||B) = \sum_{x \in X} A(x) \log\left(\frac{A(x)}{B(x)}\right) \tag{6}$$

Which is equivalent to

$$K_{KB}(A||B) = -\sum_{x \in X} A(x) \log\left(\frac{A(x)}{B(x)}\right) \tag{7}$$

Jaccard coefficient measures similarity is computed by:

$$J(A, B) = \frac{|A \cap B|}{|A \cup B|} = \frac{|A \cap B|}{|A| + |B| - |A \cap B|} \tag{8}$$

3.3 Text Classification Using the Thresholds

The recommended procedure for text classification tasks includes two stages (as shown in Fig. 1), i.e., the training phase and test phase. The training documents include 200 articles for each topic is considered. We deploy a defined of topic model mentioned in [21] to populate the sets of keywords corresponding to the topic. In testing phase, we use a set of keywords extracted from the main content of the document. The specific topic of the document is identified from the discrete probability distributions between these sets of such keywords.

4 Result and Discussion

As previously mentioned, our research aims to check the feasibility of use the automatic keyword extraction method on text classification tasks. In order to prove the efficiency, we also compare the result of the classification tasks with the set of extracted keywords to the full-text document. Besides, we focus on the meaning of extracted keywords corresponding to the considered topics. Then, we examine and consider whether such keywords can represent the corresponded topic. The experiments have implemented and executed on a PC of CPU CORE i5 with the speed of 3.3 GHz and 6 GB in RAM.

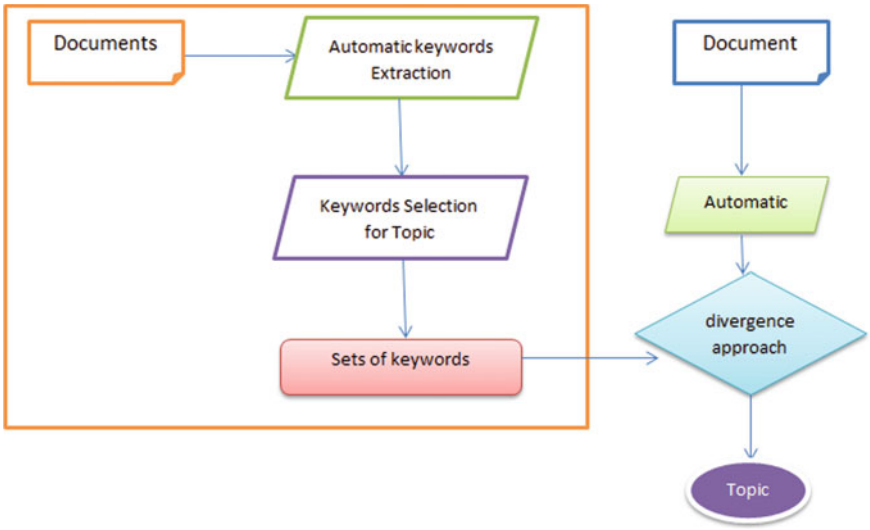

Fig. 1 Proposed approach for the text classification tasks using the thresholds calculated by divergence approach

4.1 Dataset

Our proposed method is evaluated on a dataset with 2000 articles on 10 topics [5], namely Computer, Business, Beauty, Culinary, Education, Health, Sport, Science, Society, and Travel with 200 samples for each topic. The considered articles were obtained from Vietnamese well-known online magazines or news portal including https://vietnamnet.vn, https://tuoitre.vn, https://vnexpress.net, and etc.

4.2 Experimental Results

For each topic, the articles randomly are divided into 2 subsets. The training set occupied of 75% (3/4) while the remaining part (25%) is for testing (50 samples). Our method performs the keyword extraction process on each article in the training phase. The number of extracted keywords on each article is a hyper-parameter of our method. Table 2 illustrates the words can be representatives for each topic.

As observed from Table 3, we achieve the best accuracy of 94% for Business, Education, and Sport. Moreover, we obtain 6 out of 10 topics which reach the accuracy over 90%. Travel topic seems to be the most challenging topic for the classification with only 76% in accuracy. The travel topic is usually misclassified to numerous other topics with high error prediction to sport. Most of wrong cases are corresponding to computer, society, while other topics are rarely misclassified to culinary.

Table 2 List of top 20 extracted keywords corresponding to the considered topics with threshold = log3 * N_{total} using Kullback method

No.	Topic subjects	20 keywords are translated from Vietnamese to English
1	Computer	Sell gb cellphone_screen chip product price computer usd samsung board running android sample apple video services_vietnam
2	Business	USD price increase month, decrease billion VND Ho Chi Minh City, invest-ment capital economic development, market investment turn
3	Beauty	Skin hair technology treatment methods remove zone product line˜˜ laser t c from ipl
4	Education	Exam examinee school graduation I high school study work grades depart-ment class subject hill corn different from education & 10 provinces
5	Healthy	Doctor hospital I baby sick young test tell medical province department check quang ngai case study clinic center shift
6	Sport	Match team compete player coach viet nam stadium play group good to striker quarter finals football tournament contract work
7	Science	To the United States to create a group/type research capability_electrical battery manufacturing_against university_transportation_used laser flight technology air cell
8	Travel	Tourist room price for vietnamese tourists service tour ha noi same beach hotel tourism boat cruise ha long see here island for night
9	Society	Family work homemade wife know young husband him job husband and wife mother and dad I see all ages take what want
10	Culinary	Dishes restaurant grill delicious made customer salt meat water… enjoy with fish japanese vietnamese shushi tasty

Table 3 Classification results on the datasets using 20 extracted keywords (the threshold value of log3 * N_{total} using Kullback method)

No.	Topic	Correct (%)	Wrong cases									
			1	2	3	4	5	6	7	8	9	10
1	Computer	86	–	6%	0	2%	2%	2%	0	0	2%	0
2	Business	94	2%	–	0	0	2%	0	0	0	2%	0
3	Beauty	92	2%	4%	–	0	0	0	0	2%	0	0
4	Education	94	2%	0	0	–	0	2%	0	0	2%	0
5	Healthy	86	2%	2%	8%	0	–	2%	0	0	0	0
6	Sport	94	2%	2%	0	0	0	–	0	0	2%	0
7	Science	92	2%	0	2%	0	0	0	–	0	2%	0
8	Travel	76	2%	2%	2%	2%	2%	6%	4%	–	2%	2%
9	Society	84	2%	2%	4%	2%	2%	2%	2%	0	–	0
10	Culinary	90	0	0	2%	0	0	0	2%	4%	2%	–

Table 4 Performance comparison between Kullback and Jaccard

No.	Topic name	Correct	
		Kullback (%)	Jaccard (%)
1	Computer	86	80
2	Business	94	80
3	Beauty	92	88
4	Education	94	78
5	Healthy	86	38
6	Sport	94	68
7	Science	92	50
8	Travel	76	48
9	Society	84	56
10	Culinary	90	70

4.3 Discussion

The summarized experimental results in a classification performance comparison between **Kullback** and **Jaccard** are exhibited in Table 4. As the results revealed, the performance on various topics is rather high when we deploy the Kullback method. In fact, we obtained numerous cases where the classification on the extracted keywords can achieve better than the method running on the dataset using the full-text documents.

In order to obtain the comparison in a clearer way, we plotted the results in Fig. 2. As revealed from the results, Kullback method outperforms Jaccard [22] in all considered topics. The validation sets of experiments with Kullback and Jaccard are the same. The proposed method seems be more efficient on Business, Beauty, Education, Sport, Science, and Culinary which overcome the classification accuracy of 90%. The best performance can be achieved with Business, Education, and Sport topics with 94% in accuracy. For healthy topic, Kullback method achieves the best improvement when it enhances the performance by 48% comparing to Jaccard method.

5 Conclusion

We presented a novel approach using keywords by divergence method with the thresholds, combining Kullback divergence. The method has leveraged a pair of terms whose mutual information for recommending on the trend using similarity measures, support, and confidence to do topic classification tasks. Our method reveals encouraging results using Kullback method where this method outperforms Jaccard method from 4 to 48%. The experimental results show the feasibility of our method, but data are not large enough, and only, Vietnamese texts documents are collected. Further research is expected to remain updating this work in increasing the data for

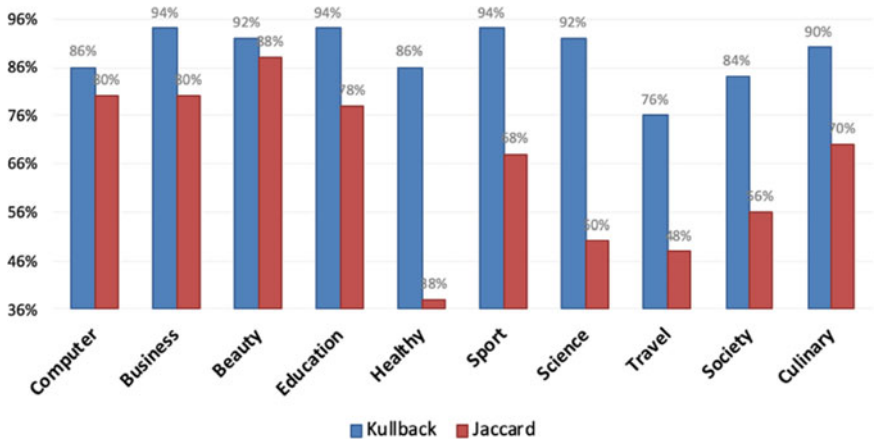

Fig. 2 Chart compares the results of Kullback algorithm and Jaccard algorithm

experiments with more languages needed to consider as well as improving accuracy of the keyword extraction approaches.

References

1. Liu, F., Pennell, D., Liu, F., & Liu, Y. (2009). Unsupervised approaches for automatic keyword extraction using meeting transcripts. In *Human Language Technologies: The 2009 Annual Conference of the North American Chapter of the ACL, NAACL'09, (June 2009)* (pp. 620–628), Boulder, Colorado.
2. Nguyen, C. T., Nguyen, T. K., Phan, X. H., Nguyen, L. M., & Ha, Q. T. (2006). Vietnamese word segmentation with CRFs and SVMs: an investigation. In *Proceedings of the 20th Pacific Asia Conference on Language, Information and Computation (PACLIC 2006).*
3. Matsuo, Y., & Ishizuka, M. (2004). Keyword extraction from a single document using word co-occurrence statistical information. *International Journal on AI Tools, 13*(1), 157–169.
4. Zaïane, O. R., & Antonie, M.-L. (2002). Classifying text documents by associating terms with text categories. *Australian Computer Science and Communications, 24*(2), 215–222.
5. Truong, Q. D., Huynh, H. X., & Nguyen, C. N. (2016). An abstract-based approach for text classification. In *Lecture Notes of the Institute for Computer Sciences, Social Informatics and Telecommunications Engineering* (Vol 168, pp. 237–245). Springer. https://doi.org/10.1007/978-3-319-46909-6_22
6. Zang, T., Goetz, T., Johnson, D., & Oles, F. (2002). A decision tree-base symbolic rule induction system for text categorization. *IBM Systems Journal,* 428–437. https://doi.org/10.1147/sj.413.0428
7. Han, E.-H. (Sam), Karypis, G., & Kumar, V. (2001). *Text categorization using weight adjusted k-nearest neighbor classification.* Springer
8. Dinh, Q. T., Le, H. P., Nguyen, T. M. H., Nguyen, C. T., & Mathias Rossignol, et al. (2008). Word segmentation of Vietnamese texts: A comparison of approaches. In *6th International Conference on Language Resources and Evaluation-LREC 2008, (May 2008)*, Marrakech, Morocco.
9. Lai, K. P., Ho, J. C. S., & Lam, W. (2020). Cross-domain sentiment classification using topic attention and dual-task adversarial training. In *Artificial Neural Networks and Machine*

Learning—ICANN 2020. ICANN 2020. Lecture Notes in Computer Science (Vol. 12397). Springer. https://doi.org/10.1007/978-3-030-61616-8_46
10. Wang, W., Guo, B., Shen, Y., et al. (2020). Twin labeled LDA: A supervised topic model for document classification. *Applied Intelligence, 50*, 4602–4615. https://doi.org/10.1007/s10489-020-01798-x
11. Aggarwal, A. G. (2018). A multi-attribute online advertising budget allocation under uncertain preferences. *Ingeniería Solidaria, 14*(25), 1–10.
12. Terrance, A. R., Shrivastava, S., Kumari, A., & Sivanandam, L. (2018). Competitive analysis of retail websites through search engine marketing. *Ingeniería Solidaria, 14*(25), 1–14.
13. Lopez-Inga, M. E., & Guerrero-Huaranga, R. M. (2018). Cloud business intelligence and analytics model for SMES in the retail sector in Peru/Modelo de inteligencia de negocios y analitica en la nube para pymes del sector retail en Peru/Modelo de inteligencia de negocios e analitica em nuvem para pmes do setor varejista no Peru. *Revista Ingenieria Solidaria, 14*(24).
14. Gupta, M., Solanki, V. K., & Singh, V. K. (2017). A novel framework to use association rule mining for classification of traffic accident severity. *Ingeniería solidaria, 13*(21), 37–44.
15. Le, H. P., Nguyen, M. H. T., Roussanaly, A., & Ho, T.V. A. (2008). Hybrid approach to word segmentation of vietnamese texts. *Language and Automata Theory and Applications,* 240–249. https://doi.org/10.1007/978-3-540-88282-4_23
16. Pak, I., & The, P. L. (2018). Text segmentation techniques: A critical review. In: *Innovative Computing, Optimization and Its Applications. Studies in Computational Intelligence* (Vol. 741). Springer. https://doi.org/10.1007/978-3-319-66984-7
17. Weisstein, E. W. Graph arc. *From MathWorld—A wolfram web resource.* https://mathworld.wolfram.com/GraphArc.html
18. Wu, C.-H., Huang, C.-L., Su, C.-S., & Lee, K.-M. (2007). Speech retrieval using spoken keyword extraction and semantic verification. In *TENCON 2007—2007 IEEE Region 10 Conference.* https://doi.org/10.1109/TENCON.2007.4429138
19. http://xltiengviet.wikia.com/wiki/Danh_s%C3%A1ch_stop_word
20. Kullback, S. (1987). Letter to the editor: The Kullback-Leibler distance. *The American Statistician, 41*(4), 340–341. https://doi.org/10.1080/00031305.1987.10475510.JSTOR2684769
21. Wallach, H. M. (2006). Topic modeling: Beyond bag-of-words. In *Proceedings of the 23rd International Conference on Machine Learning, ICML* (pp. 977–984), New York, NY, USA. ACM
22. Thi Tran, T. C., Huynh, H. X., Tran, P. Q., & Truong, D. Q. (2019). Text classification based on keywords with different thresholds. In *ACM International Conference Proceeding Series.*

Cellular Automata-Based Simulation Model for Water Quality Management of Pangasius Ponds

Hiep Xuan Huynh, Dung Tien Tran Nguyen, Huong Hoang Luong, and Hai Thanh Nguyen

Abstract Water quality is essential in aquaculture, particularly in intensive aquaculture (ponds, lakes). Aquatic animals can grow and thrive when water quality meets the standards and stability, or they will be mentally disabled or die when water is contaminated. Therefore, water's chemical, biological, and physical indexes, such as dissolved oxygen, temperature, pH, must be monitored to help fish culturists control fish farming. This article proposes the simulation model of water quality monitoring in a pangasius pond based on cellular automata theory. The experiment results are verified using water quality data collected at Phu Thuan fish farm, Hau Giang province, Vietnam.

Keywords Water quality monitoring · Pangasius pond · Simulation · Cellular automata · Fluid model

1 Introduction

A large amount of nutrients is used to feed aquatic animals, and the excess will then accumulate in the aquaculture environment. Aquaculture with a very high stocking rate will increase the amount of waste; therefore, the water quality will be poor [1]. The reasons mentioned above have significantly affected aquatic animals' development and increased disease risk in the water environment. Therefore, water quality management is critical for aquaculture's success, especially for intensive aquaculture.

H. X. Huynh (✉) · D. T. T. Nguyen · H. T. Nguyen
College of Information and Communication Technology, Can Tho University, Can Tho 900000, Vietnam
e-mail: hxhiep@ctu.edu.vn

H. H. Luong
FPT University, Can Tho, Vietnam

T. D. L. Nguyen and J. Lu (eds.), *Machine Learning and Mechanics Based Soft Computing Applications*, Studies in Computational Intelligence 1068,
https://doi.org/10.1007/978-981-19-6450-3_3

MIKE [2] and SWAT [3] are research related to water quality management, but such research focuses on large and frequent watersheds such as rivers, waterfalls. Besides, cellular automata (CA) model [4, 5] has been used extensively in building liquid flow simulation models that allow users to predict the movement direction of the fluid and also to monitor the propagation of substances in the fluid. The authors in [6] presented a model of large spherocylinder adsorption particles and small spherical TC particles with sub-micron size to perform Brownian dynamics simulations regarding adsorption and sedimentation in the gravitational field. The work in [7] explored the effects of duck manure and cefotaxime on the bacterial community and the evolution and distribution of ARGs and metal(loid) resistance genes (MRGs) in water and biofilm in a simulated fish–duck integrated pond with stress. The study in [8] investigated the effects of climate change on the fishpond ecosystem and carp growth, using 50 years long dynamic simulations to propose a well-structured dynamic balance model that may support the planning operation of pond farming systems under temperate climate. The authors in [9] conducted a quantitative measurement of the impact dispersion in the pond-side tower to show that the three schemes can obtain good performance under different engineering requirements.

This paper focuses on building the simulation model for monitoring the water quality in pangasius ponds. Using the proposed model, users can display the aquaculture areas, the propagation of the chemical and physical factors of the aquaculture area based on water quality measurements from several representative water samples, and the water quality of the aquaculture area.

2 Technical Regulations and Water Quality Factors

In this section, we present some technical regulations and water quality factors.

2.1 Technical Regulations

Pangasius farming is based on the technical regulations [10] as follows:

- The area of a pangasius pond is 2000 m^2, and the depth from the water surface to the pond bottom is from 1.5 to 4 m.
- The edge of the pond is higher than the minimum flood level, at least 0.5 m, and the slope of that edge is 30°–40° to avoid landslides.
- A pond must have an inlet and outlet system and no culverts between ponds.

To obtain an accurate result, the supervisors (fish culturists) only monitor the water quality when the pond's water is stable and is less affected by the external environment. Also, the supervisors focus on monitoring water quality fluctuation in water depths. The fluctuation of water quality in width is difficult for generalization

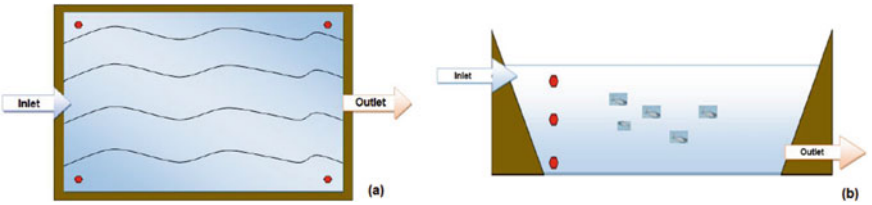

Fig. 1 Positions for collecting water samples

[1]. Therefore, water samples of ponds are collected at stable positions with little impact from the environment [11–13]: 4 or 2 corners of the pond (Fig. 1a); and two or three layers for each corner (Fig. 1b).

2.2 Water Quality Factors

The paper focuses on three water quality factors: temperature, dissolved oxygen (DO), and pH because these important factors affect other factors and can be measured directly by dedicated equipment.

Temperature affects most chemical and biological processes for pangasius's growth and development. The temperature that pangasius can be lived is from 26 °C to 32 °C, and well developed is from 28 to 30 °C. Among gases dissolved in water, oxygen is the essential gas. The appropriate dissolved oxygen concentration for fish is 6–8 mg/l (liter). The pH value shows the acidity or alkalinity present in water. If the pH is from 6 to 9, pangasius grows well. Pangasius will die if the pH is greater than 11 or less than 4; otherwise, they grow slowly.

The water quality index (WQI) calculated from the water quality monitoring factors is used to quantify the water quality and the usability of that water source [14]. There are many studies and methods for calculating WQI, such as [14–18]. For example, WQI is calculated by Bhargava [16] as the following (Eq. 1).

$$\mathrm{WQI} = \left(\prod_{i=1}^{n} \mathrm{WQI}_i\right)^{1/n} * 100 \tag{1}$$

In which:

- WQI_i: the water quality index for a water quality factor, expressed on a scale from 0.001 to 1.
- n: the number of water quality factors selected according to water use.

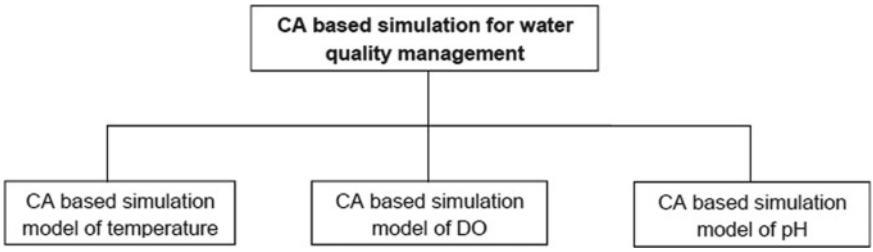

Fig. 2 Cellular automata-based simulation model for water quality management

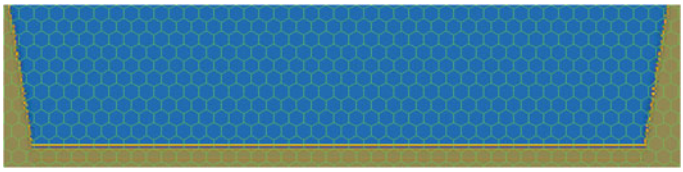

Fig. 3 Cellular space of the simulation model for water quality management

3 The Proposed Models for Monitoring Water Quality Management

3.1 Cellular Automata-Based Simulation Model for Water Quality Management

The model used for monitoring the water quality in pangasius ponds is integrated from automata cellular-based simulation models of three important factors (temperature, dissolved oxygen, and pH) as shown in Fig. 2. The proposed model consists of the 5-dimensions cellular space Z^5, the finite state set S, the neighborhood vector N, and the transition rule f.

The pangasius pond's size for simulation in length, width, and depth is 50 m, 40 m, and 4 m, respectively. *The 5-dimensions cellular space* Z^5 includes 50 cells in a horizontal direction and 40 cells in a verticle direction. The radius ratios between each cell in the simulation model and each region in the pond are 1/1 m in the horizontal direction and 1/0.1 m in the vertical direction. The cellular space of the proposed model is similar to Fig. 3.

If we call:

- X be a coordinate set of all cells in horizontal axis $X = \{x_1, x_2, x_3, \ldots, x_n\}$.
- Y be a coordinate set of all cells in vertical axis $Y = \{y_1, y_2, y_3, \ldots, y_n\}$.
- Tp be a temperature value set of all cells at a specific time $Tp = \{tp_1, tp_2, tp_3, \ldots, tp_n\}$.

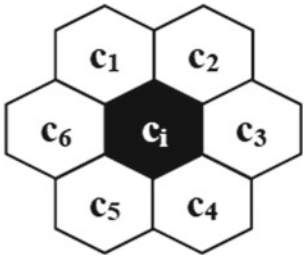

Fig. 4 Neighborhood with 6 cells

- DO be a dissolved oxygen value set of all cells at a specific time DO $= \{DO_1, DO_2, DO_3, \ldots, DO_n\}$.
- pH be a pH value set of all cells at a specific time $pH = \{pH_1, pH_2, pH_3, \ldots, pH_n\}$.

Then each cell c_i at the time t representing a water position (a water region) is specified by $(x_i, y_i, tp_{i,t}, DO_{i,t}, pH_{i,t})$.

In the proposed model, each cell will have 6 adjacent cells because the model with 6 neighbors matches the diffusion propagation properties of liquids and can also model the differences between the regions of the water layers and the considering region. Let us call c_i the considering cell, c_i has 6 neighbors as shown in Fig. 4. *The set of neighbors of* c_i is $N = \{c_1, c_2, c_3, c_4, c_5, c_6\}$. In which,

- c_1 and c_2 are cells of the water layer above c_i (the upper water layer).
- c_3 and c_6 are cells of the water layer consisting c_i (the middle water layer).
- c_4 and c_5 are cells in the water layer below c_i (the lower water layer).

For *transition rule*, the state of a cell c_i at the time t denoted by $s_{c_i,t}$ depends on the state of that cell according to three important factors (temperature, dissolved oxygen, and pH) $WQI_{c_{i,tp},t}$, $WQI_{c_{i,DO},t}$, $WQI_{c_{i,pH},t}$. The values of these factors are transformed from the states of temperature $s_{c_{i,tp},t}$ (Sect. 3.2), dissolved oxygen $s_{c_{i,DO},t}$ (Sect. 3.3) and pH $s_{c_{i,pH},t}$ (Sect. 3.3).

3.2 CA-Based Simulation Model of Temperature

The CA-based simulation model of temperature consists of the 3-dimensions cellular space Z^3, the finite state set S_{tp}, the neighborhood vector N, and the transition rule f_{tp}. N is described in Sect. 3.2. In Z^3, each cell is presented by three values: the coordinates and the collected temperature.

The finite state set of the model using temperature factor is $S_{tp} = -1, 0, 1, 2, 3, 4, 5$. The relationship between temperature value and the cell state is proposed as Fig. 5. The meaning of each state is the following.

Fig. 5 State set of the CA-based simulation model using temperature factor

State	Temperature(^{0}C)	Color
-1		
0		
1	<26	
2	>=26 and <28	
3	>=28 and <=30	
4	>30 and <=32	
5	>32	

- A cell with a state of –1 if it is not considered in the simulation.
- A cell with a state of 0 if it represents a water position in the pond and is not the cell to be analyzed. In which,
- A cell with a state of 1, 2, 3, 4, or 5 if it represents a water position in the pond and is the cell to be analyzed.
  - Pangasius will die if the temperature is less than 26 °C or greater than 32 °C (the state of a cell is 1 or 5).
  - Pangasius will develop slowly if the temperature range is from 26 to 28 °C or from 30 to 32 °C (the state of the cell is 2 or 4).
  - Pangasius will develop well if the temperature range is from 28 to 30 °C (the state of a cell is 3).

Sunlight is the main source of temperature in the pond. Temperature is propagated from high-temperature regions to low-temperature regions. This is the temperature balance trend among regions in the same water layer. The high-temperature water positions move up the water surface, whereas the low-temperature water position moves down the pond's bottom. Therefore, the temperature of the upper water layer is usually higher than that of the lower layer. The transition rule of the model using temperature factor is a function (Eq. 2):

$$f_{tp} : S^6 \rightarrow S \tag{2}$$

Let us consider the cell c_i with 6 neighbor cells $c_1, c_2, c_3, c_4, c_5, c_6$. At the time t, the state of this cell is $s_{c_i,t}$. At the time $t + 1$, the state of c_i is $s_{c_i,t+1}$ and $s_{c_i,t+1} = f_{tp}(s_{c_1,t}, s_{c_2,t}, s_{c_3,t}, s_{c_4,t}, s_{c_5,t}, s_{c_6,t})$ where f_{tp} is defined by:

- $s_{c_j,t}$ if knowing the state of only one neighbor $c_j (j = 1, \ldots, 6)$.
- average$(s_{c_3,t}, s_{c_6,t})$ if knowing the states of two neighbors in the middle layer.
- max$(s_{c_4,t}, s_{c_5,t})$ if knowing the states of two neighbors in the lower layer.
- min$(s_{c_1,t}, s_{c_2,t})$ if knowing the states of two neighbors in the upper layer.

- average($s_{c_3,t}$, $s_{c_6,t}$, max($s_{c_4,t}$, $s_{c_5,t}$), min($s_{c_1,t}$, $s_{c_2,t}$)) if knowing the states of all neighbors and there is no thermal stratification (i.e., min($s_{c_1,t}$, $s_{c_2,t}$) − max($s_{c_4,t}$, $s_{c_5,t}$) ≤ 2).
- average($s_{c_3,t}$, $s_{c_6,t}$, max($s_{c_4,t}$, $s_{c_5,t}$)) if knowing the states of all neighbors and there is the thermal stratification (i.e., min($s_{c_1,t}$, $s_{c_2,t}$) − max($s_{c_4,t}$, $s_{c_5,t}$) > 2).

3.3 CA-Based Simulation Model of Dissolved Oxygen

The CA-based simulation model of dissolved oxygen also consists of 4 elements Z^3, S_{DO}, N, and f_{DO} corresponding to the d-dimensions cellular space, the finite state set, the neighborhood vector, and the transition rule. N is similar to that of the above simulation models. In Z^3, the coordinates and the collected DO are used for presenting each cell.

DO in water is propagated in the form of diffusion. Oxygen in pangasius ponds is mainly supplied from the photosynthesis of aquatic organisms, especially algae. The variation of DO is similar to that of temperature. Therefore, *the transition rule* used by the model of the DO factor f_{DO} is similar to those used by the model of the temperature factor f_{tp}.

3.4 CA-Based Simulation Model of pH

The CA-based simulation model of pH is the 4-tuples (Z^3, S_{pH}, N, f_{pH}) where Z^3 is the 3-dimensions cellular space consisting of the coordinates and the collected pH value, S_{pH} is the finite state set, N is the neighborhood vector described in Sect. 3.2, and f_{pH} is the transition rule.

Factors affecting the pH fluctuation are the water supply and discharge, fish food, rainwater, or the photosynthesis of algae and aquatic organisms in ponds. There is less pH fluctuation among water layers in pangasius ponds. *The transition rule of model using pH factor* f_{pH} is defined by Eq. 3:

$$f_{\text{pH}} : S^6 \rightarrow S \tag{3}$$

also call c_i be the considering cell. c_i has 6 neighbor cells c_1, c_2, c_3, c_4, c_5, and c_6. The state of c_i at the time t and $t + 1$ is $s_{c_i,t}$ and $s_{c_i,t+1}$, respectively. We have $s_{c_i,t+1}$=f_{pH}($s_{c_1,t}$, $s_{c_2,t}$, $s_{c_3,t}$, $s_{c_4,t}$, $s_{c_5,t}$, $s_{c_6,t}$) where the value of f_{pH} is:

- $s_{c_j,t}$ if knowing the state of only one neighbor $c_j (j = 1, \ldots, 6)$.
- average($s_{c_1,t}$, $s_{c_2,t}$, $s_{c_3,t}$, $s_{c_4,t}$, $s_{c_5,t}$, $s_{c_6,t}$) otherwise.

4 Experiments

4.1 Water Quality Management Simulation Tool

The Water Quality Management Simulation tool (WQAS) is built on the Netgen platform [19]. WQAS has main functions: displaying the image of ponds, inputting the initial data and the set of rules acquisition for the CA-based simulation models, simulating the status change, and integrating and evaluating the water quality.

4.2 Experimental Data

Experimental data is collected at Phu Thuan fish farm pangasius ponds, Hau Giang province, Vietnam. Data is provided from an automatic water quality monitoring device supplemented by manual measurement equipment. The data is then extracted at the time points when the water quality is stable, little or not affected by the artificial events such as the water supply and discharge, the feeding.

The collected data at a water position consists of the position (near the inlet or outlet and the depth from the pond surface), the temperature, dissolved oxygen, and pH values. Each position is transformed into the model's coordinates x and y.

4.3 Scenario 1: Simulating the Water Quality After the First Feeding

Data collected at 10 a.m. on 12/05/2015 is shown in Table 1. Dataset consists of information on ten water positions (cells): the position near the inlet/outlet, the depth from the pond surface to the selected point, the temperature value, the dissolved

Table 1 Input data collected at 10 a.m. of 12/05/2015 (after the first feeding)

Position	Depth (m)	Temperature (°C)	DO (mg/l)	pH
P1 (Inlet)	0.5	32.98	7.29	9.03
P2 (Inlet)	1.0	32.60	6.56	8.32
P3 (Inlet)	1.5	30.10	5.67	7.49
P4 (Inlet)	2.0	29.53	5.52	6.78
P5 (Inlet)	3.0	28.67	5.43	6.28
P6 (Outlet)	0.5	33.24	7.02	8.92
P7 (Outlet)	1.0	32.86	5.78	7.86
P8 (Outlet)	1.5	31.64	5.54	7.12
P9 (Outlet)	2.0	30.04	5.49	6.21
P10 (Outlet)	3.0	29.34	5.45	5.91

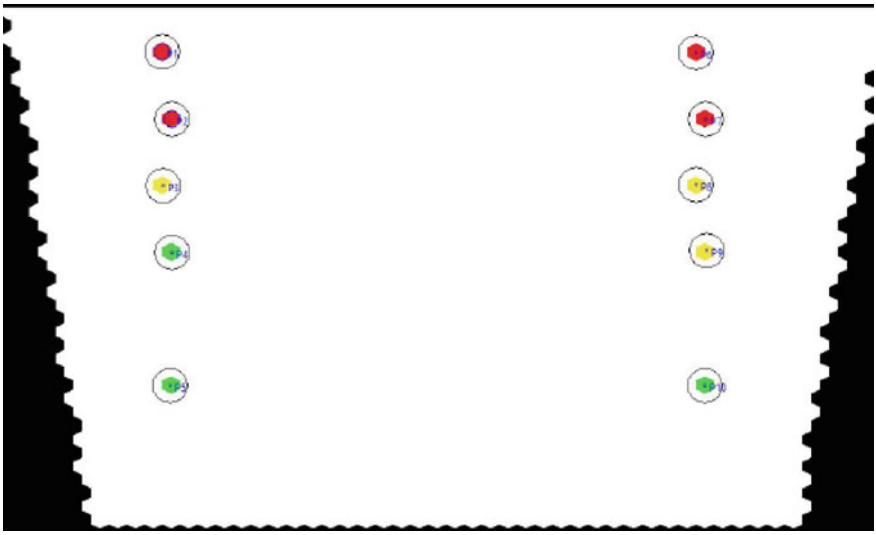

Fig. 6 The initial states of the CA-based simulation model of temperature factor after the first feeding

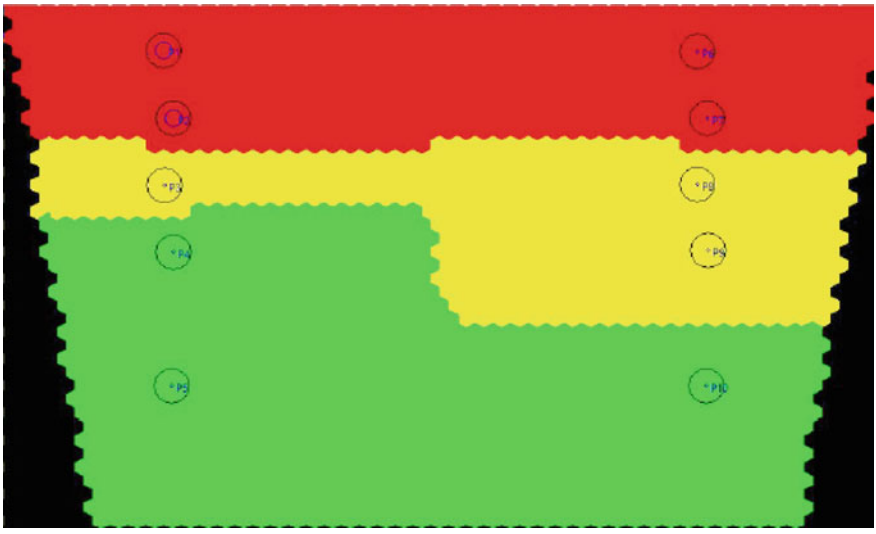

Fig. 7 The simulation result of the CA-based simulation model of temperature factor after the first feeding

oxygen value, and the pH value. The simulation is performed and stopped based on the transition rules and input data when the cells have new states.

Figure 6 shows the initial states of 10 cells according to the temperature factor. Figure 7 displays the simulation result of the temperature factor. This result shows that the temperature in the pond is disturbed, especially in the middle layer. The

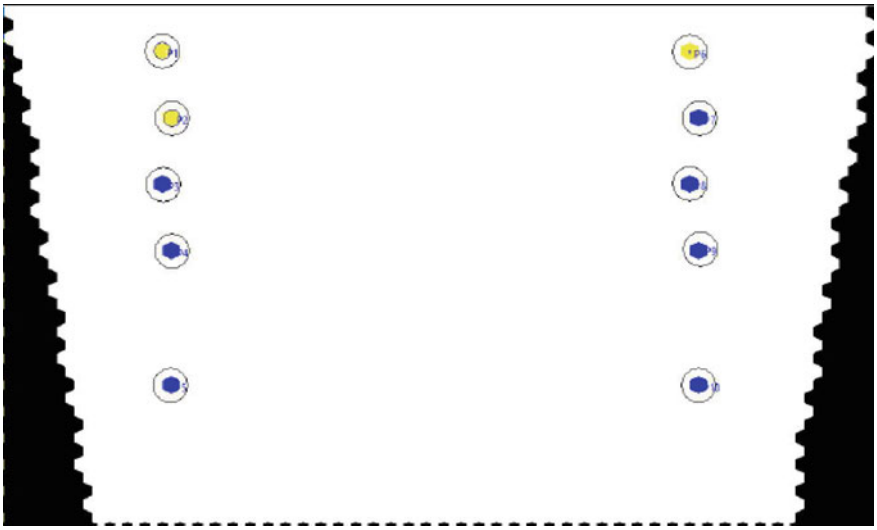

Fig. 8 Initial states of the CA-based simulation model of DO factor after the first feeding

Fig. 9 Simulation result of the CA-based simulation model of DO factor after the first feeding

average temperature of 30.1°C is suitable for pangasius. It is the first feeding of the day. Therefore, pangasius moves continuously to find food. Therefore, it affects the water quality.

According to the DO factor, the initial states of 10 cells are shown in Fig. 8. The simulation result of the CA-based model of the DO factor is shown in Fig. 9. This simulation result shows that dissolved oxygen in the pond's middle and bottom layers is reduced to an alarming level. The dissolved oxygen of 5.81mg/l is within the

endurance threshold of pangasius. It is the day's first feeding, and pangasius moves continuously to find food.

4.4 Scenario 2: Simulating the Water Quality at Noon

Data collected at 10 water positions (cells) at 12 a.m. on 12/05/2015 is shown in Table 2.

The initial states of 10 cells according to temperature factor are shown in Fig. 10. The simulation result of the CA-based simulation model of temperature factor is

Table 2 Input data collected at 12 a.m. of 12/05/2015 (at noon)

Position	Depth (m)	Temperature (°C)	DO (mg/l)	pH
P1 (Inlet)	0.5	33.02	8.01	9.11
P2 (Inlet)	1.0	32.77	7.63	8.33
P3 (Inlet)	1.5	31.54	7.51	7.45
P4 (Inlet)	2.0	30.06	7.29	7.18
P5 (Inlet)	3.0	29.60	6.77	6.28
P6 (Outlet)	0.5	33.42	7.92	9.06
P7 (Outlet)	1.0	32.68	7.87	8.34
P8 (Outlet)	1.5	31.67	7.47	7.57
P9 (Outlet)	2.0	30.54	7.21	7.01
P10 (Outlet)	3.0	29.45	5.81	6.02

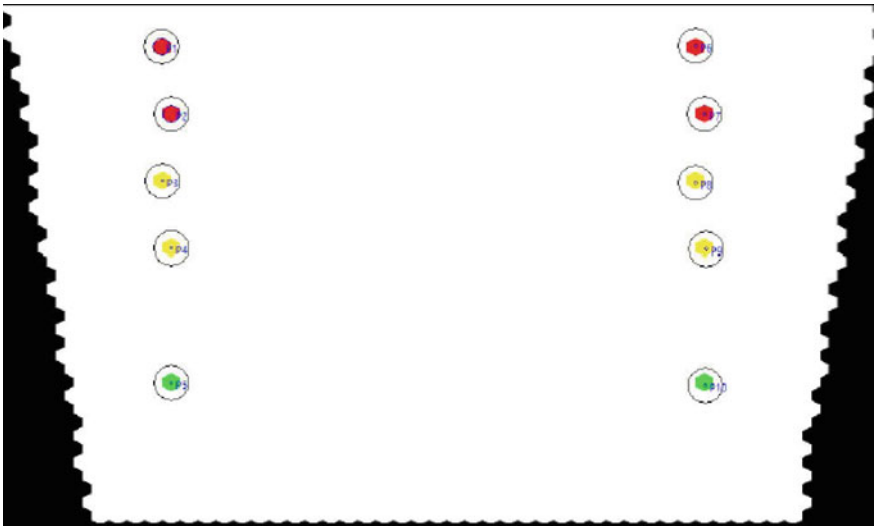

Fig. 10 Initial states of the CA-based simulation model of temperature factor at noon

shown in Fig. 11. The simulation result shows that the temperature differences among the three layers are high but not enough to appear in the temperature stratification. This is because the upper layer has a high temperature, while the lower layer has a suitable temperature for pangasius. Because the surface temperature is 33.42 °C, pangasius moves the lower layer to avoid the sun at noon.

The CA-based simulation model of the DO factor shows the initial states of 10 cells, and the simulation results are in Figs. 12 and 13, respectively. This result shows

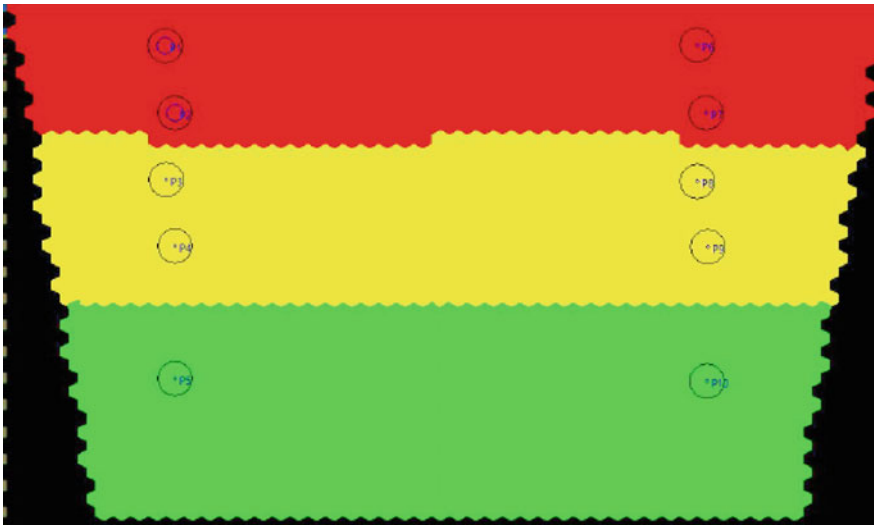

Fig. 11 Simulation result of the CA-based simulation model of temperature factor at noon

Fig. 12 Initial states of the CA-based simulation model of DO factor at noon

that DO rises at noon to adapt to the pangasius needs. As a result, the average DO is 7.32 mg/l; oxygen in the pond increases due to the algae photosynthesis at noon; and there is diffusion and uniform distribution of DO.

Figure 14 shows the initial states of 10 cells according to the pH factor. Figure 15 displays the simulation result of the pH factor. This result shows that pH in the pond has a balanced value and is consistent with pangasius adaptation. The average pH is 7.64, suitable for pangasius.

Fig. 13 Simulation result of the CA-based simulation model of DO factor at noon

Fig. 14 Initial states of the CA-based simulation model of pH factor at noon

Fig. 15 Simulation result of the CA-based simulation model of pH factor at noon

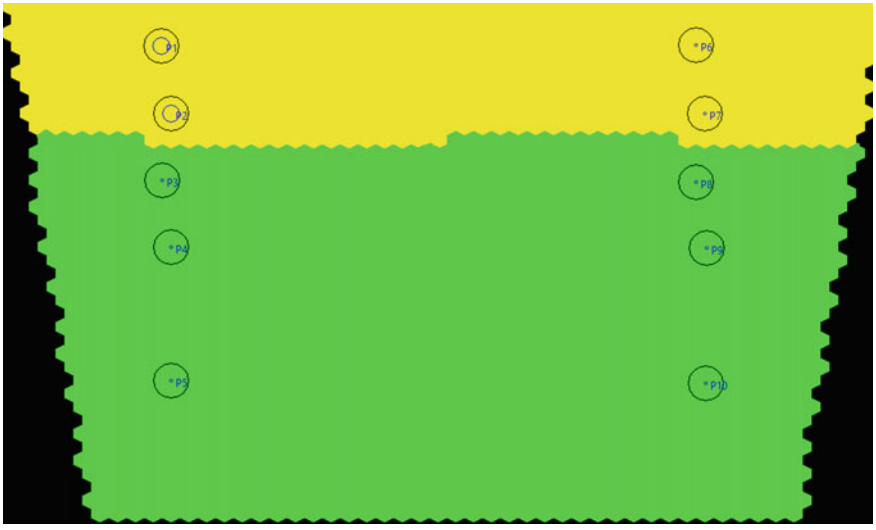

Fig. 16 Result of the CA-based simulation model for water quality management with data 10 after noon

Figure 16 shows the result of the CA-based simulation model for water quality management. The simulation shows that the water quality increases and is suitable for developing pangasius. Based on actual observations, pangasius moves to the middle and bottom layers to avoid the sun at noon; the water quality is more stable because the biochemical processes of pangasius and aquatic plant are reduced.

5 Conclusions

The water quality in ponds affects the success of fish farming. The water quality assessment is based on many important factors such as temperature, dissolved oxygen, pH, NH_3, H_2S. The first three factors are the most important because they can be collected automatically by dedicated devices and affect other factors. This paper proposes the CA-based simulation model for water quality management. The proposed model is integrated with three sub-models simulating temperature, dissolved oxygen, and pH. The simulation result on datasets collected at Phu Thuan fish farm ponds is valid. We will test the proposed simulation model on a large and continuous dataset in the future.

References

1. Boyd, C. E., & Tucker, C. S. (1998). *Pond aquaculture water quality management*. Springer.
2. Denmark Hydraulic Institute. (2007). *MIKE 11 user guide*.
3. Arnold et al., J. (2009). *Soil and water assessment tool (SWAT) global applications*.
4. Gomez-Orejuela, I. A., & Viancha-Sanchez, Z. H. (2017). Good agricultural practices as a clean production alternative in the citrus and mango production process in the municipality of viota (cundinamarca, colombia). *Revista ingenieria solidaria, 13*(22), 137–152.
5. Gualdron Prieto, L. Y., Acosta Romero, J. M., & Bohórquez Arevalo, L. E. (2017). Organizational structures and adaptation to changing environmental conditions: Challenges and implications.
6. Okada, K., & Satoh, A. (2020). Sedimentation characteristics of spherical and rod-like particles in the gravitational field by Brownian dynamics simulations: To improve the visibility of small lakes and ponds. *Environmental Fluid Mechanics, 20*, 765–790. https://doi.org/10.1007/s10652-019-09722-9
7. Zhou, M., Xu, Y., Ouyang, P., Ling, J., Cai, Q., Huang, L., Zhou, X., & Zheng, L. (2020). Evolution and distribution of resistance genes and bacterial community in water and biofilm of a simulated fish-duck integrated pond with stress. *Chemosphere, 245*, 125549. ISSN 0045-6535, https://doi.org/10.1016/j.chemosphere.2019.125549
8. Varga, M., Berzi-Nagy, L., Csukas, B., & Gyalog, G. (2020). Long-term dynamic simulation of environmental impacts on ecosystem-based pond aquaculture. *Environmental Modelling and Software, 134*, 104755. ISSN 1364-8152, https://doi.org/10.1016/j.envsoft.2020.104755
9. Gao, Z., Huang, J., Ma, Y., Liu, X., & Ren, H. (2020). Study on the distribution optimization scheme of the grounding device of the transmission line pole tower next to the fish pond. In *2020 5th Asia Conference on Power and Electrical Engineering (ACPEE)*, Chengdu, China, 2020 (pp. 1800–1804). https://doi.org/10.1109/ACPEE48638.2020.9136318
10. Directorate of Fisheries. (2014). *National technical regulation on Striped catfish (Pangasianodon hypophthalmus Sauvage, 1878) culture farm in pond*. Ministry of Agriculture and Rural Development of Vietnam.
11. Cat, L. V., Nhung, D. T. N., & Cat, N. N. (2006). *Aquaculture water—Quality and quality improvement solutions*. Science and Technics Publishing House.
12. Giang, H. T., Ut, V. N., & Phuong, N. T. (2008). Study on water quality of intensive catfish (pangasianodon hypophthalnos) ponds in An Giang province. *Can Tho University Journal of Science, 1*, 1–9.
13. Nguyen, P. Q., Le, H. Y., Congvá, N. V., & Phu, T. Q. (2014). Variation of some water quality parameters in intensive catfish (Pangasianodon hypothalamus) ponds. *Can Tho University Journal of Science, 34,* 128–136.

14. Center For Environmental Monitoring. (2011). *Method of calculating water quality index (WQI)*. Vietnam Environment Administration.
15. APHA. (1998). *Standard methods for examination of water and waste water*. American Public Health Association (APHA Inc.).
16. Bhargava, D. S. (1983). Use of a water quality index for river classification and zoning of the Ganga River. *Environmental Pollution*.
17. Parmar, K., & Parmar, V. (2010). Evaluation of water quality index for drinking purposes of river Subernarekha in Singhbhum District. *International Journal Of Environmental Sciences, 1*, 77–81
18. Pandey, M., & Sundaram, S. M. (2002). Trend of water quality of river Ganga at Varanasi using WQI approach. *International Journal of Ecology and Environmental Science, 28*, 139142.
19. NetGen Website. *A generator of concurrent systems*. http://wsn.univ-brest.fr/NetGen/Presentation.html

Heuristic Methods Solving Markowitz Mean-Variance Portfolio Optimization Problem

Ta Anh Son, Bui Quoc Bao, and Luu Quang Luc

Abstract In this paper, we introduce two heuristic methods for solving Markowitz mean-variance portfolio optimization problem with cardinality constraints and bounding on variables: genetic algorithm (GA) and heuristic branching (HB) with some proposed improvements. There are exact methods for solving the problem: outer approximation, branch-and-bound, etc. They are efficient for small-size problems, which is under five hundred stocks. However, they are not applicable for larger size problems. We implement the algorithms on Vietnam and the United States stock market data. Numerical experiments show that GA and HB give good results and have some advantages, especially in computation times.

Keywords Portfolio optimization · Heuristic method · Genetic algorithm · Heuristic branching

1 Introduction

In 1990, Harry Markowitz was awarded the Nobel Prize in Economic Science for his work on portfolio theory. One of the basic ideas is modeling the portfolio selection process in the form of a nonlinear program, and by solving the problem, investors will have more information to choose their portfolios. The objective of the problem is to minimize investment risk or to maximize the expected return of the portfolio. In his work, Markowitz used the variance of the portfolio as an investment risk measure and a linear combination of the expected return on assets as the expected return on the portfolio. Our goal is to find the proportions of the assets in the portfolio.

Let a_i be the proportion of the total invested funds of asset i and μ_i represent expected return for each asset ($i = 1, 2, \ldots, n$ with n is number of assets). Moreover, for any two assets i and j, σ_{ij} is their covariance.

T. A. Son (✉) · B. Q. Bao · L. Q. Luc
School of Applied Mathematics and Informatics, Ha Noi University of Science and Technology, Hanoi, Viet Nam
e-mail: taanhson123@gmail.com

T. D. L. Nguyen and J. Lu (eds.), *Machine Learning and Mechanics Based Soft Computing Applications*, Studies in Computational Intelligence 1068,
https://doi.org/10.1007/978-981-19-6450-3_5

We can calculate the expected return μ_i using formula:

$$\mu_i = E\left(r^i\right) = \frac{\sum_{t=1}^{m} r_t^i}{m} \tag{1}$$

where r_t^i is the return value of asset i between periods of time and m is the number of periods. In practice, the data of assets (such as stocks) often statistics by day. So, the return on each asset between day t and day $t+1$ can be calculated as below [1]:

$$r_t = \frac{G_{t+1} - G_t}{G_t} \tag{2}$$

where G_{t+1}, G_t are the closing prices of asset at day $t+1$ and day t.

From formula (1) and (2), covariance σ_{ij} between two assets i and j is calculated by [2]:

$$\sigma_{ij} = \text{Cov}\left(r^i, r^j\right) = \frac{\sum_{t=1}^{m}\left(r_t^i - \mu_i\right)\left(r_t^j - \mu_j\right)}{m} \tag{3}$$

since, we have covariance matrix:

$$\Sigma = \begin{pmatrix} \sigma_{11} & \sigma_{12} & \dots & \sigma_{1n} \\ \sigma_{21} & \sigma_{22} & \dots & \sigma_{2n} \\ \vdots & \vdots & \ddots & \vdots \\ \sigma_{n1} & \sigma_{n2} & \dots & \sigma_{nn} \end{pmatrix}$$

The expected return and the variance of the portfolio are as follows [3]:

$$E[a] = a_1\mu_1 + a_2\mu_2 + \cdots + a_n\mu_n = \mu^T a \tag{4}$$

$$\text{Var}[a] = a^T \Sigma a \tag{5}$$

where $a = (a_1, \dots, a_n)$ and $\mu = (\mu_1, \dots, \mu_n)$.

In this paper, we build a model to minimize the objective function, which is the risk measure of the portfolio. The model is described below:

$$\begin{aligned} \min_a \quad & a^T \Sigma a \\ \text{s.t.} \quad & \mu^T a \geq R, && (6) \\ & \sum_{i=1}^{n} a_i = 1, && (7) \\ & a_i \geq 0, \qquad i = 1, 2, \dots, n. && (8) \end{aligned}$$

The constraint (6), we want the expected return greater than a predefined threshold R. The constraint (7) shows that the sum of investment proportions for each asset a_i equals to one. The purpose of the last constraints (8) is to prevent short sales.

1.1 Cardinality Constraints and Bounding on Variables

In practice, in order to select the portfolio, the investors must consider their preferences and limitations, which stem from real features. They can be added as constraints to the model (6)–(8). Two types of constraints we consider here are cardinality constraints and bound constraints.

Cardinality Constraints We introduce binary variables b_i $(i = 1, 2, \ldots, n)$ to represent the cardinality constraint.

$$b_i = \begin{cases} 1, & \text{if asset } i \text{ is selected,} \\ 0, & \text{otherwise} \end{cases} \tag{9}$$

In practice, we may want to invest in a certain amount range of assets from $K_{\min}$ to $K_{\max}$:

$$K_{\min} \leq \sum_{i=1}^{n} b_i \leq K_{\max} \tag{10}$$

For convenience in programming, we can also express the constraint as follows:

$$\sum_{i=1}^{n} b_i = K \tag{11}$$

Bounds on Investment For each selected asset, we limit their investment weight with given lower and upper bound:

$$l_i\, b_i \leq a_i \leq u_i\, b_i, \quad i = 1, 2, \ldots, n \tag{12}$$

We can see that if asset i is not selected, then the value a_i equals to one, so the bounds are apply only when the asset is selected.

Apply the two constraints (11) and (12) to the model (6)–(8), we have:

$$\begin{aligned}
\min_a \quad & a^T \Sigma a \\
\text{s.t.} \quad & \sum_{i=1}^{n} \mu_i a_i \geq R, && (13)\\
& \sum_{i=1}^{n} a_i = 1, && (14)\\
& \sum_{i=1}^{n} b_i = K, && (15)\\
& l_i\, b_i \leq a_i \leq u_i\, b_i, \quad i = \overline{1,n}, && (16)\\
& a_i \geq 0, \qquad\qquad i = \overline{1,n}, && (17)\\
& b_i \in \{0,1\}, \qquad\quad i = \overline{1,n}. && (18)
\end{aligned}$$

As we can see, the model includes continuous and discrete variables, with the objective function is a convex quadratic function. Therefore, the problem is mixed-integer quadratic program (MIQP), which is NP-Hard [4]. In this paper, two heuristic methods: genetic algorithm and heuristic branching, will be introduced to solve this problem.

2 Related Work

The portfolio optimization problem in general has many variations. One of the main approaches is to minimize risk. There are many measure functions for assessing risk: Gini's mean difference [5], mean absolute deviation [6], etc. An other approach that is using expected return as objective function or using a linear combination of risk measure and expected return.

In the thesis [3], the author introduces an exact method—the outer approximation algorithm [7] and a heuristic branching algorithm for solving Markowitz mean-variance model. In this work, the data samples were randomly generated using the continuous uniform distribution in MATLAB.

Heuristic algorithms for cardinality constrained portfolio optimization were introduced in 2000 by Chang et al. [8]. In this work, they represent three heuristic algorithms based upon genetic algorithms, tabu search and simulated annealing. The model they used has an objective function that is a linear combination of the mean-variance risk measure and expected return. The data are five datasets including the Hang Seng (Hong Kong), Nikkei 225 (Japan), FTSE 100 (UK), DAX 100 (Germany), and S&P 100 (USA).

3 Genetic and Heuristic Branching Algorithm

In this section, we will present genetic algorithms and heuristic branching solving model (13)–(18).

3.1 Genetic Algorithm

GAs are based on the evolutionary process of biological organisms in nature. The evolutionary process shows the optimum in that the next generation is always better than the previous. Genetic algorithms include basic factors: Represent the solution of the problem as a chromosome, initial population, genetic operations, evaluate fitness function, and parameters. In the following, we will present the main factors for solving (13)–(18):

1. Representation

We use a vector with size $2n$ to represent each solution:

$$X = [a_1, a_2, ..., a_n, b_1, b_2, ..., b_n], \tag{19}$$

where $a_i \in [0, 1]$ and $b_i \in \{0, 1\}$.

2. Fitness function

   We construct fitness function by adding constraint (13) as a penalty to the objective function:

$$g(X) = a^T \Sigma a + H \cdot \max\left(0, R - \sum_{i=1}^{n} \mu_i a_i\right) \tag{20}$$

   where H is some positive constant; the bigger H is, the stronger the constraint.

3. Initial population

   Let P be the size of the population, each chromosome in the population set will be encoded such that they satisfy constraint (15), (17), (18). We create an initial population:

   (a) First, we randomly generate K different natural numbers; $D = \{d_1, d_2, ..., d_K\}$, for each $d_k : 1 \le d_k \le n$.

   (b) Then, we set:

$$b_i = \begin{cases} 1, & \text{if } i \in D \\ 0, & \text{otherwise} \end{cases} \tag{21}$$

$$a_i = \begin{cases} rand(i), & \text{if } i \in D \\ 0, & \text{otherwise} \end{cases} \tag{22}$$

   where $rand(i)$ is a random number in [0,1].

4. Selection
   Let Q be the size of the selection set ($Q < P$), chromosomes are selected based on their fitness values using a roulette wheel approach. The chromosome with a smaller fitness value has a greater probability of being selected.
5. Crossover
   Choose randomly two parent chromosomes from the selection set:

$$X^{(1)} = [a_1^{(1)}, a_2^{(1)}, ..., a_n^{(1)}, b_1^{(1)}, b_2^{(1)}, ..., b_n^{(1)}], \tag{23}$$

$$X^{(2)} = [a_1^{(2)}, a_2^{(2)}, ..., a_n^{(2)}, b_1^{(2)}, b_2^{(2)}, ..., b_n^{(2)}]. \tag{24}$$

   To create a pair of offspring chromosomes from $X^{(1)}$ and $X^{(2)}$ without violating constraint (15), we only apply a crossover operation where $a_i^{(1)}$ and $a_i^{(2)} \neq 0$. Generate random number ran in [0,1], if $ran < p_c$, with p_c is crossover probability, we have:

$$\hat{X}^{(1)} = [a_1^{(1)}, ..., \underline{a_i^{(2)}}, ..., a_n^{(1)}, b_1^{(1)}, b_2^{(1)}, ..., b_n^{(1)}], \tag{25}$$

$$\hat{X}^{(2)} = [a_1^{(2)}, ..., \underline{a_i^{(1)}}, ..., a_n^{(2)}, b_1^{(2)}, b_2^{(2)}, ..., b_n^{(2)}]. \tag{26}$$

6. Mutation
   Let children chromosome X:

$$X = [a_1, a_2, ..., a_n, b_1, b_2, ..., b_n], \tag{27}$$

   Similarly, we only apply a mutation operation where $a_i \neq 0$. Generate random number ran in [0,1], if $ran < p_m$, with p_m is mutation probability, we have:

$$\hat{X} = [a_1, a_2, ..., \underline{r_i}, ..., a_n, b_1, b_2, ..., b_n], \tag{28}$$

   where r_i is a random number in [0,1].
7. Normalize chromosomes
   We can see that after each process: initial population, selection, crossover, and mutation; constraints (15), (17), (18) are satisfied. However, constraints (14), (16) can be violated. Therefore, we need to normalize chromosome; the idea is based on Chang et al. [8] 's work :

   (a) If $\sum_{i \in D} l_i \geq 1$ or $\sum_{i \in D} u_i \leq 1$, the solution is infeasible.
   (b) Otherwise, we set:

$$A = \sum_{i \in D} a_i, \tag{29}$$

$$L = 1 - \sum_{i \in D} l_i, \tag{30}$$

$$w_i = l_i + a_i \frac{L}{A}, \ \forall i \in D. \tag{31}$$

(c) Let $W = \{i \in D | w_i \geq u_i\}$, we set:

$$A = \sum_{i \in D-W} a_i, \tag{32}$$

$$L = 1 - \left(\sum_{i \in D-W} l_i + \sum_{i \in W} u_i \right), \tag{33}$$

$$w_i = l_i + a_i \frac{L}{A}, \ \forall i \in D - W, \tag{34}$$

$$w_i = u_i, \ \forall i \in W. \tag{35}$$

(d) Update $a_i = w_i, \ \forall i \in D$.

Algorithm 1: Genetic Algorithm

```
Algorithm parameters:
  iter: max number of iteration.
  P: the size of the population.
  p_c: crossover probability.
  p_m: mutation probability.
  Q: the size of the selection set
Generate an initial population
Normalize chromosomes
Evaluate the fitness value of chromosomes
While t < iter:
  Selection
  for i from Q to P:
    Crossover
    Mutation
    Normalize chromosomes
  Update population
  Evaluate the fitness value of each chromosome
  t := t + 1
```

3.2 Heuristic Branching

Next, we will solve the model (13)–(18) by HB algorithm introduced in the paper. This algorithm decomposes the problem into a relaxed problem and a MILP problem.

Relaxed problem:

$$\begin{aligned}
\min_a \quad & a^T \Sigma a \\
\text{s.t.} \quad & \sum_{i=1}^{n} \mu_i a_i \geq R, && (36)\\
& \sum_{i=1}^{n} a_i = 1, && (37)\\
& \sum_{i=1}^{n} b_i = K, && (38)\\
& l_i\, b_i \leq a_i \leq u_i\, b_i, \quad i = \overline{1,n}, && (39)\\
& a_i \geq 0, \qquad i = \overline{1,n}, && (40)\\
& b_i \in [0,1], \qquad i = \overline{1,n}. && (41)
\end{aligned}$$

The relaxed problem is a continuous convex quadratic problem. CPLEX can solve it to optimality in a very timely manner. We denote a^* is the solution of relaxed problem. This solution is a lower bound for the original problem. Next, we put solution a^* into master problem. We denote κ^* is the solution of master problem. κ^* is an upper bound.

Master problem:

$$\begin{aligned}
\underset{\kappa}{\text{minimax}} \quad & \sum_{i=1}^{n} \left|\kappa_i - a_i^*\right| \\
& \text{s.t} \sum_{i=1}^{n} \mu_i \kappa_i \geq R, && (42)\\
& \sum_{i=1}^{n} \kappa_i = 1, && (43)\\
& \sum_{i=1}^{n} b_i = k, && (44)\\
& l_i\, b_i \leq \kappa_i \leq u_i\, b_i, \quad i = \overline{1,n}, && (45)\\
& \kappa_i \geq 0, \qquad i = \overline{1,n}, && (46)\\
& b_i \in \{0,1\}, \qquad i = \overline{1,n}. && (47)
\end{aligned}$$

We seek to minimize the maximum distance. If we linearize the objective function, then we have a MILP problem.

We linearize by adding ρ_i and constraints $-\rho_i \leq \kappa_i - a_i^* \leq \rho_i$ to the master problem, $i = 1, 2, \ldots, n$. We can quickly solve MILP problem by CPLEX.

We have MILP problem of master problem:

$$\begin{aligned}
\min_{\rho} \quad & \sum_{i=1}^{n} \rho_i \\
\text{s.t.} \quad & \sum_{i=1}^{n} \mu_i \kappa_i \geq R, && (48)\\
& \sum_{i=1}^{n} \kappa_i = 1, && (49)\\
& -\rho_i \leq \kappa_i - a_i^* \leq \rho_i, && (50)\\
& \sum_{i=1}^{n} b_i = K, && (51)\\
& l_i\, b_i \leq \kappa_i \leq u_i\, b_i, \quad i = \overline{1,n}, && (52)\\
& \kappa_i \geq 0, \qquad i = \overline{1,n}, && (53)\\
& \rho_i \geq 0, \qquad i = \overline{1,n}, && (54)\\
& b_i \in \{0,1\}, \qquad i = \overline{1,n}. && (55)
\end{aligned}$$

After solving the two above problems, we need to tighten the lower bound by cuts. We do the cuts by adding conditions on b_i in the relaxed problem.

We consider the cut in the [3]: $b_i' - (b_i')^2 = 0 \ \forall\ i$ to define a condition on b_i', where b_i' is the value of b_i in Relaxed problem. In the positive cuts with $i = 1, \ldots, n$, we choose the minimum cut to fix $b_i' = 0$ and choose the maximum cut to fix $b_i' = 1$ in Relaxed problem.

Before we do the cuts, we change the value of b_i by the following method:

$$b_i = b_i(1 + \varepsilon_i) \quad \text{if } \lambda_i \geq 0.5, \tag{56}$$

$$b_i = b_i(1 - \varepsilon_i) \quad \text{if } \lambda_i < 0.5. \tag{57}$$

where ε_i, λ_i is random value in [0, 1]. After changing value of b_i, we check value of b_i.

$$\text{If } b_i > 1 \text{ then } b_i := 1 \tag{58}$$

Then, we do the cuts.

We define the optimality gap as bellow:

$$\text{GAP}_{\text{opt}} := (((\kappa^*)^T)\Sigma\kappa^*) - (((a^*)^T)\Sigma a^*). \tag{59}$$

Table 1 US stock data (size 500–1200)

Number of assets	The solution of the original problem		GA		HB	
	Result	Time (s)	Result	Time (s)	Result	Time (s)
500	$2.21815e^{-5}$	2267.91	$7.2623e^{-5}$	31.65	$2.3984e^{-5}$	35.61
600	$2.02839e^{-5}$	153.74	$7.6669e^{-5}$	35.17	$2.2409e^{-5}$	47.04
700	$1.95769e^{-5}$	1602.51	$9.5275e^{-5}$	41.15	$2.1019e^{-5}$	66.90
800	$1.95769e^{-5}$	4492.28	$7.3633e^{-5}$	46.67	$2.1042e^{-5}$	99.57
900	NA	NA	$7.1940e^{-5}$	51.61	$2.2009e^{-5}$	119.27
1000	NA	NA	$8.6629e^{-5}$	57.94	$2.1987e^{-5}$	152.11
1100	NA	NA	$8.2264e^{-5}$	64.44	$6.09011e^{-5}$	199.39
1200	NA	NA	$7.1584e^{-5}$	70.07	$3.8761e^{-5}$	240.58

We denote the maximum optimal gap by θ.

Algorithm 2: Heuristic Branching

Solve Relaxed problem and get solution a^*;
Apply a^* to Master problem and solve it. We have solution κ^*;
Update GAP_{opt} by solution a^* and κ^*;
IF $GAP_{opt} > \theta$ then:
  Apply the above change;
  Apply the cut to Relaxed problem;
  Repeat;
ELSE: STOP and return the solution

4 Numerical Results

In this section, we provide numerical results comparing GA, HB, and the exact method using CPLEX for solving. The data we use are from the Vietnamese and American stock markets. The Vietnamese datasets are downloaded from the Web: https://cafef.vn, start from 12/12/2018 to 12/11/2020 of over 1200 companies. The American datasets are of the top 3000 companies on the US stock exchange, start from 19/2/2016 to 25/11/2020. We will compare the results as follows:

1. First, we use the American datasets to compare the objective values and computation time between GA, HB, and the exact method on datasets with sizes from 500 to 1200.
2. Then, we implement the algorithms on the Vietnamese datasets and also perform a comparison of the objective values and computation time between GA and HB. The reason we do not compare them with the exact method is that its computation time is over 3 h with a dataset of size 500.

Table 2 US stock data (size 1500–3000)

Number of assets	GA		HB	
	Result	Time (s)	Result	Time (s)
1500	$6.2497e^{-5}$	93.80	$6.5408e^{-6}$	451.61
2000	$6.5897e^{-5}$	129.75	$4.8932e^{-5}$	843.56
2500	$5.4843e^{-5}$	162.96	$4.5872e^{-6}$	1083.72
3000	$5.2001e^{-5}$	186.45	$10.0018e^{-5}$	1507.12

Table 3 Vietnamese stock data

Number of assets	GA		HB	
	Result	Time (s)	Result	Time (s)
500	$4.1553e^{-5}$	33.73	$8.7949e^{-6}$	55.61
600	$4.9257e^{-5}$	35.93	$1.2211e^{-5}$	83.56
700	$2.7815e^{-5}$	42.63	$6.4953e^{-6}$	91.72
800	$3.6540e^{-5}$	48.77	$1.7018e^{-5}$	120.12
900	$3.6943e^{-5}$	54.70	$3.1983e^{-5}$	164.26
1000	$3.7545e^{-5}$	60.90	$6.31e^{-5}$	206.03
1100	$4.0752e^{-5}$	68.28	$1.1048e^{-5}$	220.8
1200	$3.4166e^{-5}$	72.94	$2.7353e^{-5}$	266.51

From Table 1, we can see that datasets with sizes larger than 900, the computation time of the exact method is not applicable. Otherwise, it only takes 70 s with GA and 240 s with HB. However, the objective values of GA are twice time as HB.

In Tables 2 and 3, in some cases (size 1000, 1500, and 3000), the result of GA is better than HB, and the computation times of GA are much faster than HB.

Besides the computation time, HB and GA have another advantage. After each time we execute the algorithms, it gives different results. That helps investors to have more options for their portfolio

5 Conclusion and Future Work

Conclusion

This section is a summary of the results in Sect. 4. According to the results in Table 1, when the size of the data is larger, finding exact solution for the original problem in the time allowed is impossible while the two heuristic algorithms can solve it in a timely manner.

In Tables 2 and 3, we compare GA and HB algorithm on US stock data. The result of HB is better than GA, but the computation times of GA are faster than HB. In some cases, the result and the computation times of GA are better than HB.

Therefore, developing heuristic algorithms will be great option, especially for huge data size problems.

Future Work
We will research and build a investment decision-making support system.

Acknowledgements This research is funded by Ha Noi University of Science and Technology (HUST) under the grant number T2020-PC-303.

References

1. Campbell, J., Lo, A., & MacKinlay, C. (1997). The econometrics of financial markets. Princeton University Press.
2. Chacko, G., & Viceira, L. (2005). Dynamic consumption and portfolio choice with stochastic volatility in incomplete markets. *Review of Financial Studies, 18,* 1369–1402.
3. Rahnama, H. (2016). *A Portfolio optimization model*. Montreal University.
4. Garey, M. R., & Johnson, D. S. (1979). *Computers and intractability: A guide to the theory of NP-completeness*. W. H. Freeman and Company.
5. Shalit, H., & Yitzhaki, S. (1989). Evaluating the mean-Gini approach to portfolio selection. *The International , Portfolio Journal of Finance, 1*(2), 15–31.
6. Konno, H., & Yamazaki, H. (1991). Mean-absolute deviation portfolio optimization model and its applications to Tokyo Stock Market. *Management Science, 37,* 519–531.
7. Duran, M. A., & Grossmann, I. E. (1986). An outer-approximation algorithm for a class of mixedinteger nonlinear programs. *Mathematical Programming, 36,* 307–339.
8. Chang, T.-J., Meade, N., Beasley, J. E., & Sharaiha, Y. M. (2000). Heuristics for cardinality constrained portfolio optimisation. *Computers & Operations Research, 27*, 1271–1302.

Context-Based and Collaboration-Based Product Recommendation Approaches for a Clothes Online Sale System

Hai Thanh Nguyen, Vi Hung Ngo, and Tran Thanh Dien

Abstract E-commerce systems have developed remarkably and provided a considerable profit for commercial companies and groups. Customers also benefit from such systems. However, the rapidly increasing volume and complexity of data lead customers to find that it is a challenge to find suitable products for their interests. Numerous product recommended methods have been researched and developed to support users when they visit E-commerce websites. This study proposes a recommendation system for a Clothes Online Sale system based on analyzing context-based and collaboration-based methods. Each type was divided into memory-based and model-based approaches. The results give the same product, but the cosine distance of the Word2vec + IDF algorithm is the lowest. We have also deployed algorithms including the K-nearest neighbor's algorithm (KNN), singular value decomposition (SVD), non-negative matrix factorization (NMF), and matrix factorization (MF) for the comparison. The method is evaluated on Amazon women's clothing, including 50,046 samples and six features. We proposed a content-based memory-based method using Word2vec + IDF and a collaboration-based model-based method using the SVD algorithm with the result of RSME as 1.268 to deploy on the sales system.

Keywords Recommendation system · Content-based · Amazon · Collaboration-based · E-commerce website · Clothes

H. T. Nguyen (✉) · V. H. Ngo · T. T. Dien
College of Information and Communication Technology, Can Tho University, Can Tho 900000, Vietnam
e-mail: nthai.cit@ctu.edu.vn

T. T. Dien
e-mail: thanhdien@ctu.edu.vn

T. D. L. Nguyen and J. Lu (eds.), *Machine Learning and Mechanics Based Soft Computing Applications*, Studies in Computational Intelligence 1068,
https://doi.org/10.1007/978-981-19-6450-3_6

1 Introduction

E-commerce websites have been trendy and are growing day by day. E-commerce site managers always want to increase sales while customers want convenience when buying, so the recommendation system is developed and increasingly optimized for E-commerce sites. Thence, we consolidate studies and analyze key types of recommendations, such as content-based and collaboration-based recommendations. Our goal is to synthesize system methods that recommend appropriate products to customers using popular algorithms so that E-commerce site administrators can easily select and implement a recommendation system for their website. In addition, we have compared different algorithms in the same product recommendation method to help people make good choices.

This study introduces a content-based memory-based method using Word2vec + IDF and a collaboration-based model-based method with the SVD algorithm and obtains an RSME of 1.268. In the next sections of the paper, we present some research related in Sect. 2. Section 3 includes our steps to perform the recommendations for an E-commerce website. We also exhibit the results and compare the performance of various methods in Sect. 4. Finally, Sect. 5 is the conclusion and direction of development.

2 Related Work

Many different types of recommendations have been studied [1] as well as the development of various algorithms within those types of recommendations [2, 3]. Moreover, every kind of recommendation has its unique method and evaluation [4], and it develops in many directions, such as building the framework of recommendation system [5], perennial customer information [6]. Typically, the recommended system will be divided using data such as content-based [7] and collaboration-based [8], or even a combination of the two [9].

2.1 Related Work on Text Vectorization

The authors in [10] studied to convert text to vector using TF and IDF, and both give good performance. However, the formula seems simple. Later on, many other methods appear to compare efficiency. The authors in [11] studied the quality of the vector representations of words derived by different models over a set of syntactic and semantic linguistic tasks. They observed that it is possible to train high-quality magnetic vectors using a simple model architecture compared to standard neural network models (straight and repetitive).

2.2 Related Work on the Algorithm for Matrix Factorization

We combine the ability to predict supplementary information and the ability to simulate nonlinear relationships of a multi-layered neural network in the problem of predicting user ratings (explicit) by using the architecture based on Neural Collaborative Filtering and the equation in the article "Neural Collaborative Filtering" [12]. The authors in [13] gave a non-negative matrix factorization(NMF) to solve the problems. We see this as an applicable method for the situation we are studying. Again mentioned the method of improving the accuracy, dividing the matrix into many parts, so the Singular Value Decomposition (SVD) method appears in an article [14]. The question here is whether these methods, which are more efficient when integrating into a particular sales system, are the startup sales system we have built to study.

3 The Proposed Method

Our recommendation system is divided into a context-based method that uses data about each user's context and behavior and the collaboration-based method to use another user's behavior data as the primary user. Each category evolved in two directions: memory-based (memory-based is the use of direct, untrained data) and model-based (model-based is the use of trained data). These four types all use the following architectures:

In Figure 1, memory-based recommendations will stop at the algorithm selection process and then move directly to the top-N product process.

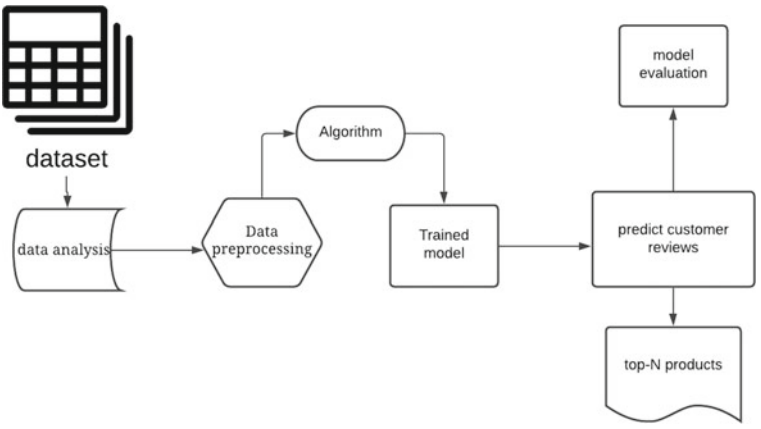

Fig. 1 Processes in the recommended system study

3.1 Data Description

Our method is evaluated on two datasets from the website Kaggle [15] with the following description. The first dataset includes 28,395 samples and seven features on products. The set of considered features contains data on Amazon's standard identification number, title the title of the product, the brand, color information of apparel, and the type of the apparel, the URL of the image (for small image) to show the product image, and the URL of the large image. The other is about product evaluation with 50,046 samples and six features, a collection of customer reviews for a product. The second dataset contains 6584 products and 6670 customers. Features include: ASIN (Amazon standard identification number), title (title of the product), review_userId (identification number of reviewer), review_score (rating score), review_summary (summary comment section), review_text (comment section content). Our data analysis mainly looks at the top-rated products or the most appreciated products, the statistics of the features, and customer opinion through product reviews.

3.2 Data Preprocessing

In dealing with **loss data**, we removed rows because there are many unique types and a little bit of data loss.

Remove **duplicate title data**: Because we use the title to suggest products with similar titles in the contextual suggestion, we have to deal with each word in the title duplicate. Therefore, the data will be duplicated as follows: Products with almost the same title only differ in size, and products with nearly the same title vary only by color.

Remove Stop Words in title data: Stop Words are some words partially or completely ignored by search engines. Words like: "a, a, a, of, or, many, etc... ". These words have nothing to do with the content and meaning of the article.

Handling special characters such as.,?! -_ + \ [] { } " ;: '= /: We will proceed to remove all these special characters. Because these special characters affect the comparison of the filter.

Text vectorization: We use different equations to find the best one**,** those equations include **IDF** (Inverse Document Frequency), **TF-IDF** (Term Frequency-Inverse Document Frequency).

Word2vec [11] is an unsupervised learning model trained from a large corpus. The dimension of Word2vec is much smaller than one-hot encoding, where the dimension is $N \times D$, where N is the number of documents, and D is the number of word embedding. Word2vec represents each separate word with a list of specific numbers called vectors.

We deploy Word2vec and IDF, as shown in Eq. 1. IDF calculates the titles of the product to find the weight of each word. When using the Word2vec model, synonyms will multiply by the IDF weight of each corresponding word.

3.3 Algorithm and Trained Model and Predict Customer Reviews

In the case of memory-based recommendations, we skip the model training and move straight to the customer rating prediction process or the top-N product. In memory-based context-based recommendations, we used cosine distance to calculate the distance of the vector of products other than the vector of the proposed product. Evaluating the two vectors by "cosine distance" has the following equation [16]:

$$\text{cosine distance} = 1 - \cos(\mathbf{A}, \mathbf{B}) = \frac{\mathbf{AB}}{\|\mathbf{A}\|\|\mathbf{B}\|} = \frac{\sum_{i=1}^{n} \mathbf{A}_i \mathbf{B}_i}{\sqrt{\sum_{i=1}^{n} (\mathbf{A}_i)^2}\sqrt{\sum_{i=1}^{n} (\mathbf{B}_i)^2}} \quad (1)$$

In Eq. 1, A_i and B_i are components of vectors A and B, respectively. After applying Eq. 1, we have sorted the list of products according to the products with the smallest distance, and we have the list of top N similar products. While calculating the cosine distance, we can calculate other product features such as brand, product_type_name, and color by converting the vector as shown in the Bag of Words section and blending it. Then, we get a different characteristic spacing and title characteristic spacing.

$$\text{dist} = (W_1 * \text{titleDist} + w_2 * \text{extraDist})/(w_1 + w_2) \quad (2)$$

In Eq. 2, w_2 is the weight of title, w_2 is the weight of extra features, titleDist is title difference measured by distance, extraDist is additional features difference measured by the distance, and dist is the combination of these two parameters.

In memory-based collaboration-based recommendations [17], we also studied and built a user-item matrix, then calculated the correlation between users to form the human correlation matrix. User is referred to as user-based. Similar to products, we calculate the correlation between products to form a product correlation matrix called item-based. The correlation equation is as follows:

$$r = \frac{\sum_{i=1}^{n}(x_i - \overline{x})(y_i - \overline{y})}{\sqrt{\sum_{i=1}^{n}(x_i - \overline{x})^2(y_i - \overline{y})^2}} \quad (3)$$

In Eq. 3, r = correlation coefficient, x_i = value of the variable x in the sample, $\overline{x}$ = mean value of variable x, y_i = value of the variable y in the sample, $\overline{y}$ = mean value of variable y. After calculating the similarity between users or between products, we can predict the rating of user u on the product i using the following formula:

$$\widehat{r_{ui}} = \overline{r_u} + \frac{\sum_{u' \in K_u} \text{sim}(u, u').(r_{u'i} - \overline{r_{u'}})}{\sum_{u' \in K_u} |\text{sim}(u, u')|} \quad (4)$$

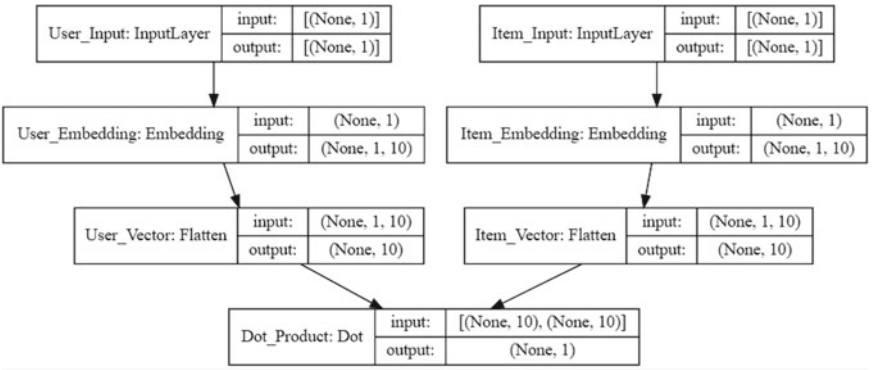

Fig. 2 Deep learning architecture 1

In Eq. 4, $\widehat{r_{ui}}$ is the prediction for user u on product i, sim(u, u') similarity between user u and u', K_u is the number of users whose proximity is near user u.

In model-based collaboration-based recommendations, we divided the sample data set into two parts to train and evaluate the model. We used algorithms: K-nearest neighbor (KNN), SVD, and NMF. The algorithms NMF and SVD have same the following equation:

$$\widehat{r_{ui}} = \mu + b_u + b_i + {q_i}^T p_u \tag{5}$$

In Eq. 5, $\widehat{r_{ui}}$ is the score which the customer u like the product i, while μ is the global average of all user ratings across all products. b_i is the deviation of the product (mean value of products relative to the global mean), and b_u is the user's deviation (the average of the users close to the global mean). If customer u is undefined, b_u is expected, and the factors p_u are assumed to be 0. The same applies to product i with b_i and q_i. To expand our research, we have referenced article [12] and proposed two more deep learning types for this problem. The architecture of those two deep learning types is as follows:

Figure 2 shows this architecture mainly after embedding the input layer and then calculating those two vectors' scalar product. The dot layer is the layer used to combine two layers of user input and product input by calculating the scalar product corresponding to each user of the embedded layer and the embedded layer's product.

In Fig. 3, we did not use the scalar product, we used the join layer to join, and the dense layer called the sigmoid function to compute the input vector. The output at each layer is equal to the product of the input vector with the weight matrix, and each element of the output vector is applied the nonlinear operator σ

$$y = \sigma(wx) \tag{6}$$

σ is a space matrix $\mathbb{R}_{m_x n}$ whose elements are applied nonlinear operator σ. The activation function σ of the classes is a **sigmoid function**.

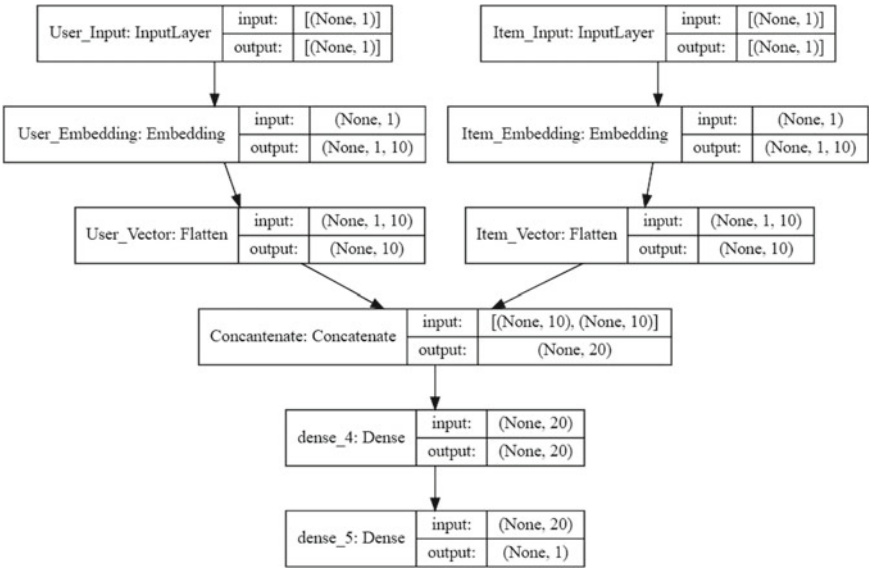

Fig. 3 Deep learning architecture 2

3.4 Model Evaluation

Evaluate the model by two main measures: RMSE and MAE. The mean squared error (MSE) of an estimate is the mean of the error square. In other words, it is the difference between the values predicted by the model and the actual value. We take the root of MSE to get RMSE. The mean absolute error (MAE) is a method of measuring the difference between two continuous variables. The MAE is calculated as follows:

$$\text{MAE} = (\frac{1}{n}) \sum_{i=1}^{n} \left| Y_i - \widehat{Y}_i \right| \tag{7}$$

$$\text{RMSE} = \sqrt{\frac{1}{n} \Sigma_{i=1}^{n} \left(Y_i - \widehat{Y}_i \right)^2} \tag{8}$$

In Eqs. 7 and 8, n is the number of elements in the set, Y_i is worth real evaluation, $\widehat{Y}_i$ is the value of the prediction.

4 Experimental Results

The main presentation compares the algorithms and then compares the recommended methods.

4.1 Text Vectorization Methods

The process steps in this form are mainly about calculating the cosine distance of the products other than the input product, and we will reorder which products have the smallest cosine distance Eq. 1 relative to the input product, which is also a list of similar products. We test to find similar products with the title "*women's unique 100 kinds of cotton special Olympics world games 2015 white size L*" for all three algorithms Bag of Words, TF-IDF, IDF. All three algorithms return the same products "*women's new 100 kinds of cotton special Olympics world games 2015 red size*" but different in distance calculation. Table 1 shows that the most similar product results are the same but different indicators in that the cosine distance using Word2vec+IDF is somewhat smaller.

Table 1 Cosine distance results on the same product

	Womens new 100 cotton special olympics world games 2015 red size
Bag of Words	0.18181818181818166
TF-IDF	0.12748023262076247
IDF	0.11689768372442932
Word2vec	0.05564171
Word2vec+IDF	0.03939116

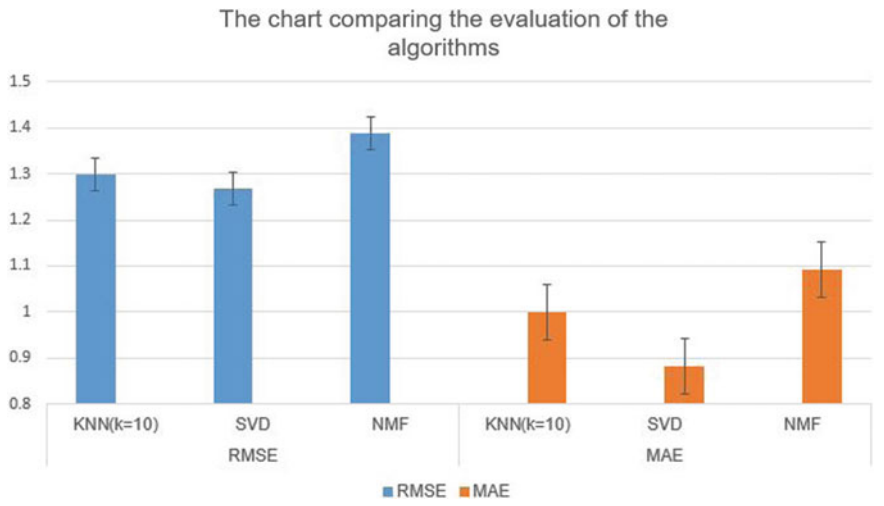

Fig. 4 Average performance comparison KNN, SVD, NMF in RMSE and MAE. The standard deviations are shown in error bars

4.2 Recommended Methods

We can use the machine learning model in the content-based recommended method, but because we comply with the method's rules based on each user's data, the data is greatly lacking. Besides, many users only rate very few products, this user data is very little, so when training the model, the results are not satisfactory. However, we still research to recognize the weaknesses and strengths of this method. We will present it in the comparison of methods. In the collaboration-based recommended method, we compare three algorithms to train the model: **KNN, SVD, and NMF** with fivefold cross-validation on the dataset.

From Fig. 4, we see that the SVD algorithm is the best algorithm for RMSE and MAE results, but we have to pass the corresponding parameter to get this result. We will choose the RMSE measure for SVD comparison with two deep learning structures, all three algorithms divide the data sample set (50,046 samples and 3 features) with a training rate of 0.8, a test rate of 0.2, and the number of epoch is 50, N_factor(the number of feature vectors) = 10.

Table 2 shows that architecture 2 of deep learning has a smaller measure than SVD and proves that the algorithm is better. The standard is to choose the right recommendation method for a newly opened sales system to split deals by new product, new user, both new product and new user, to choose the method that could predict in the case. In Table 3, we can see that in the context-based approach, the memory usage method works well in case the sales system is just starting up. In collaboration-based methods, we see that using memory to calculate the correlation takes time. Using the deep learning model is unpredictable due to the use of embedded

Table 2 Measure comparison between SVD and deep learning algorithms

	SVD	Deep learning architecture 1	Deep learning architecture 2
RMSE	1.2680594415447108	2.1875152570896508	1.2665433273283626

Table 3 Method for new product, new user

		New product	New user	Both new product and new user
Content-based	Memory	Still works	Still works	Still works
	Model	New data training is required	New data training is required	New data training is required
Collaborate-based	Memory	Still works time-consuming	Still works time-consuming	Time-consuming to rebuild corr-matrix
	Model	Still works but not with deep learning	Still works but not with deep learning	Still works but not with deep learning

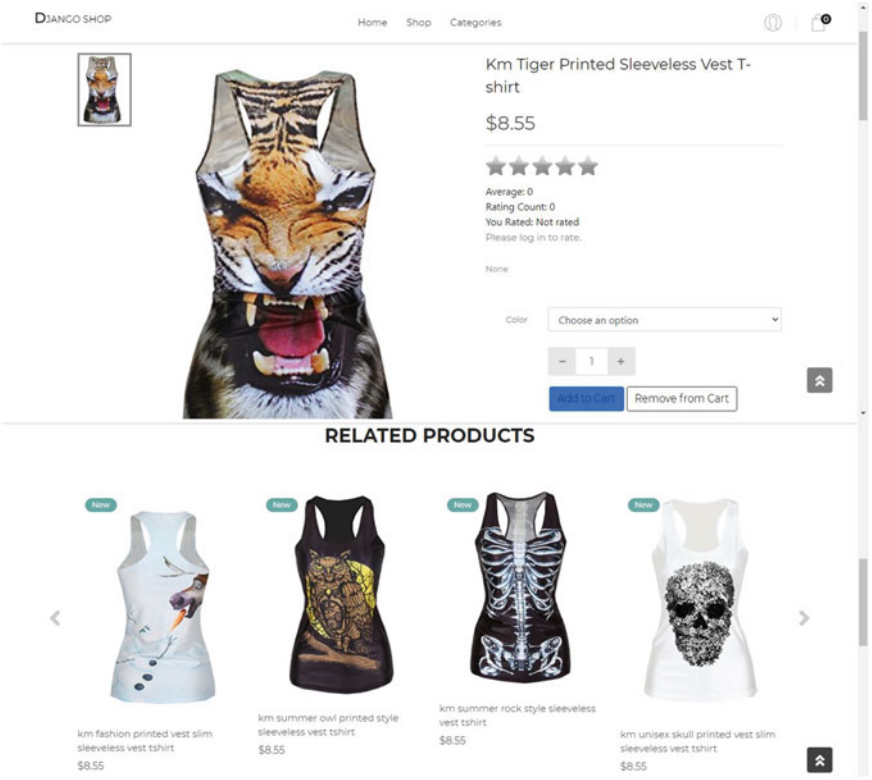

Fig. 5 Recommended product interface when deployed on a sales system

layers, but solving SVD techniques is still predictable. Finally, we implemented the referral system into the sales web system. Figure 5 shows the input product interface and shows the proposed output product interface (similar to the input product).

5 Conclusion

Regular E-commerce sites usually have basic information about the product, so in this study, we propose a method based on content, using memory, using Word2vec + IDF algorithm for text vectorization to find similar products through the product's contextual information because of the lowest cosine distance (0.03939116). We propose a model-based, collaborative-based approach that uses the SVD algorithm for the launch sales system to predict ranking scores. SVD model is predictable, with RMSE being 1.2681 for new users and new products, so it is suitable for E-commerce startups and E-commerce sites with big data. In the future, we should apply the A/B testing method (also known as split testing) to compare according to customers'

feelings to increase convenience for customers. A/B testing is a process in which two versions (A and B) are compared together in a defined environment/situation, thereby evaluating which version is more efficient.

References

1. Thu, T. N. M., & Hien, P. X. (2016). Evaluation methods for recommender systems (in Vietnamese). *Can Tho University Journal of Science., 42,* 18–27. https://doi.org/10.22144/ctu.jvn.2016.023.
2. Bao, L. H. Q., Dat, Q. N. , & Nghe, N. T. (2015). Model of combination of fisheries and the law of the number of east for ranking in the recommendation system (in Vietnamese). *Can Tho University Journal of Science IT*, 1–8.
3. Dung, N. H., & Nghe, N. T. (2014). Product recommendation system in online sales using collaborative filtering techniques (in Vietnamese). *Can Tho University Journal of Science, 31*, 36–51.
4. Isinkaye, F. O., Folajimi, Y. O., & Ojokoh, B. A. *Recommendation systems: Principles, methods and evaluation*. https://www.sciencedirect.com/science/article/pii/S1110866515000341b0175.
5. Abumalloh, R. A., Ibrahim, O., & Nilashi, M. (2020). Loyalty of young female Arabic customers towards recommendation agents: A new model for B2C E-commerce. *Technology in Society, 61*, 101253. https://doi.org/10.1016/j.techsoc.2020.101253
6. Tareq, S. U., Habibullah Noor, Md., & Bepery, C. (2019). The framework of dynamic recommendation system for e-shopping. *International Journal Information Technology, 12*, 135–140. https://doi.org/10.1007/s41870-019-00388-6
7. Beleveslis, D., & Tjortjis, C. (2020) Promoting diversity in content based recommendation using feature weighting and LSH. In: I. Maglogiannis, L. Iliadis, & E. Pimenidis (Eds.), *Artificial intelligence applications and innovations. AIAI 2020. IFIP Advances in information and communication technology* (Vol. 583). Springer. https://doi.org/10.1007/978-3-030-49161-1_38
8. Singh, M. K., & Rishi, O. M. (2020). Event driven recommendation system for E-commerce using Knowledge based collaborative filtering technique. *Scalable Computing: Practice and Experience, 21*(3), 369–378. https://doi.org/10.12694:/scpe.v21i3.1709, ISSN 1895-1767
9. Cai, X., Hu, Z., Zhao, P., Zhang, W., & Chen, J. (2020). A hybrid recommendation system with many objective evolutionary algorithm. *Expert Systems with Applications, 159*, 113648. https://doi.org/10.1016/j.eswa.2020.113648
10. Jones, K. S. (1972). A statistical interpretation of term specificity and its application in retrieval. *Journal of Documentation, 28*(1), 11–21.
11. Mikolov, T., et al. (2013). Efficient estimation of word representations in vector space. arXiv preprint arXiv:1301.3781.
12. He, X., Liao, L., & Zhang, H. (2017). Neural collaborative filtering. In *WWW '17: Proceedings of the 26th International Conference on World Wide Web* April 2017, pp. 173–182. https://doi.org/10.1145/3038912.3052569
13. Hernando, A., & Bobadilla, J. (2016). FernandoOrtega-A non negative matrix factorization for collaborative filtering recommender systems based on a Bayesian probabilistic model. *Knowledge-Based Systems, 97*(1), 188–202.
14. Li, C., & Yang, C. (2016). The research based on the Matrix Factorization recommendation algorithms. In *2016 IEEE Advanced Information Management, Communicates, Electronic and Automation Control Conference (IMCEC)*.
15. Amazon (May 1996–July 2014). Apparels review. https://www.kaggle.com/thekenjin/amazonapparelsdata

16. Wen, H., Ding, G., Liu, C., & Wang, J. (2014). Matrix factorization meets cosine similarity: Addressing sparsity problem in collaborative filtering recommender system. In: L. Chen, Y. Jia, T. Sellis, & G. Liu, (Eds.), *Web technologies and applications* (Vol. 8709). APWeb 2014. Lecture Notes in Computer Science. Springer. https://doi.org/10.1007/978-3-319-11116-2_27
17. Stephen, S. C., Xie, H., & Rai, S. (2017). Measures of similarity in memory-based collaborative filtering recommender system: A comparison. In *Proceedings of the 4th Multidisciplinary International Social Networks Conference (MISNC '17). Association for Computing Machinery*, New York, USA, Article 32, 1–8. https://doi.org/10.1145/3092090.3092105

A Cost-Effective Control System of the Biogas-Based Electrical Generator

Hoang Anh, Duc Tung Trinh, Vu Thanh Nguyen, Hung Dung Pham, and Duc Chinh Hoang

Abstract Increment of energy consumption in a fast-developing country like Vietnam has put high pressure on conventional power generation such as thermal power and hydroelectricity. In order to supplement energy demand, renewable energy sources are playing crucial roles. Among those sources, biogas energy has great potential, especial in livestock farm, for its ability to convert waste into heat and electricity. In this work, a control system has been developed to facilitate the operation of a biogas-based electrical generator. Self-customized generator of 25–100 kW is used to supply power to a hog farm. As the biogas production which is impacted by the livestock and the electrical load may vary over the time, it is required to manage the system in such a way that it can stabilizes the generator speed and thus its output power frequency. In this paper, we present a control system equipped with an industrial programmable logic controllers (PLC) and adopting PID algorithm which has been integrated to the biogas-based generators. The self-developed biogas base generation systems have been deployed in a few hog farms in the rural area of northern Vietnam. The experimental results have shown that the control system is able to supply power to the farm with stable frequency within 49.5 and 50.5 Hz while the load varies.

Keywords Biogas · Composed speed control · Electrical generator · Renewable energy

1 Introduction

Biogas is a type of organic gas created from the decomposition of various organic matter such as landfill waste, industrial wastewater, and livestock wastewater. Raw biogas mainly consists of methane (CH_4, 40–75%) and carbon dioxide (CO_2, 15–60%). The minority of the gas includes other components such as water (H_2O, 5–10%), hydrogen sulfide (H_2S, 0.005–2%), oxygen (O_2, 0–1%), and carbon monoxide

H. Anh · D. T. Trinh · V. T. Nguyen · H. D. Pham · D. C. Hoang (✉)
Hanoi University of Science and Technology, Hanoi, Vietnam
e-mail: chinh.hoangduc@hust.edu.vn

T. D. L. Nguyen and J. Lu (eds.), *Machine Learning and Mechanics Based Soft Computing Applications*, Studies in Computational Intelligence 1068,
https://doi.org/10.1007/978-981-19-6450-3_7

(CO, < 0.6%) [1, 2]. Biogas can be considered as a type of renewable energy sources which is used in the form of thermal energy for cooking or heating in winter [3]. It is also employed as fuel for electrical generator to generate power which is the interest in this work.

Large and medium-sized livestock farms are popular in Vietnam where agriculture is still an important part of the country economy. Waste generated by these farms is usually disposed to the environment directly, and thus, it causes serious pollution issues. Biogas is a solution to convert waste into useful energy source and to avoid contaminating the surroundings simultaneously. The overall procedure of energy conversion is illustrated in Fig. 1 where the waste produced by the animal is gathered in the treatment tank to be processed and subsequently transformed into to biogas in the gasholder. In this study, the biogas generated in hog farms is partially used for heating, and the rest of gas is fed to an electrical generator to power the farms. In fact there were some domestic and foreign research works to use biogas as a fuel supply for the operation of electrical generators [4, 5]. However, there may be some risks to develope and run such generators which actually are costly. These risks come from the fact that: the aforementioned biogas has a high proportion of CO_2 content and some highly corrosive impurities such as hydrogen sulfide which may causes damage to engine parts. Therefore, in order to use biogas as a fuel for the engine to run for a long time, it needs to be cleaned with the filtration system as shown in Fig. 1. Biogas filtration helps to increase the concentration of methane. The heating efficiency of this renewable fuel is then improved when harmful compounds such as hydrogen sulfide and carbon dioxide are removed. The methane concentration can be increased to a higher value than natural gas (NG), and in this case, the biogas becomes biomethane [1]. The authors in [6] conducted simulation studies to compare the performance of the generators using gasoline, liquefied petroleum gas (LPG), natural gas, and biogas. The results that the biogas can reduce significant amount of contamination gas like CO, HC, and NO_x, and thus, it helps decrease the bad effect of harmful greenhouse gas emission.

The biogas generation system which can be cooperated with power grid or other energy sources like wind or solar as discussed in [7–9]. Electricity produced from biogas to supply to the grid requires a large scale generation system. Such system as well as the infrastructure is not currently available in Vietnam to the best of our knowledge. This study mainly considers small scale biogas-based generators which run in off-grid mode most of the time. The generator combustion engines are usually classified as biogas-diesel, dual-fuel engine generator, and ignition biogas engine generator. Their performance comparison is presented in [10], among those purely biogas ignition type can achieve higher efficient energy conversion and is used in this work. To have a cost-effective solution, our approach is to modify a diesel engine to make it work with biogas as fuel. Although, there is a built-in governor inside the diesel generator, it is not really suitable to be used with other types of fuel. Thus, it is required to retrofit the control system for the enhanced generator to operate properly.

In this study, we present a design of such control system which includes sensing devices, a PID controller, and actuators integrated in the biogas generators. The main purpose is to stabilize the electrical generator speed and thus the power frequency

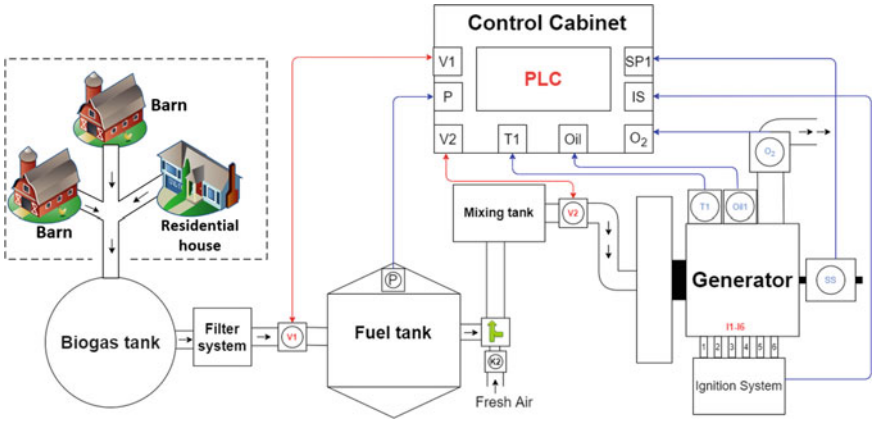

Fig. 1 Biogas production and energy conversion in livestock farms

should be maintained within the safe range of 49.5–50.5 Hz while the system can respond quickly to load changes. It would help to operate the generator safely and prolong its lifetime.

The structure of the paper is as below: Sect. 1 introduces the background of the biogas generation system, the system description is presented in Sect. 2, the control system development is discussed in Sects. 3 and 4 provides the experimental results, and finally, we conclude the paper in Sect. 5.

2 System Description

The biogas-powered generator in this research is converted from an original diesel generator with a capacity of 110 kW. It is converted to use entirely biogas fuel with about 60% of pre-modified system capacity.

The generator consists of an internal combustion engine (ICE) EP100T 4-cycle, 6-cylinder, vertical, turbo-type air intake system and a SAE J149 Gross generator with standby power of 110 kW. The ICE rotation speed varies from 0 to 3000 rpm; the optimum operating point according to the engine's application is 1500 rpm. At that optimum speed, the engine can provide prime power of 94 kW. The ICE and SAE J149 Gross generator is directly coupled to compose the generator set used in this work.

The overall control system is also depicted in Fig. 1, including the filtration system and fuel tank with purified biogas. The mixing tank is responsible to combine biogas and ambient air. The mixture is then fed into the biogas generator.

Several sensors equipped with the system are oxygen sensor (O_2), tank pressure sensor (P), water temperature sensor (T_1), oil pressure sensor (Oil), engine

speed sensor (SS). The actuators are two throttle valves (V_1 and V_2) and an ignition system (IS). The ignition system facilitates to start the engine. Meanwhile, V_1 throttle is responsible to maintain stable gas flow and ensure safe pressure level in the tank. V_2 throttle is the main actor which regulates the flow of fuel so that the generator speed 1500 rpm during the operation as long as total electrical loads in the farm changes within generator power capacity. The sensing measurements are collected and processed at a control cabinet which also makes decision on adjusting the actuators based on the feedback information.

3 Control System Development

Hardware. A control cabinet has been developed as shown in Fig. 2. It consists of (a) Raspberry Pi and switch, (b) power card controls two throttle valves (V_1 and V_2) actuators, (c) intermediate relays and a circuit breaker, (d) a PLC S7-1212 DC/DC/DC and an 8 analog inputs expansion module (e) ignition system control board and buck boost converter, (f) DC/DC converters to provide 12 V DC and 5 V DC from the 24 V DC, and voltage to current converter 0–10 V to 4–20 mA. The PLC S7-1212 module is the main controller of the system which gather all the sensing values, process and make the decision of the control output. The system also includes a single board computer, Raspberry Pi to acquire the information of its operation and transfer to a remote server for subsequent analysis.

Controller A PID controller is designed and integrated to adjust the running speed of the generator. The adopted PID controller structure is described as below [11]

$$y = [b.w - x) + \frac{1}{T_I \cdot s}(w - x) + \frac{T_D \cdot s}{a \cdot T_D \cdot s + 1}(x \cdot w - x) \tag{1}$$

It needs to change valve V_2 opening position as desired. In case the load demand increases, throttle valve V_2 opens wider to provide more fuel gas into the engine cylinder so that it can produce more power and vice versa. However, the frequency must be kept within the range of 49.5–50.5 Hz or the speed of the three phase synchronous motor should be maintained around the set point of 1500 rpm. Due to the characteristics of the biogas fuel, the mixing ratios of the gases required during the starting phase, no load and full load operation are different. Two set of PID tuning parameters are used in this work to serve different machine working conditions.

4 Experimental Results

Several biogas generation systems have been installed and operated to supply power in some hog farms in the north of Vietnam. Figure 3 shows an example of a real

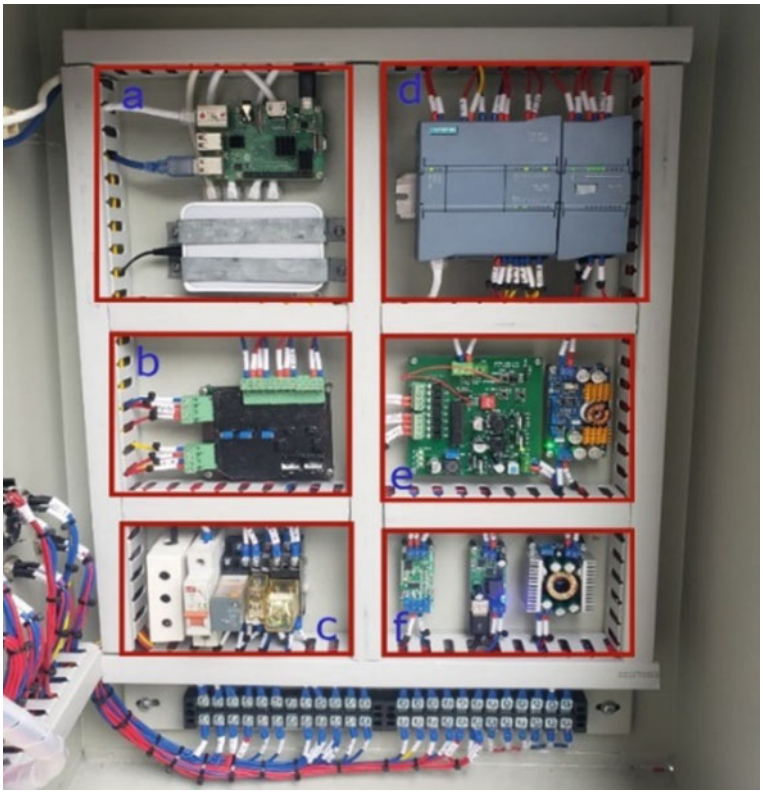

Fig. 2 Control cabinet of the biogas generation system

biogas generation system which we have developed. Two bio-generators with post-conversion capacity 70 kW in two different farms have been selected for experimental studies. The electrical loads in the farm are organized in to three groups, each group is supplied power via an individual branch from the main distribution board. Group one consists of the loads inside the livestock barns which are ventilation and cooling fan, heating system and indoor lighting. These loads are critical as they serve to maintain the comfort indoor environment of the livestock; they also consume the highest energy, around 35 kW totally. Group two is the pumping system and the wastewater treatment system of 15 kW. Group three include all the appliances and loads of the residential area consuming 10 kW. The investigation of system response is carried out for various scenarios of load changes.

Fig. 3 Biogas generation system deployment in a hog farm

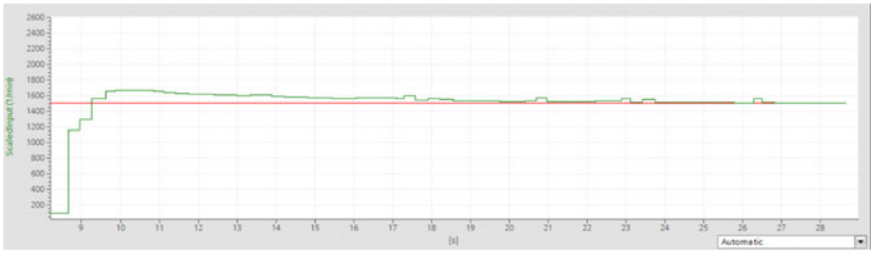

Fig. 4 Startup process of generator 1

4.1 Case Study 1

The starting processes of the biogas generators when no load is connected are shown in Figs. 4 and 5. The speeds of the generators are increased from zero to 1500 rpm less than 15 s. Generator 1 starts up slightly faster than the generator 2 due to the difference of their internal construction and the input fuel conditions.

4.2 Case Study 2

Once the generators are running stably at no load, the responses of the two systems when different loads are connected are investigate. Firstly, a total load of 35 kW load

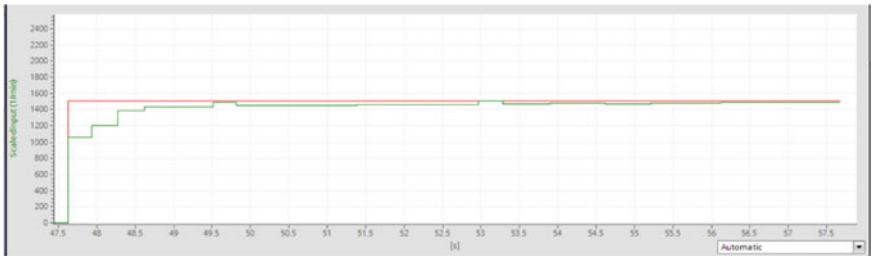

Fig. 5 Startup process of generator 2

is turned on. The response of the two systems is shown in Figs. 6 and 7. Generator speeds are reduced slightly but can quickly get back to the set point.

In the next scenario, the load changes from zero to a 50 kW load which is accomplished by first supplying electricity to the livestock barns and then the wastewater treatment and pumping system which consumes around 15 kW. It can be seen in Figs. 8 and 9 that both the systems are able to reach the stable speed set point within 4 s.

We then change the load from no load to the full load of 60 kW by turning on the livestock barn loads, the wastewater treatment system, and then the residential area. The similar results are shown in Figs. 10 and 11.

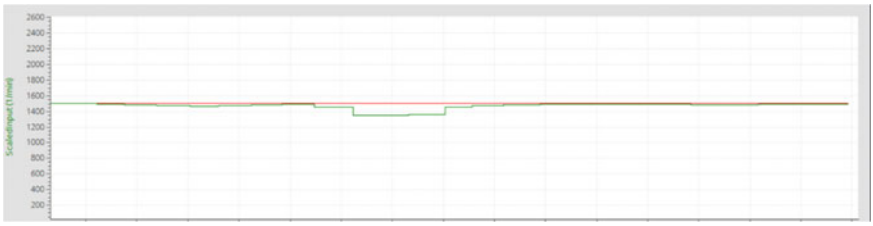

Fig. 6 Total load of 35 kW is connected to the generation system 1

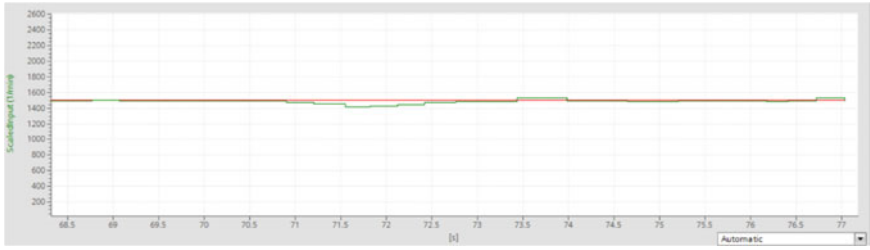

Fig. 7 Total load of 35 kW is connected to the generation system 2

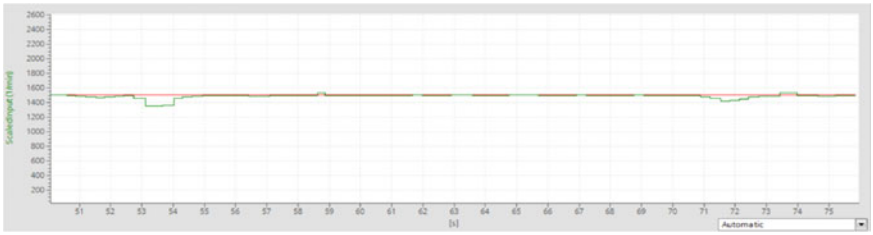

Fig. 8 Total load of 50 kW is connected to the generation system 1

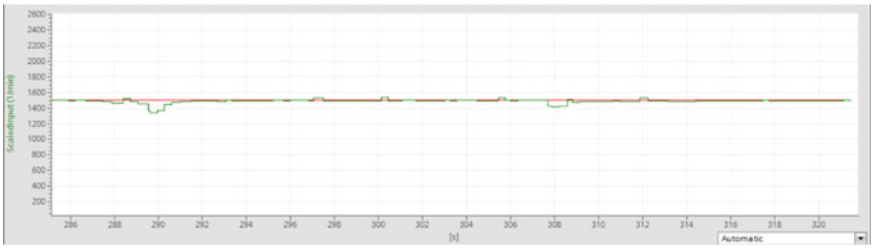

Fig. 9 Total load of 50 kW is connected to the generation system 2

Fig. 10 Full load of 60 kW is connected to the generation system 1

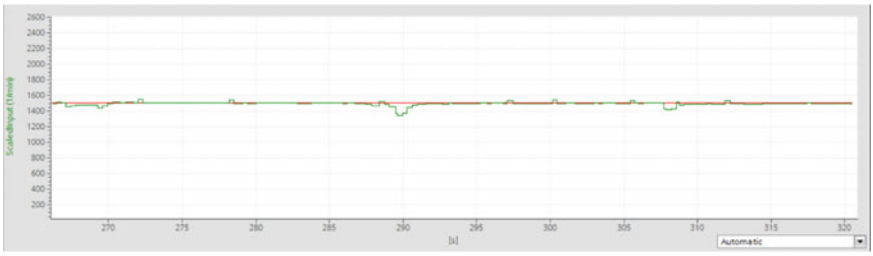

Fig. 11 Full load of 60 kW is connected to the generation system 2

Fig. 12 Generator 1: decrease from full load by no load

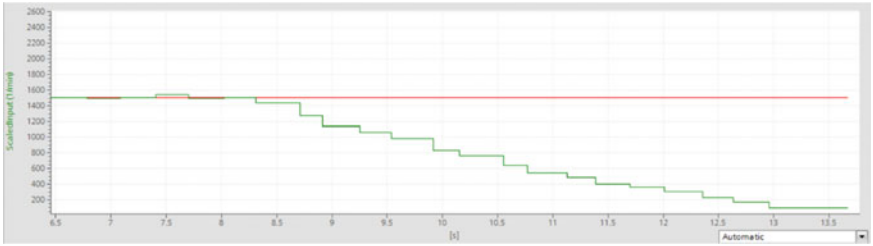

Fig. 13 Switch from no load to shutdown

4.3 Case Study 3

After operating at full load, we then disconnect the entire load from the generation system and shut it down. The responses of generator 1 when turning off the load and shutting down the system are shown in Figs. 12 and 13, respectively. It can be seen that after disconnecting the load, the generator speed overshoots shortly, but the controller can quickly adjust to make it be steady at 1500 rpm as desired.

Table 1 shows a summary of the system performance in different operation modes of starting up and varying the loads of the generation systems. In all the cases, the overshoots of the generator speeds are less than 12% or almost 0. Time response, T_{res}, is also within required duration T_{req} for appropriate power distribution in farm.

5 Conclusions

A proposed speed control controller specialized for biogas generators has been described. It is shown the system is able to maintain a stable operation and keep the generated electrical frequency within the required range for safely supply to any normal appliances in the farm. The cost of the control unit is around 40% of the governor sold together with the original generator and may be cheaper when being mass produced. The generation systems have been deployed in nine farms located

Table 1 Overshoot and time response of the system with changes in load

Operation modes		T_{req} (s)	T_{res} (s)	Overshoot (%)
Startup	Generator 1	≤ 30	15	12
	Generator 2	≤ 30	9	0
Switch from no load to 35 kW	Generator 1	≤ 20	5	0
	Generator 2	≤ 20	3	0
Switch from no load to 50 kW	Generator 1	≤ 45	23	0
	Generator 2	≤ 45	24	0
Switch from no load to full load of 60 kW	Generator 1	≤ 60	48	0
	Generator 2	≤ 60	50	0
Decrease from full load to no load	Generator 1	≤ 60	11.5	8

at different places mostly in the north of Vietnam and a few in the south so far. The generators in the north are being operated for 15–20 h daily depending on the available amount of fuel and load demand. In the south, we have installed two generators in the same farm for the trial of 24-7 service, and thus, it is not required to get the power from the grid. In the future work, the control systems will be enhanced further to include other inputs such as air quality conditions and the deterioration of actuators' accuracy under extreme working environment conditions. In fact, the biogas generation is a component of the farm management system. Thus, the secondary control at system level which cooperates other sub-systems will also be integrated to optimize overall energy consumption while ensuring reliable operation of the farm.

Acknowledgements This research is funded by the Hanoi University of Science and Technology (HUST) under project number T2018—PC—051.

References

1. Pedro, D., Lucas, C. d., Jarbasa, S., & William, B. (2019). Novel composed speed controller applied to biogas generator set. In *2019 IEEE PES Innovative Smart Grid Technologies Conference—Latin America* (ISGT Latin America), Gramado, Brazil.
2. Ryckebosch, E., Drouillon, M., & Vervaeren, H. (2011). Techniques for transformation of biogas to biomethane. *Biomass and Bioenergy, 35*(5), 1633–1645.
3. Sheng, S., & Wang, F. (2020). Energy-saving and economic analysis of anaerobic reactor heating system based on biogas and sewage source heat pump. In Z. Wang, Y. Zhu, F. Wang, P. Wang, C. Shen, & J. Liu, (Eds.), *Proceedings of the 11th International Symposium on Heating, Ventilation and Air Conditioning (ISHVAC 2019). ISHVAC 2019. Environmental Science and Engineering*. Springer, Singapore.
4. Wang, L., & Lin, P.-Y. (2009). Analysis of a commercial biogas generation system using a gas engine–Induction generator set. *IEEE Transactions on Energy Conversion, 24* (1).
5. Dalpaza, R., Konrada, O., Cândido da Silva Cyrneb, C., Panis Barzottoc, H., Hasana, C., & Guerini Filhod, M. (2020). Using biogas for energy cogeneration: An analysis of electric and

thermal energy generation from agro-industrial waste. *Sustainable Energy Technologies and Assessments, 40*.
6. Hassan, S., & Ya, H. (2019). Experimental study on electrical power generation from a 1-kW engine using simulated biogas fuel. In S. Sulaiman, (Eds.), *Rotating machineries*. Springer Briefs in Applied Sciences and Technology.
7. Yadav, D. K., & Bhatti, T. S. (2016). Voltage and frequency control in a wind-PV-Biogas based rural micro grid with limited grid operation. In *2016 IEEE 7th Power India International Conference (PIICON)*, Bikaner, India.
8. Bhamu, S., Pathak, N., & Bhatli, T. S. (2018). Power control of wind-biogas-PV based hybrid system. In *2018 International Conference on Computing, Power and Communication Technologies (GUCON)*, Greater Noida, Uttar Pradesh, India.
9. Abaye, A. E., & Haro, R. D. (2018). Assessment of resource potential and feasibility study of standalone PV-wind-biogas hybrid system for rural electrification. In *2018 2nd International Conference on Electronics, Materials Engineering & Nano-Technology (IEMENTech)*, Kolkata, India.
10. Jiang, Y.-H., Xiong, S.-S., Shi, W., He, W.-H., Zhang, T., Lin, X.-K., Gu, Y., Lv, Y.-D., Qian, X.-J., Ye, Z.-Y., Wang, C.-M., & Wang, B. (2009). Research of biogas as fuel for internal combustion engine. In *2009 Asia-Pacific Power and Energy Engineering Conference*, Wuhan, China.
11. Siemens, https://cache.industry.siemens.com/dl/files/465/36932465/att_106119/v1/s71200_system_manual_en-US_en-US.pdf. Last accessed November 2020, 25.

Parallel, Distributed Model Checking of Composite Web Services with Integrated Choreography and Orchestration

D. Sungeetha and B. S. Sathish Kumar

Abstract Business Process Execution Language (BPEL) specification is transformed into communicating finite state machines (CFSMs) specification for interacting, synchronizable web services. Computational distributed tree logic (CDTL) logic over a set of Kripke structures, called communicating minimal-prefix machines (CMPMs) which together constitute sum machine was proposed in previous work. Sum machine has a much better scalability of variety of peers as opposed to the more traditional product machine. This paper discusses about using sum machine and CDTL logic to model-check a web-service specification by integrating both choreography and orchestration in a modular fashion with bottom-up approach. We do a couple of case studies of Virtual Travel Agency (VTA) protocol and Fresh Market Update (FMU) service and illustrate the model-checking procedure on these protocols to verify the synchronizability and reachability properties of the protocol in an efficient manner, with parallel, distributed algorithm incurring polynomial time complexity.

Keywords BPEL · Synchronizability · Scalability · CFSMs · Sum machine · Minimal-prefix state vectors · CDTL · State-space-explosion · Product machine · Choreography · Orchestration

1 Introduction

These days, web services are commonly applied in several fields, like business to business and incorporation of enterprise usage [1]. In BPEL, [2] used to agree the roadmap of web-service composition.

D. Sungeetha (✉)
Department of Electronics and Communication Engineering, Saveetha School Engineering, SIMATS, Chennai, Tamil Nadu, India

B. S. Sathish Kumar
A.V.C. College of Engineering, Mayiladuthurai, India

T. D. L. Nguyen and J. Lu (eds.), *Machine Learning and Mechanics Based Soft Computing Applications*, Studies in Computational Intelligence 1068,
https://doi.org/10.1007/978-981-19-6450-3_8

Model checking (MC) projected the authentication and validate of software systems [3, 4]. Model checking [5] is an authentication of profoundly and automatically execute starts at early stage and exhibit in each way. We propose the two techniques for MC for distributed protocols.

Past research focus on use of MC logic is important in computer science [6, 7]. For major reviews of model checking, kindly refer to [3, 4]. An extensive limitation of MC for authentication of distributed systems is often unattainable [8]. An intensive search is used in MC to verify temporal-logic specification of the concurrent system. This spectacle is called as "*state-space-explosion problem*", is our present work.

1.1 Web-Service Choreography, Orchestration, State-Space Explosion and Scalability of Peers

In web-service specification taxonomy, *choreography* refers to abstract processes and *orchestration* refers to executable processes [9, 10]. Choreography covers the interaction of messages among different services while orchestration includes internal process actions, in this work. Choreography concerns *messages* across services in *concurrency*, while orchestration concerns *activities* in *sequence* and *choice/conflict* within a service. Choreography specifies the *inter-behaviour* transitions and orchestration, the *intra-behaviour* transitions. There are also contexts [11] in which orchestration is used as an alternative to choreography, the latter with decentralized control and the former with centralized control. Both choreography and orchestration have to be consolidated into the web-service CFSM specification before composing the component CFSMS of multiple peers into a global composite product machine.

But unfortunately, the traditional composition of the *synchronous product* of the component CFSMs blow-up *exponentially* for the number of input CFSMs as the interaction of message sequences in the choreography and huge value of peers increase. The problem is even more compounded when the choreographed message sequences are interleaved with the orchestrated local/asynchronous actions/operations of the specification. Therefore, instead of composing the component CFSMs into one single synchronous product, we build its quotient transition system called the sum machine which incorporates global environment as well as maintains the local identity of the peers thus contributing to their *scalability*.

We illustrate the above in our case study of Virtual Travel Agency in the sequel.

1.2 Top–Down and Bottom–Up Approaches and Synchronizable Conversations

There are two ways of composite web service as follows [12]:

(1) In the *bottom-up approach,* each peer in the web service is specified uniquely and composed system is combined behaviours of individual peer specifications. In our work, we follow this approach. We calculate the synchronization of the composite web service [12]. If it is synchronically we use synchronous communication semantic to authenticate the *temporal-logic* properties of its conversations. Even in the presence of unbounded message queues, the results we achieve in this case hold for all conversation created by the composite web service.

(2) In the *top-down approach,* the chosen behaviour is defined first, followed by the comprehensive peer implementations. Conversation protocols are a formalism for specifying composite from the up down. A discussion protocol is a single, global finite state machine that defines group of conversations. It is difficult to control the *state-space explosion* in the top-down approach. Also in the top-down approach, only choreography can be represented and not the autonomous local orchestration.

1.3 Related Work

Many researches based on model-checking web services are being conducted. The work by Ankolekar et al. [13] verifies the contact protocol of web providers outlined in OWL-S using automated methods. Fu et al. [14] suggests a top-down approach consists of desired conversations and provides a tool. The EFA, according Shin [15] should check the service flows in [2]. In paper, [16] shapes a structure that makes instinctive proof of business processes. Jun et al. [17] uses pi-calculus to define and model web service and their structure and then tests the model's validity.

For the benefits of this, we advise to quotation behavioural specifications and agent interaction protocols [18, 19] and it may translating method to transform the model into asynchronous communication with model checker SPIN.

The work reported [1] makes the use of agent interaction protocols to establish the BPEL work flow. Our work begins from the BPEL specification of [1] which consists of multiple agents each of which is modelled as a communicating limited state machine with synchronous communication/rendezvous interactions. We make sure the synchronizability condition [20] is satisfied after transforming the BPEL input specifications into CFSMs and then from CFSMs to corresponding CMPMs constituting the sum machine.

In remaining portion of paper, the preliminary of the computational model of sum machine is summarized in Sect. 2, giving its syntax and semantics. It then introduces sum machine comprising the set of n CMPM trees generated from n CFSM graphs

(corresponding to *n* peers of the web service) and its relationship with the traditional product machine structure. In comparison with our previous work [21, 22], Sect. 3 introduces the logic, its updated formats over sum machine. Section 4 does the case study of VTA protocol using which the CDTL specification of properties and their verification are illustrated, and Sect. 5 conclusion and future directions are discussed.

2 The Computational Model of Sum Machine

2.1 What is the Idea Behind Sum Machine as Opposed to Traditional Product Machine?

A given specification consisting of a set of *n communicating finite state machines* (CFSMs), represented as a set of *n* CFSM *graphs*, is transformed into a corresponding set of *n unfolded trees* whose leaves correspond to what are defined as *cut-off* states. Each CMPM state represents not only its corresponding local CFSM state, but also a vector of non-local CFSM states that are its causal predecessors due to synchronization in the most recent past.

2.2 The BPEL-Transformed CFSMs Specification

The CFSM specification is based on Hoare's CSP model [23].

2.3 The Simulation of CFSMs into a Novel Sum Machine as Opposed to Traditional Product Machine

The given set of CFSMs represented as *cyclic, rooted, directed graphs* is *simulated in their respective global environments* into a corresponding set of CMPMs, each represented by a *directed, rooted tree* structure.

We assume a given specification of *n* CFSMs that are in general non-terminating. We convert a set of n CFSM graphs into a set of n CMPM trees given a set of n CFSM graph [21]. In the following context, the unfolding mechanism is recursive: A corresponding CFSM state s_{fi} exists for each unfolded CMPM state s_i.

2.4 Minimal-Prefix Vectors of CMPM States

Definition 2.4 *: The minimal-prefix* vector Mp(s_i) of a CMPM state s_i is the vector of size n that should n*ecessarily/minimally* be reached according to *causality order* $\leq$ in order to guarantee the entry of state s_i in question. The ith component of the *Mp*-vector of a state s_i is itself. That is, $\mathrm{Mp}_i(s_i) = s_i, \quad \forall i \in \{1, \ldots, n\}$.

In order to fulfil the possible requirements, the unfolding of one CFSM necessitates the unfolding of the other non-local CFSMs.

f vec : $X_{i=1\ldots n} S_i \rightarrow X_{i=1\ldots n} S_{fi}$ where f vec is the function that maps the CMPM-state vectors into corresponding CFSM-state vectors with the instance numbers dropped/omitted. The fvec function is used to map the Mp-vectors into corresponding CFSM-state vectors, to identify the *cut-off states* of the CMPMs as will be related in the sequel.

2.5 Sequence, Conflict/Choice and Concurrency Among States of Sum Machine

Definition 2.5 : sequence (seq), conflict (conf) *and* concurrency (co) viz. are the three fundamental binary relations *defined using* R_i, $i \in \{1\ldots n\}$ *and* $\leq$ *relations.*

To summarize, CMPMs *statically* produce only a minimal state vectors, which can be *enthusiastically* made by navigating non-local CMPM trees asynchronously. Any two CMPM states, non-local in general, can be reachable from one another iff: all the n components of their respective Mp-vectors are reachable from each other. This notion will be elaborated in the model-checking procedure in the sequel.

2.6 Sum Machine Simulates Product Machine

In this paper [22–24], by virtue of the construction of conventional product machine and the sum machine compositions, the set of all reachable configurations S of sum machine correspond to product machine states S_f. Based on configurations and transitions among them, a single transition system corresponding to a product machine simulated by the sum machine can be defined as follows:

$C = (S, R, P, s_0)$ where S is the set of all configurations, R is the transition relative where $R = \cup_{i=\{1\ldots n\}} R_i$, P is the conventional of all intentions of configurations $P = \cup_{i=\{1\ldots n\}} P_i$ and s_0 is the initial configuration, replicated in all CMPMs as the initial Mp-vectors.

The conventional transition system of the product machine of given CFSMs is given by $C_f = (S_f, R_f, P_f, s_{0f})$ such that $s_0 \rightarrow s_{0f}$, $R \rightarrow R_f$, $P \rightarrow P_f$ and $S \rightarrow S_f$ are subjective mappings, where each reachable configuration s of sum machine is a CMPM-state vector while the vectors s_f of product machine is the set of reachable

CFSM-vectors, whose components correspond to CMPM-vector components with instance numbers dropped. Henceforth in the sequel, by product machine, we refer to $C = (S, R, P, s_0)$.

3 The Specification Language CDTL over Sum Machine for Specifying Web-Service Properties

CDTL formulas over sum machine can be specified [21, 22, 24, 25] to pose the properties of the global paths of configurations of sum machine as well as the local properties of local paths of CMPM states. In addition, the global properties can be expressed as conjunction and/or disjunction of local properties which is implemented to model-check the properties efficiently and in a modular fashion and deduce the global properties in terms of local properties.

We use s to denote a configuration, p to denote a global path of configurations traced from local paths of CMPM states and Π to denote a set of n concurrent local paths, Π_i, $i = \{1..n\}$. $\models_i$ denotes local satisfiability and $\models$ the global satisfiability.

Global CDTL formulas over sum machine

- $C, s \models \cup_{i=\{1..n\}} (P_i(s_i))$ such that s_i is the ith component of s.
- $C, s \models \vdash(q)$ iff: $\vdash(C, s \models q)$
- $C, s \models (q \wedge r)$ iff: $(C, s \models q) \wedge (C, s \models r)$
- $C, s \models q \mathbf{U} r$ iff: there exists a path p emanating from s such that

  $C, p \models q \mathbf{U} r$.

- $C, s \models \mathbf{A}q$ iff: $\forall$ paths p emanating from s it is true that
- $C, p \models q$ where q is a p formula.
- $C, s \models \mathbf{A}q$ iff: $\forall$ concurrent path sets Π from s,

  $C, \Pi \models q$ where q is a cp formula.

- $C, p \models q$ iff: $C, s \models q$ where s is the initial configuration of the path p.
- $C, p \models Xq$ iff: $C, s' \models q$ where $p = (s\ R\ s'\ R \ldots)$
- $C, p \models F$q iff: $\mathrm{C}, s' \models q$ where $p = (s\ R^+\ s' \ldots)$
- $C, p \models q\ \mathrm{U}\ r$ iff: for $p = (s^1\ R\ s^2\ R\ C^3 \ldots R\ s^k \ldots)$ it is the case that

  $C, s^k \models r$ and $\forall m \leq k, M, s^m \models q$

- $C, p \models q$ iff: $C, s \models q$ where s is the initial configuration of the concurrent path-set Π.
- $C, \Pi \models q$ iff: $C, p \models q$ where p is one of the global paths from concurrent path-set Π.
- $C, \Pi \models Xq$ iff: $C, p \models Xq$ where p is one of the global paths of concurrent path-set Π.
- $C, \Pi \models Fq$ iff: $C, p \models Fq$ where p is one of the paths of concurrent path-set Π.

- $C, \Pi \models q \mathbf{U} r$ iff: $C, p \models q \mathbf{U} r$, where p is one of the traces of concurrent path-set Π.

Local CDTL formulas over CMPMs

- $C_i, s_i \models_i P_i(s_i)$, s_i is the ith component of s, $i = \{1...n\}$.
- $C_i\ s_i \models_i \neg(q_i)$ iff: $\neg(C_i, s_i \models q_i)$
- $D_i, s_i \models_i (q_i \bigwedge r_i)$ iff: $(D_i, s_i \models q_i) \bigwedge (D_i, s_i \models r_i)$
- $C_i, {s_i}^1 \models_i q_i\ \mathbf{U_i}\ r_i$ iff: there exists a $\Pi_{i=}$ $({s_i}^1\ R_i\ {s_i}^2\ R_i\ {s_i}^3 \ldots R_i\ {s_i}^k \ldots)$ emanating from ${s_i}^1$ such that $M_i, {s_i}^k \models_i r_i$ and $\forall m \leq k$, $C_i, {s_i}^m \models_i q_i$.
- $C_i, s_i \models_i \mathbf{A_i} q_i$ iff: $\forall$ i-local paths Π_i emanating from s_i it is true that $C_i, \Pi_i \models_i q_i$ where q_i is a p formula$_i$.
- $C_i, \Pi_i \models_i q_i$ iff: $C_i, s_i \models_i q_i$
- $C_i, \Pi_i \models_i \mathbf{X_i} q_i$ iff: $C_i, s_i' \models_i q_i$ where $\Pi_i = (s_i\ R_i\ s_i'\ R_i \ldots)$
- $C_{i,\,\Pi i} \models_i \mathbf{F_i} q_i$ iff: $C_i, s_i' \models_i q_i$ where $\Pi_i = (s_i\ {R_i}^+\ s_i' \ldots)$

Deduction of global formulas from local formulas

Following equivalences between global and local formulae follow from the definition of *configurations* and *concurrent local path sets.*

- $C, s \models q \leftrightarrow \bigwedge_{i=\{1..n\}} (C_i, s_i \models_i q_i)$, where $(s_i \text{ co } s_j)$, $i1 \neq j1$, $i1, j1 = \{1...n1\}$.
- $C, \Pi \models \mathbf{X}(\vee_{i=\{1\ldots n\}}\ q_i) \leftrightarrow \bigwedge_{i=\{1\ldots n\}} (C_i, \Pi_i \models_i \mathbf{X_i} q_i)$ where s_{0i} is the initial state of path Π_i, $(s_{0i}\ R_i\ s_i)$, $s_i \models_i q_i\ \forall i\ = \{1...n\}$ and $(s_1 \text{ co } s_2 \text{ co} \ldots\ s_n)$.
- $C, \Pi \models \mathbf{F}(\bigwedge_{i=\{1...n\}}\ q_i) \leftrightarrow \bigwedge_{i=\{1...n\}}\ (C_i, \Pi_i \models_i \mathbf{F_i} q_i)$, where s_{0i} is the initial state of path Π_i, $(s_{0i}\ {R_i}^+\ s_i)$, $s_i \models_i q_i\ \forall i = \{1 \ldots n\}$ and $(s_1 \text{ co } s_2 \text{ co} \ldots\ s_n)$.
- $C, \Pi \models \mathbf{AX}(\bigwedge_{i=\{1...n\}}\ q_i) \leftrightarrow \bigwedge_{i=\{1...n\}}\ (C_i, \Pi_i \models_i \mathbf{A}_i \mathbf{X_i} q_i)$, where s_{0i} is the initial state of path Π_i, $(s_{0i}\ R_i\ s_i)$, $s_i \models_i q_i\ \forall i = \{1...n\}$ and $(s_1 \text{ co } s_2 \text{ co} \ldots\ s_n)$.
- $C, \Pi \models \mathbf{AF}(\bigwedge_{i=\{1...n\}}\ q_i) \leftrightarrow \bigwedge_{i=\{1...n\}}\ (C_i, \Pi_i \models_i \mathbf{A}_i \mathbf{F_i} q_i)$, where s_{0i} is the initial state of path Π_i, $(s_{0i}\ {R_i}^+\ s_i)$, $s_i \models_i q_i\ \forall i = \{1...n\}$ and $(s_1 \text{ co } s_2 \text{ co} \ldots\ s_n)$.

From the above equivalences, ($\leftrightarrow$ is the equivalence operator) it follows that in order to check the property of a global formula, to deduce the global property a simple search of the consistent value CMPM based on the belongings being verified and check the concurrency of local states.

4 Model-Checking Case Study of Fresh Market Update (FMU) Service and Virtual Travel Agent (VTA) Protocol Using Sum Machine and CDTL Logic

Here, we verify the properties of FMU protocol of *stock broker*, *research department* and *investor* web services and VTA protocol of *user, VTA, flight booking service and hotel booking service.* These *peer-services* are transformed/mapped from their respective BPEL (version 2.0) flowchart specifications into CFSM specifications using which we construct the joint behaviour of sum machine in *bottom-up* approach and perform synchronizability and reachability analysis of the VTA protocol. The

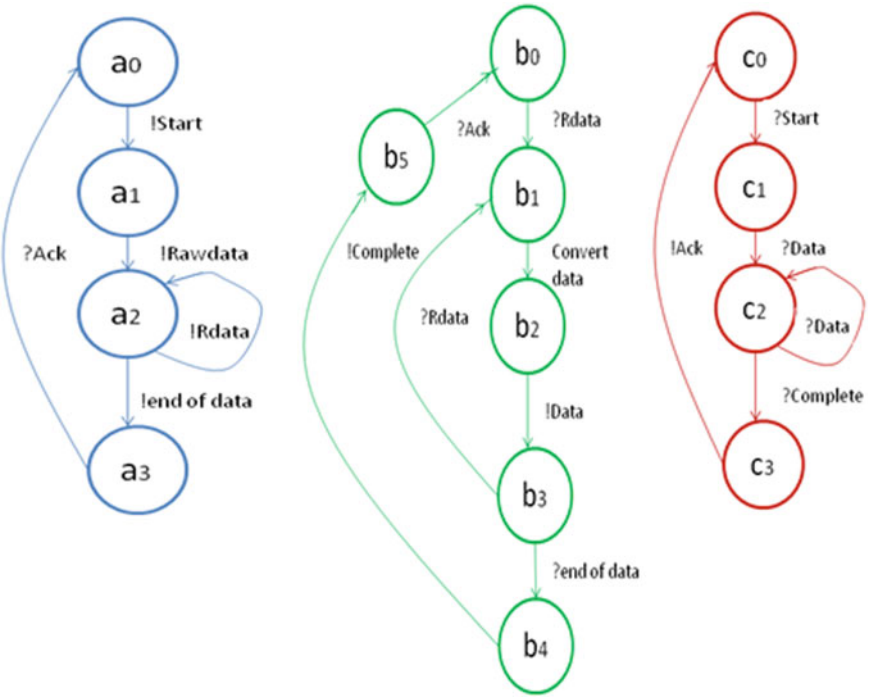

Fig. 1 CFSM of stock broker, research development, investor

local identities of individual services are maintained in the composite service with only a polynomial blow-up of the state space depending on their *degree of coupling,* thus making the composition *scalable* and *modular.*

Figure 1 shows the CFSM graphs of the *stock broker*, *research department* and *investor*. The corresponding CMPM trees constituting the sum machine composition is shown in Fig. 2.

Since the sum machine is modular global properties can be deduced from local properties. Synchronizability is verified hand-in hand with the construction of the sum machine. Since the research-department service coordinates with both stock-broker and investor services, many interesting properties can be deuced from the CMPM of research department. In addition, the autonomous event "*convert to data*" from raw data can be *orchestrated* by introducing the invocation and response of the sub-services within the research-department service. The orchestration can be followed by model checking the research department independently but taking into account, the global environment using the concept of Mp-vectors.

Figure 3 shows the CFSM graphs of the VTA protocol consisting of the agent *VTA, flight agent service, hotel agent service* and *user*. Since VTA interacts with all other services and user, it is enough to check the correctness of synchronizability and reachability of CMPM states of the VTA service. The events "*process request*" of

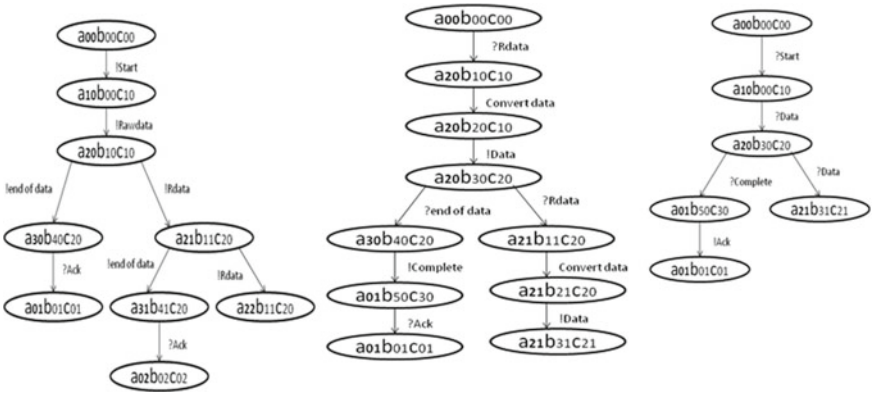

Fig. 2 CMPM of stock broker, research development, investor

flight agent and that of hotel booking agent can be *orchestrated* to introduce the sub-services of the respective agents. That is the advantage of the modular sum machine as opposed to the single synchronous product machine. Figure 4 shows the CMPM of the VTA service, which is sufficient to check the correctness of the properties to be satisfied by the composite service, since VTA interacts with all other services.

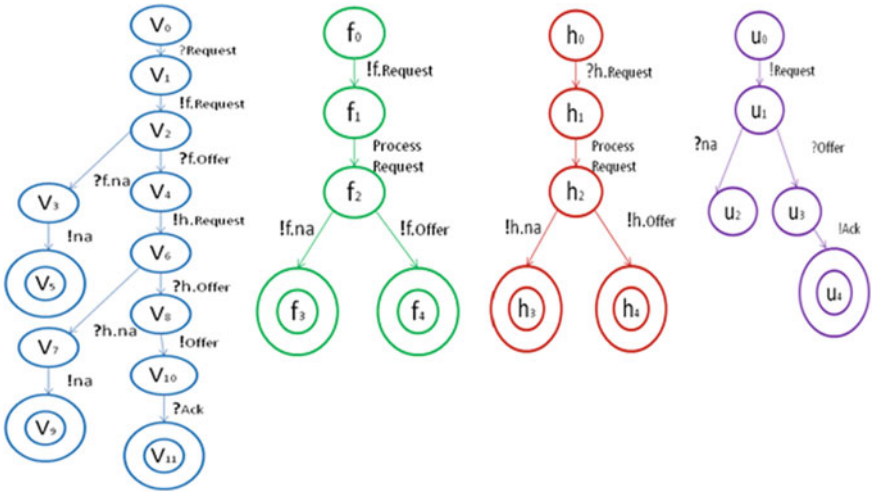

Fig. 3 CFSM of VTA, flight agent, hotel agent, user

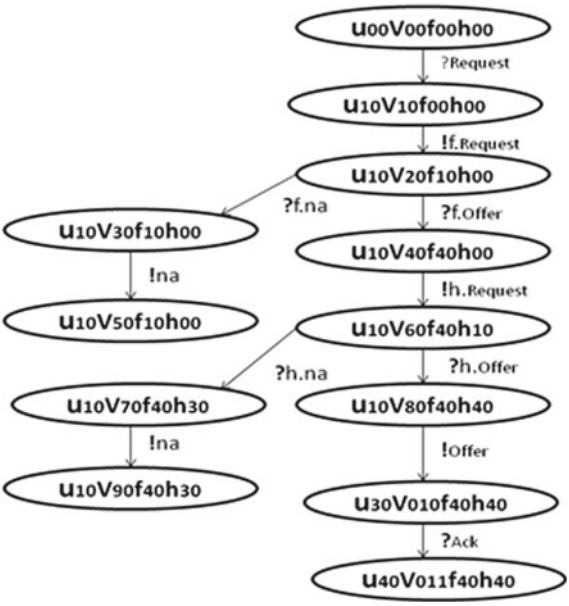

Fig. 4 CMPM of VTA

4.1 Orchestration Along with Choreography in Model Checking

Since the sum machine composite is modular, in FMU service, the research-department CMPM can be expanded to orchestrate the raw data to data conversion. Similarly in VTA service, the CMPMs corresponding to flight agent and hotel agent can be individually expanded (in global environment) to orchestrate the event "*process request*" by replacing it with invocation and response of *sub-services* required to process the *flight request* and similarly for the *hotel booking request*. If it were a one single composite product machine, it would be difficult to verify the orchestration of the above services autonomously and with less complexity.

4.2 Discussion of Model-Checking Complexity

As reported in [22, 26], the model-checking complexity of the sum machine is polynomial peer CFSMs specification while the under complexity of product machine is exponential in group of peer CFSMs. Specifically, the worst-case time complexity in sum machine is $(d * N_f + \log n)$ in the sum of CFSMs n with N_f, maximum quantity of states per CFSM and d, a constant depending on degree of coupling, $|R\text{sync}_{fi}|$ given in the specification, with $O(n^2)$ number of processors. This result is as opposed to the traditional *PSPACE–complete* complexity of CTL over *product machine.*

5 Conclusions

Given choreography of global message sequence and orchestration of local activities in WS-CDL/BPEL specification, we extract *n* CFSM specifications. The relations *sequence, choice* come from local orchestration and communication (using synchronous message passing) come from global choreography, resulting in *concurrency*. Having extracted the set of *n* CFSMs specification of Web services, instead of composing them into a traditional product machine, we construct the sum machine which can simulate product machine and is also distributed and multi-threaded. The *synchronizability* is verified during the construction of sum machine whose components are the *n* CMPMs. In the case of CMPMS/sum composition, the correctness properties of protocols can be verified using polynomial time.

References

1. Dong, R., Wei, Z., & sLuo, X. (2008). Model checking behavioral specification of BPEL web services. In *Proceedings of the World Congress on Engineering 2008* (Vol. 1, pp. 2–4). London: U.K.
2. Arkin, A., Askary, S., Bloch, B., Curbera, F., Goland, Y., Kartha, N., Liu, C. K., Thatte, S., Yendluri, P., & Yiu, A. *Web Services [BPEL].* http://www.oasis-open.org/committees/tc_home.php?wg_abbrev=
3. Clarke, E., Grumberg, O., & Peled, D. (1999) Model checking, The MIT Press
4. Holzmann, G. J. (1997). The Model checker SPIN. *IEEE Transaction on Software Engineering, 23*, 76–95.
5. Park, J., et al. (2013). A theorem prover for boolean BI. In *ACM International conference on Principles of Programming Language* (pp. 219–232)
6. Clark, E. M., & Emerson, E. A. (1982). 'Design and Synthesis of Synchronization skeletons for branching time temporal logic': Workshop. *LNCS, 131*, 52–71.
7. Clarke, E., Emerson E. A., & Sistla, A. P. (1983) Automatic verification of finite-state concurrent system using temporal logic. In *Proceedings of the 10th Annual ACM Symposium on Principles of Programming Languages (POPL)* (pp.164–176)
8. Clarke, E., & Schlingloff, H. (2001) Model checking (Chap. 21). In J. Robinson & Voronkov (Eds.), *Handbook of automated reasoning* (pp 1369–1468) Elsevier.
9. Clarke, E., et al. (2001) Progress on the state-explosion problem in model-checking. *Informatics*, 176–194
10. Daniel, F., & Pernici, B. (2006). Insights into web service orchestration and choreography. *International Journal of E-Business Research*, *2*(1), 58–77, Idea Group Publishing.
11. Karande, A., et al. (2011). Orchestration and choreography using business process execution language for SOA with web-services. IJCSI International Journal of Computer Science *Issues*, 8(2).
12. Bultan, T., et al. (2006). Analyzing converstions of web services. *IEEE Internet Computing, 10*(1), 18–25.
13. Ankolekar, A., Paolucci, M., & Sycara, K. (2004). Spinning the OWL-S process model-toward the verification of the OWL-S process models. In *Proceedings of the ISWC 2004 Workshop on Semantic Web Services: Preparing to Meet the World of Business Applications.* Hiroshima, Japan.
14. Fu, X., Bultan, T., & Su, J. (2004). *Model checking interactions of composite web services.* (UCSB Computer Science Department Technical Report (2004–05))

15. Nakajima, S. (2006). Model-checking behavioral specification of BPEL applications. *Electronic Notes in Theoretical Computer Science, 151*, 89–105.
16. Mongiello, M., & Castelluccia, D. (2006). Modelling and verification of BPEL business processes. In *4th Workshop on Model-Based Development of Computer-Based Systems and Third International Workshop on Model-Based Methodologies for Pervasive and Embedded Software (MBD/MOMPES'06)*. IEEE
17. Jun, L., Hao, T., & Jin-De, L. (2005). Describing and verifying web service using pi-calculus. *Chinese Journal of Computers, 4*, 635–643.
18. Jun, W., Shing-Chi, C., & Xu, W. (2001). Towards a methodology for forma l design and analysis of agent interaction protocols. *Wuhan University Journal of Natural Sciences, 6*(122), 126–139.
19. Wu, Z., Verma, K., Gomadam, K., Sheth, A. P., & Miller, J (2006). *Process Mediation and Interaction Protocol for Web services [document/word]*. http://lsdis.cs.uga.edu/~wroposal.doc
20. Fu, X., Bultan, T., & Su, J. (2005). Synchronizability of Conversations among Web-services. *IEEE Transactions on Software Engineering*, *31*(12), 1042–1055.
21. Narayanan, V. K., et al. (2015). A branching-time logic to verify synchronously coupled concurrent systems and their relevance to web-based systems. *International Journal of Web engineering and technology, 10*(4), 311–333.
22. McMillan, K. (1992). *Symbolic model checking: An approach to the state explosion problem* (Ph.D. Thesis). CMU-CS-92-131.
23. Dakshinamurthy, S., & Narayanan, V. (2013). A model-checking algorithm for formal-verification of Peer-to-peer fault-tolerant networks (LNIT ISSN 2301-3788) *Lecture Notes on Information theory*, *1*(3), 128–131.
24. Dakshinamurthy, S., & Narayanan, V. (2014). Fault-tolerance verification in a distributed collective collaborative robotic system. *International Journal of Scientific and engineering research, 5*(3), 541–546.
25. Dakshinamurthy, S., & Narayanan, V. (2013). A component-based approach to verification of formal software models to check safety properties of distributed systems (LNSE ISSN 2301-3559), *1*(2), 186–189
26. Narayanan, V. K. (1997). *A state-oriented, partial-order model and logic for distributed systems verification* (Ph.D. Thesis). Concordia University, Montreal.

An Application of Logistic Regression Model in the Student's Academic Performance at HUST, Vietnam

Ta Anh Son and Nguyen Tuan Dat

Abstract In this paper, we use logistic regression model to study the factors affecting students' results in the subject named 'Analysis III (MI1130)'. The data is collected from the results of the questionnaires and the actual students' academic performance given by the School of Applied Mathematics and Informatics (SAMI) of HUST. Data analysis provides a precise estimate of 5 factors that make an impact on students' learning results in the subject, including the living environment, the CPA result, self-study time, difficulty in solving some Analysis III problems, and awareness of the application of the subject in reality. Then, some suggestions can be made to improve the quality of training and learning outcomes of students.

Keywords Logistic regression · The student's academic performance

1 Introduction

Analysis III (MI1130) is a compulsory subject in the student training program of HUST. This module is the necessary foundation for advanced math modules and other disciplines in science and engineering. Over the years, it has been reported that student scores have been uneven across all faculties [1, 2]. This inequality occurs not only in HUST but also in other colleges and universities in Vietnam. There are also other subjects in which students perform poorly, and thus finding the factors that influence students' performance has become the subject of research. Therefore, this paper focuses on identifying such factors among HUST's students as the basis for strategic intervention in course delivery.

T. A. Son (✉) · N. T. Dat
School of Applied Mathematics and Informatics, Ha Noi University of Science and Technology, Hanoi, Vietnam
e-mail: taanhson123@gmail.com

T. D. L. Nguyen and J. Lu (eds.), *Machine Learning and Mechanics Based Soft Computing Applications*, Studies in Computational Intelligence 1068,
https://doi.org/10.1007/978-981-19-6450-3_9

2 Logistic Regression Model

We use logistic regression for the binary variable Y:

- With scores 0.0, 1.0, 1.5, assigned the value 1: Student has the possibility to fail Analysis III (MI1130).
- With scores 2.0, 2.5, 3.0, 3.5, 4.0, assigned the value 0: Student does not have the possibility to fail Analysis III (MI1130).

Predictor variables are factors under investigation, which may have an effect on the reaction variable. The logistic model equations according to Sule, Adjumo [3, 4] have the form

$$\text{Log}\left[\frac{p(x)}{1-p(x)}\right] = \alpha + \beta_1 X_1 + \beta_2 X_2 + \cdots + \beta_k X_k. \tag{1}$$

where X_i, $i = 1, 2, ..., k$ are influential factors being investigated and

$$P(x) = P(Y = 1|X = x) = \frac{1}{1 + \mathrm{e}^{\sum_{i=1}^{k} X_i Y_i}}. \tag{2}$$

where the vector, $X = (x_1, x_2, ..., x_k)$.
Hence, the odds ratio presented by Sule and Saporu [3] is

$$\prod(x) = \frac{p(x)}{1-p(x)}. \tag{3}$$

3 Research Scope

The tool used is to develop a list of survey questionnaires for students from HUST. The questionnaire includes 20 questions that make up the predictor variable to be investigated. The questionnaire was checked for the validity of the content and tested–re-tested in reliability before being issued to students. The survey target is about 200 students from School of Applied Mathematics and Informatics and Institute of Information Technology. In fact, we obtained a survey of 153 random students at HUST. The response rate is 100% of the questions in the survey. The detailed list of questions is presented in the appendix.

4 The Data

Questionnaires are managed for students using appropriate codes. Student's score in the surveyed course is a binary-dependent variable, encoded as mentioned earlier. The questionnaire which consists of 20 independent variables was investigated.

Standardize data:

- Code answers from 1 to 4.
- Normalize the answer data set to the segment [0;1] by the formula

$$\overline{x} = \frac{x - \min(x)}{\max(x) - \min(x)}. \tag{4}$$

where $\overline{x}$ is the newly encoded value.

Example: Question 1 has four answers: 1, 2, 3, 4.
The new value is 0, 0.33, 0.67, 1.
Result variable

- where $y = \{0; 1; 1.5\}$ is assigned the value 1 (possibility to fail);
- where $y = \{2.0; 2.5; 3.0; 3.5; 4.0\}$ is set to 0 (impossibility to fail).

5 Data Analysis Methods

We use the statistics package for the social sciences (SPSS) for data analysis. Binary logistic regression is performed step-by-step. Neglerke R^2, chi-square Test, and Hosmer–Lemeshow test are used to evaluate the suitability of the model.

Chi-Square test The chi-square test is used when we want to evaluate whether there is a relationship between categorical or categorical variables in a data set.

In linear regression, according to goodness of fit in logistic regression [5], the residual can be defined as

$$y_i - \hat{y}_i. \tag{5}$$

When we apply the chi-square test to the logistic regression model, where y_i is necessarily equal to either 1 or 0, and

$$\hat{y}_i = \hat{\pi}_i(x_i) = \frac{e^{(\alpha+\beta_1 x_{i1}+\cdots+\beta_p x_{ip})}}{1 + e^{(\alpha+\beta_1 x_{i1}+\cdots+\beta_p x_{ip})}}. \tag{6}$$

We have the normalized remainder using the following formula:

$$r_i = \frac{y_i - \hat{y}_i}{\sqrt{\hat{y}_i(1 - \hat{y}_i)}}. \tag{7}$$

A statistic according to the χ^2 distribution is generated:

$$X^2 = \sum_{i=1}^{n} r_i^2. \tag{8}$$

The X^2 statistic follows a χ^2 distribution with $n - (p + 1)$ degrees of freedom, so we can calculate the p-value value.

Hosmer–Lemeshow test The inspection formula takes the form [6, 7]:

$$\mathrm{HL} = \sum_{i=1}^{k} \frac{n_i(p_i - \hat{p}_i)^2}{\hat{p}_i(1 - \hat{p}_i)} \sim \chi^2(k - 2). \tag{9}$$

The Hosmer–Lemeshow test is a statistical test for goodness of fit for logistic regression models.

Coefficient R^2 A commonly used linear mode the suitability measure is to determine the coefficient R^2 [8]. Idea of building formula R is to divide the variation of the dependent variable into two parts: the part that varies due to regression and the part that does not due to regression (also known as the residual). The higher the R^2 value if the smaller the regression variability, or the higher the regression variability [5].

6 Forecast Results

From the data analysis chart, we see that the proportion of women is smaller than that of men. This is due to the fact that fewer women enrolled in surveyed institutes than men. Also, most of the surveyed students are freshmen and sophomores at HUST (See Figs. 1, 2, 3, 4, 5, 6, 7, 8, 9, 10, and 11).

The three indexes of Step, Block, and Model in Table 1 all have sig equal to $0.000 < 0.05$ (95% confidence level). Thus, the general model shows that the correlation between the dependent and independent variables is statistically significant with a confidence interval of over 99%.

In the results from Fig. 12 we see that the coefficient -2 log likelihood is small, so the model is appropriate. At the same time, the coefficient Nagelkerke R Square

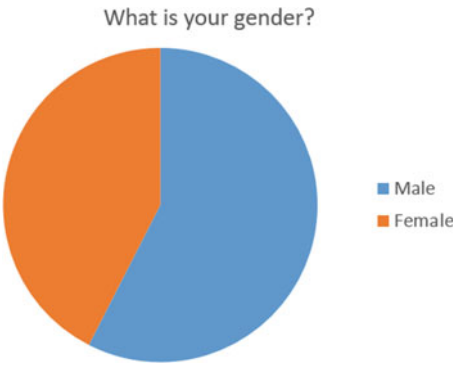

Fig. 1 Gender of the person to be surveyed

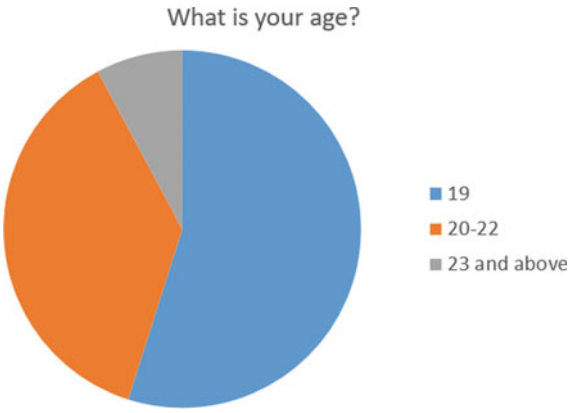

Fig. 2 Age of surveyed person

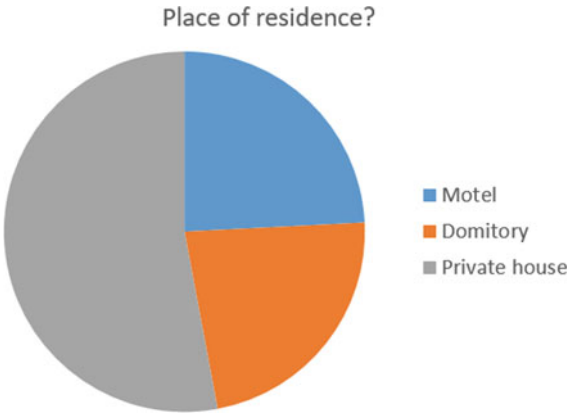

Fig. 3 Place of residence of the surveyed person

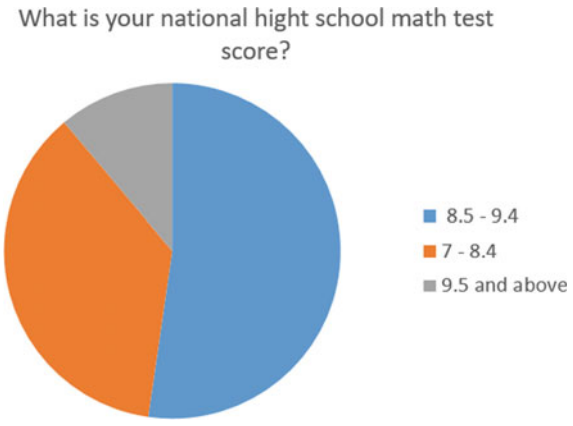

Fig. 4 High school test score of the person being surveyed

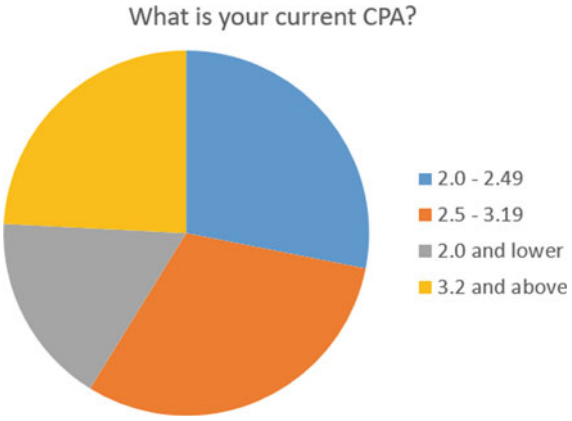

Fig. 5 CPA score at the time of the survey

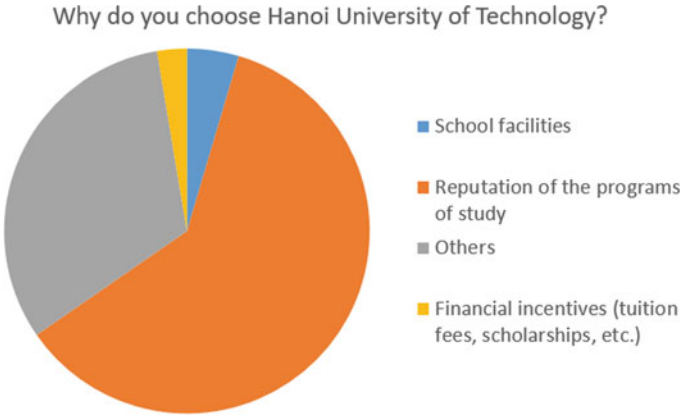

Fig. 6 Reason you chose HUST

= 0.756 shows that 75.6% of the change of the dependent variable is explained by the independent variables in the model, and the rest is due to other factors.

The results of checking the conformity of Hosmer–Lemeshow in Fig. 13, with the p-value = 0.491, show that the logistic regression model is suitable for analyzing the data that we have collected.

In Fig. 14, the probability of predicting students who will not slip correctly is 96.7%, and the ability to predict students with accurate slip is 76.7%. The results show that the model has 92.8% accuracy.

The results in Fig. 15 indicate that only five variables are determined to be statistically significant, or that the above five factors influence student achievement at HUST. These variables are the current residence, CPA score, the perception of the difficulty of the subject, the reason for choosing HUST, the student's awareness of

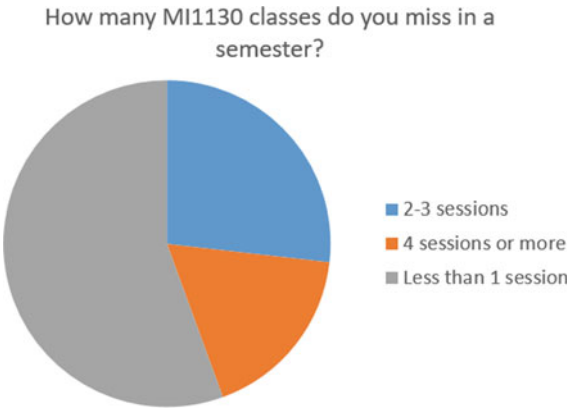

Fig. 7 Number of absences in the course

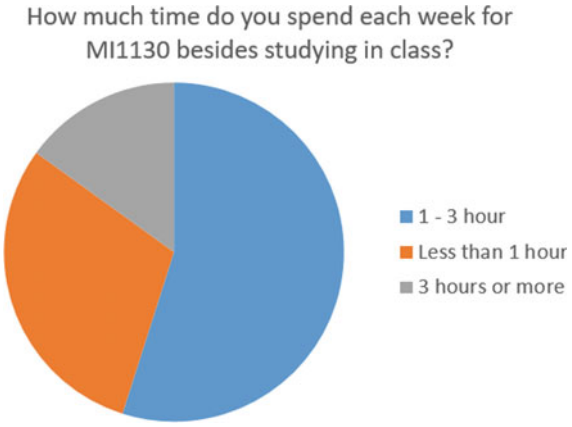

Fig. 8 Self-study time in a week

the application of the subject in reality, and self-study time. Therefore, they are the only variables that have a significant effect on the predictive results of the model. The seventh column of Fig. 15 provides the corresponding estimated difference values, Exp(β). These estimates show that students who live in boarding houses have high CPA scores, spend more time on self-studying, and think that the subject is easy and applicable in reality will be unlikely to fail the course.

From Fig. 11 with value R^2, 75.6% log changes are explained by independent variables. The unexplained change is 24.4%. This suggests that there are other important independent variables that have not been included in the model. From the above tests, it shows that the logistic regression model is suitable. We find five variables that affect the exact prediction results of the model.

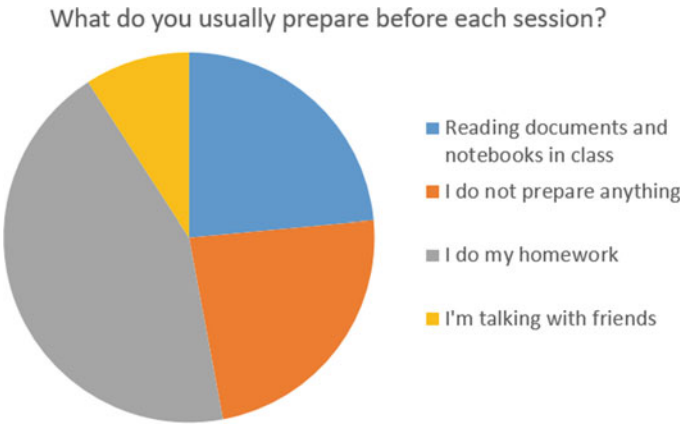

Fig. 9 Prepare before each class

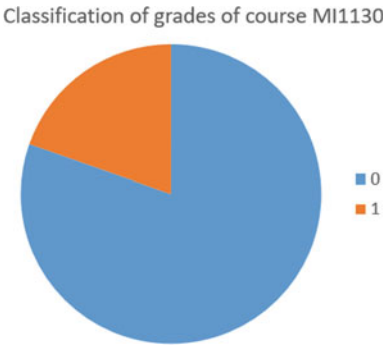

Fig. 10 Classification of grades of course MI1130

Omnibus Tests of Model Coefficients

		Chi-square	df	Sig.
Step 1	Step	98,173	20	,000
	Block	98,173	20	,000
	Model	98,173	20	,000

Fig. 11 Chi-square test

Model Summary

Step	-2 Log likelihood	Cox & Snell R Square	Nagelkerke R Square
1	52,833[a]	,476	,756

a. Estimation terminated at iteration number 8 because parameter estimates changed by less than ,001.

Fig. 12 Value R^2

Hosmer and Lemeshow Test

Step	Chi-square	df	Sig.
1	7,430	8	,491

Fig. 13 Hosmer–Lemeshow test

Classification Table[a]

Observed			Predicted		
			result		Percentage Correct
			,00	1,00	
Step 1	result	,00	118	4	96,7
		1,00	7	23	76,7
	Overall Percentage				92,8

a. The cut value is ,500

Fig. 14 Classification table

The regression equation found is

$$\log \frac{P(X)}{1-P(X)} = 8.269 + 2.318X_1 - 7.561X_2 - 8.513X_3 - 7.772X_4 - 5.117X_5 \tag{10}$$

where

$$P(X) = \frac{e^{(8.269+2.318X_1-7.561X_2-8.513X_3-7.772X_4-5.117X_5)}}{1+e^{(8.269+2.318X_1-7.561X_2-8.513X_3-7.772X_4-5.117X_5)}} \tag{11}$$

and

- X_1 = Place of residence
- X_2 = C.P.A result
- X_3 = Feeling of difficulty
- X_4 = Awareness of the applications of math in the real world
- X_5 = Self-study time

Variables in the Equation

		B	S.E.	Wald	df	Sig.	Exp(B)	95% C.I.for EXP(B)	
								Lower	Upper
Step 1[a]	C1DL	-1,668	1,388	1,444	1	,230	,189	,012	2,866
	C2DL	1,099	,999	1,210	1	,271	3,001	,423	21,262
	C3DL	2,321	1,172	3,919	1	,048	10,185	1,023	101,355
	C4DL	-,123	2,322	,003	1	,958	,884	,009	83,759
	C5DL	1,871	1,910	,960	1	,327	6,493	,154	274,099
	C6DL	-1,242	1,898	,428	1	,513	,289	,007	11,911
	C7DL	-7,557	2,303	10,765	1	,001	,001	,000	,048
	C8DL	-8,506	2,523	11,369	1	,001	,000	,000	,028
	C9DL	1,930	1,616	1,426	1	,232	6,893	,290	163,756
	C10DL	2,552	1,570	2,641	1	,104	12,831	,591	278,451
	C11DL	-2,774	1,500	3,423	1	,064	,062	,003	1,179
	C12DL	-1,599	1,630	,962	1	,327	,202	,008	4,933
	C13DL	2,447	2,105	1,351	1	,245	11,553	,187	715,333
	C14DL	-7,766	2,390	10,562	1	,001	,000	,000	,046
	C15DL	-,416	1,245	,112	1	,738	,660	,058	7,571
	C16DL	-1,784	1,514	1,389	1	,239	,168	,009	3,262
	C17DL	-5,120	2,327	4,841	1	,028	,006	,000	,572
	C18DL	,965	1,312	,541	1	,462	2,625	,200	34,371
	C19DL	-2,128	1,562	1,857	1	,173	,119	,006	2,542
	C20DL	,028	1,182	,001	1	,981	1,028	,101	10,429
	Constant	8,265	2,860	8,353	1	,004	3885,180		

a. Variable(s) entered on step 1: C1DL, C2DL, C3DL, C4DL, C5DL, C6DL, C7DL, C8DL, C9DL, C10DL, C11DL, C12DL, C13DL, C14DL, C15DL, C16DL, C17DL, C18DL, C19DL, C20DL.

Fig. 15 Results of the model

7 Conclusion

Some suggestions to university and students are as follows:

- Improve the quality of lectures, lecturers can inspire students to learn.
- Demonstrating the importance of the subject to reality.
- Students need to spend a reasonable time for self-study at home.
- Appropriate residence is also a factor affecting learning results.

The article has briefly presented the current situation of studying Analysis III of today's students at HUST. We see that the survey data set is quite small and the results of the Hosmer–Lemeshow test are quite low, but with the R-squared test of 75.6%, the model is quite suitable. The accuracy of the model is 92.8%, so the logistic regression model shows that the students' ability to accurately predict the results of Analysis III is quite good. Our future research direction will be to find more factors that affect students' in the subject Analysis III to increase the accuracy of the model and expand the research model of factors that affect the students' learning outcomes in the training program.

References

1. Akanle, O. B. (2007). *Socio-economic factors influencing students academic performance in Nigeria some explanation from a local survey*. Free Online Library: Sociology and social work community.
2. Angela, C., Maria, P., & Belen, M. (2013). Predicting academic performance and attritution in undergraduates students. *Revista de Psicologia, 19*(1), 101–112.
3. Sule, B. O., & Saporu, F. W. O. (2015). A Logistic Regression Model of Students' Academic Performance in University of Maiduguri, Maiduguri, Nigeria. *Mathematical Theory and Modeling*. ISSN 2224-5804 (Paper) ISSN 2225-0522 (Online).
4. Adejumo, A. O. (2013). Application of ordinal logistic regression in the study of students' performance. *Mathematical Theory and Modeling*. ISSN 2224-5804 (Paper) ISSN 2225-0522.
5. http://www.medicine.mcgill.ca/epidemiology/joseph/courses/epib-621/logfit.pdf
6. Guffey, D. (2012). *Hosmer-Lemeshow goodness-of-fit test: Translations to the cox proportional hazards model*. University of Washington.
7. https://www.real-statistics.com/logistic-regression/hosmer-lemeshow-test/
8. Allison, P. D. (2014). Statistical horizons LLC and the University of Pennsylvania.: Measures of fit for logistic regression. Paper 1485-2014.

Soft Robotics-Fingered Hand Based on Working Principle of Asymmetric Soft Actuator

Hiep Xuan Trinh, Phung Van Binh, Le Duc Manh, Nguyen Van Manh, and Ngo Van Quang

Abstract This study presents a prototype of the soft-fingered hand based on the operating principle of an asymmetric soft actuator, which is designed as a tube with the different thickness and stiffness of two sides and is activated by the pneumatic actuation. Based on such design, four soft fingers were fabricated from the silicone rubber material by using the molding method and then were assembled to the connectors and base to complete the soft-fingered hand. The ability of the proposed soft-fingered hand is validated by conducting the simulations and gripping experiments. The simulation and experimental results show that under the pneumatic activation, the soft fingers have a good bending deformation, and the proposed hand can grip several objects with different shapes, sizes, and weights.

Keywords Soft robotics · Soft gripper · Asymmetric soft actuator

1 Introduction

Soft robotics has been introduced as a novel frontier in robotic research. In general, soft robotics is fabricated by soft materials such as silicone elastomers, urethane, hydrogels, and so on [1]. The deformable properties of soft material enable soft robotics which is much inherently compliant and withstand large strains in comparison with the traditional rigid robot. Thus, soft robotics has many advantages such as adaptable to the unpredicted surrounding environment, safe for human interactions, light-weight, and so on [2, 3]. The area research of soft robotics is a wide range from locomotion, manipulation, actuating, or sensing [4–6]. In which the development of the soft-fingered robotics hand recently is an emerging area in soft robotics research and achieved significant results. The soft robotics hand has exposed many benefits on the dexterous manipulation, grasping delicate objects in unstructured environments [7, 8]. Many studies focused on proposing, developing soft-fingered hand for adapt-

H. X. Trinh (✉) · P. V. Binh · L. D. Manh · N. V. Manh · N. V. Quang
Le Quy Don Technical University, 236 Hoang Quoc Viet, Cau Giay, Ha Noi, Vietnam
e-mail: hieptx@mta.edu.vn

T. D. L. Nguyen and J. Lu (eds.), *Machine Learning and Mechanics Based Soft Computing Applications*, Studies in Computational Intelligence 1068,
https://doi.org/10.1007/978-981-19-6450-3_10

ing various tasks. One of the first authors who proposed the gripping mechanism based on the softness design in Suzumori et al. [9], they used four micro-actuators to construct a soft gripper for grasping various objects. Pneumatic and hydraulic actuating mechanics have recently widely utilized in the design of soft gripper, due to their advantages such as low cost, high gripping efficiency, simple fabrication, easy control, and fast responses [10, 11]. For instance, the authors in [12] presented the soft robotic gripper with the bellow soft pneumatic actuator for delicate manipulation and collecting the sample fragile species on the deep reef. Park et al. [13] proposed the soft gripper based on the electrohydraulic actuator, fabricated by polyethylene film and silicone material. However, most pneumatic or hydraulic mechanics-based soft-fingered hands consist serial chambers with specially-designed thin walls to generate the gripping shape under pressurization activation. The thin walls design causes easily the failures such as torn, wears, or bulge. Moreover, the construction with many chambers leads to the complication of mathematical models and the difficulty to fabricate and calculate exactly the curvature shape or contact gripping force. In [14], Ho et.al proposed the novel concept of soft-fingered hand with contact feedback based on the idea of morphological computation with the unbalanced deformation mechanism. In this design, the soft finger structure includes a softer layer much thicker than a stiffer layer, and the gripping energy is generated from the elastic energy of the pre-stretched softer layer. Nonetheless, this design requires the external motor to pull or release the tendon string for controlling the opened state of soft fingers.

In this paper, based on the operating principle of asymmetric soft actuator, we present the soft-fingered hand that is easy to design, fabricate, and model. The robotic hand consists of four soft fingers; each finger is a simple asymmetric tube and is activated by air pressure. The remainder of this paper includes the principle, design, fabrication, simulation, and preliminary gripping test of the soft-fingered hand.

2 Principle and Design of Soft-Fingered Hand

Principle of Soft-Fingered Hand In this study, the soft finger is operated based on the principle of the asymmetric soft actuator that has a cross-section of the asymmetric hole [15]. Due to the different thickness and stiffness between two sides of the asymmetric tube, under the actuation of internal pressure, the actuator is curved in the direction of the thicker side. The cross section of the soft finger is circular, with different thicknesses t_1 and t_2 of the top and bottom side, where is smaller than (Fig. 1). The thicker side is partly flat to improve the gripping contact area. The bending effect of the soft actuator can be considered as the bending of the cantilever beam. In which, the actuator is closed at the free end; the air pressure is input into the soft actuator from the fixed end through a small tube. Under the pneumatic actuation, the different thickness leads to the different expansion between two sides, and the eccentricity causes the bending moment. The bending curvature of the soft actuator depends on its geometrical design and the pressure value.

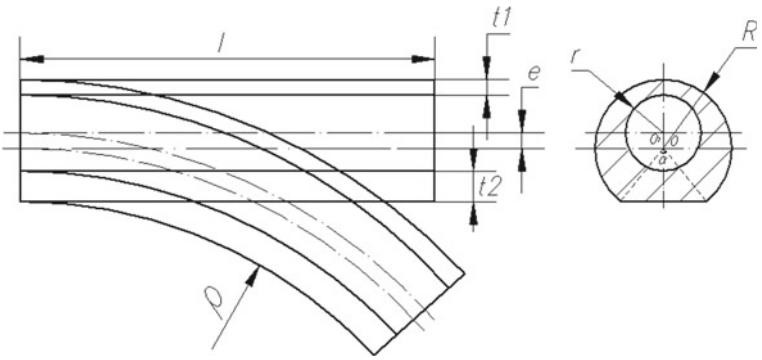

Fig. 1 Curved principle of the asymmetric soft actuator and its cross section

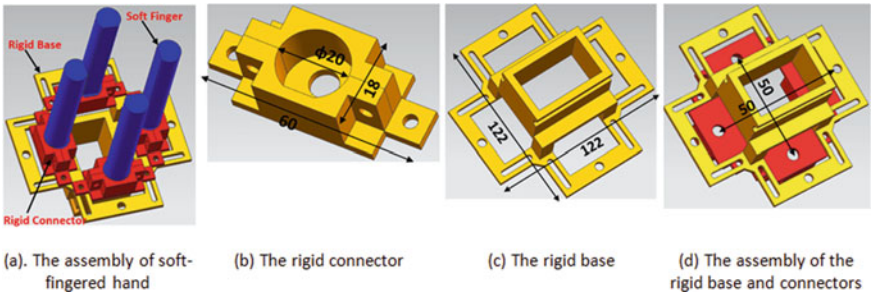

Fig. 2 Design of soft-fingered hand

Design of Soft-Fingered Hand The robotics hand consists of four soft fingers, a rigid connector, and a rigid base (Fig. 2). The rigid connector is an assembly of two parts. It has a hole with a diameter of 20 mm to fix the soft finger. Four rigid connectors are assembled to rigid based by using the screws. All parts of the rigid connectors and rigid based are designed by the SolidWork software, then fabricated by using a 3D printer. The soft finger is an eccentric tube, a free end is closed, and the fixed end has a small hole for directing the compressed air into the tube. The prototype soft finger has a dimension of designed parameters as $l = 100$, $R = 8$, $r = 5$, $e = 2$, $t_1 = 2$, $t_2 = 4$ mm. The overall dimension of the soft finger is similar to the size of the human finger.

3 Fabrication

The soft fingers were made from silicone rubber of RTV 225 and fabricated with two 3D printing molds. The first mold is the assembly of three parts and is used to fabricate a main part of the soft finger (Fig. 3a, b). The remained mold (Fig. 3c) is

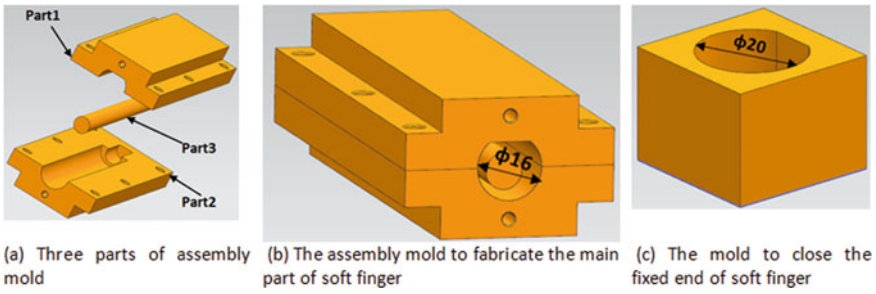

Fig. 3 Molds for fabricating the soft finger

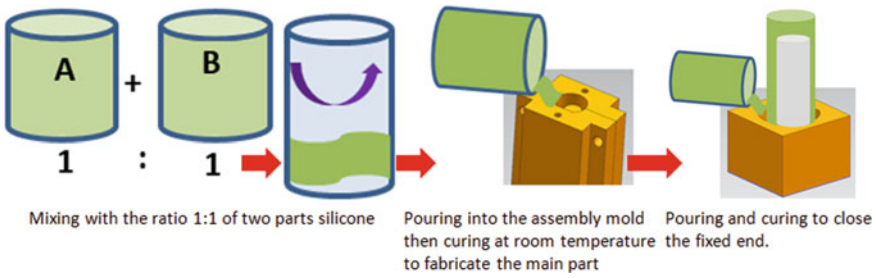

Fig. 4 Schematic of fabricating process

used to seal the fixed end of the finger. The fabrication process of the soft finger by molding method is depicted as in Fig. 4 and can be summarized as follows. First, two components of the liquid silicone rubber were mixed with the ratio of 1:1, then the mixed liquid silicone is poured into the assembly mold and is cured at room temperature after ten hours. After the curing process, by removing the assembly mold, we get the main part of the soft finger. At this stage, the soft finger still has an open end. This end was closed with the same mixed silicone by using the second mold and a similar curing method. Finally, after taking out that mold, we get the soft finger. The soft fingers were then fixed to the connector and the base to complete the soft-fingered hand.

4 Simulation and Preliminary Gripping Test

To clarify the principle of the soft finger and the effect of geometrical parameters on its bending curvature, we conducted the simulation with the commercial software Abacus. The soft finger was modeled as a deformable solid with the hyper-elastic material. The Yeoh model with the parameters of $C_{10} = 0.1$, $C_{20} = 0.02$, $C_{30} = 0.0002$, $D_1 = D_2 = D_3 = 0$ was used in the simulations [16]. The FE model was meshed with the linear hexahedral elements of type C3D8R. The bending angle

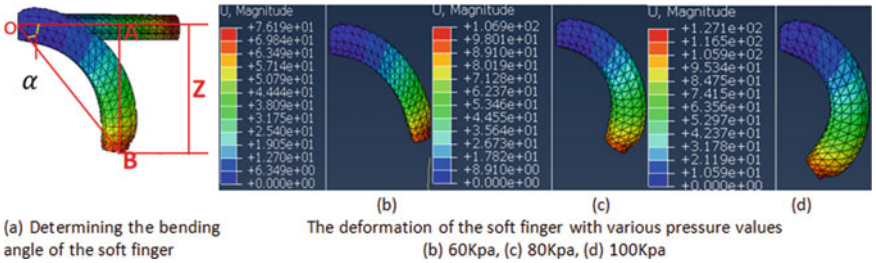

Fig. 5 Deformation of soft finger

Table 1 Various cases of finger's geometrical parameters

Parameter	R (mm)	r (mm)	e (mm)	t_1 (mm)	t_2 (mm)
Case 1	8	5	2	2	4
Case 2	8	5	2.4	1.6	4.4
Case 3	8	5	2.8	1.2	4.8
Case 4	8	5	3	1	5

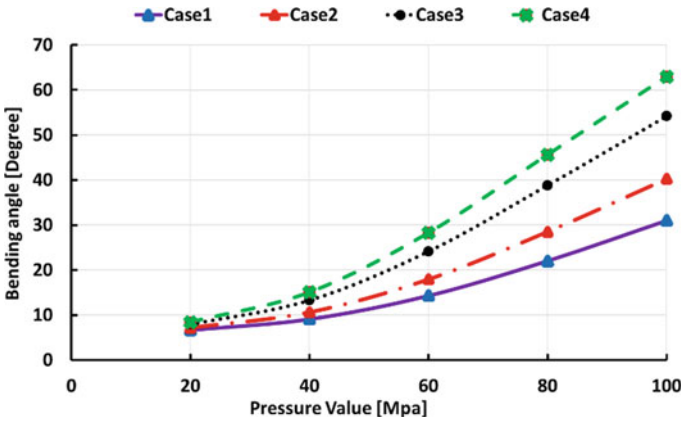

Fig. 6 Bending angle's values with different pressure of various case designs

α of the soft finger is determined through the positions of two nodes at the fixed and free ends (Fig. 5). To investigate the effect of the designed structure on the bending curvature of the soft finger under the air pressure activation, we conducted the simulations with various cases of the finger's geometrical design as shown in Table 1. The bending angle α of these soft fingers with different pressure values is shown in Fig. 6.

From Fig. 6, we can see that when the pressure value increases, the bending angle of the soft finger does not increase linearly, and it grows up noticeably with high pressure. It is due to the physical nonlinearity of the silicone material and the

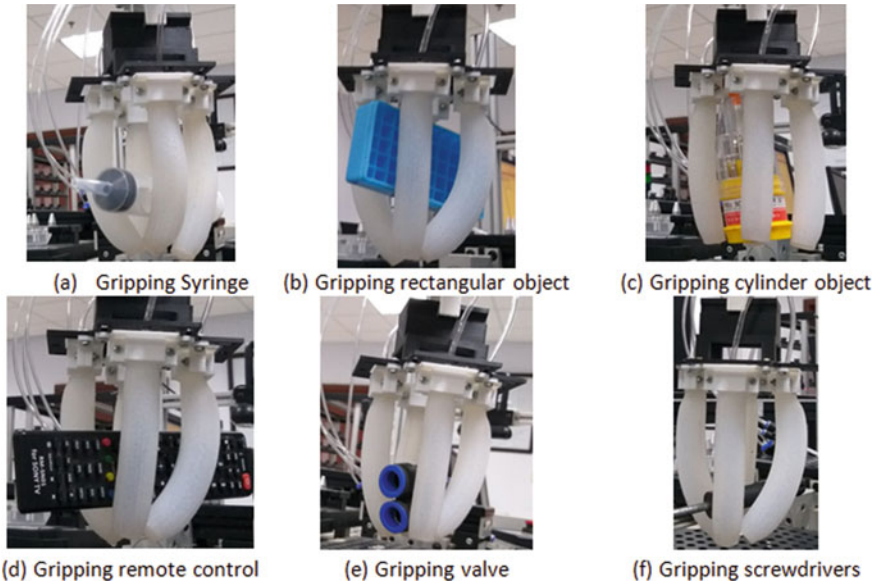

Fig. 7 Gripping tests of the soft-fingered hand

geometrical nonlinearity of the large deformation. In the comparisons of the bending angle with the different designed parameters under the same pressure conditions, we see that the values of bending angle rise with the increase of the eccentricity e, thickness t_2, and the decrease of thickness t_1.

We conducted the experiments to test the preliminary gripping ability of the soft-fingered hand. The hand was mounted onto the SCORRA ER-14pro robotics arm. The soft fingers were activated by air pressure through the pump system. Several objects with different shapes, sizes, and weights were used for gripping tests, and the results were shown in Fig. 7. This figure indicates that the proposed hand has a good gripping ability with different objects.

5 Conclusion

The study presented in this paper is our first step toward a soft robotics hand that has a simple design, easy to fabricate, modeling, and control. In future, we will address some aspects to improve the performance of the soft-fingered hand. First, we will focus on proposing a novel mathematical model to estimate the bending deformation of the soft finger under the pneumatic actuation. This model would build based on the deformation laws of the nonlinear material and consider the geometrical nonlinearity of the large deformation. Then, based on the mathematical model, optimization algorithms would be proposed to improve the soft finger's design

for obtaining desired bending shapes that attempts to imitate the shape of human fingers when handling operations. Finally, a rigid nail will be embedded to the free end to limit the tip inflation, which will make better pick-and-place performance of the soft finger. The technical pre-stressed deformation will be used to extend the gripping area of the soft-fingered hand.

References

1. Rus, D., & Tolley, M. (2015). Design fabrication and control of soft robots. *Nature, 521,* 467–475.
2. Chiwon, L., Myungjoo, K., Yoong, K., et al. (2017). Soft robot review. *International Journal of Control, Automation and Systems, 15*(1), 1–13.
3. Iida, Fumiya, & Laschi, Cecilia. (2011). Soft robotics: Challenges and perspectives. *Procedia Computer Science, 7*(7), 99–102.
4. Lin, H. T., Leisk, G. G., & Trimmer, B. (2011). GoQBot: A caterpillar-inspired soft-bodied rolling robot. *Bioinspiration & Biomimetics, 6,* 026007.
5. Calisti, M., Giorelli, M., Levy, G., Mazzolai, B., Hochner, B., Laschi, C., & Dario, P. (2011). An octopus-bioinspired solution to movement and manipulation for soft robots. *Bioinspiration & Biomimetics, 6,* 036002.
6. Stefan, M., Benjamin, T., Randall, M., et al. (2010). Highly sensitive flexible pressure sensors with microstructured rubber dielectric layers. *Nature Materials, 9,* 859–864.
7. Amend, J., Cheng, N., Fakhouri, S., & Culley, B. (2016). Soft robotics commercialization: Jamming grippers from research to product. *Soft Robotics, 3*(4), 213–222.
8. Deimel, R., & Brock, O. (2015). A novel type of compliant and underactuated robotic hand for dexterous grasping. *The International Journal of Robotics Research*.
9. Suzumori, K., Iikura, S., & Tanaka, H. (1991). Development of flexible microactuator and its applications to robotic mechanisms. In *Proceedings. IEEE International conference on robotics and automation* (pp. 1622–1627). Sacramento.
10. Boyras, P. et.al. (2018). An overview of novel actuators for soft robotics. *Actuators, 7*(48).
11. Robertson, M. et al. (2016). Soft pneumatic actuator fascicles for high force and reliability. *Soft Robotics, 4*(1).
12. Galloway, K. C., Becker, K. P., Phillips, B., Kirby, J., Licht, S., Tchernov, D., et al. (2016). Soft robotic grippers for biological sampling on deep reefs. *Soft Robotics, 3*(1), 23–33.
13. Park, T. et al. (2020). Electrohydraulic actuator for a soft gripper. *Soft Robotics, 7*(1).
14. Ho, V., & Hirai, S. (2017). Design and analysis of a soft-fingered hand with contact feedback. *IEEE Robotics and Automation Letters, 2*(2), 491–498.
15. Udupa, G. et al. (2010, October) Robotic gripper driven by flexible micro actuator based on an innovative technique. In *IEEE workshop on advanced robotics and its social impacts*. KIST.
16. Martins, P., et al. (2006). *A comparative study of several material models for prediction of hyperelastic properties: Application to silicone-rubber and soft tissues strain* (Vol. 42, pp. 135–147).

Control Design for 400 Hz Ground Power Unit

Tran Que Son, Nguyen Kien Trung, Dich Nguyen Quang, Do Ngoc Quy, and Do Ba Phu

Abstract In this paper, a design of Sinusoidal Pulse Width Modulation (SPWM) 400 Hz inverter is proposed for Ground Power Unit (GPU) in airlines industry. In which, the inductor filter is integrated into the isolated transformer, for reducing the production volume, also enhancing the system flexibility and reliability. In the control scheme, resonant controller with parallel structure is performed to control fundamental harmonic voltages. The computation delay always existed in digital systems is considered to handle through the phase compensator technique. Simulation studies in Matlab software and Hardware in the Loop (HIL) show that the controller can regulate the output voltage, with the Total Harmonic Distortion (THD) is just 1.21% and 2.31%, respectively, even under the nonlinear load condition. The 20 kVA GPU experimental prototype using digital signal processing (DSP) has been implemented verify the validity and feasibility of the proposed controller. The control strategy steady state and the dynamic performance are tested in carefully, which show that the steady state error is relatively small, the transient response is fast and THD is 2.24% for the rectifier load.

Keywords Ground power unit · Resonant controller · Unipolar SPWM · Three single phase combine inverter

T. Q. Son · D. N. Quang · D. N. Quy · D. B. Phu
Institute for Control Engineering and Automation, Hanoi University of Science and Technology, Dai Co Viet, Hai Ba Trung 11657, Ha Noi, Viet Nam
e-mail: tranqueson.ktdt@tnut.edu.vn

D. N. Quang
e-mail: dich.nguyenquang@hust.edu.vn

T. Q. Son
Faculty of International Training,Thai Nguyen University of Technology, 3/2, Tich Luong 24000, Thai Nguyen, Viet Nam

N. K. Trung (✉)
Department of Industrial Automation, Hanoi University of Science and Technology, Dai Co Viet, Hai Ba Trung 11657, Ha Noi, Viet Nam
e-mail: trung.nguyenkien1@hust.edu.vn

T. D. L. Nguyen and J. Lu (eds.), *Machine Learning and Mechanics Based Soft Computing Applications*, Studies in Computational Intelligence 1068,
https://doi.org/10.1007/978-981-19-6450-3_11

1 Introduction

Recently, the airline industry has achieved an incredible growth either in civil or military sectors. Additionally, it is demanded by airport regulations that external power units must be used to energize the aircraft while stopping to reduce the noise and air pollution. This rises continuously the demands to the Ground Power Unit (GPU), a device providing external power to aircraft when parked on the airport. The GPU voltage supply standard is 115V RMS-400 Hz, and the main objective of GPU design is to meet the requirement in which the THD is smaller than 2% even when feeding unbalanced and nonlinear loads.

The classical GPU is composed of a input rectifier, an inverter, an transformer, and output LC filters [1]. However, the passive LC circuit makes the system become larger, heavier, and more difficult to install. In this paper, a GPU configuration is proposed in which, the filter inductor is integrated in the transformer to improve the system portability and flexibility.

Design the GPU with the THD content are $\leq$2% under different types of load conditions, create research challenges. Reference [2] presents a GPU system based on the Deadbeat control technique with the disturbance decoupling networks are taken into consideration. The phase corrector scheme is also applied to compensate the time delay. However, the system output power is limited at only 1 kVA and the THD is 3.53%, which is relatively high. FPGA based on Repetitive Control for high performance GPUs is proposed in [3], but both the simulation and experimental results are not evaluated specifically. Active neutral point clamped converter technology is also applied, a 5-level active neutral point clamped (5L-ANPC) multilevel converter is given in [4] which benefits in increasing the carrier ratio, decreasing the output dv/dt, reducing the inductance, boosting GPU voltage control capability. Nevertheless, the THD is still high and the number of switches used is large. To overcome this problem, the improvement of 5L-ANPC topology is presented in [5]. In which, a hybrid active-neutral-point-clamped (HANPC) converter with 25 levels is introduced to the GPU. Though, the control complexity has narrowed its application in practice.

Recently, the resonant controller has been widely used in many fields, and it is one of the most popular approaches for AC voltage control because of high performance of zero steady state tracking error [6, 7]. In this paper, a single loop resonant controller with the phase delay technique is proposed for the GPU. Simulation and experiment results show that this system can provide high performance output voltages under different load conditions.

This paper is organized as follows. In Sect. 2, 400 Hz GPU topology and the GPU model are analyzed. In Sect. 3, the modified resonant controller in combination to phase delay compensation technique is analyzed and implemented. In Sect. 4, a case study is conducted in which, simulation and experiment results are carefully analyzed to verify the efficiency of the proposed system. Finally, the conclusion and reference is presented at the end of the paper.

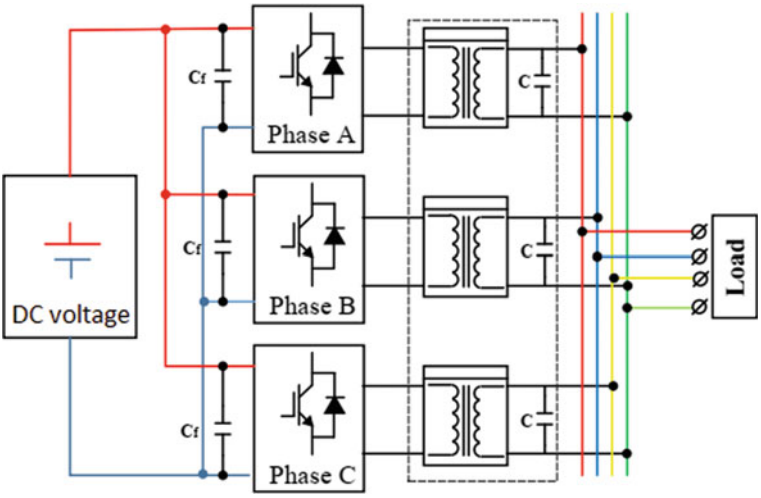

Fig. 1 The proposed GPU system

2 GPU Model

2.1 Inverter Topology

A standard three single-phase combined inverter is used because it profits especially in the case of operation with an unbalanced load. The GPU system is shown in Fig. 1.

2.2 State-Space Model and Transfer Function of the GPU

With the transformer ratio $N = 1$, the equation of one second order LC filter is as follows:

$$\begin{bmatrix} \frac{di_L}{dt} \\ \frac{dv_O}{dt} \end{bmatrix} = \begin{bmatrix} \frac{-r}{L} & \frac{-1}{L} \\ \frac{1}{C} & 0 \end{bmatrix} \begin{bmatrix} i_L \\ v_O \end{bmatrix} + \begin{bmatrix} \frac{1}{L} & 0 \\ 0 & \frac{-1}{C} \end{bmatrix} \begin{bmatrix} v_I \\ i_O \end{bmatrix} \tag{1}$$

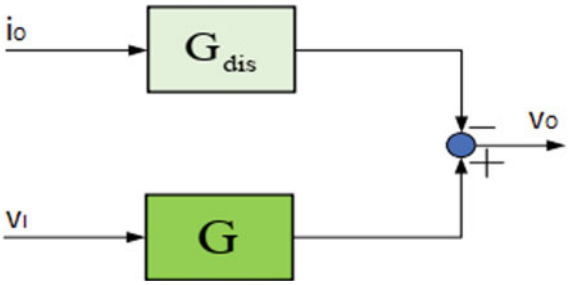

Fig. 2 GPU model

The GPU transfer function then can be written as:

$$v_O = \frac{v_I}{LCs^2 + rCs + 1} - \frac{(sL + r)i_O}{LCs^2 + rCs + 1} \tag{2}$$

PWM transfer function The total digital delay time, which includes the sampling time, computation and PWM process, is approximated one and half of the sampling period, $1.5T_s$. So, the PWM function can be expressed:

$$G_{PWM} = \frac{1}{1.5T_s s + 1} \tag{3}$$

Consider the load current i_O is the disturbance to the model, the dynamics model of the system can be expressed in Fig. 2. In which:

$G = \frac{1}{(1.5T_s s + 1)(LCs^2 + rCs + 1)}$ is the GPU transfer function

$G_{dis} = \frac{(sL + r)i_O}{LCs^2 + rCs + 1}$ is the load disturbance funcion.

3 Digital Resonant Controller Design

3.1 Discrete Model of Resonant Controller

Overall control structure The parallel resonant controller shown in Fig. 3 is implemented to control fundamental as well as the harmonics [6].

The controller transfer function is written as [7]:

$$R_n(s) = K_{rn} \frac{s\cos(\theta_n) - \omega_n \sin(\theta_n)}{s^2 - \omega_n^2} \tag{4}$$

with K_{rn}: resonant gain and ω_n: resonance frequency for the nth resonant compensator.

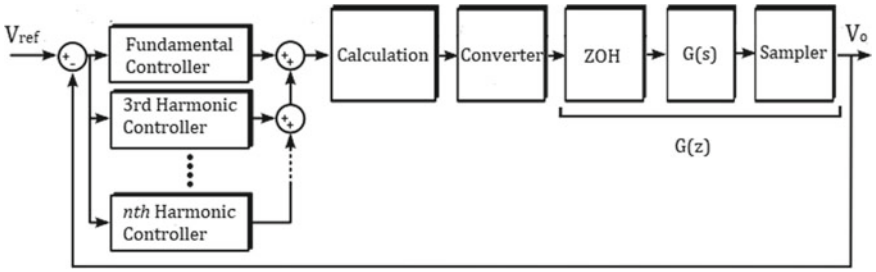

Fig. 3 The overall control structure

Phase delay compensation Each compensator phase can be changed by adjusting θ_n in (4). θ_n is determined from the phase angle of the GPU open-loop frequency response.

By Zero Order Hold (ZOH) transform, the model of resonant controller in the discrete domain can be obtained:

$$R_n(z) = \frac{(z-1)\sin(\omega_n T_s)\cos(\theta_n) - (z+1)\left[1-\cos(\omega_n T_s)\right]\sin(\theta_n)}{\left[z^2 - 2\cos(\omega_n T_s)z + 1\right]\omega_n} \tag{5}$$

4 A Case Study

4.1 The GPU Parameters

System parameters listed in Table I is used for following analysis.

4.1.1 Simulation Results

Matlab Simulations The first simulation is designed for the situation where only fundamental is used to control the output voltage with resistive load. The output voltage, as shown in Fig. 4, is maintained at the desired RMS value only within 0.015 s, with excellent overlapping, indicating that the phase and amplitude differences are considerable zero. Figure 5 shows the THD content which is just 0.97%.

A nonlinear load included a single phase diode H—bridge converter, a $50\mu F$ capacitance and a load 1.09Ω is next apply to investigate the performance of fundamental controller. The waveform of output voltage and current with the significant distortions are expressed in Fig. 6. It can be observed from the Fig. 7 that the THD is risen to 6.7% due to large increments in the 3rd and 5th harmonic percentage.

To overcome, the 3rd harmonic compensator is designed in combination to the fundamental controller for compensating the 3rd harmonic, with the THD content

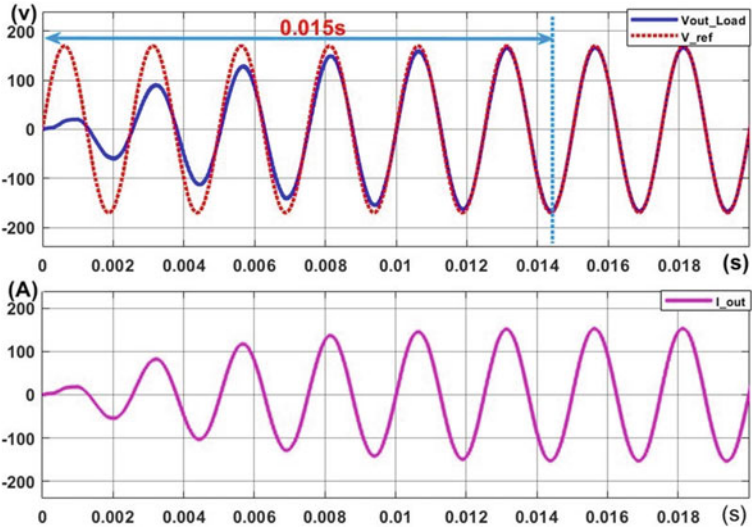

Fig. 4 Output voltage waveform

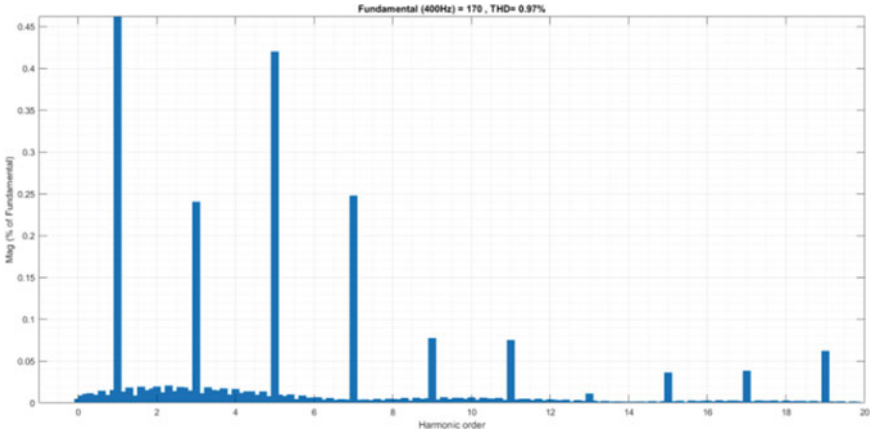

Fig. 5 THD content with linear load

is depicted in Fig. 8. It can be seen that the percentage of 3rd harmonic is almost completely eliminated, being kept at 0.44%, the output voltage THD content now is just 1.21%.

HIL Simulations System simulation is then implemented in the Hardware In Loop (HIL) device to test the proposed GPU with a real time system. The real HIL sumulation system is illustrated in Fig. 9.

The HIL simulation is focused on the situation under the rectifier load condition ($C = 50\mu F$ and $R = 1.09\Omega$). Figure 10a) exhibits the THD content of the output

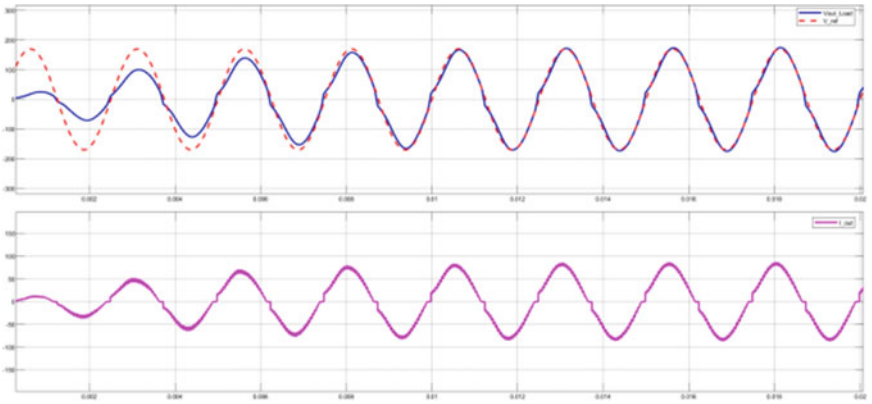

Fig. 6 Distorted output voltage waveform

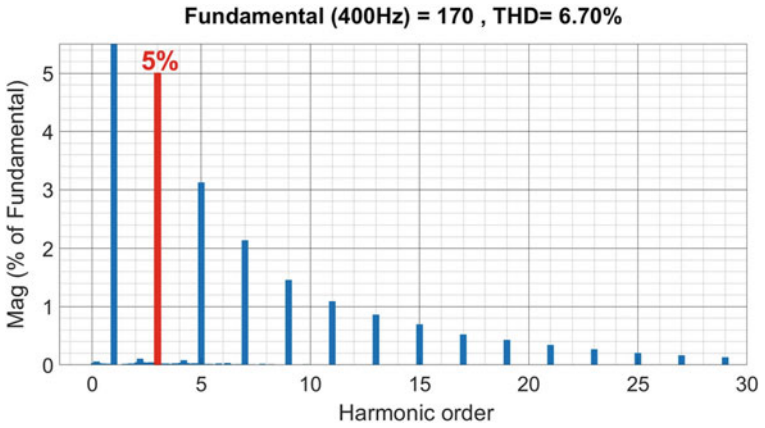

Fig. 7 THD of output voltage waveform

voltage when only fundamental controller is used, the 3rd harmonic is at high level, which is 4.3%, and the THD is 4.95%, consequently, highly distorted output voltages are obtained.

By adding the 3rd harmonic compensator, it can bee seen from the Fig. 10b that the the 3rd harmonic value is significantly lowered from 4.3% to 0.6, also, the THD is strongly improved to the value of 2.31%, just few above 2%.

4.2 Experiment Results

To evaluate the proposed design method, a 20 kVA GPU prototype was built as shown in Fig. 11. The inverter was constructed based on Infineon FF450R12KT4

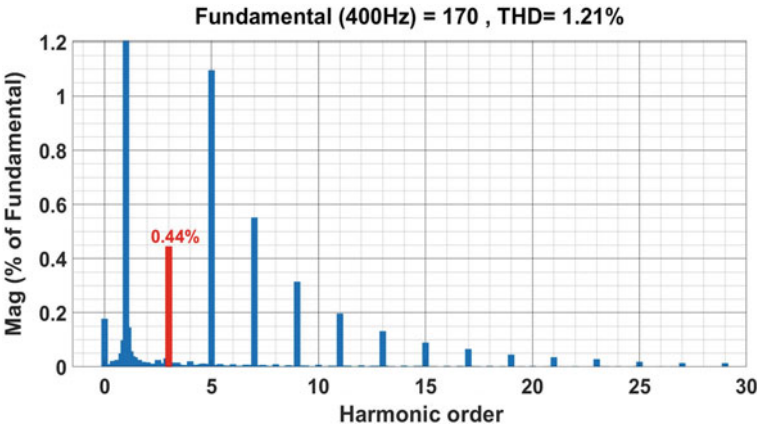

Fig. 8 THD of output voltage waveform is significantly improved with 3rd harmonic compensator

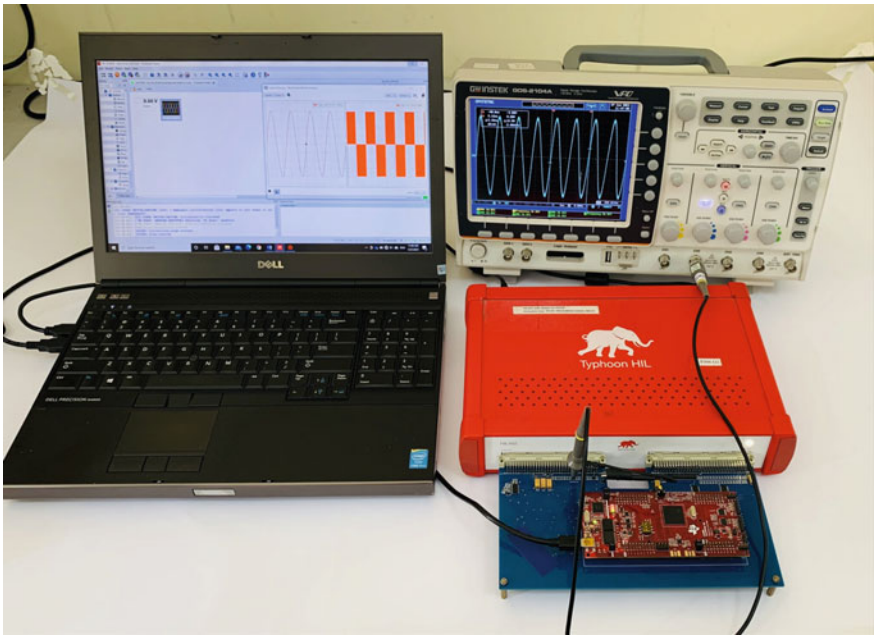

Fig. 9 HIL simulation system

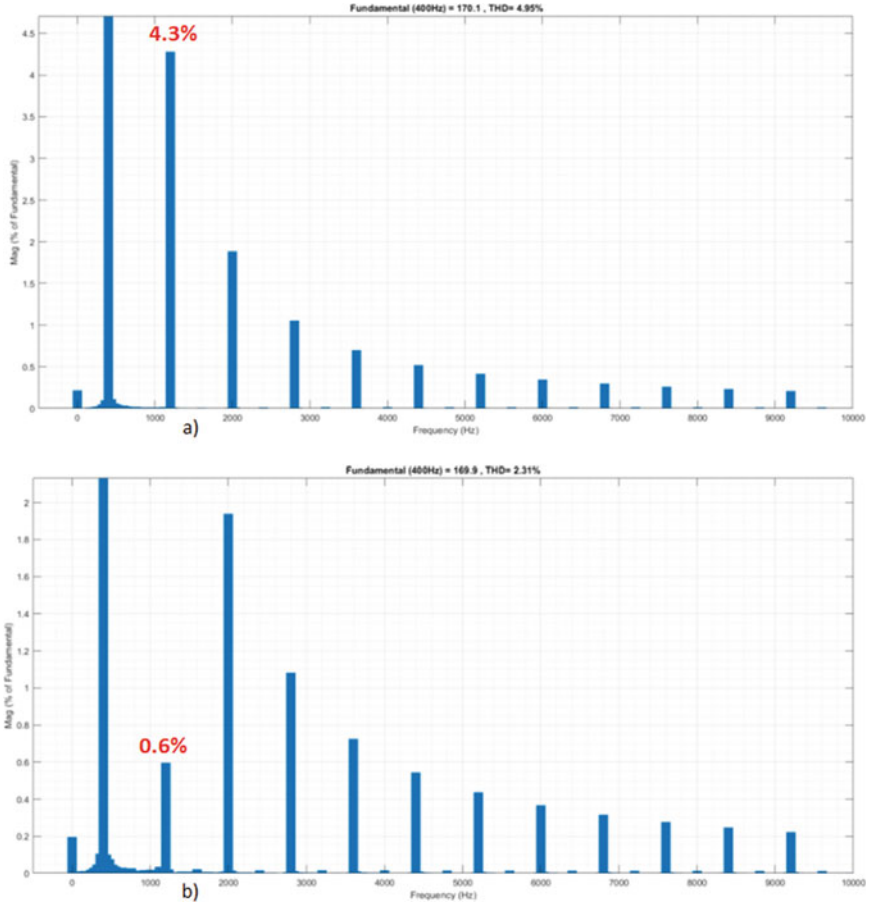

Fig. 10 **a** Output voltage with fundamental controller only, **b** The case in which 3rd harmonic compensator is applied

IGBT. Texas Instrument TMS320F28379D microcontroller has been exploited to control the system.

The experiment is first considered to test system response with only fundamental under the resistive load, the results are depicted in Fig. 12, in which (a) is the output voltage, and (b) is the THD content. It is possible to realize that output voltage quality is good with only little distortion, THD is maintained at a low level of 1.35%.

The second test is conducted with the rectifier load ($C = 50\mu F$, $R = 1\Omega$). With only the fundamental controller, output voltage is distorted, the THD increases to 3.29% with the 3rd harmonic value is 2.5%, as exhibited in Fig. 13. When the 3rd compensator is implemented, the 3rd harmonic is decremented to 1.85% and the THD content is now 2.24%, illustrated by Fig. 14.

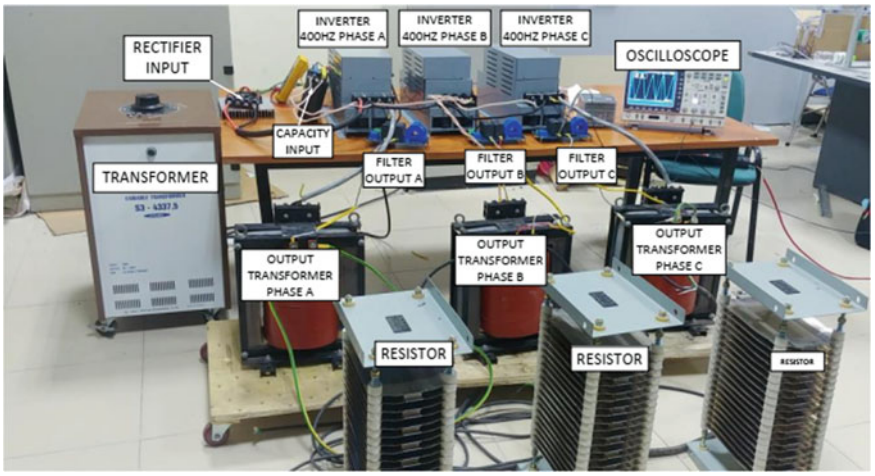

Fig. 11 The experiment system

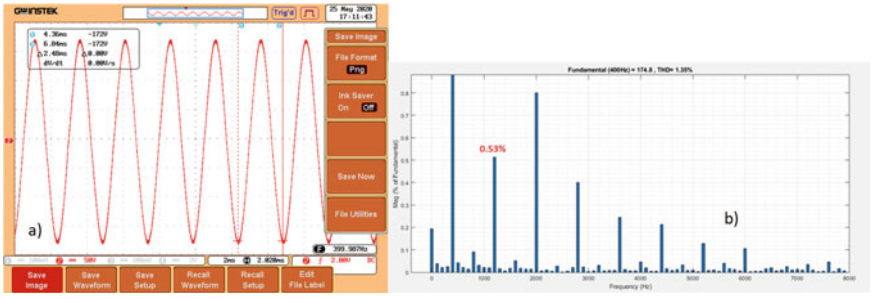

Fig. 12 **a** The output waveform, **b** The THD

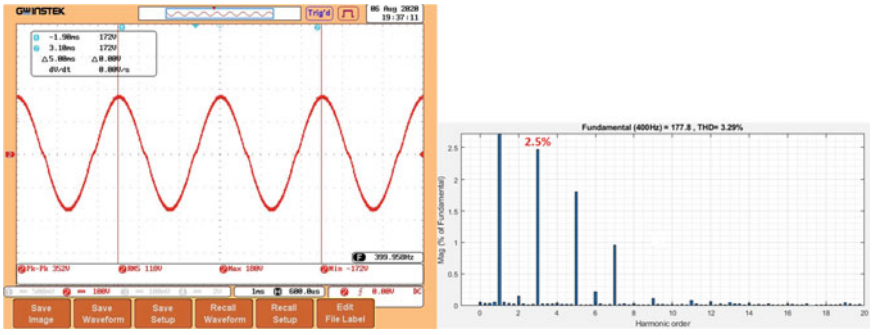

Fig. 13 The experiment system

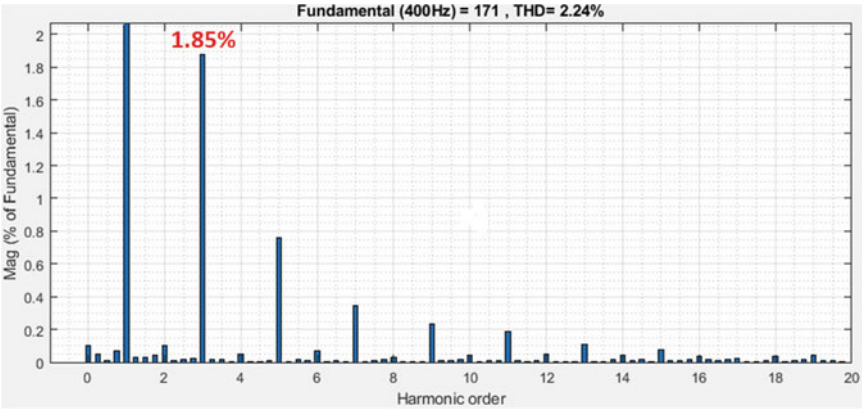

Fig. 14 The THD with compensator added

5 Conclusion

This paper has introduced a configuration of GPU in which, the standard three single-phase inverter topology are used with the filter inductance L is formed by transformer leakage inductance to reduce the production volume. The dynamic model of the inverter are investigated with the effect of the computation delay is taken into consideration. The control system is made up with the use of resonant controller in combination with phase delay compensation that aims to compensate the phase difference caused by the computation delay and the LC filter, to enhance the quality of output voltage. The simulation result on both Matlab software package and HIL, also the experiment resuls have approved the effectiveness of the proposed controller in regulating the fundamental component as well as compensating the high order harmonic distortions, in both the linear and nonlinear load situations. In the future work, the higher order harmonic compensators will be applied to further improve the system dynamic.

Acknowledgments. This work was funded by the Institute for Control Engineering and Automation (ICEA), Hanoi University of Science and Technology (Vietnam) under project number DTDL.CN-14/18.

References

1. Jensen, U. B., Blaabjerg, F., & Pedersen, J. K. (2000, January/February). A new control method for 400-Hz ground power units for airplanes. *IEEE Transactions on Industry Applications, 36*(1).
2. Manohar, D., & Seema, P.N. (2015). Deadbeat controller with phase corrector for 400-Hz inverter used in ground power units of aircrafts. In *IEEE International Conference on Technological Advancements in Power & Energy*, 978-1-4799-8280-6/15.

3. Lidozzi, D. A., Solero, L., Crescimbini, F., Ji, C., Bifaretti, S., & Zanchetta, P. (2017). FPGA-based direct repetitive control for high performance ground power units. In *IEEE Energy Conversion Congress and Exposition (ECCE)*, pp. 3063–3068.
4. Abarzadeh, M., Madadi Kojabadi, H., & Chang, L. (2015). A modified static ground power unit based on active natural point clamped converter. In *IEEE Energy Conversion Congress and Exposition (ECCE)*, pp. 3508–3514.
5. Abarzadeh, M., & Kojabadi, H. M. (2016, December). A static ground power unit based on the improved hybrid active neutral-point-clamped converter. *IEEE Transactions on Industrial Electronics, 63*(12), 7792–7803.
6. Rojas, F., Cardenas, R., Clare, J., Diaz, M., Pereda, J., & Kennel, R. (2019, August). A design methodology of multiresonant controllers for high performance 400 Hz ground power nits. *IEEE Transactions on Industrial Electronics, 66*(8), 6549–6559.
7. Li, Z., Li, Y., Wang, P., Zhu, H., Liu, C., & Gao, F. (2010, February). Single-loop digital control of high-power 400-Hz ground power unit for airplanes. *IEEE Transactions on Industrial Electronics, 57*(2), 532–543.

Rapid Design of Square-Spiral Metamaterial for Enhanced Wireless Power Transfer Applications Using Artificial Neural Networks

Bui Huu Nguyen, Quoc-Dong Hoang, and Luan N. T. Huynh

Abstract Wireless power transfer (WPT) is an appropriate method of delivering power without connecting wires to multiple devices. To further increase WPT performance, metamaterials' extraordinary properties, such as electromagnetic field focusing, have been used successfully. Normally, metamaterial properties depend on multiple parameters. Several metamaterial designs require a significant amount of time to complete numerical simulation. In this work, we propose a rapid design square-spiral metamaterial method using an artificial neural network (ANN). When ANN is used, the results show an accuracy of 97.4% and a collective mean square error (MSE) less than 0.7×10^{-3}. For synthesizing the design parameters, the results show an accuracy of 95.6% and the MSE less than 7×10^{-3}. Besides, the computation time of 1000 samples can be reduced 93×10^3 times compared to the HFSS simulation.

Keywords Metamaterial · Artificial machine learning · Wireless power transfer

1 Introduction

The WPT is a convenient method of delivering power to multi-device without connecting wires. However, the previous approaches indicate that the antenna's field is much leakage to the unload because the receiver coil is small or not close to the source coil [1]. As a result of this, the wireless power transfer efficiency is reduced.

B. H. Nguyen
Department of Physics, Hanoi University of Mining and Geology, 18 Pho Vien, Duc Thang ward, Bac Tu Liem District, Hanoi, Vietnam
e-mail: buihuunguyen@humg.edu.vn

Q.-D. Hoang
Institute of Mechanical Engineering, Vietnam Maritime University, Hai Phong, Vietnam
e-mail: hoangquocdong.vimaru@gmail.com

L. N. T. Huynh (✉)
Thu Dau Mot University, Binh Duong, Vietnam
e-mail: luanhnt@tdmu.edu.vn

T. D. L. Nguyen and J. Lu (eds.), *Machine Learning and Mechanics Based Soft Computing Applications*, Studies in Computational Intelligence 1068,
https://doi.org/10.1007/978-981-19-6450-3_12

Recently, cavity-metamaterials are useful in WPT for enhanced efficiency. Pham et al. [2] investigate the 2D metamaterial, which improves WPT efficiency by using cavities unit cells as the power hotspots. The cavity unit cell metamaterial is created by tuning its properties, which depend on multiple parameters. Thus, the metamaterial design process takes a long time of simulation or complex computation. For numerous designs, the traditional method is unpreferred.

Recently, the ANN has been improved high accuracy and computing rate beyond the human level. The ANN's advantages providing the designed an arbitrary metamaterial structure with high accuracy were approached [3–5]. In [3], the result shows that the ANN has been usefully used to predict the chiral metamaterial's transmission spectra. Furthermore, with extraordinary computing, the ANN shows the significance in reduced calculated time of the metamaterial parameters as investigated in the report [5].

Follow of this trend, in this paper, we propose a rapid design of square-spiral metamaterial parameters using an ANN. Using 2000 (13.3%) testing data of 15,000 random samples, we investigate that the ANN can rapidly successfully predict the square-spiral metamaterial's reflection spectra (S_{11}).

2 Design

Figure 1A shows a schematic of the wireless charging table using the cavity in metasurface assembled by 81 square-spiral unit cells. Six parameters decide the unit cell properties, including the strip width $\boldsymbol{W}$, the metal thickness $\boldsymbol{t_m}$, the spacing $\boldsymbol{S}$, the dielectric thickness $\boldsymbol{t_d}$, unit cell size $\boldsymbol{a}$, and the capacitor $\boldsymbol{C_S}$. Same as our previous work, there are 3.4×10^{11} designs when considering all the combinations of the parameters [6].

Figure 1b shows the simulation result of the H-field distribution of the metasurface. Figure 1c shows the measured relative field magnitude by scanning over the metasurface. The unit cells shaping the cavity area resonate at $\omega_0 = 14$ MHz. Besides, the unit cells of the non-cavity area resonate at $\omega_1 = 0.89\ \omega_0$. The result shows that the relative field amplitude in the cavity region is higher than in the surrounding region, confirmed the simulation result. This phenomenon can be explained by the Fano constructive interference phases between the continuous incident wave and the cavity resonance [2]. Thus, the amplitude of the H-field in the cavity can be increased. As a result, the WPT efficiency can be improved by using a cavity.

Figure 2a indicates four samples of the square-spiral unit cell with a different W. Figure 2b shows the simulated reflection spectra as a frequency function for different W. The graph shows that the square-spiral unit cell's resonance frequency moves to a higher value when W increases dimension. This result can be explained by decreasing the self-inductance of the square-spiral coil.

Figure 3 indicates the illustration of the whole neural network. Two fully-connected networks (FCNs) are used to synthesize the design parameters. The FCN consists of a series of fully-connected layers. Then, the output of the fully-connected

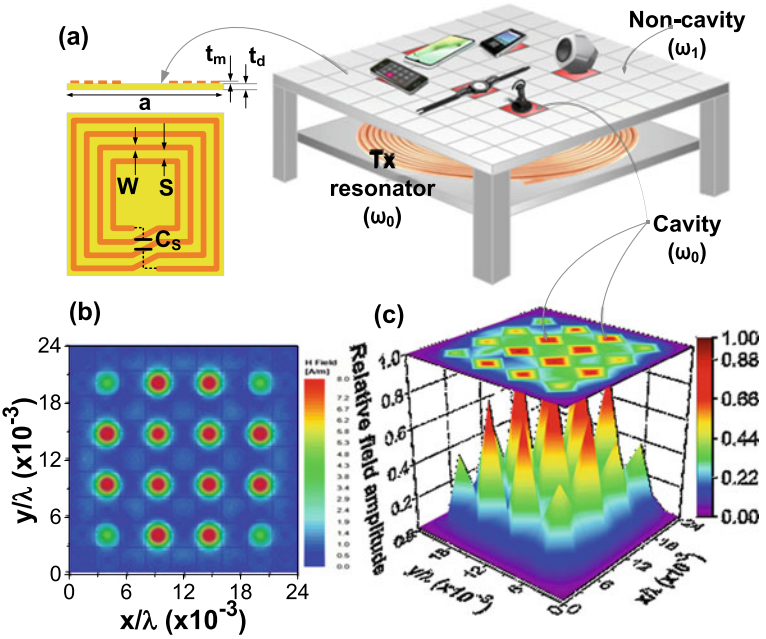

Fig. 1 **a** The WPT charging table using cavity metasurface and six square-spiral unit cell parameters, **b** simulated field distribution on metasurface, **c** measured relative field amplitude distributes on metasurface

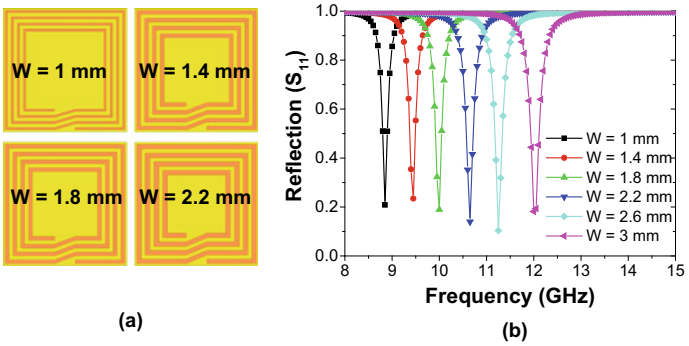

Fig. 2 **a** Four samples of the square-spiral unit cell have different strip widths (***W***), **b** simulated reflection spectra for different strip widths as a function of frequency

layer *i*-th is computed as

$$Y_{\mathrm{i}} = W^{\mathrm{T}} X_{\mathrm{i}} + b_{\mathrm{i}} \tag{1}$$

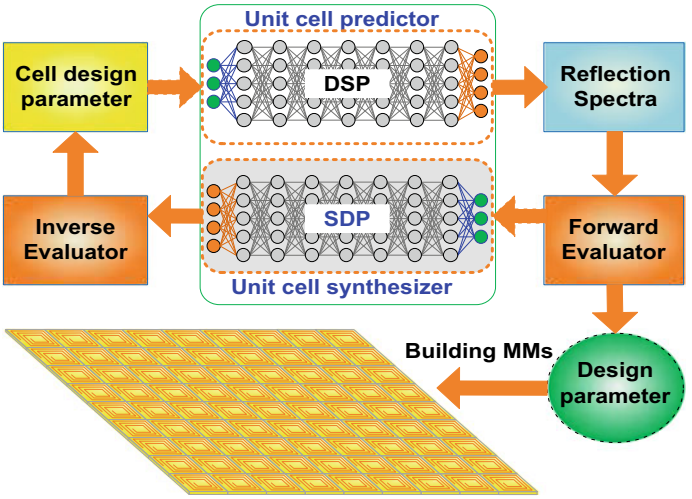

Fig. 3 The DSP and SDP networks are used to predict the reflection spectra and create the design parameters of the square-spiral unitcell

where X_i and Y_i are the input and output of the layer i-th, W^T is called the kernel transposed weight matrix, and b_i is the bias.

The first fully-connected network is the DSP network that predicts reflection spectra from the design parameter. The second fully-connected network is the SDP network that predicts the design parameter from the reflection spectra. Both DSP and SDP networks have nine layers, including an input layer, an output layer, and seven hidden layers with 1024 nodes.

Figure 4 indicates predicting the reflection spectra process of the DSP network. The DSP network creates a 581 point of the reflection spectra (S_{11}). The EM solver and the DSP network create the simulated (R_{Sim}) and predicted (R_{Pre}) reflection spectra. The EM solver and DSP network outputs are used to determine the mean square error (MSE). The MSE is a norm error assessor as

$$\mathrm{MSE}(a, b) = \frac{1}{n}\sum_{i}^{n}(a-b)^2 \tag{2}$$

Figure 5 indicates synthesizing the square-spiral unit cell's design parameters process of the SDP network. From the desired spectra (R_{Des}), the SDP network creates the predicted design parameters (D_{Pre}) compared with the desired design parameters (D_{Des}) for the training process. The D_{Pre} is input to the trained DSP network to create the predicted reflection spectra (R_{Pre}). Both R_{Pre} and R_{Des} are used to achieve test error.

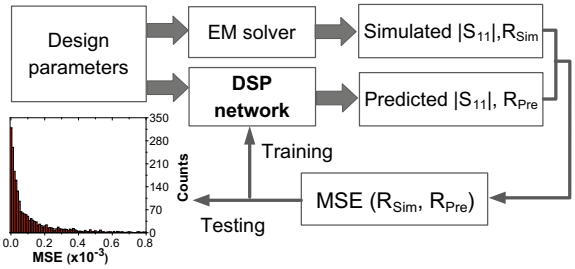

Fig. 4 Schematic of predicting the reflection spectra process of the DSP network

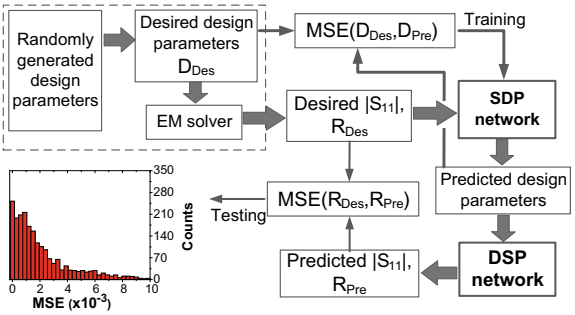

Fig. 5 Schematic of synthesizing the square-spiral unit cell's design parameters process of the SDP network

3 Result and Discussion

Figure 6 displays the samples of testing data for the DSP network operating at the 2500 epoch. The MSE is also shown in each sub-figure. There is 97.4% of the 2000 testing sets have MSE $<0.7 \times 10^{-3}$ when we collect the MSE. The results show that the ANN staunchly recreates the reflection spectra.

Figure 7 displays the samples of testing data for the SDP network operating at the 2500 epoch. There is 95.6% of the 2000 testing sets have MSE $<7 \times 10^{-3}$ when we collect the MSE. The results show that the ANNs can be utilized for synthesizing the dimension of the square-spiral metamaterial unit cell.

We use Tensorflow version 2.1 for ANN and HFSS version 2019 for the EM solver. To compare the computation time, both ANN and HFSS are run on the Dell computer having a 32 GB memory, a GTX1080 GPU, and a core i7 processor. When

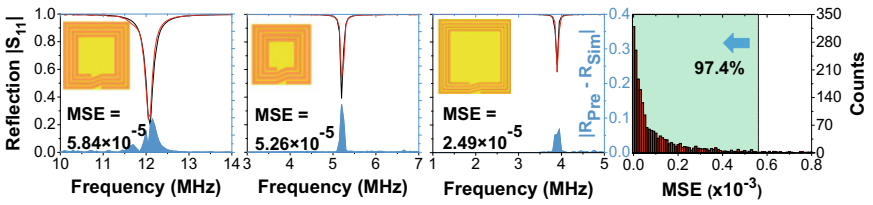

Fig. 6 Samples of random testing data were collected using the DSP network

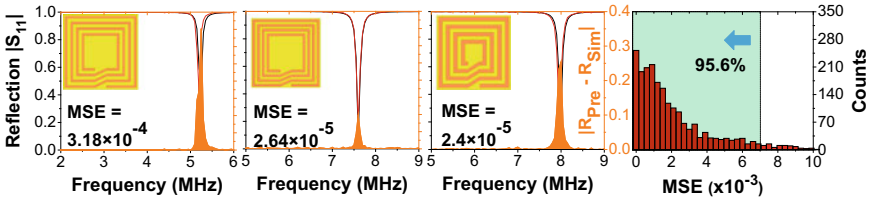

Fig. 7 Samples of random testing data were collected using the SDP network to synthesize the design parameters

Table 1 Comparison with similar studies

	Tahersima et al. [7]	Akashi et al. [8]	Hou et al. [9]	So et al.[10]	An et al. [11]	This work
Sample	20,000	27,000	22,500	18,000	50,000	15,000
Testing set	4000	5000	2500	1800	15,000	2500
Max. layer	8	7	11	6	6	9
MSE	0.58	4.4×10^{-2}	2.95×10^{-4}	6.5×10^{-3}	3.5×10^{-4}	1.5×10^{-4}

1000 samples are calculated, the HFSS simulator takes 195,030 s (54.18 h) while ANN takes 2.1 s. The result shows that the ANN method greatly decreases the simulation time.

The relation with related studies is shown in Table 1. Since each work uses a different ANN structure to analyze a particular physical phenomenon, the comparison between them is difficult. Using this method, they can rapidly predict the device's design parameter from the spectra response; however, a large MSE is obtained. In our work, using nine ANN layers, we realized a comparatively small MSE of 1.5×10^{-4} by using 15,000 samples.

4 Conclusion

In this work, we investigated the ANNs can successfully predict the reflection spectra and synthesize the design parameters. For predicting the reflection spectra, the DSP network approaches 97.4% of the 2000 testing set having MSE $<0.7 \times 10^{-3}$. For synthesizing design parameters, the SDP network approaches 95.6% of the 2000 testing set having MSE $<7 \times 10^{-3}$. Using ANN for 1000 metamaterial designs, the process's computation time was reduced around 93×10^3 times compared to the HFSS simulation.

Acknowledgements This work was supported by Hanoi University of Mining and Geology and by Thu Dau Mot University.

References

1. Ho, J. S., Kim, S., & Poon, A. S. (2013, June). Midfield wireless powering for implantable systems. *Proceedings of the IEEE, 101*, 1369–1378.
2. Pham, T. S., Ranaweera, A. K., Ngo, D. V., & Lee, J. W. (2017, July). Analysis and experiments on Fano interference using a 2D metamaterial cavity for field localized wireless power transfer. *Journal of Physics D: Applied Physics, 50*, 305102.
3. Ma, W., Cheng, F., & Liu, Y. (2018, June). Deep-learning-enabled on-demand design of chiral metamaterials. *ACS Nano, 12*, 6326–6334.
4. Nadell, C. C., Huang, B., Malof, J. M., & Padilla, W. J. (2019, September). Deep learning for accelerated all-dielectric metasurface design. *Optics Express, 27*, 27523–27535.
5. Qiu, T., Shi, X., Wang, J., Li, Y., Qu, S., Cheng, Q., Cui, T., & Sui, S. (2019, April). Deep learning: A rapid and efficient route to automatic metasurface design. *Advancement of Science, 6*, 1900128.
6. Bui, H. N. (2020, October). Design of tunable metasurface using deep neural networks for field localized wireless power transfer. *IEEE Access, 8*, 194868–194878.
7. Tahersima, M. H., Kojima, K., Koike-Akino, T., Jha, D., Wang, B., Lin, C., & Parsons, K. (2019, February). Deep neural network inverse design of integrated photonic power splitters. *Science and Reports, 9*, 1–9.
8. Akashi, N., Toma, M., & Kajikawa, K. (2019, November). Design of metamaterials using neural networks. *Proceedings of SPIE, 11194*, 111940U.
9. Hou, J., Lin, H., Xu, W., Tian, Y., Wang, Y., Shi, X., Deng, F., & Chen, L. (2020, November). Customized inverse design of metamaterial absorber based on target-driven deep learning method. *IEEE Access, 8*, 211849–211859.
10. So, S., Mun, J., & Rho, J. (2019, June). Simultaneous inverse design of materials and structures via deep learning: Demonstration of dipole resonance engineering using core-shell nanoparticles. *Applied Materials & Interfaces, 11*, 24264–24268.
11. An, S., Fowler, C., Zheng, B., Shalaginov, M. Y., Tang, H., Li, H., Zhou, L., Ding, J., Agarwal, A. M., Baleine, C. R., Richardson, K. A., Gu, T., Hu, J., & Zhang, H. (2019). A deep learning approach for objective-driven all-dielectric metasurface design. *ACS Photonics, 6*, 3196–3207.

GIS and RS Application for Land Use Status Quo Mapping in 2020 and Land Use Change Assessing in Thu Dau Mot City

Dang Trung Thanh, Nguyen Huynh Anh Tuyet, Vo Quang Minh, and Pham Thanh Vu

Abstract Effective land utilization and management will be an important foundation for economic and social development. In recent decades, information technology has developed rapidly and has been applied in all areas of life. However, the application of informatic technology, especially digital map system for professional purposes in land management at the commune level in Vietnam, is still limited. Thu Dau Mot city has a total natural land area of 11,890.58 ha, accounting for 4.41% of the total area of Binh Duong province. In recent years, the urbanization rate in Thu Dau Mot city is very high, every year, the fact that the area of agricultural land converted to non-agricultural is very large causes rapid changes in the reality of land use and pressures for management faced by the local government. With the aim of establishing land use status quo map in 2020 quickly, saving time and money for monitoring and evaluating land use changes over the past 5 years, this study is conducted. On the basis of inheriting the maps and data of the past years, processing remote sensing images and applying GIS software in combination with collecting field data, the map of current land use in 2020 is established, and changes of current land use in comparison with that of the year 2015 are assessed. Research results show that the area and percentage of main land use groups of Thu Dau Mot City by the end of 2020 are as follows: (1) Non-agricultural land group is 8929.53 ha (accounting for 75.10% of natural area of Binh Duong province), that area in 2015 is 7530.03 ha (63.33%), increasing an area of 1399.50 ha in 5 years (11.77%); (2) the group of agricultural land in 2020 is 2961.05 ha (24.90%) while that in 2015 is 3133.07 ha (26.35%), that means in 5 years agricultural land decrease an area of 172.02 ha (1.45%); and (3) the group of unused land is 0.00 ha (0.00%), in compared to 2015, that area is 1227.48 ha (10.32%), decreasing 1227.48 ha in 5 years (10.32%). The combination of GIS software with remote sensing images helps to create a land use status quo map effectively. The results of the research are the necessary information for the local government to ensure the sustainable use of land resources.

D. T. Thanh (✉) · N. H. A. Tuyet
Thu Dau Mot University, Binh Duong, Vietnam
e-mail: thanhdt@tdmu.edu.vn

V. Q. Minh · P. T. Vu
Can Tho University, Can Tho, Vietnam

T. D. L. Nguyen and J. Lu (eds.), *Machine Learning and Mechanics Based Soft Computing Applications*, Studies in Computational Intelligence 1068,
https://doi.org/10.1007/978-981-19-6450-3_13

Keywords GIS · Remote sensing image · Current land use · Land use change · Thu Dau Mot City

1 Introduction

Thu Dau Mot City is an administrative, economic, and social center of Binh Duong province. Thu Dau Mot is located about 30 km far from Ho Chi Minh City. The total natural area is 11,890.58 ha [1]. Thu Dau Mot has 14 communal administrative units (Chanh My, Chanh Nghia, Dinh Hoa, Hiep An, Hiep Thanh, Hoa Phu, Phu Cuong, Phu Hoa, Phu Loi, Phu My, Phu Tan, Phu Tho, Tan An, and Tuong Binh Hiep) with an average population of 246,555 people in 2017 and a population density of 1052 people/km^2, higher than that of Binh Duong province (718 people/km^2) [2].

The use of Geographic Information System (GIS) and remote sensing (RS) to monitor the current status and changes of the land cover in recent years has been implemented by many experts and research organizations. There are lots of scientific articles in the world related this research field such as in 2015, Boori MS. et al. studied on the impact of tourism on land use in Jeseníky mountains by using Landsat time-series data (1991, 2001, and 2013) [3]. In 2012, K. Sundarakumar et al. used Landsat TM and ETM$^+$ images captured in Vijayawada City to identify different land use types, and the accuracy obtained is between 73 and 80% for all classified objects [4]. In 2014, O. S. Olokeogun et al. applied GIS and RS to assess the land cover change in Shasha Forest Reserve, Nigeria [5]. In 2018, Pentile Thong et al. studied the shifting cultivation in the Champhai district of Mizoram by using Landsat time-series data in the period of 1999–2016 [6]. In 2019, Sadaf Khan et al. analyze the land use change by using Landsat images in 2011 and 2018; the study noted the gradual decrease of agricultural land in Aligarh, Uttar Pradesh, India [7]. In 2011, Suzanchi, K. and R. Kaur used RS data and GIS to access the agricultural land use changes in the capital of India [8]. Tanveer Ahmed et al., in 2015, used GIS to map the spatial and temporal changes of urban and peri-urban land [9]. In 2019, Wang Yuncai et al. forecasted future land use by simulating land use changes in the past use using GeoSOS-FLUS software and ArcGIS for the peri-urban area of Shanghai [10]. Similar studies were done in Nile Delta [11], Cairo (Egypt) [12], and Kuala Lumpur (Malaysia) [13].

In Vietnam, many studies have been conducted, such as in 2019, Nguyen Van Chung used MicroStation and Famis software to update and adjust the changes of each land parcel and helped the locality to solve their problem accurately, fastly, and economically [14]. Huynh Van Chuong et al., in 2017, applied GIS and Markov chain to evaluate and foresee the trends of land use change in Nha Trang city by 2020 [15]. Nguyen Thuy Cuong et al., in 2019, used time-series remote sensing data and GIS to assess land use changes in Buon Ma Thuot city in the period of 2010–2019 [16]. Trinh Le Hung et al., 2017, used Landsat data captured from 2000 to 2015, Markov CA model, multi-criteria analysis method, and time-based regression method to evaluate and foresee the urban land use change in Hanoi to 2020 [17].

Similar to other studies were done in Kon Tum province [18], Vinh city (Nghe An province) [19], Dong Hy district (Thai Nguyen province) [20]. In Thu Dau Mot City, using GIS and RS to build maps of current land use and assess land use changes has not been published.

In this study, unlike the above scientific publications, we apply GIS, Landsat-8 remote sensing images and MicroStation software to establish the land use status quo map in 2020, and combining with the Tk-tool statistical software, output current land use data according to the land classification table specified by Ministry of Natural Resources and Environment and the land use changes in the last 5 years from 2015 to 2020 will be statisticed as well.

2 Data, Research Process and Method

In this study, the used data, implementation procedure, and method are presented as follows:

2.1 Data and Tool

Data. Land use status quo maps in 2015 and 2019 of Thu Dau Mot City, Cadastral map in 2019 (land parcel map updated to 2019).

Land statistics in 2015; List of land allocation, lease, change of land use purpose of organizations, units, households, and individuals (from January 1 to December 31, 2020).

Landsat-8 remote sensing image with scene indentifier of LC08_L1TP_125052_20201121_20201210_01_T1 downloaded from: https://earthexplorer.usgs.gov/.

GIS. A Geographic Information System designed to work with data in a reference coordinate system. A GIS includes a database system and methods for manipulating that data. GIS is a computer system for collecting, storing, processing, and displaying data related to positions on the Earth's surface. Its functions include:

Data collecting: Data is collected from different sources such as other digital data, scanners, satellite images, and aerial images.

Data storing: After collected and aggregated, data will be stored to ensure the data security, integration, numerical filtering, and evaluation and data maintaining. GIS stores real-world information into separate data layers, these layers are placed in the same coordinate system and they are linked with each other.

Data processing: Data processing is performed to generate information. It helps the user decide what to do next. The result of data processing is the creation of images, reports, and maps. Analysis and modeling: Aggregate and transformation data is only one part of GIS. The next requirements are the ability to decode and analyze qualitatively and quantitatively the information collected.

Data displaying: One of the aspects of GIS technology is the variation of different methods to display the processed information. The traditional methods are tables and graphs that can be supplied with maps and holograms.

MicroStation. It is a Computer-Aided Design—CAD software developed and distributed by Bentley Systems. MicroStation has very powerful graphic tools that allows to construct and manage vector objects for digital map. MicroStation is also designed to be compatible with other software such as Famis, Geovec, MSFC, Irasb, Mrfclean and eMap, and eTools. It helps to digitize objects from raster data, then edit data and display maps. It also supports to import and export vector data from other data format via *.dxf, *.dwg files.

Especially in map editing and displaying, it is easier to design point, line, and region objects and use lots of map layout methods than other softwares such as MapInfo, CorelDraw, AutoCAD, and Adobe Freehand.

Tk-tool. It runs on desktop without an Internet connection and helps to statictis and inventory the data on land use for the administrative level of commune. There are two steps in using this tool: (i) importing the statistics and inventory data for the commune level and (ii) exporting the imported data to *.data file.

2.2 Research Process and Method

Preparation. Using the land use status quo maps in 2019 to update and adjust changes in land use purposes basing on the statistical data of performed projects in 2020.

Using Landsat-8 image to internally adjust the fluctuating areas compared to the 2019 map on the MicroStation software, note the unknown areas and print out paper files for field inspection.

Field survey. Use printed paper file maps to survey the above suspicions about contents such as land parcel boundaries, land correction, and delineation and check the area of the fluctuated parcels of land.

Mapping. Land use status quo map of Thu Dau Mot City was generated from the land use quo maps wards located in Thu Dau Mot City by MicroStation software. This process requires to prepare following digital maps:

Files of maps are in the format of *.dgn of MicroStation Software and contains the map information and symbol source file. They must be an open format that allow to edit and update information, be able to convert to other formats, and have Vietnamese fonts, numbers, Unicode encoding; the independent symbols are available in the "HT" library with many scale ranges named ht1-5.cell, ht10-25.cell, ht50-100.cell, respectively.

Parameters of seed file include working units; master units of meters (m); sub-units of millimeters (mm); resolution of 1000; and the Storage Center point of X: 500,000 m and Y: 1,000,000 m.

Line objects must be continuous, not breaking and only ending line at the intersection points between the lines of the same object type; region objects must be closed

areas; and point objects must be shown by point symbol types pre-designed in *.cell files.

Data aggregation. On the land use status quo map, it is necessary to make the region objects that need to calculate their area (including land blocks or objects occupying land that not forming the land parcel) be closed and determine their spatial relationship.

For same region objects (such as traffic objects or hydrological objects), when they intersect at the same level, these objects are calculated according to the outermost land occupation boundary. On the other hand, when the different region objects intersect or the same region object intersect at the different level, intersection area of the vertical projection of these objects is calculated for the objects laying on the ground).

The area of land parcels is calculated based on the shape of region objects on the digital maps. Then, that area is checked again with the total area of the communes based on the administrative boundary. In case of having any difference, it is necessary to check the overlapping and omission of land parcels.

The data of land use status of the wards are synthesized from the data of land plots using Tk-tool. Thu Dau Mot City data is aggregated from ward data. In the process of synthesizing data of the city, if detecting errors, return to check and edit from the ward level to correct and aggregate them to ensure consistency from ward to city.

Accuracy requirements are ensured at two levels (direct implementation, and inspection), in accordance with the provisions of Circular No. 49/2016/TT-BTNMT of Ministry of Natural Resources and Environment dated December 28, 2016, about Regulations on the supervision, inspection, appraisal, and acceptance of works and products in the field of land management. Specifically, at level 1, the authors check at least 60% of the total zoning on the map, and then survey and inspect the 20% of the zoning in the field. At level 2, the authorities will be checked for 15% of the total zoning and 5% of the zoning in the field for their approval. In this study, at level 1 of inspection, we randomly checked internally 1272/2120 plots of land with the realistic image captured by Landsat-8 satellite. Among them, there are 1082 plots of land having the same land use type, reaching an accuracy rate of 85%. After that, the 424 other land plots were checked externally, and 361 blocks of land are correct (reaching the accuracy rate of over 85%). Currently, level 2 inspection is being performed (Fig. 1).

3 Results and Discussions

The research results are the land use status quo map, data of agricultural and non-agricultural land use reality of Thu Dau Mot City at the end of 2020 and data of their changes over the past 5 years. Details are as follows.

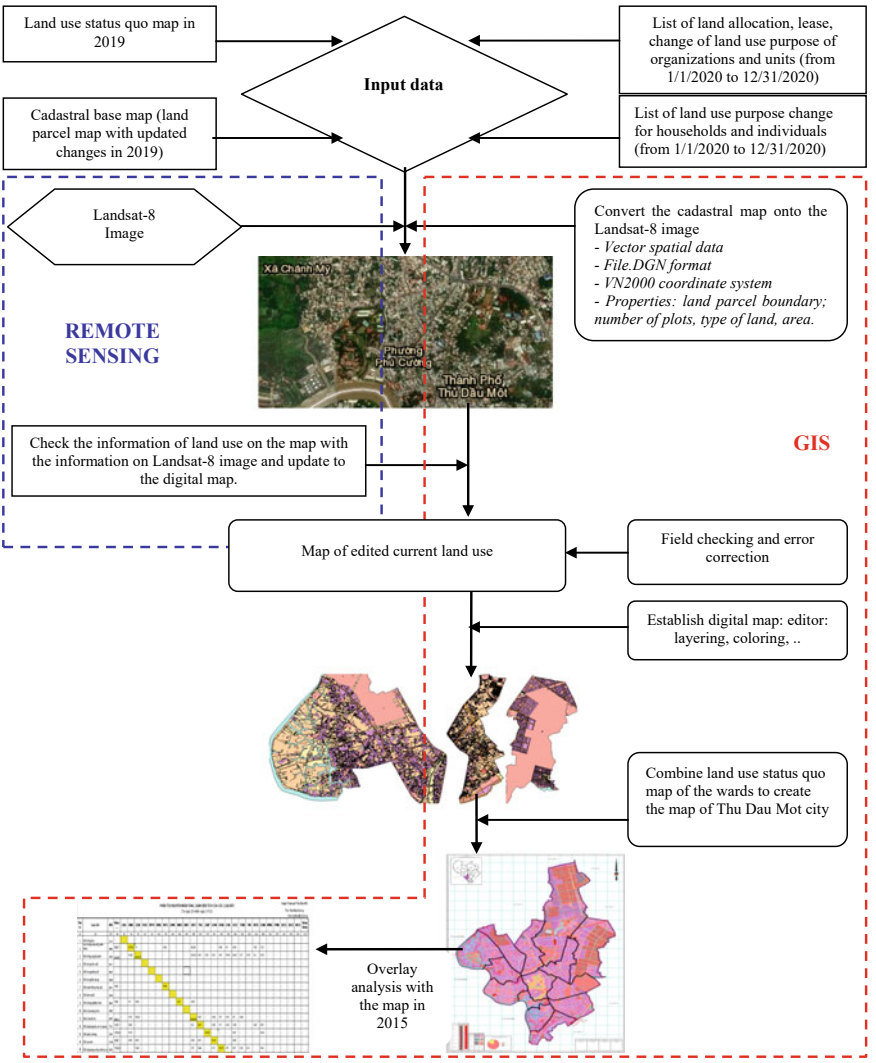

Fig. 1 Implementation progress diagram

3.1 Land Use Status Quo Map of Thu Dau Mot City

Land use status quo map in 2020 of each ward is established on the MicroStation software by overlaying the work or project's boundaries and land parcels that changes in land use purpose of organizations, households, or individuals in 2020 onto land use status quo map in 2019, after that checking with land use shown on Landsat-8 satellite images and field inspection.

Land use status quo map in 2020 of Thu Dau Mot City was established on the basis of borderline and aggregation the land use status quo maps of the wards.

From the land use status quo map in 2020, area of each block can be calculated and data of all kinds of land use for each administrative unit of wards and the whole city can be exported with the supporting of Tk-tool (Fig. 2).

3.2 Reality of Agricultural Land

The area of agricultural land of Thu Dau Mot City is 2961.05 ha by the end of 2020, accounting for 24.90% of the total natural area of the city.

In the group of land for agriculture, the land for perennial crops has the largest area of 2252.99 ha (76.09% over total agricultural land area) and other agricultural land has the smallest area of 10.79 ha (0.36%), this is the land used for the purpose of making livestock barns, warehouses for machinery, and agricultural materials.

Tan An ward has the largest agricultural land area of 579.99 ha, accounting for 19.59% of the agricultural land of Thu Dau Mot City. This is a ward located in the northwest of the city, next to Saigon River, so its alluvial soil is suitable for growing vegetables, fruit trees, and developing ecotourism serving urban residents (Table 1).

3.3 Reality of Non-agricultural Land

In 2020, the area of the non-agricultural land of Thu Dau Mot City is 8929.53 ha, making up 75.10% of the total area of the City (Table 2).

Among non-agricultural land types, specialized land has the largest area of 5316.29 ha (accounting for 59.54% of the total non-agricultural land area) and religious land has the smallest area of 15.14 ha (0.17%). This is the land used for the construction of religious works, including communal houses, temples, shrines, and clan ancestral house.

Hoa Phu ward has the largest area of non-agricultural land at 2778.62 ha, accounting for 31.12% of the non-agricultural land area of Thu Dau Mot City, because the ward has large construction works such as the new city's administrative areas with resettlement areas, urban industrial parks, services, and complexes, so the land area for non-agricultural purposes accounts for a high proportion.

3.4 Land Use Changes in the Period of 2015–2020

Land use changes in the period of 2015–2020 are obtained by overlap analysis the two land use status quo maps in 2020 and 2015, the results are presented in Table 3 and Fig. 3.

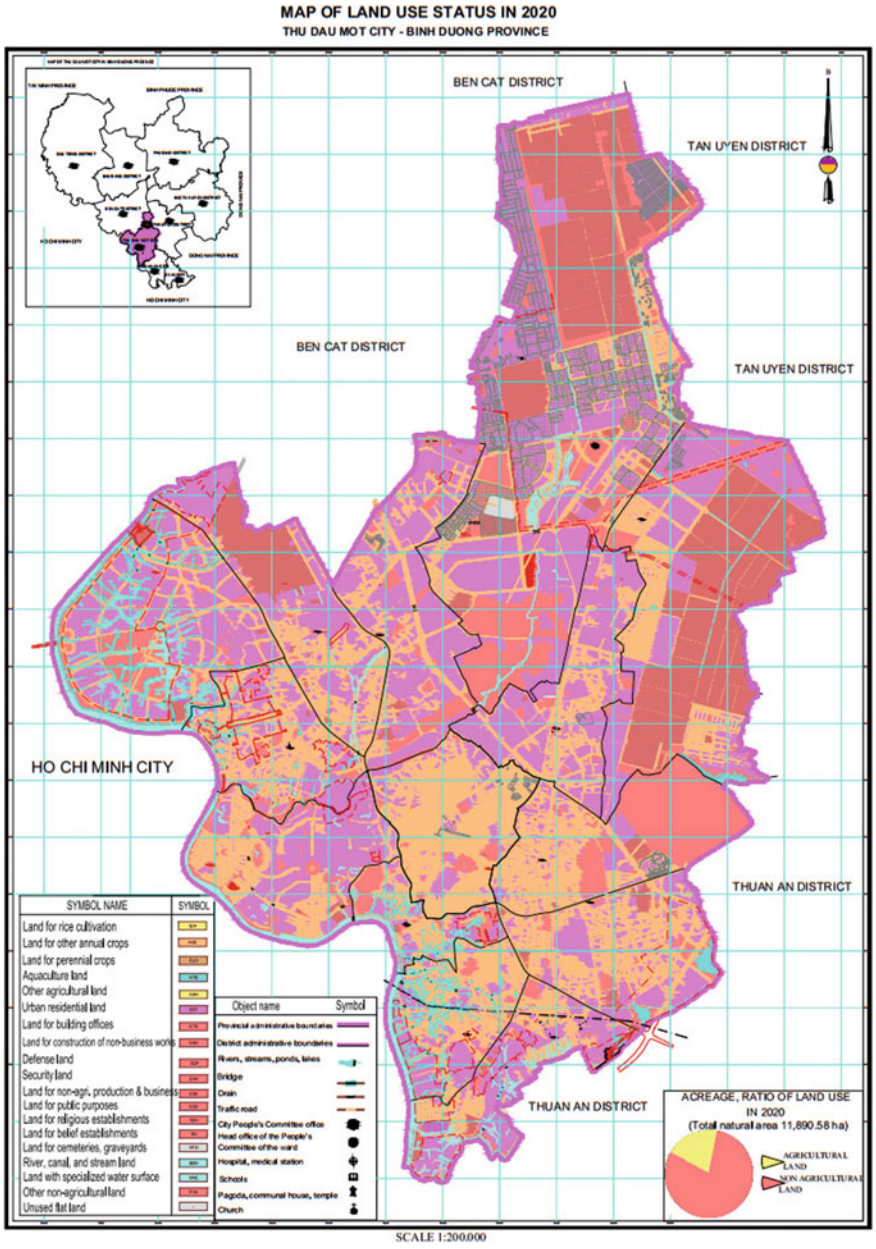

Fig. 2 Land use status quo map of Thu Dau Mot in 2020

Table 1 Current agricultural land in 2020

No.	Land use type	Total area	Area at ward level													
			Chanh My	Chanh Nghia	Đinh Hoa	Hiep An	Hiep Thanh	Hoa Phu	Phu Cuong	Phu Hoa	Phu Loi	Phu My	Phu Tan	Phu Tho	Tan An	Tuong Binh Hiep
(1)	(2)	(3) = (4) + ⋯ + (17)	(4)	(5)	(6)	(7)	(8)	(9)	(10)	(11)	(12)	(13)	(14)	(15)	(16)	(17)
	Agricultural land	**2961.05**	**259.00**	**146.47**	**413.15**	**225.49**	**158.81**	**70.70**	**2.45**	**196.55**	**104.93**	**287.97**	**15.21**	**210.63**	**579.99**	**289.73**
1.1	***Land for agriculture production***	***2938.35***	***252.28***	***146.45***	***413.15***	***225.41***	***158.81***	***70.70***	***2.45***	***196.55***	***104.93***	***281.45***	***15.21***	***209.77***	***578.09***	***283.10***
1.1.1	Annual crop land	685.35	167.50	4.95	30.68	40.52	18.05		0.34	126.86	44.97	35.66	2.24	32.08	115.73	65.78
1.1.1.1	Land for rice cultivation															
1.1.1.2	Land for other annual crops	685.35	167.50	4.95	30.68	40.52	18.05		0.34	126.86	44.97	35.66	2.24	32.08	115.73	65.78
1.1.2	Land for perennial crops	2252.99	84.78	141.50	382.48	184.89	140.76	70.70	2.11	69.69	59.95	245.79	12.97	177.69	462.36	217.32
1.2	***Forestry land***															

(continued)

Table 1 (continued)

No.	Land use type	Total area	Area at ward level													
			Chanh My	Chanh Nghia	Đinh Hoa	Hiep An	Hiep Thanh	Hoa Phu	Phu Cuong	Phu Hoa	Phu Loi	Phu My	Phu Tan	Phu Tho	Tan An	Tuong Binh Hiep
(1)	(2)	(3) = (4) + ⋯ + (17)	(4)	(5)	(6)	(7)	(8)	(9)	(10)	(11)	(12)	(13)	(14)	(15)	(16)	(17)
1.3	***Aquaculture land***	***11.93***	***6.72***	***0.02***		***0.07***								***0.86***	***0.69***	***3.58***
1.4	***Salt production land***															
1.5	***Other agricultural land***	***10.78***										***6.52***			***1.21***	***3.05***

Table 2 Current non-agricultural land in 2020

No.	Land use type	Total area	Area at ward level													
			Chanh My	Chanh Nghia	Đinh Hoa	Hiep An	Hiep Thanh	Hoa Phu	Phu Cuong	Phu Hoa	Phu Loi	Phu My	Phu Tan	Phu Tho	Tan An	Tuong Binh Hiep
(1)	(2)	(3) = (4) + ⋯ + (17)	(4)	(5)	(6)	(7)	(8)	(9)	(10)	(11)	(12)	(13)	(14)	(15)	(16)	(17)
	Non-agricultural land	**8929.53**	**430.39**	**329.96**	**379.37**	**455.83**	**427.74**	**2778.62**	**242.01**	**460.23**	**608.02**	**342.10**	**1522.47**	**279.68**	**442.39**	**230.73**
2.1	***Residential land***	***3142.58***	***209.60***	***158.05***	***154.75***	***168.76***	***244.35***	***656.16***	***119.34***	***290.18***	***160.66***	***218.54***	***298.30***	***119.16***	***220.91***	***123.84***
2.2	***Specialized land***	***5316.30***	***123.02***	***131.88***	***216.03***	***275.47***	***170.59***	***2077.92***	***95.03***	***162.34***	***444.89***	***117.78***	***1224.17***	***124.88***	***71.25***	***81.05***
2.2.1	Land for building offices	33.31	1.73	0.99	0.60	1.53	4.80	8.12	5.30	1.19	3.57	0.49	2.72	0.34	1.54	0.39
2.2.2	Defense land	367.03			3.78		12.12		34.74	4.70	311.69					
2.2.3	Security land	19.48		9.93	0.31	0.23	3.36	0.72	0.07	0.16	0.06	3.94	0.35	0.08	0.08	0.17
2.2.4	Land for construction of non-business works	844.78	11.24	11.27	41.77	8.10	25.34	651.94	7.65	24.05	10.33	11.59	7.51	14.40	6.92	12.67
2.2.5	Land for non-agricultural production and business	2278.40	17.26	28.47	35.47	212.94	25.68	846.38	3.38	46.04	47.36	12.52	938.85	34.28	13.24	16.52

(continued)

Table 2 (continued)

No.	Land use type	Total area	Area at ward level													
			Chanh My	Chanh Nghia	Đinh Hoa	Hiep An	Hiep Thanh	Hoa Phu	Phu Cuong	Phu Hoa	Phu Loi	Phu My	Phu Tan	Phu Tho	Tan An	Tuong Binh Hiep
(1)	(2)	(3) = (4) + ⋯ + (17)	(4)	(5)	(6)	(7)	(8)	(9)	(10)	(11)	(12)	(13)	(14)	(15)	(16)	(17)
2.2.6	Land for public purposes	1773.30	92.80	81.21	134.10	52.67	99.28	570.76	43.90	86.19	71.87	89.24	274.75	75.77	49.48	51.29
2.3	***Land for religious establishments***	***33.72***	***2.28***	***4.48***	***3.68***	***0.58***	***4.36***	***2.02***	***7.34***	***1.19***	***0.65***	***0.12***		***3.44***	***3.20***	***0.39***
2.4	***Land for belief establishments***	***15.14***	***0.30***	***0.40***	***1.87***	***0.78***	***0.24***		***0.00***	***1.08***	***0.79***	***3.58***		***0.92***	***4.86***	***0.32***
2.5	***Land for cemeteries, graveyards, and funeral homes***	***41.36***	***0.85***	***2.79***	***0.94***	***4.24***	***3.90***	***19.46***		***0.26***	***1.04***	***1.41***		***0.10***	***5.87***	***0.51***
2.6	***Land for rivers, canals, channels, and streams***	***363.00***	***94.34***	***32.36***	***2.09***	***6.01***	***2.60***	***7.71***	***20.30***	***5.19***		***0.66***		***31.19***	***135.93***	***24.63***
2.7	***Land with specialized water surface***	***17.43***					***1.72***	***15.35***							***0.37***	
2.8	***Other non-agricultural land***															

Table 3 Changes of land use types' area in the period of 2015–2020

No.	Land use type	Code	2015	LUA	HNK	CLN	RSX	RPH	RDD	NTS	NKH	ONT	ODT	TSC	CQP	CAN	DSN	CSK	CCC	TON	TIN	NTD	SON	MNC	PNK	BCS	Total decrease	Change	2020
(1)	(2)	(3)	(4)	(5)	(6)	(7)	(8)	(9)	(10)	(11)	(12)	(13)	(14)	(15)	(16)	(17)	(18)	(19)	(20)	(21)	(22)	(23)	(24)	(25)	(26)	(27)	(28)	(29)	(30)
1	Land for rice cultivation	LUA																											
2	Land for other annual crops	HNK	**685.70**		607.67	11.00				0.02			43.26				9.14	5.10	6.85			1.32	1.33				78.02	−0.35	**685.35**
3	Land for perennial crops	CLN	**2430.50**		18.29	2136.27							231.23	0.81	3.78	0.07	1.91	13.68	21.38	0.17	0.78	1.40	0.76				294.26	−177.51	**2252.99**
4	Production forest land	RSX																											
5	Protection forest land	RPH																											
6	Special-use forest land	RDD																											
7	Aquaculture land	NTS	**11.93**							11.92									0.02								0.02		**11.93**
8	Other agricultural land	NKH	**4.94**		0.50	0.08					4.27		0.09						0.01								0.68	5.84	**10.78**
9	Rural residential land	ONT																											
10	Urban residential land	ODT	**1956.06**		0.78	14.62							1924.65	0.01		0.05	1.75	5.93	7.60	0.64							31.38	1186.52	**3142.58**
11	Land for building offices	TSC	**39.91**		0.02								0.20	29.30		0.09	1.71	4.36	3.96			0.27	0.01				10.62	−6.60	**33.31**
12	Defense land	CQP	**375.03**		12.13										361.47		1.00		0.07				0.36				13.56	−8.00	**367.03**
13	Security land	CAN	**18.08**		0.09	0.03							0.07	0.15		17.48			0.26								0.60	1.40	**19.48**
14	Land for construction of non-business works	DSN	**778.63**			11.24							1.79	0.66		0.18	752.77	1.77	9.77	0.19	0.11		0.16				25.87	66.15	**844.78**
15	Land for non-agricultural production and business	CSK	**2404.07**		20.24	50.99							90.90	0.03	1.78	0.16	1.64	2180.70	55.85			1.79					223.38	−125.67	**2278.40**
16	Land for public purpo ses	CCC	**1447.75**		2.03	3.12							0.42	0.14			0.49	1.71	1438.52				1.34				9.25	325.55	**1773.30**
17	Land for religious establishments	TON	**32.63**														0.73		0.15	31.75							0.88	1.09	**33.72**
18	Land for belief establishments	TIN	**14.86**										0.06						0.43	0.12	14.26						0.61	0.28	**15.14**
19	Land for cemeteries, graveyards, funeral homes	NTD	**81.54**		15.86	21.77							0.80			0.90	1.05		4.58			36.57					44.96	−40.18	**41.36**
20	Land for rivers, canals, channels and streams	SON	**356.94**													0.03			2.84				354.07				2.87	6.06	**363.00**
21	Land with specialized water surface	MNC	**17.85**																				0.42	17.43			0.42	−0.42	**17.43**
22	Other non-agricultural land	PNK	**6.68**								6.52								0.16								6.68	−6.68	
23	Unused flat land	BCS	**1227.48**		7.73	3.90							849.08	2.22		0.52	72.60	65.16	220.87	0.85			4.55				1227.48	−1227.48	
24	**Total increase**				**77.67**	**116.75**				**0.02**	**6.52**		**1217.90**	**4.02**	**5.56**	**2.00**	**92.02**	**97.71**	**334.80**	**1.97**	**0.89**	**4.78**	**8.93**						

Note Change (29) = Total increase (24) − total decrease (28) for each land use type

Data in this cell is the unchanged area of each land use type in 5 years

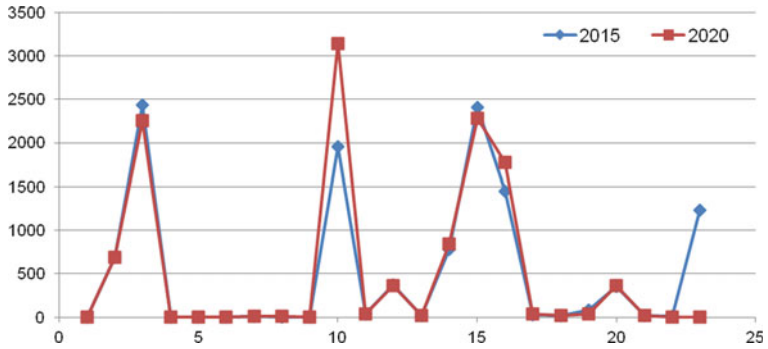

Fig. 3 Chart of land use changes in 2015–2020

Changes of agricultural land: Agricultural land area in 2020 decreases 172.02 ha in comparison to that of 2015, an average decrease of 34.40 ha/year, details are as follows:

- Other annual crop land area in 2015 is 685.70 ha, in 5 years it increases 77.67 ha due to the conversion of other land and decreases 78.02 ha due to conversion to non-agricultural land. In general, it decreases by 0.35 ha, so its area in 2020 is 685.35 ha.
- Perennial land area in 2015 is 2430.50 ha, in 5 years it increases 116.75 ha due to other land conversion, and at the same time it reduces 294.26 ha due to conversion to non-agricultural land. In general, its area decreases by 177.51 ha, so its area up to 2020 is 2252.99 ha.
- Aquaculture land area in 2015 is 11.93 ha, in the past 5 years this land type increased 0.02 ha due to the conversion of land for other annual crops, and it also decreased 0.02 ha due to conversion to public land. In general, its area is not changed and the area by 2020 is 11.93 ha.
- Other agricultural land area in 2015 is 4.94 ha, in the past 5 years, it increases by 6.52 ha due to the conversion of other non-agricultural land, at the same time, it decreased by 0.68 ha due to the conversion to other annual crop land (0.5 ha), land for perennial crops (0.08 ha), residential land (0.09 ha) and land for public works (0.01 ha). In general, it increases by 5.84 ha, and the area by 2020 is 10.78 ha.

Changes of non-agricultural land: The area of non-agricultural land increases by 1399.50 ha in comparison with that of 2015, an average increase of 279.90 ha/year.

Changes of unused land: The unused land area has been fully used by 1227.48 ha in 2020; the unused land decreases with an average area of 245.50 ha/year, unused land decreases due to changing into other using purposes.

The chart 3 shows that the type of urban residential land (land type No. 10) in the past 5 years has drastically increased, caused by the economic development, the strong growth of real estate market in the period from 2017 to 2019. In this period, there were many residential projects built in Thu Dau Mot City such as Takara Residence (Chanh Nghia ward) with an area of 19 ha, Chanh My ecological urban

area (Chanh My ward) with an area of 372 ha, Happy One detached apartment (Phu Hoa ward) with an area of 0.6 ha, Luxcity project area (Tuong Binh Hiep ward) with an area of 2.5 ha, and Sun Casa Binh Duong residential area (Phu Hoa ward) with an area of 6.0 ha.

4 Conclusion

Application of GIS software and remote sensing images helps to create land use status quo map and assess land use change quickly, economically, and accurately, makes the land management at the commune and district level more convenient and effective.

The results have contributed to establish the land use status map in 2020 serving for the land management of the local government as well as the future development planning of relevant areas. Aggregate data from the study have demonstrated that area of agricultural land has rapidly reduced due to the urbanization and industrialization that lead to the transition of agricultural land to non-agricultural land in the past 5 years (34.40 ha on average/year), at the same time, the unused bare land area has been exploited and used with an average area of 245.50 ha per year.

Due to budget limitation, the study used free images with medium spatial resolution so the results did not get highest accuracy. In subsequent studies, for better results, images with higher spatial resolution would be used to provide the most accurate information for policymakers in the future. At the same time, it is necessary to continue to study technical solutions to fully automate the convertible input data source to create land use status quo maps and ensure the accuracy for each 6-month and annual report of the professional sector and administrative management levels from commune to district and province.

References

1. Thu Dau Mot Town People's Committee, Land Inventory 2019.
2. Thu Dau Mot Town People's Committee—Thu Dau Mot Town Statistics Office, Statistical Yearbook 2020.
3. Boori, M. S., Vozenilek, V., & Choudhary, K. (2015). Land use/cover disturbances due to tourism in Jeseniky Mountain, Czech Republic: A remote sensing and GIS based approach. *The Egyptian Journal of Remote Sensing and Space Sciences, 17*, 01–10. https://doi.org/10.1016/j.ejrs.2014.12.002
4. Sundarakumar, K., Harika, M., Aspiya Begum, S. K., Yamini, S., Balakrishna, K. (2012). Land use and Land cover change detection and urban Sprawl analysis of Vijayawada city using multitemporal landsat data. *International Journal of Engineering Science and Technology, 4*(01), 170–178, ISSN: 0975-5462.
5. Olokeogun, O. S., Iyiola, K., & Iyiola, O. F. (2014). Application of remote sensing and GIS in land use/land cover mapping and change detection in Shasha Forest Reserve, Nigeria.

ISPRS-International Archives of the Photogrammetry. *Remote Sensing and Spatial Information Sciences, XL-8*, 613–616. https://doi.org/10.5194/isprsarchives-XL-8-613-2014
6. Thong, P., et al. (2018). A Geospatial approach to understand the dynamics of shifting cultivation in Champhai District of Mizoram, North-East India. *Journal of the Indian Society of Remote Sensing, 46*(10), 1713–1723.
7. Khan, S., et al. (2019). The impact of urban expansion on agricultural land use changes in Aligarh, Uttar pradesh, India. In *Workshop on "Earth Observations for Agricultural Monitoring"*, 18–20 February, 2019, New Delhi, India. The International Archives of the Photogrammetry, Remote Sensing and Spatial Information Sciences, Volume XLII-3/W6, 2019 ISPRS-GEOGLAM-ISRS Joint Int, pp. 381–384.
8. Suzanchi, K., & Kaur, R. (2011). Land use land cover change in National Capital Region of India: A remote sensing and GIS based two decadal spatial-temporal analyse. *Procedia-Social and Behavioral Sciences, 2011*(21), 212–221.
9. Ahmed, T., et al. (2015, August). Change of agricultural land use in residential land and its impact on the socio-economic status of the farmer in Bahawalpur city. *Asian Journal of Social Sciences & Humanities, 4*(3), 120–127.
10. Yuncai, W., et al. (2019). Backcasting approach with multi-scenariosimulation for assessing effects of land use policyusing GeoSOS-FLUS software. *Elsevier B.V. MethodsX, 6*(2019), 1384–1397.
11. Hereher, M. (2010). Vulnerability of the Nile Delta to sea level rise: An assessment using remote sensing. *Geomatics, Natural Hazards and Risk, 1*, 315–321.
12. Hereher, M. E. (2012). Analysis of urban growth at Cairo, Egypt using remote sensing and GIS, Department of Environmental Sciences, Faculty of Science at Damietta, Mansoura University, Mansoura, Egypt, Natural Science 4, 4(6), 355–361.
13. Boori, M. S., Choudhary, K., & Kovelskiy, V. (2015). Kuala Lumpur city growth study through remote sensing and GIS. *Journal Remote Sensing & GIS, 4*(2), 1000e112.
14. Van Chung, N. (2009). Application of MicroStation and Famis software in updating and adjusting land changes on the cadastral map of Tan Quy Ward, Tan Phu District, Ho Chi Minh City. Graduated thesis of bachelor of Land Management—Agriculture and Forestry University of Ho Chi Minh City, DH05QL: 2005–2009.
15. Van Chuong, H. Vo Trung Thong, C., & Hung, H. C. (2017). Research and forecast land use changes in Nha Trang city, Khanh Hoa province by applying Markov chains and GIS. *Journal of Science and Agriculture, 1*(1), 37–46, ISSN 2588-1256.
16. Cuong, N. T., Vung, N. X., & Linh, N. B. (2019). Assessing land use changes based on analysis of multi-time remote sensing data sources and GIS technology in Buon Ma Thuot city, Dak Lak province. In *Proceedings of National GIS Application Workshop*, pp. 431–441, ISBN: 978-604-60-3104-8.
17. Le Hung, T., Nga, N. T. T., Tuyen, V. D., & Phuong, B. T. (2017). Assessment and forecast of urban change in Hanoi city inner area by remote sensing and GIS data. *Journal of Ho Chi Minh City University of Pedagogy, 14*(3), 176–187.
18. Nguyen, U. K. (2014). Application of GIS to assess land use change in Kon Tum province in the period of 2005–2010, graduation thesis, Environmental Information System, Faculty of Environment and Natural Resources, University Ho Chi Minh City agriculture and forestry.
19. Ngoc Phi, N. (2006). *Remote sensing application to monitor soil changes in Vinh city*, Nghe An province, Institute of Geology, Institute of Science and Technology of Vietnam, 84—Chua Lang, Dong Da, Hanoi.
20. Viet, T. V. (2014). Application of Microstation and Famis software for editing, making cadastral maps and adjusting land use changes. Graduated thesis of bachelor of Environment Cadastral of Agriculture and Forestry University (Thai Nguyen University), 42B: 2014–2019.

Particle Swarm Optimization for Acceleration Tracking Control of an Actuator System

Quoc-Dong Hoang, Bui Huu Nguyen, and Luan N. T. Huynh

Abstract In this study, a platform of a fluid-power actuator system with a combination of electro-hydraulic and pneumatic for acceleration tracking control is proposed. Furthermore, a control strategy is provided to obtain high-performance results in controlling the piston's motion. Here, the particle swarm optimization (PSO), a computational method, is appropriately utilized for selecting the parameters of the classical proportional integral derivative (PID) control. The tracking errors are eliminated without the challenge of the tuning process, and the control performance is further enhanced. In order to validate the effectiveness of the control strategy, the numerical simulation results are eventually given. The remarkable result of the paper is that the position tracking control is precisely guaranteed when applying only a traditional PID controller with optimized parameters by using the PSO algorithm.

Keywords Hydraulic servo actuator (HPA) system · Acceleration tracking · Actuator position tracking · Velocity control · Particle swarm optimization (PSO)

1 Introduction

Pneumatic and hydraulic are the kinds of fluid-power technologies that are commonly utilized in industries, such as in robotics, factories, handling and lifting machine, and constructions. They show the high-performance abilities in control areas with

Q.-D. Hoang
Institute of Mechanical Engineering, Vietnam Maritime University, Hai Phong, Vietnam
e-mail: hoangquocdong.vimaru@gmail.com

B. H. Nguyen
Department of Physics, Hanoi University of Mining and Geology, 18 Pho Vien, Duc Thang ward, Bac Tu Liem District, Hanoi, Vietnam
e-mail: buihuunguyen@humg.edu.vn

L. N. T. Huynh (✉)
Thu Dau Mot University, Binh Duong, Vietnam
e-mail: luanhnt@tdmu.edu.vn

T. D. L. Nguyen and J. Lu (eds.), *Machine Learning and Mechanics Based Soft Computing Applications*, Studies in Computational Intelligence 1068,
https://doi.org/10.1007/978-981-19-6450-3_14

transmission from the high energy place to the lower in order to drive the actuator or implement the machines' actions. Hydraulic is typically used in heavy-load and high-precision systems, whereas pneumatic is a technical feature that provides elasticity by utilizing compressed gas. This research proposes a hybrid system that combines the electro-hydraulic and pneumatic to obtain the accuracy of the rapid tracking accelerations. The system will utilize the advantages of both types of fluid transmission technologies.

Numerous methods have been developed and effectively implemented to address the problem of the control actuator. There are various studies to enhance system reliability, such as classical PID control [1], LQR control [2], nonlinear control [3–5], and intelligent control [6].

Using particle swarm optimization (PSO) [7], a high-level heuristic (i.e., metaheuristic) achieved satisfactory results in solving a difficult optimization problem. PSO is capable of solving large-scale NP problems in polynomial time while maintaining convergence within specified limits. PSO has the advantages of being simple to implement and fast to converge, as well as the ability to escape local optima and converge to a near-global optimum. Therefore, the application of this algorithm is increasing, for example, communication [8] and in the control area [9].

For rapid tracking acceleration control, the paper presents an approach based on a combination of traditional PID and PSO algorithms to save time and effort for defining controller coefficients, enhancing the controller's quality. The performance of the entire job is surveyed through simulations. The main contribution of this research is developing and providing a new approach for fluid-power actuator control with high performance and optimized controller parameters.

2 Formula Problem and Control Strategy

In Fig. 1, the structure of the hybrid pneumatic–hydraulic actuator is provided. This is a combination that takes advantage of the superior properties of both hydraulic and pneumatic transmission [9]. The energy of the compressible pneumatic plays the role of driving the piston moving with the external mass. The hydraulic brake's restricting force controls the precise acceleration of the piston and its mass. As a result, active forces and frictional restraining forces affect the operating actuator. Based on [9], the motion of the piston and the mass $\chi_P(t)$ is illustrated by the equations as

$$\begin{bmatrix} (m_P + m_L)\ddot{\chi}_P + b_P\dot{\chi}_P + K_L\chi_P + (a_P - a_R)p_{p1} + sgn(\dot{\chi}_P)F_{fc0} \\ +sgn(\dot{\chi}_P)F_{fs0}e^{\frac{-|\dot{\chi}_P|}{c_s}} - a_P p_{P2} + \mu_{d0}(n_v e^{-m_v\dot{\chi}_P} + 1)a_B p_B \end{bmatrix} = 0, \quad (1)$$

where m_L and m_P are the masses of external load and the piston; b_P is the coefficient of the piston–cylinder friction; K_L denotes the equivalent stiffness; F_{fc0} and F_{fs0} represent the parameters for static and Coulomb friction; and a_R and a_P are cross-piston rod section areas and the piston effective, respectively. Additionally, p_B is the

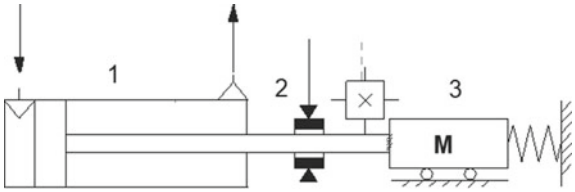

Fig. 1 Experimental HEHPA system configuration (*1-pneumatic cylinder, 2-hydraulic brake system, 3-external mass*)

brake chamber pressure; a_B indicates the brake piston effective area; μ_{d0} denotes the steady-state friction coefficient between the piston rod and brake pad; and m_v and n_v denotes parametric coefficient of the exponential function and the multiplication factor of the friction speed.

The function $sgn(\dot{\chi}_P)\left(F_{fc0} + F_{fs0}e^{\frac{-|\dot{\chi}_P|}{c_s}}\right)$ describes the external friction force, and the signum function of actuator's velocity $\dot{\chi}_P(t)$ is defined as

$$sgn(\dot{\chi}_P) = \begin{cases} +1 & \dot{\chi}_P \geq 0 \\ 0 & \dot{\chi}_P = 0 \\ -1 & \dot{\chi}_P < 1. \end{cases} \tag{2}$$

The general control structure is given in Fig. 2, in which U_C is the control signal of the system. Y is the system state which needs to be controlled. R and e are the reference value and the tracking error, respectively. K_p, K_i, and K_d represent the controller gains.

The controller for the system is given as

$$U_C = \lambda_p \sigma_{A_p} + \lambda_d \dot{\sigma}_{A_p} + \lambda_i \int \sigma_{A_p} \mathrm{d}\tau, \tag{3}$$

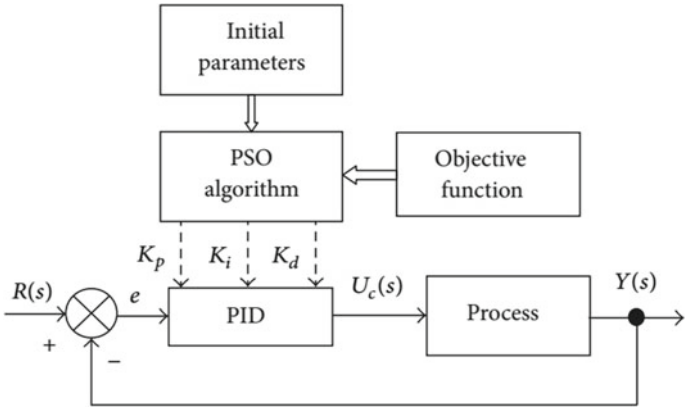

Fig. 2 PSO-based PID controller structure

where U_C is the input signal providing to the system; λ_p, λ_d, and λ_i are the controller parameters; and σ_{A_p} is the tracking error.

Unlike conventional approaches to determine the controller gains, the PSO method is suitably applied in this article to optimize the mentioned parameters. Figure 2 illustrates the control structure with the integration of the PID control and the PSO algorithm.

PSO was initially provided by Eberhart and Kennedy in 1995 [10]. It is established based on the clustering behavior of birds where the birds' properties suggest the decision-making of the human. The theoretical fundamentals of the algorithm are provided in [10]. Its mathematic presentations for the standard PSO [10] are given as follows.

Firstly, the particles adjust their displacement by learning by themselves from their best individual displacements and the best displacement in the global swarm. With considering a problem of minimization with D-dimensional search space, the velocity and displacement are updated by the formula as follows

$$V_{ij}^{t+1} = \omega V_{ij}^{t} + c_1 r_1 \left(P_{ij}^{t} - X_{ij}^{t}\right) + c_2 r_2 \left(G_{j}^{t} - X_{ij}^{t}\right) \tag{4}$$

$$X_{ij}^{t+1} = V_{ij}^{t+1} + X_{ij}^{t} \tag{5}$$

where $1 \leq i \leq D$; $1 \leq i \leq M$ with M being the population size; ω is the inertia weight to better balance the exploitation and exploration; c_1 and c_2 are the coefficients of the acceleration; r_1 and r_2 in the interval (0, 1) are the mutually independent random numbers uniformly distributed; and P_{ij}^{t} and G_{j}^{t} are the best displacement of the particle i and the global optimized displacement in the swam that satisfies the conditions

$$P_{ij}^{t} = \begin{cases} X_i^t, & \text{if } f\left(X_i^t\right) < f\left(P_i^t\right) \\ P_i^{t-1}, & \text{if } f\left(X_i^t\right) \geq f\left(P_i^t\right) \end{cases} \tag{6}$$

$$G^t = P_g^t, \quad g = \arg \min_{1 \leq i \leq M} \left[f\left(P_i^t\right)\right] \tag{7}$$

3 Numerical Simulation

The simulation results of actuator trajectory control are provided in Figs. 3, 4, 5 and 6.

Figure 3 describes the convergence process of the weight along with the iteration. It can be clearly observed that from the fifth cycle, the weight is converged to somewhere nearby the value of 115.051. Coincidingly, the tracking error is forced to zero (Fig. 4), and the acceleration trajectory is converged to its reference curb,

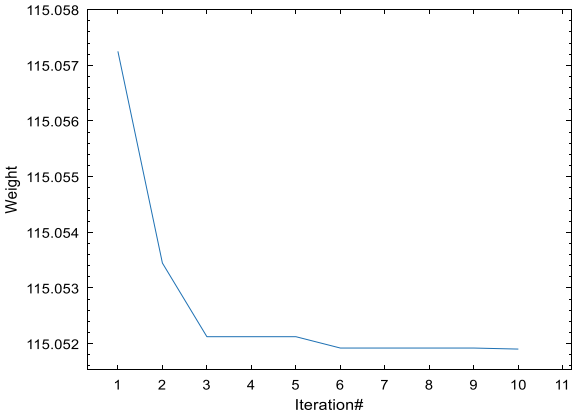

Fig. 3 The weight following the iteration

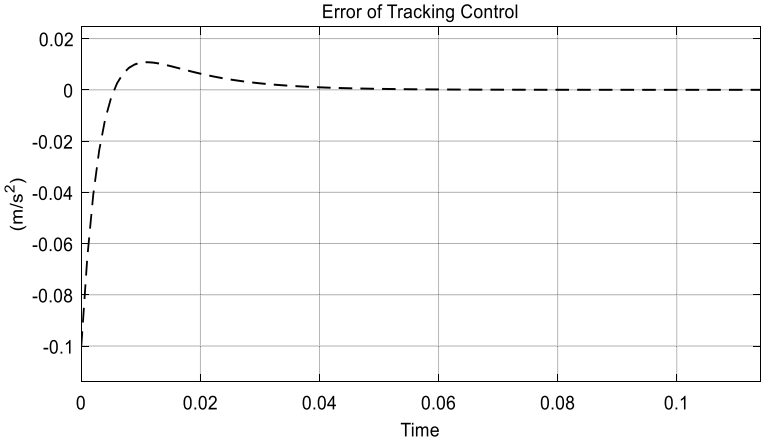

Fig. 4 Tracking error of acceleration tracking

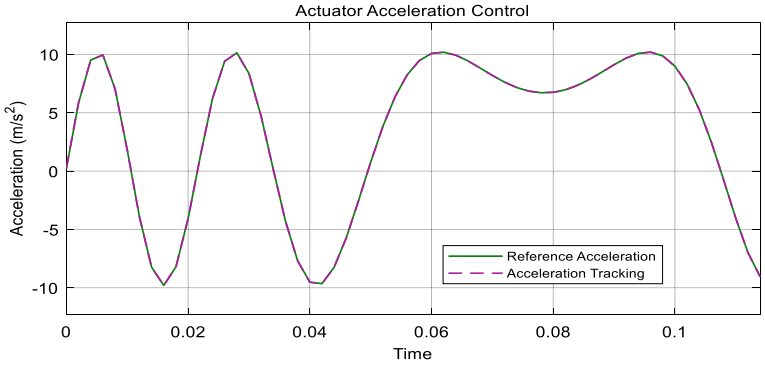

Fig. 5 Acceleration tracking control

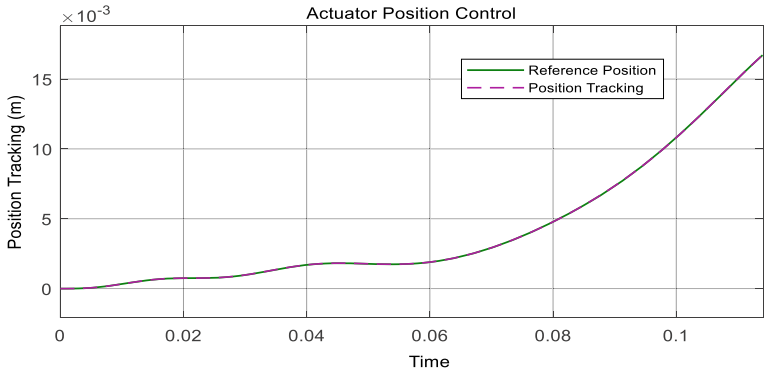

Fig. 6 Displacement tracking control

as shown in Fig. 5. Consequently, the tracking condition of piston displacement is further satisfied (Fig. 6).

4 Conclusion

This research proposes a control strategy to control the hybrid pneumatic–hydraulic actuator system, in which the controller gains of a conventional PID control are optimized. Consequently, the tracking errors are forced to zero, and the control tracking conditions are guaranteed. The numerical computation results are shown to investigate the effectiveness of the designed control law.

Acknowledgements This research was supported by the Institute of Mechanical Engineering, Vietnam Maritime University and by Thu Dau Mot University.

References

1. Ishak, N., Tajjudin, M., Adnan, R., Ismail, H., & Md Sam, Y. (2011). Real-time application of self-tuning PID in electro-hydraulic actuator. In *2011 IEEE International Conference on Control System, Computing and Engineering*, pp. 364–368.
2. Pourebrahim, M., Ghafari, A. S., & Pourebrahim, M. (2016). Designing a LQR controller for an electro-hydraulic-actuated-clutch model. In *Proceedings of 2016 2nd International Conference on Control Science and Systems Engineering*, pp. 82–87.
3. Schkoda, R. F. (2015). Sliding mode control of a hydraulically actuated load application unit with application to wind turbine drivetrain testing. *IEEE Transactions on Control Systems Technology, 23*(6), 2203–2215.
4. Vu, M. T., et al. (2021). Station-keeping control of a hovering over-actuated autonomous underwater vehicle under ocean current effects and model uncertainties in horizontal plane. *IEEE Access, 9*, 6855–6867.

5. Vu, M. T., Le, T. H., Thanh, H. L. N. N., Huynh, T. T., Van, M., Hoang, Q. D., & Do, T. D. (2021). Robust position control of an over-actuated underwater vehicle under model uncertainties and ocean current effects using dynamic sliding mode surface and optimal allocation control. *Sensors, 21*(3).
6. Liu, Y.-J., Zeng, Q., Liu, L., & Tong, S. (2020). An adaptive neural network controller for active suspension systems with hydraulic actuator. *IEEE Transactions on Systems, Man, and Cybernetics: Systems, 50*(12), 5351–5360.
7. Huynh, L.N., Pham, Q.V., Pham, X.Q., Nguyen, T.D., Hossain, M.D. and Huh, E.N., 2019. Efficient computation offloading in multi-tier multi-access edge computing systems: A particle swarm optimization approach. Applied Sciences, 10(1), p.203.
8. Cen, Y., & An, J. (2019). Intelligent control strategy based on PSO-Elman prediction model for ignition temperature in sintering process. In *2019 Chinese Control Conference*, pp. 2846–2851.
9. Hoang, Q.-D., Lee, S.-G., & Dugarjav, B. (2019). Super-twisting observer-based integral sliding mode control for tracking the rapid acceleration of a piston in a hybrid electro-hydraulic and pneumatic system. *Asian Journal of Control, 21*(1), 483–498.
10. Kennedy, J., & Eberhart, R. (1995). Particle swarm optimization. In *Proceedings of ICNN'95—International Conference on Neural Networks*, Vol. 4, pp. 1942–1948.

Count the Number of Steel Bars Based on Deep Learning

Dinh-Thuan Dang, Jing-Wein Wang, Van Nghia Luong, Van Lam Ha, and Van Trinh Truong

Abstract Object detection is one of the most fundamental tasks in digital image processing and has been widely applied in industries. Advances in deep learning are accelerating object detection methods. This work presents the end-to-end two-stage object detection method and the steel bars counting application. In the first step, we collect data and labeling. Second, data is trained and fine-tuned by the Faster-RCNN FPN model. Finally, predict the test data from the trained model. Based on the mean Average Precision metric, the steel bars detection result is 67%. The experience shows that this approach is feasible for counting the steel bars.

Keywords Steel bar counting · Object detection · Deep learning · Two-stage detector

1 Introduction

Humans make object recognition look trivial. Although they are different in color and texture or partly occluded, we can quickly identify objects in our surroundings. Even things appear in many various forms, like shape deviations. Nevertheless, to go from human object recognition to automatic object recognition is a large step. In the past decades, the computer vision field has developed many different theories on how computer systems perform object recognition. The traditional computer vision techniques use feature presentations such as scale-invariant feature transform

D.-T. Dang (✉)
Department of Electronic Engineering, National Kaohsiung University of Science and Technology, Kaohsiung 80778, Taiwan
e-mail: ddthuan@pdu.edu.vn

J.-W. Wang
Institute of Photonics Engineering, National Kaohsiung University of Science and Technology, Kaohsiung 80778, Taiwan

D.-T. Dang · V. N. Luong · V. L. Ha · V. T. Truong
Department of Information Technology, Pham Van Dong University, 509 Phan Dinh Phung Rd, Quang Ngai 57000, Viet Nam

T. D. L. Nguyen and J. Lu (eds.), *Machine Learning and Mechanics Based Soft Computing Applications*, Studies in Computational Intelligence 1068,
https://doi.org/10.1007/978-981-19-6450-3_15

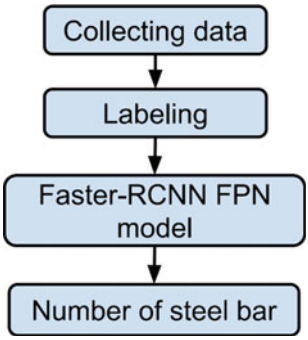

Fig. 1 Diagram presents the main tasks of the paper

(SIFT) and histogram of oriented gradients (HOGs). The other outstanding object recognition method is theorized from deep learning [1].

Deep learning integrates end-to-end learning where the feature extraction, classification, and regression phases are combined pipeline. Convolutional neural networks (CNNs) play a primary role in the feature extraction phase. It is responsible for a big jump in the ability to recognize objects. All classification and objection detection models use CNNs, such as AlexNet, ResNet, MobileNet, and VGG [2].

Deep learning-based object detection engineering consists of two basic approaches, one-stage detectors and two-stage detectors. Two-stage detectors generate region proposals before classifying and positioning them. One-stage detectors do not need to generate region proposals. The one-stage detectors have a speed advantage, but the two-stage detectors have advantages in accuracy [3].

In this work, we select two-stage detectors for an overview, which have higher accuracy. We fine-tuned this two-stage-based model to build the steel bar counting application. Our work presents in detail as in Fig. 1. The first step is to collect data; the second step is to label data. In the third step, we train the Faster Region-based convolutional neural networks (Faster-RCNNs) [4] and feature pyramid networks (FPN) [5] model. The final step is to infer the trained model to count the number of steel bars.

Next, we describe the object detection problem and explain the working principles of Faster-RCNN FPN in Sect. 2; Sect. 3 creates the steel dataset and some augmentation techniques. The results and the future work are in Sect. 4.

2 Method

To count the number of steel bars from an image, we assume that sum of steel bars is equal to the sum of one end of the bars [6]. So, we only need to detect the ends of steel bars that can count the number. Now the work of counting will be attributed to the object recognition problem. The method is to train a neural network that can

detect the ends of steel bars. We choose the advanced model that combines the Faster-RCNN and FPN. In the next section, we declare the object detection problem and present the Faster-RCNN FPN architecture.

2.1 Object Detection Problem Setting

Description Given an image, determine whether or not there are instances of objects from predefined classes and, if present, return the box bounding of each instance.

Input. A collection of N annotated images X_{train} and a label set Y_{train}.

$$X_{\text{train}} = \{x_1, x_2, \ldots, x_N\} \tag{1}$$

$$Y_{\text{train}} = \{y_1, y_2, \ldots, y_N\} \tag{2}$$

where y_i is annotation in image x_i, and each y_i has M_i objects belong to C classes.

$$y_i = \left\{\left(b_1^i, c_1^i\right), \left(b_2^i, c_2^i\right), \ldots, \left(b_{M_k}^i, c_{M_k}^i\right)\right\} \tag{3}$$

With b_j^i and c_j^i denote bounding-box of jth object in x_i and the class, respectively.

Algorithm Optimize the loss function $\mathcal{L}$ of classification $\mathcal{L}_{\text{cls}}$ and bounding-box regression $\mathcal{L}_{\text{box}}$:

$$\mathcal{L} = \mathcal{L}_{\text{cls}} + \mathcal{L}_{\text{box}} \tag{4}$$

Formally, $\mathcal{L}_{\text{box}}$ is based on the sum of squared error (SSE) loss function, and $\mathcal{L}_{\text{cls}}$ is based on the cross-entropy loss function. The loss function is optimized by training the neural network after a specific amount of epochs.

Prediction For x_{test}^i, the prediction result is y_{pred}^i,

$$y_{\text{pred}}^i = \left\{\left(b_{\text{pred}_1}^i, c_{\text{pred}_1}^i, p_{\text{pred}_1}^i\right), \left(b_{\text{pred}_2}^i, c_{\text{pred}_2}^i, p_{\text{pred}_2}^i\right), \ldots\right\} \tag{5}$$

With $b_{\text{pred}_j}^i, c_{\text{pred}_j}^i, p_{\text{pred}_j}^i$ are results of the bounding-box, object class, and reliability. For filtering the object detection results, we can use a predefined threshold that compares the reliability.

Evaluation Metric For evaluating the detection algorithms' performance, the primary metric used is the mean Average Precision (mAP). This metric considers the prediction of correct category labels and accuracy location. An Intersection-Over-Union (IoU) measure refers to the accuracy of object location.

$$\text{IoU}\left(b_{\text{pred}}, b_{\text{lb}}\right) = \frac{\text{area}\left(b_{\text{pred}} \cap b_{\text{lb}}\right)}{\text{area}\left(b_{\text{pred}} \cup b_{\text{lb}}\right)} \tag{6}$$

With b_{pred} and b_{lb} are bounding-box of prediction and label, respectively.

2.2 Network Architecture

This section will present some main neural blocks in Faster-RCNN and FPN architecture. The RCNN family is the state of the art of two-stage object detectors. This approach splits the detection task into two stages: The first is to generate the anchor-boxes, and the second stage makes predictions for these anchors. In the first stage, the detector identifies the potential regions in the image that may cover objects. In the Faster-RCNN model, the proposal region generator algorithm created rectangles randomly, which may either be backgrounds or fourth-growths. In the second stage, the algorithm classifies and regresses the Regions of Interest (ROIs).

To improve better performance in the feature extraction, the Faster-RCNN model usually combines the FPN network. The FPN network shows to be the efficient feature extractor in many applications. FPN implements the multi-scale, pyramidal hierarchy of convolutional networks to construct feature pyramids. The combination between the Faster-RCNN detector and FPN realizes an accuracy solution for detecting tiny to large objects. This method achieves state-of-the-art (SOTA) object detection algorithms as described in the Detectron2 [7] framework.

The composite structure of Faster-RCNN and FPN includes three blocks, which are the backbone network (backbone), regional proposal network (RPN) [8], and ROI-Head network (ROI-Head) [9, 10]. Figure 2 presents a flowchart of the object detection process. The backbone extracts multi-scale features, the RPN block creates and filters anchor-boxes, and the ROI-Head block warps anchors to detect objects. The below sections will be the details of each block.

Backbone. Backbone's role is to extract the feature maps from the input image at different scales. It is an associate ResNet architecture with FPN. The backbone block takes a single-scale image of arbitrary size as input; outputs proportionally sized feature maps at multiple levels. For example, input as a single image of size H = 800 and W = 800, the output of backbone is a feature dictionary "p2", "p3", "p4", "p5", "p6" there are shapes [1, 256, 200, 320], [1, 256, 100, 160], [1, 256, 50, 80], [1, 256, 25, 40], [1, 256, 13, 20], respectively. This step is important to create anchor boxes of different proportions and sizes.

RPN. Goal of RPN is to learn to identify object regions from the multi-scale features. The five feature maps (P2 → P6) fed to RPN one by one. The output feature maps at one level are boxes and the probability of object existence of boxes. First, RPN generates a set of anchor boxes that have different sizes and aspect ratios. The anchor boxes compare box labels to choose some candidate anchors. This step also

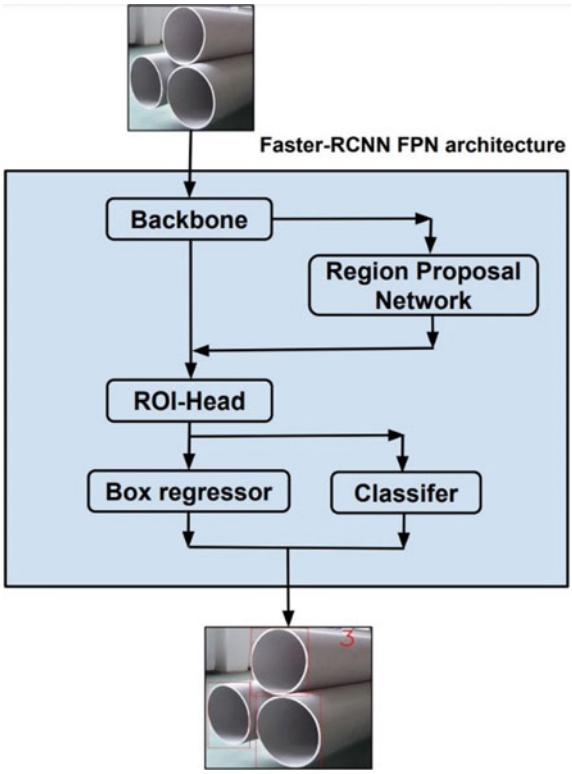

Fig. 2 Main neural blocks in Faster-RCNN architecture

classifies candidate boxes to foreground (objectness = 1) or background (objectness = 0).

ROI-Head. The main tasks of ROI-Head are to crop the ROI by the proposal boxes. It then classifies object boxes and regress positions and shape of the candidate boxes.

The combination of these three neural blocks makes a SOTA object detection method in deep learning [11].

3 Dataset

3.1 Data Gathering and Labeling

We had collected images of steels on the internet. Two hundred and seventy images were labeled with totals are 947 circles. An additional ten images were labeled to be used as test images.

Fig. 3 Steel images are labeled by Labelme tool

To label the images, we use the Labelme [12] utility. It is a graphical image polygonal annotation tool developed by Wada. The steel tree ends were marked with a rectangle box whose coordinates were saved together in JSON file format. Examples of two annotated images are shown in Fig. 3a, b.

3.2 Data Augmentation

Neural networks learn generalized characteristics from training data: The more training data, the better the learning process. However, the labeling procedure is the most time-consuming part of the data collecting process. One method that overcomes this problem is data augmentation. This approach will save time to expand the dataset. The augmentation methods are vertical and horizontal flips, brightness, rotation, translations, and scale changes. Figure 4b is a result of horizontal flip transforms from Fig. 4a. Figure 4c changes the contrast, and Fig. 4d applies the ColorJitter and rotation transforms of Fig. 4a.

4 Result and Future Work

We train the Faster-RCNN FPN model with ResNet50 [13] backbone and predict the above dataset's result. Training and testing are based on Detectron2 framework. The training procedure lasts for 100 epochs, using the Stochastic Gradient Descent optimizer with the momentum of 0.9 and weight decay of 0.0001. The learning rate is set to 0.01. We obtain an accuracy 67% with the mAP metric under IoU thresholds of 0.5. Evaluation results are detailed in Fig. 5.

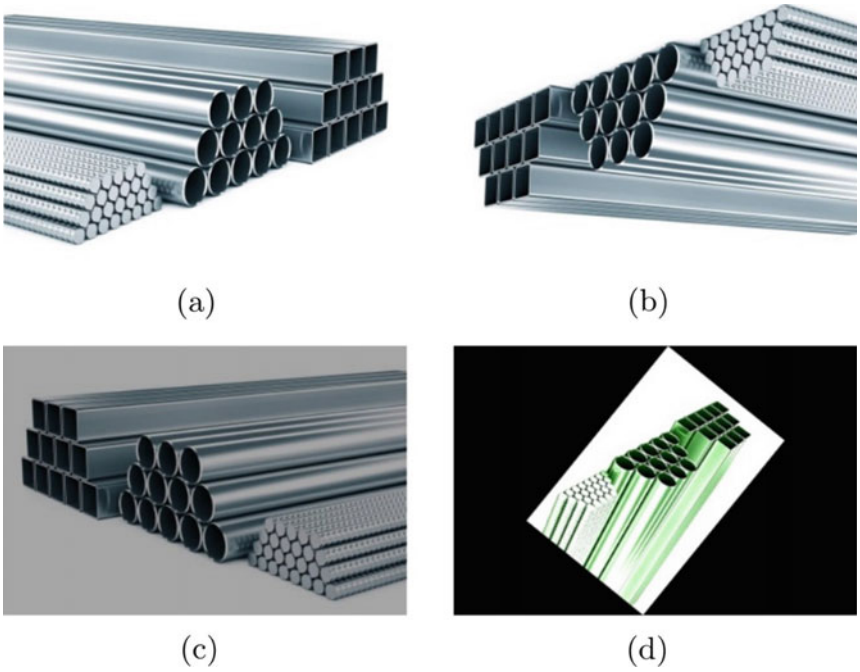

Fig. 4 **a** Root image, **b** horizontal flip, **c** contrast, **d** ColorJitter and rotation

```
Average Precision  (AP) @[ IoU=0.50:0.95 | area=   all | maxDets=100 ] = 0.670
Average Precision  (AP) @[ IoU=0.50      | area=   all | maxDets=100 ] = 0.771
Average Precision  (AP) @[ IoU=0.75      | area=   all | maxDets=100 ] = 0.571
Average Precision  (AP) @[ IoU=0.50:0.95 | area= small | maxDets=100 ] = 0.200
Average Precision  (AP) @[ IoU=0.50:0.95 | area=medium | maxDets=100 ] = 0.350
Average Precision  (AP) @[ IoU=0.50:0.95 | area= large | maxDets=100 ] = 0.670
```

Fig. 5 Evaluation results based on mAP metric

Besides, we also manually test some cases. Figure 6b is the detection result from Fig. 6a. The results show bounding-box and reliability. The counting accuracy of this image is 100%. Figure 7a, b show the counting results that get 100% accurate, but Fig. 7c, d cannot. The result of Fig. 7c is even wrong with the bounding-box.

We solved the stated problem by collecting and labeling the data. The counting problem was solved by fine-tuning the Faster-RCNN FPN model. The future work will improve performance and deploy on mobile devices.

Fig. 6 **a** Prediction image and **b** the detection result with bounding-box and reliability

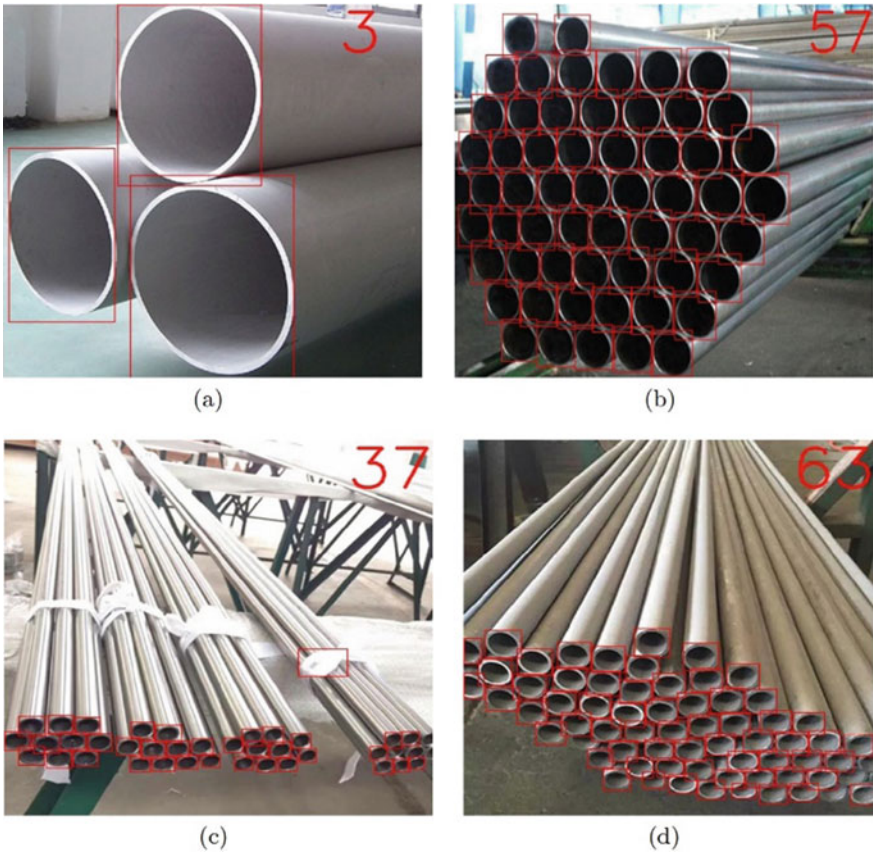

Fig. 7 Counting results get the high precision

References

1. Wu, X., Sahoo, D., & Hoi, S. C. H. (2020, July). Recent advances in deep learning for object detection. *Neurocomputing, 396*, 39–64. https://doi.org/10.1016/j.neucom.2020.01.085.
2. Khan, A., Sohail, A., Zahoora, U., & Qureshi, A. S. (2020, December) A survey of the recent architectures of deep convolutional neural networks. *Artificial Intelligence Review, 53*(8), 5455–516. https://doi.org/10.1007/s10462-020-09825-6
3. Du, L., Zhang, R., & Wang, X. (2020, May) Overview of two-stage object detection algorithms. *Journal of Physics: Conference Series, 1544*, 012033. https://doi.org/10.1088/1742-6596/1544/1/012033
4. Ren, S., He, K., Girshick, R., & Sun, J. (2017, June). Faster R-CNN: Towards real-time object detection with region proposal networks. *IEEE Transactions on Pattern Analysis and Machine Intelligence, 39*(6), 1137–1149. https://doi.org/10.1109/TPAMI.2016.2577031
5. Lin, T.-Y., et al. (2017). Feature pyramid networks for object detection. In *2017 IEEE Conference on Computer Vision and Pattern Recognition (CVPR)* (pp. 936–944). IEEE. https://doi.org/10.1109/CVPR.2017.106
6. Hernández-Ruiz, A. C., et al. (2021, February). Steel bar counting from images with machine learning. *Electronics, 10*(4), 402. https://doi.org/10.3390/electronics10040402
7. Wu, Y., Kirillov, A., Massa, F., Lo, W.-Y., & Girshick, R. (2019). Detectron2. https://github.com/facebookresearch/detectron2
8. Chen, Y. P., et al. (2018, September). An enhanced region proposal network for object detection using deep learning method. *PLOS ONE, 13*(9), e0203897, X. Li (Ed.). https://doi.org/10.1371/journal.pone.0203897
9. Girshick, R., et al. (2014). Rich feature hierarchies for accurate object detection and semantic segmentation. In *2014 IEEE Conference on Computer Vision and Pattern Recognition* (pp. 580–587). IEEE. https://doi.org/10.1109/CVPR.2014.81
10. Wu, Y., et al. (2020). Rethinking classification and localization for object detection. In *2020 IEEE/CVF Conference on Computer Vision and Pattern Recognition (CVPR)* (pp. 10183–10192). IEEE. https://doi.org/10.1109/CVPR42600.2020.01020
11. He, K., et al. (2017). Mask R-CNN. In *2017 IEEE International Conference on Computer Vision (ICCV)* (pp. 2980–2988). IEEE. https://doi.org/10.1109/ICCV.2017.322
12. Wada, K. (2016). labelme: Image polygonal annotation with python. https://github.com/wkentaro/labelme
13. He, K., Zhang, X., Ren, S., & Sun, J (2016). Deep residual learning for image recognition. In *2016 IEEE Conference on Computer Vision and Pattern Recognition (CVPR)* (pp. 770–778). https://doi.org/10.1109/CVPR.2016.90

Hybrid SARIMA—GRU Model Based on STL for Forecasting Water Level in Red River North Vietnam

Pham Dinh Quan, Vu Hoang Anh, Nguyen Quang Dat, and Vijender Kumar Solanki

Abstract The Red River Delta is formed by the Red River System, which is the greatest river system in Vietnam's northern region. The primary river, the Red River, has neither an water storage dam nor a hydroelectric dam. Because of this disadvantage, water level forecasting is critical for regulating agricultural water in Vietnam's second-largest rice-producing region. We present a model to anticipate the water level of Red River water level in Viet Tri, which is near Ha Noi, in this study. The new model is known as the SARIMA-GRU hybrid model, which can fully exploit seasonal patterns in the data. In comparison to the single models SARIMA and GRU, as well as the model ARIMA-RNN, published by Xu et al. in 2019, the new model has produced better results.

Keywords SARIMA · GRU · Hybrid · Water level · Forecasting

1 Introduction

The Red River system is the Northern Vietnam's largest river system. Red River Delta which—the largest delta in Northern Vietnam, Vietnam's second largest, and Vietnamese second largest agricultural sector is mostly made by the sediment of Red River system.

P. D. Quan (✉) · V. H. Anh · N. Q. Dat
High School for Gifted Students,Hanoi University of Science—Vietnam National University,Hanoi, Vietnam
e-mail: phamdinhquan_hsgs2021@hus.edu.vn

V. H. Anh
e-mail: vuhoanganh_hsgs20@hus.edu.vn

N. Q. Dat
e-mail: nguyenquangdat@hus.edu.vn

V. K. Solanki
Department of Computer Science and Engineering, CMR Institute of Technology, Hyderabad, India

T. D. L. Nguyen and J. Lu (eds.), *Machine Learning and Mechanics Based Soft Computing Applications*, Studies in Computational Intelligence 1068,
https://doi.org/10.1007/978-981-19-6450-3_16

As a result, Red River Delta irrigation water level forecasting is critical. Furthermore, it is more vital than ever in today's circumstances, when the climate is changing and there is worldwide food insecurity. On the rivers of the Red River system, many hydroelectric and irrigation systems are built in large numbers with the goal of regulating water for the North's huge irrigation systems. This has helped to mitigate most of the agricultural damage caused by natural catastrophes.

The Red River system is divided into three main branches: the Red River, the Black River, and the Chay River. All three tributaries of these rivers meet in Viet Tri city, which is also known as "the city of three rivers". The Red River, the largest tributary, is also the river system's primary branch. The Red River system receives the most water from this branch too. As a result, the management of water for the plain's irrigation system is heavily reliant on the flow rate of this Red River tributary. The Black River is home to three massive hydroelectric dams and there is one huge hydroelectricity dam, it is also the irrigation on the Chay River, both of them have a significant impact on river water regulation. Ironically, the Red River is the largest branch of the main river, yet there are no irrigation dams.

Currently, water restriction measures are only in place on two tributaries of the Black and Chay rivers. Therefor, anticipating the water flow (or river level) of the Red River tributary is a critical irrigation problem in northern Vietnam.

Using machine learning approaches to identify seasonality is a highly practical path, especially since it is not controlled by humans (the main branch of the Red River) because the water in VietNam's rivers has a distinct seasonality throughout the year. Moreover, deep learning algorithms can also be used to deal with irregular data. In our study, we propose the SARIMA in conjunction with GRU, which can fully exploit the seasonal features of the data, while also utilizing the capability of artificial neural network models. As a consequence, rather than applying each standard model individually, we hope to get better outcomes (Fig. 1).

2 Related Works

In 2021, author Thammarat et al. [2] analyzed the monthly average water level from April of 2007 to March of 2020 across multiple measuring stations of the Yom River in Thailand using the SARIMA method. The author has tried to use many SARIMA models with different parameters, and compared with AutoRegression (AR), Moving Average (MA), Seasonal AR, Seasonal MA models, thereby showing a good method. Best for practical use.

When comparing SARIMA and SARIMAX in the heart of Sulaymaniyah city in 2021, Bakhan Hoshyar Qadir and Monem Aziz Mohammed [10] utilized groundwater level data from January 2013 to May 2020. After considerable comparison, they discovered that SARIMAX $(0,1,0)\times(1,0,1)_{12}$ with AIC (456.744) is the best model.

In 2019, Xu and colleagues [22] attempted to forecast water levels on Lake Taihu using a combination of ARIMA and RNN models, creating an ARIMA-RNN hybrid approach. Experimentally, the authors have shown that the proposed model's results

Fig. 1 Red river system. There are no hydroelectric dams or irrigation dams on the main river

are much better than that of single models such as ARIMA and RNN, based on RMSE and FA criteria, with the results of RMSE criteria being 0.021 (scaled data) and the FA criterion is 99.17%.

The Oyoda River in Japan will experience flooding in 2021, according to Shuofeng et al. [4] , who discusses the use of the LSTM and Tank models in tandem. After considerable comparison, it was determined that the LSTM-based hybrid model had more accurate long-term predictions and that the RMSE values had increased from 0.64 to 0.86.

Yu Liu and colleagues [11] will anticipate the trend of urban river water levels in the short run in 2021 using the LSTM Forecast Model. After comparing the observed and simulated water levels, students may notice that the error of the model they are investigating behaves similarly under different rolling intervals within the same forecast period.

Five models were developed in 2022 as a result of the work of Noor et al. [8], including Artificial Neural Network, LSTM, Spatial Attention LSTM, Temporal Attention LSTM, and Spatiotemporal Attention LSTM.The outcomes demonstrated that the combined application of focusing spatially and temporally improved the LSTM model's ability to predict outcomes, outperforming existing attention-based LSTM models. The flood control strategies for Bangladesh and other countries might be informed by the STALSTM-based flood warning system that was created in this work.

Anh et al. [5] estimated water levels in 2020 using the WAANN-TS at the Yen Bai station for a variety of purposes, including agricultural and flood forecasting. They may see that, while comparing the outcomes from the ARIMA model, ANN model, WAANN model, and Zhang's model, the error of the model they are investigating has the lowest error. Average error is 2.9579.

Sang-Soo Baek et al. [6] demonstrated a CNN-LSTM and profound understanding strategy in 2020 to forecast water levels and the Nakdong river basin's water quality. The outcomes showed that the NSE value for the CNN-LSTM in combination with a deep learning approach was over 0.75, which is in the "very good" performance range.

To increase the precision of the Lake Michigan and Lake Ontario WL predictions, Barzegar et al. [12] will adopt the CNN-LSTM DL Model in 2021. After considering the results, they may conclude that selecting the ideal model parameter settings can enhance model performance by 5 to 20 %.

In 2021, Yue Zhang and colleagues[7] suggested a STA-LSTM model for forecasting accuracy about the quantity and timing of flood water levels in urban locations like the city of Toronto, and this method had the lowest incidence of error at roughly 3.98 % for a twelve-hour forecast .

In 2021, Van et al. [3] use the Seasonal-Wavelet-LSTM model to forecast water level on Red River. After comparing the result from the SARIMA method, LSTM model, ARIMA-RNN model and Seasonal-Wavelet-LSTM method they can point out that the error of the model that they are researching get the lowest error. The MSE value is 0.344907 and 0.443847 for MAPE.

3 Methodology

3.1 SARIMA

Box and Jenkins examined the ARIMA models [1] in 1970 ; and Brockwell and Davis [14]; Both the auto regressive and moving average methods are helpful for predicting. According to ZHANG (2003), their hybrid method (AR + MA) outperforms component methods [13] and is applicable to a larger range of applications.

For period planning and prediction, the SARIMA model, an enhanced variant of the ARIMA model with an additional seasonal component, is frequently employed. In 1982, ARIMA estimating model with periodic coefficients based on the hybrid model concept was created by Salas et al.

A time series $\{X_t | t = 1,2, \ldots, N\}$ is produced by a SARIMA (p,d,q)(P,D,Q) process using the following equation:

$$\phi(L)(1-L)^d \Phi(L^s)(1-L^s)_t^{Dy} = c + \theta(L)\Theta(L)\varepsilon_t \tag{1}$$

with $\phi(L) = 1 - \phi_1 L - \phi_2 L^2 - \cdots - \phi_p L^p$ is the Auto Regressive operator (AR) of order p. $\Phi(L) = 1 - \Phi_1 L^s - \Phi_2 L^{2s} - \cdots - \Phi_P L^P$ is the Seasonal Auto Regressive operator (S-AR) of order P. $\theta(L) = 1 - \theta_1 L - \theta_2 L^2 - \cdots - \theta_q L^q$ is the Moving Average operator (MA) of order q. $\Theta(L) = 1 - \Theta_1 L^s - \Theta_2 L^{2s} - \cdots - \Theta_Q L^Q$ is the S-MA operator of order Q, where d is the quantity of regular variations. Seasonal fluctuations' amount is D. In the majority of situations, $D = 1$ if a seasonality

impact exists and $D = 0$ otherwise. ε_t is a white noise signal, and $varepsilon_t$ is the predicted residue at move t that is distributed evenly and freely as a normal random variable with an average value of 0 (σ_ε^2).

3.2 Gated Recurrent Unit—GRU

Long-Short term memory—LSTM
In 1997 [18], Hochreiter and Schmidhuber introduced that recurrent neural network has a modification named LSTM. The occurring issues of recurrent neural network can be solved by Long-Short term memory, which appears while RNN networks is being trained with long-term interdependence [17]. To accomplish these, 3 gates and memory cells have been included in the design of LSTM, in such a way that it can keep data for whole the RNN network's training.

The input of the LSTM unit is xt at step t, and the output is $(ht - 1)$ at step t. Gates that load the input using the sigmoid function have an output range of [0, 1]. If the output value is 0, then all inputs are eliminated. From a different angle, if the output value is 1, all the information has been transmitted. Thus, the output from t-step (ht) and the $cell\ state$ from t-step will be handled in 4 steps:

– **Step 1:** Forgotten gates erase information obtained from the $cell\ state$:

$$f_t = \sigma(W_f.[h_{t-1}, x_t] + b_f) \tag{2}$$

– **Step 2:** The $cell\ state$ is where new data is kept. The input gate (with the function $sigmoid$) receives fresh values during the 1st phase., which are subsequently used to update this node. The tanh class receives a new vector $\tilde{c}_t$ in the 2nd phase:

$$i_t = \sigma(W_i.[h_{t-1}, x_t] + b_i); \qquad \tilde{c}_t = \tanh(W_{\tilde{c}}.[h_{t-1}, x_t] + b_{\tilde{c}}) \tag{3}$$

– **Step 3:** The $state\ cell$ value is changed from $Ct - 1$ to Ct:

$$c_t = f_t \otimes c_{t-1} \oplus i_t \otimes \tilde{c}_t \tag{4}$$

– **Step 4:** Output: The data that will be shown outside the LSTM unit is initially determined by the output gate. Following that, $state$ becomes a passed node with a value ranging from –1 to 1. The following formula will be used to calculate the final result:

$$o_t = \sigma(W_o.[h_{t-1}, x_t] + b_o); \qquad h_t = o_t \otimes \tanh(h_t) \tag{5}$$

with W_f, W_i, $W_{\tilde{c}}$, W_o which are LSTM parameters and b_f, b_i, $b_{\tilde{c}}$, b_o are LSTM model biases.

Gated recurrent unit—GRU

KyungHyun Cho et al. proposed in October 2014 [16] a simplification of LSTM named gated recurrent unit (GRU). It works on a range of applications and employs some gate functionalities. Different from LSTM, the GRU model doesn't have a memory cell. GRU operations can be summarized using the following formulas:

$$h_t = (1 - z_t)h_{t-1} + z_t\tilde{h}_t$$

$$z_t = \sigma\left(W_{zxt} + U_z h_{t-1}\right)$$

$$\tilde{h}_t = \left(W_{hxt} + U(r_t \cdot h_{t-1})\right)$$

$$r_t = \sigma\left(W_{rxt} + U_{rht-1}\right)$$

where h_t and z_t are the GRU outputs, r_t is the update and reset gate, $\tilde{h}_t$ is the candidate output, and Wz, Wh, W_r, U_z, and U_r are the GRU matrices.

3.3 STL Trend-Seasonal Decompose

For seasonal data, the accuracy of the model will increase when we can accurately separate the season series from the original data.

To do this, we use the STL method provided by Cleveland and others. [19] in 1990. This is a very popular method today in separating seasonality from time series.

This technique separates the three-part time series: $y_t = T_t + S_t + R_t$where T_t is the trend, S_t is seasonal, and R_t is the remaining component.

The inner loop and outer loop are the two recursive components of the STL method. Each time the inner loop iterates, the seasonal component is adjusted, and the smoothing method is then used to update the trend. After this iteration, we go on to the outer loops where the weights of the model are produced and utilized to update the seasonal and trend in time series for the following inner loop while reducing the interference from outliers (Fig. 2).

3.4 Proposed Model: Hybrid SARIMA-GRU with STL Model

Forecasting trend and seasonal time series (linear components) has shown to be successful using the SARIMA model, but not for nonlinear components. Additionally, the model uses fewer computer resources. The GRU model (this is the nonlinear component), can handle residual data sets successfully but consumes more resources.

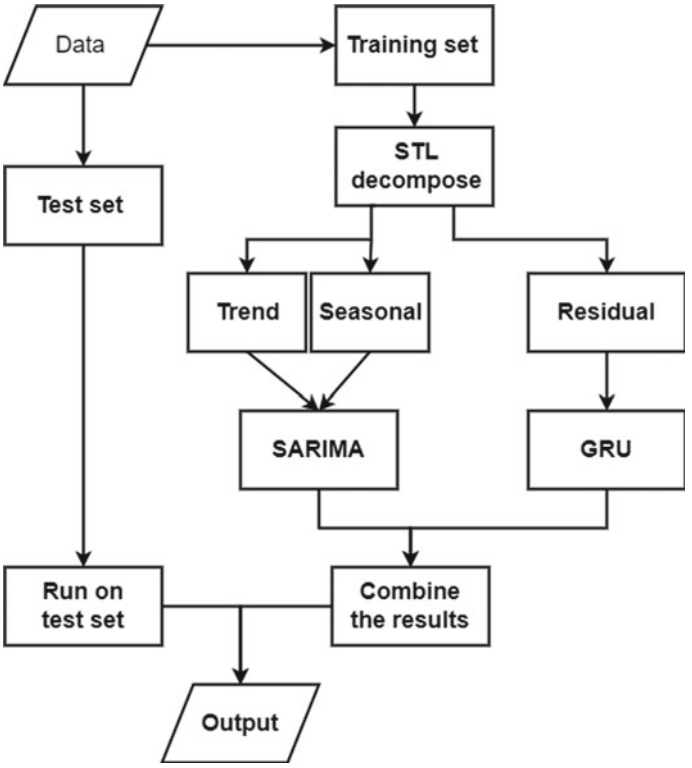

Fig. 2 Proposed model

Therefore, it is hoped that by combining the SARIMA and GRU models, the hybrid model's outcomes will be superior to those of the individual approaches.

Algorithm 1 SARIMA - GRU hybrid model based on STL

Require: original_data = $\{y_i\}$;
$\{y_i\} = y_{train} + y_{test}$ (90% + 10%);
$\text{STL}(y_{train}) = \text{train}_{trend} + \text{train}_{seasonal} + \text{train}_{residual}$;
$\text{train}_{linear} = \text{Combine}(\text{train}_{trend} + \text{train}_{seasonal})$;
SARIMA model:
    $\text{train}_{linear\_predict} = \text{SARIMA}(\text{train}_{linear})$;
GRU model:
    $\text{train}_{residual\_predict} = \text{GRU}(\text{train}_{residual})$;
$\text{train}_{total\_predict} = \text{Reconstruct}(\text{train}_{linear\_predict}, \text{train}_{residual\_predict})$;
$\text{test}_{total\_predict} = \text{hybrid\_model}(y_{test})$;
Evaluate:
    $\text{MSE} = \text{MSE}(\text{test}_{total\_predict})$; $\text{MAPE} = \text{MAPE}(\text{test}_{total\_predict})$;

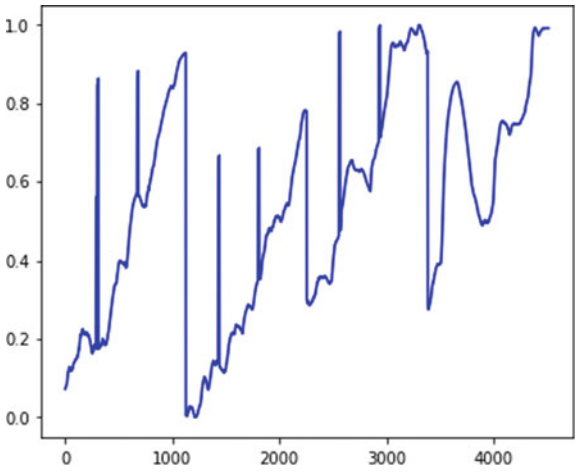

Fig. 3 North Vietnam's Viet Tri city, on the Red River, and the station there where daily inflows pass

4 Application

4.1 Data and Area

Daily influx via Viet Tri city

The data were taken at the measuring station in Viet Tri city, on the main river (Red River), right in front of where the Black river and Chay river join the main river.

The data consists of 4512 values, taken every 2 h, collected for 4 years 2017–2020, taken during the rainy season (June 15–September 15) every year (Fig. 3).

4.2 Criteria for Comparison

To compare the outcomes, two criteria are used: Mean Absolute Percentage Error (MAPE) and Mean Squared Error (MSE):

$$MSE = \frac{1}{n} \cdot \sum_{i=1}^{n} (\hat{y}_i - y_i)^2 \qquad MAPE = \sum_{i=1}^{n} \left| \frac{\hat{y}_i - \bar{\hat{y}}_i}{n} \right|$$

4.3 Results from the Daily Inflow via the Reservoir at the Viet Tri Station Dataset

We will rebuild the model of Van [3] and Xu [22], two models with high similarity with our proposed model. From there, we can consider the advantages and disadvan-

Table 1 Result of Viet Tri data (scaled data)

	MSE	***MAPE***	
ARIMA	7.5011	1.0765	
SARIMA	5.2708	0.8806	
LSTM	2.2815	0.2184	
GRU	2.2115	0.2003	
Wav.-Seas.-LSTM	2.2101	0.2100	(*Van's model*) [3]
ARIMA-RNN	2.2270	0.2101	(*Xu's model*) [22]
Proposed model	**2.0102**	**0.1785**	

tages of the proposed model, along with that we can evaluate the superiority of the models.

The proposed models were trained using the dataset, along with the rebuild of the model Wavelet-Seasonal-LSTM of Van et al. [3], the model ARIMA-ANN model from Xu et al. [22], the pure ARIMA, SARIMA, LSTM and GRU models (Figs. 4 and 5).

After using existent data of influx to Viet Tri hydroelectric dam, the result of the model is illustrated in the Table 1.

Each combination model's outcomes are better than the results of the individual segment models, as illustrated in the table. The basic ARIMA model'MSE is the highest of 7.5011, followed by SARIMA, which has an MSE of 5.2708 and and a remarkable high MAPE of 1.0765, a sign of inaccuracy. Aside from ARIMA and STL-SARIMA-GRU, the SARIMA-GRU model performs the worst across all criteria, except for the exception of MAPE. However, this model's MAPE was higher than that of the hybrid STL-SARIMA-GRU model. Because the MAPE criteria is based on a relative error, which is more delicate too mimimal numbers, which illustrates the superior the linear SARIMA model's reliability in modeling water levels. The difference between 0.20685 and 0.0316 is comparatively insignificant. The MSE and MAPE differences between STL-SARIMA-GRU and the hybrid model ARIMA-RNN are just 0.20685 and 0.0316, respectively. The suggested STL-SARIMA-GRU model had the lowest MSE and MAPE values, with a 10.3% lower MSE and a 15% better MAPE than its hybrid adversary.

5 Conclusion

We have suggested a model to suit the need of forecasting water level on the on the Red River in Viet Tri, right before the intersection of the big rivers in the Red River Delta in this study. The seasonal aspect of the input data with this model can be taken use of, increasing the model's precision. Furthermore, the adoption of a powerful neural network, such as the GRU, yields superior outcomes compared to some previous

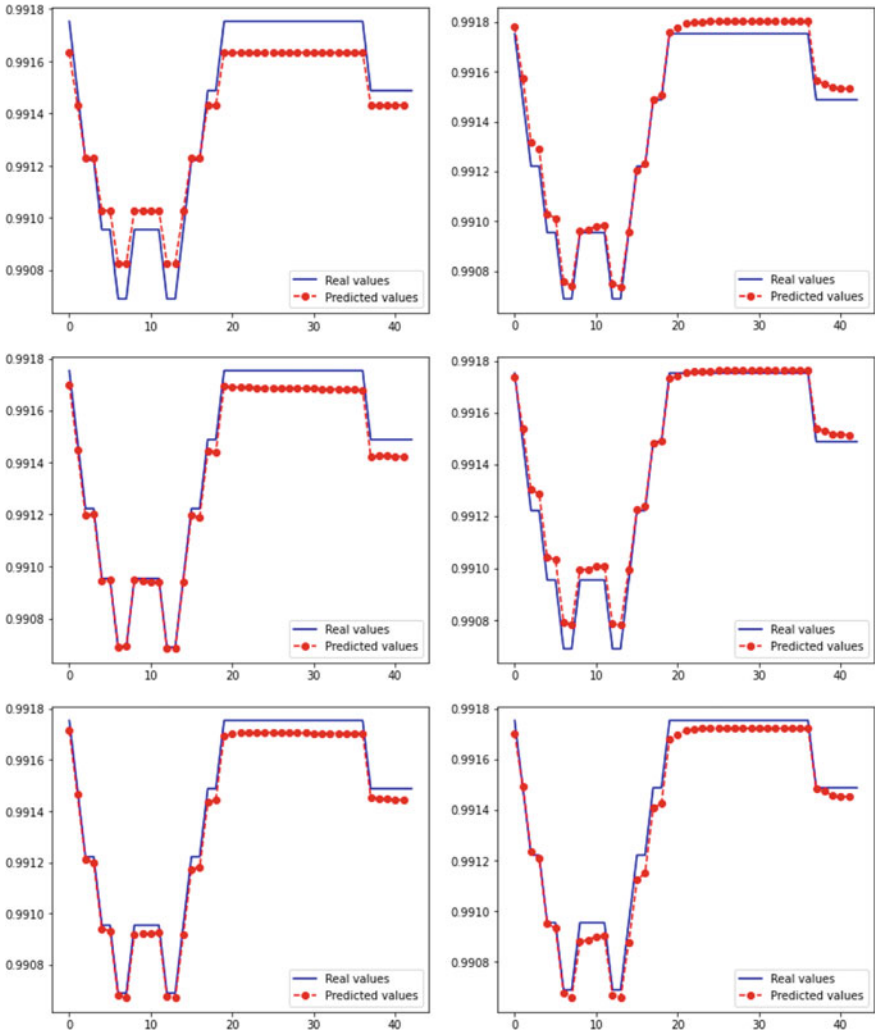

Fig. 4 The following are the results of numerous models for the water level at the Viet Tri station: ARIMA (1st row-lelf), SARIMA (1st row-right), LSTM (2nd row-left), GRU (2nd row-right), Xu's model (ARIMA-RNN)(3rd row-left), Van's model (Wavelet-Seasonal-LSTM) (3rd row-right)

studies [3, 22].The hybrid model has generated the greatest results when compared to the pure models and the hybrid model from Xu et al. and the Seasonal-Wavelet-LSTM of Van et al. The ability to make use of the unique elements of the data (which have never been used previously), the best comparison has been produced with less errors in the results by the hybrid model.

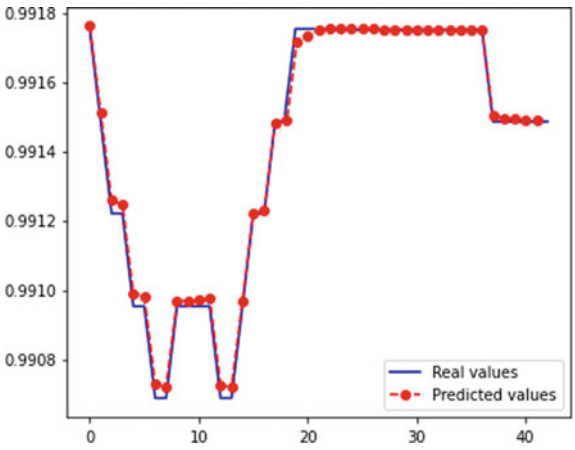

Fig. 5 Results of the suggested model STL-SARIMA-GRU

We will strive to fix some of the model's present shortcomings in the future work: noice reducing (SAX, Wavelet, etc.), more inputs (statistics about rainfall, etc.), and an online model. We believe that this is a viable solution to the problem in Vietnam.

Acknowledgements We owe heartfelt gratitude to WARM group for their assistance for the previous version this article's previous version being edited (Thuy Loi University's WARM group, Vietnam).

References

1. Box, G. E. P., & Jenkins, G. (1970). *Time series analysis, forecasting and control*. San Francisco, CA.: Holden-Day.
2. Thammaarat, P., Piyawan, K., Ronnason, C., & Pijitra, J. (2021). High performance approach for water level forecasting in Yom river basin of Thailand. *J. Math. Comput. Sci., 11*(3), 3102–3129.
3. Van, D. T., & Lan, L. H. (2021). Using data mining to pre-process data for the neural network model to predict water level applied for Northern Vietnam's agriculture. Conference ICCIML.
4. Shuofeng, L., Puwen, L., & Koyamada, K. (2021). LSTM based hybrid method for basin water level prediction by using precipitation data. *J. Adv. Simult. Sci. Eng., 8*(1), 40–52.
5. N. T. N. Anh. (2020). Prediction of water level using time series. Wavelet Neural Netw Approachs.
6. Baek, S., Pyo, J., & Chun, J. A. (2020). Predictionn of water level and water quality using a CNN-LSTM combined deep learning approach. *Water, 12,* 3399.
7. Zhang, Y., Gu, Z., & The, J. V. G. (2022). The Discharge Forecasting of Multiple Monitoring Station for Humber River by Hybrid LSTM Models. *Water, 14*, 1794.
8. Fahima Noor and colleagues. (2022). Water level forecasting using spatiotemporal attention-based long short-term memory network. *Water, 14,* 612.
9. Babu, C. N., & Reddy, E. (2014). A moving-average filter based hybrid ARIMA-ANN model for forecasting time series data. *App. Soft Comp., 23,* 27–28.
10. B. H. Qadir, M. A. Mohammed, "Comparision Between SARIMA and SARIMAX Time Series Models with Application on Ground Water in Sulaymaniyal", p30-48, Vol. 5, Issue 2, Dec 2021.

11. Liu, Y., Wang, H., Feng, W., & Huang, H. (2021). Short term real-time rolling forecast of urban river water levels based on LSTM: A case study in Fuzhou city, China. *Int. J. Environ. Res. Public Health, 18,* 9287.
12. Barzegar, R., Aalami, M. T., & Adamowski, J. (2021). Coupling a hybrid CNN-LSTM deep learning model with a boundary corrected maximal overlap discrete wavelet transform for multiscale lake water level forecasting. *J. Hydrol., 598*(2021), 126196.
13. Zhang, G. (2003). Time series forecasting using a hybrid ARIMA and neural network model. *Neurocomputing, 50,* 159–175.
14. Brockwell, P. J. & Davis, R. A. (1991). Time series: Theory and methods. Int. Conf. Mach. Learning.
15. Salas, J. D., Boes, D. C., & Smith, R. A. (1982). Estimation of ARMA models with seasonal parameters. *Water Resour. Res., 18*(4), 1006–1010.
16. Cho, K., van Merrienboer, B., Gulcehre, C., Bougares, F., Schwenk, H., & Bengio, Y. (2014). Learning phrase representations using RNN encoder-decoder for statistical machine translation. *CoRR, 1406*(1078), 1724–1734.
17. Razvan, P., Tomas, M., & Yoshua, B. (2013). On the difficulty of training recurrent neural networks. Int. Conf. Mach. Learning, pp. 1310-1318.
18. Hochreiter, S., & Schmidhuber, J. (1997). Long short-term memory. *Neural Comput., 9*(8), 1735–1780.
19. Cleveland, R. B., Cleveland, W. S., McRea, J. E., & Tepenning, I. (1990). STL: A seasonal-trend decomposition produre base on Loess. *J. Official Stat., 6*(1), 3–73.
20. Xiong, Tao, Li, Chongguang, & Bao, Yukun. (2018). Seasonal forecasting of agricultural commodity price using a hybrid STL and ELM method: Evidence from the vegetable market in China. *Neurocomputing, 275,* 2831–2844.
21. Qin, L., Li, W., & Shijia, L. (2019). Effective passenger flow forecasting using STL and ESN based on two improvement strategies. *Neuralcomputing, 356,* 244–256.
22. Xu, G., Cheng, Y., Liu, F., Ping, P., & Sun, J. (2019). A water level prediction model based on ARIMA-RNN. In 2019 IEEE Fifth International Conference on Big Data Computing Service and Applications (BigDataService), pp. 221–226.

Activity-Based Learning: An Analysis to Teach Learners Using Online Methodologies

Deepanjali Mishra, Dilrabo Bakhronova, and Umida Djalilova

Abstract Activity-based learning is one of the most trending methodology of learning. It is a teaching methodology which enables a learner to learn as per his or her natural pace using a series of activities which is more interactive, engaging and beneficial for young learners. It also has the facility of monitoring and evaluating the activities. However, the online activity-based learning became a new mode of teaching during the COVID-19 when the entire world went under lockdown. The situation was indeed very difficult for everyone to make their ends meet during that time. People were not allowed to come out of their homes except to purchase the daily needs. All the educational institutions including schools, colleges and universities were shut down for an indefinite period. The faculties were left with no other alternative but to take classes through online mode. This was a challenging task not only for students but also for the teachers. Therefore, the basic objective of the paper would be to discuss about the effectiveness of the implementation of activity-based learning through online mode and how far it has succeeded in creating an impact among the trainers as well as the learners.

Keywords Activity-based learning · Online · Multimedia · Trainers · Effectiveness

1 Introduction

Activity-based learning is a widely known concept which emphasizes more on practical approaches to learning something. The method of learning by doing was coined by a well-known educationist from UK, named David Horsburgh taking cues from the ancient methodology that was used by the sages in their ashrams in 1944 when the Second World War was going on [1]. Learning needs to be creative and as well as exploratory which could be gained only through practice. Involvement of learners

D. Mishra (✉) · D. Bakhronova · U. Djalilova
KIIT University, Uzbekistan State World Languages University, Tashkent, Uzbekistan
e-mail: nguyenquangdat@hus.edu.vn

Tashkent Chemical-Technological Institute, Tashkent, Uzbekistan

T. D. L. Nguyen and J. Lu (eds.), *Machine Learning and Mechanics Based Soft Computing Applications*, Studies in Computational Intelligence 1068,
https://doi.org/10.1007/978-981-19-6450-3_17

or the students makes a class much more lucrative and interesting which has more meaning and the class more interesting. Positive learning outcomes are achieved only when the learners are not afraid to take up challenges of doing something new even in an unfavourable atmosphere. It involves oneself in order to induce oneself to achieve self-learning. However, a social amicable environment is needed between the trainers and the learners for activity-based learning. As English is our second language, and more of our students are first generation students, it is a Herculean to make the students get interested in the language [2]. Moreover, English is a language where all the subjects travel and it is great challenge for the English teachers to make the classroom interactive and full-fledged. Basically, teaching must include two major components sending and receiving information. Ultimately, a teacher tries his best to impart knowledge as the way he understood it. So, any communication methods that serve this purpose without destroying the objective could be considered as innovative methods of teaching. Using new innovative techniques in schools and colleges having the potential to bring about latest advancement in educational technologies. It brings about empowerment administration is strengthened and efforts are galvanized so that sustainable human development goals are achieved for any nation. Globalization has been responsible in bringing information and technological revolution which has led to reformation of the entire education system [3]. It becomes very necessary for any trainer to change his or her conventional method of teaching and adopt the latest mode of training that involves technology enabled teaching. In the words of a famous leader, Jonathan Schattke, "*Necessity is the author of change*" which is indeed very true. As it is very necessary for the current generation to change, therefore, it becomes very important to adopt the latest technologies and pedagogy which enhances the training and understanding process for learning all subjects including English language. It is true that traditional techniques is not alone sufficient for a student to improvise on his or her communication skills and developing the interpersonal skills. It is very necessary to combine both technological pedagogy as well as the conventional methodologies in order to achieve effective results for both the teacher and the student. Another important point is to keep in mind that the teacher should make the class. Further, it is necessary to know the student's interest, and attraction as the class would be meaningful without these aspects.

2 Review of Literature

Ericksen (1978) emphasized that "powerful studying in the lecture room relies upon on the trainer's ability to keep the hobby that brings college students to the route in the first region." The emphasis of effective mastering in a classroom has vital importance in pupil retention. The lecturers are required to be adaptive to the changing school room and pupil needs' such that the students enjoy the path and set up goals. One such method is interest-based mastering (ABL) that is defined as a gaining knowledge of process wherein college students are constantly engaged [4]. Hobby based getting to know is defined as a setup where students actively participate inside

the gaining knowledge of enjoy rather than take a seat as passive listeners. These writers emphasize that energetic getting to know technique is not the same as the traditional method of teaching by using: (a) the active position and involvement of students within the school rooms and (b) collaboration among the scholars in a learning surroundings. These two gadgets are the important thing to ABL and aim to establish a fine getting to know surroundings inside the study room. Churchill (2003) propagates that hobby-primarily based learning aids students and freshmen to construct intellectual models that permit for better-order performance consisting of applied trouble fixing and switch of data and skills. Schumaker and Deshler (2006) have the opinion on getting to know techniques as "a person's approach to a mission. It consists of how a person thinks and acts while making plans, executing and evaluating performance on an assignment and its effects." It assures mastering method is a deliberate character practice to organize and bear in mind matters in studying system. Several studies had been performed approximately the effectiveness of online getting to know, and the demanding situations and regulations that it can cause to students had been considered. Among these are research conducted by means of Hazwani et al. (2017), Irfan and Iman (2020), Awal et al. (2020), Wildana et al. (2020), Muhammad and Kainat (2020) and Nurul Haidah et al. (2020). Furthermore, Wildana et al. (2020) do not forget online learning to be effective as it helps using various programmes together with "WhatsApp," "Zoom" and "Google lecture room." However, Wildana et al. additionally concur that net get right of entry to and net packages restriction the effectiveness of online mastering. A examine with the aid of Muhammad and Kainat (2020) found that Internet access problems, a loss of interplay between teachers and students and a lack of technological facilities project the efficacy of online mastering. In step with a observe carried out by Hazwani et al. (2017), an group's infrastructure plays an enormous position in making sure that online studying operates successfully. Bad infrastructure will restriction students' capacity to get right of entry to the net.

3 Concept of Online Activity-Based Learning

India is one of the leading countries of the world which has taken initiatives to implement the Rights to Education act in the year 2009. It allows rights to all the students who are interested to study each and every child a right of clock-watching elementary education based on the principles of equity and non-discrimination. Activity-based learning or ABL is beneficial to those students who learn by asserting their freedom. They follow all the rules and regulations that aim to provide freedom. It provides a sociable model to impart learning in a spontaneous way so that the learners do not face any insecurity or anxiety or strain. The present scenario in India is such that almost all elementary schools follow the conventional methodology of teaching for English language and literature [5]. A diligent endeavour towards keen observation of teachings in different schools has been taken to heighten an awareness of the issues involved with activity-based learning for re-examination of some prevalent myths relevant to the pedagogical implementations. We can have better teachings in our

state if we have some understandings on the practical challenges coming across the path of second language teaching. This study is an in-depth analysis of the current teaching strategies and the challenges to be surmounted in this domain. The study of teachings in various primary and upper primary schools of Bolagarh block in the district of Khordha reveals the real circumstances and opens a door for wide discussion. The development and execution of various language activities are viewed as internal regulating processes and project impulsions to discover the challenges in the way of teaching learning process [6]. This research work characterizes the current status of activity-based learning through the four basic techniques of teaching such as visual memory development technique (VMDT), chain drill (CD), brain storming (BS) and mental talk (MT) earmarked in text books and the development of procedures of teaching consistent with it, challenges coming across the path of English language teaching in elementary education and a few possible ways to overcome those. Various study preferences and educational practices pertaining to the theories of learning styles are collected from different literature reviews and depicted below with prevailing categorizations [7]. Various study preferences and educational practices pertaining to the theories of learning styles are collected from different literature reviews and depicted below with prevailing categorizations [8].

(1) **Showing Visual Aids to the Students**: It is one of the tools which enables a reader to see and learn. The trainer could use white board and virtual markers and try to elaborate his or her points using various technologies. For example, PowerPoint presentations could be one of the basic technology that can be used. Slides could be prepared on a topic and it could include graphics, animation and other aids. This would not only make the class interesting but also it would make the students glued to the class for a longer duration of time. There are various virtual classrooms like zoom, Google Classrooms, Microsoft teams, etc., which enable the teachers to perform Various activities like viewing the slides and answering the questions, doing activities based on the topics that are shown in the slides [9].

(2) **Listening**: It is a learning methodology where a learner understands through listening. The trainer shows the students a video or are made to listen an audio which could be of shorter or longer duration of time. Then, they are given questions to answer. It could be multiple choice questions or elaborate questions and the answers are expected spontaneously [10]. This enables the learner comprehend and analyse and enhance his or her listening skills.

(3) **Verbal Expression**: It is taught through classroom deliberation, speaking some rhymes in the classroom, asking the students to make guesswork teaching them tongue twisters, mutual teaching as well as learning. The students also learn how to use mnemonics. The students are taught to use acronyms, how to write and memorize words and form sentences. They are asked to read paragraphs, and it helps the students to improve their reading speed, pronunciation and have a neutral accent [11]. They could be given activities like group discussion, speaking impromptu on any topic of their choice. They can record their voice and listen to them. In that way, they could regulate their reading speed.

(4) **Kinaesthetics**: It is taught using non-verbal communication in the form of gestures and postures of the human body. A virtual lab could be developed and a student's gestures, movements of the body could be displayed and that could be monitored through a virtual mode in presence of all the students. The teacher may display after which the students could be asked to perform. This concept is called, TPR or total physical response. In the same way, the students could be taught rhymes and asked to demonstrate it in-front of the class using body language communication [12].

(5) **Tactile**: It is a teaching methodology which is performed by the use of usable teaching and learning materials like the students learn how to make collages by using the multimedia technologies. There are lot of multimedia technologies available and the students could use them which would make their work look more attractive.

(6) **Socio-interpersonal Interaction**: It is one of the most innovative learning methodology where a learner learns through online interaction with people and working with them across the globe. It is a technique where a learner learns by using notes from the social media, interacting with friends and other people through social media platforms [13]. For examples, students can benefit from attending online webinars, conferences, related to their field of study and they can also enhance their intellectual resources through various question and answer sessions that are held for their benefit.

(7) **Individual Learning**: It is a mode of learning where the learner learns by himself or herself. The learners are taught to look for various websites that are beneficial to them in their studies. They are taught to prepare personal bio-sketch, prepare resumes, how to express their hobbies and interests and their perception about any topic.

(8) **Multimedia Mode**: The learners are shown various online applications like PowerPoint and taught through the slides which are prepared by the trainers. They are given pdfs of the notes so that that could be used by the students to study for their exams [14]. This is one of the most important technique of teaching and learning as it makes the class more interesting and creates more impact on the learners

(9) **Online Debates**: Pick a subject associated with your problem and pair college students together. Assign one pupil to argue for the "pro" facet of the argument and the alternative pupil to argue the "con." the usage of your selected video assembly software, allow your students to debate the subject. Debates force college students to dig deeply into a subject and to apprehend both factors of view of the topic. It can growth empathy and enhance studies competencies. There's not anything like a bit opposition to get your students excited and to check their know-how. Inspire your students to think rapid through posting a couple of choice questions and having them answer as rapid as viable [15]. Trivia competitions can be performed in teams to lower the strain and to inspire bonding even when students are not in the equal school room. It is also a superb way to help college students practice for upcoming tests and quizzes [16].

(10) **Comic Strip** Upload a little humour in your school room by assigning your college students to create comedian strips after which put up them to your classroom discussion channel. That is an outstanding alternative for artwork students, overseas language training, English instructions, records instructions etc. Step back and watch the creativity drift. A few college students may additionally need to draw their comics on paper and experiment them. Others may create their personal memes, at the same time as others put together animated comic strips. You will be amazed at what they come up with video newscast.

(11) **Virtual Newspaper**, you are now the director of an information software. Send your "reporters" out to report news memories which are applicable on your current lesson. Drama students can file evaluations of famous films even as biology students can explain ground breaking new studies. Inspire your college students to research their topics, write their tales, then report them as an information report. Older college students may additionally need to use video software to feature photos or videos to decorate their stories.

(12) **Reciting a Poem**: Every other high-quality way to get innovative is to assign your college students to write down and carry out a music or poem on a particular subject matter. That is a super project for song college students, but it does not need to forestall there [17]. Your English college students can write slam poetry from the factor of view of a famous literary individual. Your history college students can write a global war II fight music. Your technology college students can write and carry out a rap about the sun gadget. The alternatives are endless, and the outcomes might be incredibly a laugh [18].

4 Effectiveness

Online activity-based learning is one of the most used learning methodology that is used by the majority of people across the world during the pandemic COVID-19. Online activity-based learning is implemented by various educational institutions across the globe. KIIT University, one of the premier engineering institutions in India was the first to incorporate in the online activity-based learning among the students in all the subjects of B. Tech stream. Almost the entire syllabus was revised which was challenging in a very short duration of time which consisted of applied science and humanities subjects. Among all these subjects, it was professional communication which posed to be more challenging [19]. Professional communication was offered to B. Tech first year students in the first semester. Apart from this, English is being taken by the faculties in medical science and nursing. This would help the students to in placement, enhancement of communication skills, in research and in bridging the gap between the learners and trainers. Since professional communication is more effective when its practised, the syllabus is designed in such a way that there are activities.

5 Advantages and Limitations

Online activity is comparatively new mode of teaching. Even then it has so many advantages [20]. It is beneficial for the students to take up any course irrespective of places and time. Similarly, the facilitator too could take his or her classes wherever he or she is present. It is not limited to only office hours. Sometimes classes could be taken outside office hours. Online activity-based learning has advantages as well as disadvantages. One of the major positive point is a learner can get access to the training irrespective of his presence. He or she can study without being physically present in the classroom. Same is for the trainer too who can impart education without being in the classroom. Due to availability of virtual classrooms and meeting links, it facilitates the trainers to teach. Apart from the meeting link, the classroom enables the teacher to check plagiarism content of the submitted assignments which makes the evaluation much easier. E-learning can produce a flexible and distributed learning system [21]. Due to flexibility in opting so many learning platforms, the trainer might use that platform which could be convenient for the faculty as well as the students. It is the duty of the teacher to make the class more interactive and make it as much elaborative as well as explanatory in nature.

6 Challenges Faced Due to Activity-Based Online Learning

Undoubtedly, online activity-based learning has many advantages, yet it is not free from challenges as well. Not all the students have the facility of Internet connection and laptops to access the online methodology of teaching. Due to sudden cause of pandemic in 2019, nobody was prepared for facing it, the governments had to impose lockdown across the country and schools and colleges were closed. As a result, the students had to rush to their hometowns. There were so many students living in rural areas and they could not have access to Internet [22]. Their classes got disrupted and they could not access the online mode of education. Not only that they had to face problems in their exams as many of them could not appear the exams too and had to drop their semesters. Apart from that there were some situations where the teachers were not technology saavy due to which they face problems while accessing the multimedia modes while taking classes. There were some senior faculties who could not take classes due to which they even lost their jobs. Other issues that the students faced was that they could not understand the deliberations of the faculties due to unstable network and sometimes when their data got exhausted. Another problem was the teacher was unable to know who are not attending the classes as sometimes it was not mandatory for students to keep their cameras on [23]. It was more natural that some students did not listen to the teacher even though they were online in the class. Another challenge the faculties faced was with the assignments of the students. It was quite easy for them to copy and paste them from the sources that were available online [24].

7 Conclusion

Due to technological advancement, online activity-based learning has proved to be more effective to the learners and the trainers who could not only take classes, but also it was possible to conduct online exams, and perform the evaluation too [25]. It also generated more interest among the learners who glued to their computer screens or mobile display screen. However, it is challenging for the new learners who did not have much Internet competency. Looking into the advantages and disadvantages, it would not be wrong to conclude that online activity-based learning has indeed created a platform among its audience and learners are more interested to explore its benefits rather than lacunae [26]. Therefore, this mode of learning is here to stay in the long run.

Scope for Further Research More and more learning oriented activities could be formulated and could be experimented on the young learners as it would create more impact on them due to their age and their inquisitiveness to explore new things.

References

1. Nasional, B. (17 March 2020). Kronologi Covid-19 di Malaysia. Berita Nasional. Dilayari di laman www.bharian.com.my pada 28 Oktober 2020.
2. Barnard-Bark, L., Burley, H., & Crooks, S. M. (2010). Explaining youth mentoring behavior using theory of planned behavior perspective. *International Journal of Adolescence and Youth, 15*, 365–379.
3. Bernard, R. M., Lou, Y., Abrami, P. C., Wozney, L., Borokhovski, E., & Wallet, P. A. (2003). How does distance education compare to classroom instruction? A meta-analysis of the empirical literature. In Paper presented at the annual meeting of the Association for Educational Communication and Technology.
4. Panko, M., Kenley, R., Davies, K., Piggot-Irvine, E., Allen, B., Hede, J. & Harfield, T. (2005). Learning styles of those in the building and construction sector. Rep Build Res, New Zealand.
5. Anaheim, C. A., & Datnow, A. (2020). The role of teachers in educational reform: A 20-year perspective. *Journal of Educational Change, 21*(1), 109–113.
6. Schneider, S. L., & Council, M. L. (2020). Distance learning in the era of COVID-19. *Archives of Dermatological Research.* https://doi.org/10.1007/s00403-020-02088-9
7. Shiue, Y. (2007). Investigating the sources of teachers' instructional technology use through the decomposed theory of planned 534 behavior. *Journal of Educational Computing Research, 36*(4), 425–453.
8. Mishra, D. (2021). Learning how to learn: An analysis through styles and strategies. *International Journal of Web-Based Learning and Teaching Technologies, 15*(3), 46–59.
9. Oxford, R. (1989). *The role of styles and strategies in second language learning.* ERIC Digest.
10. Oxford, R. (1990). *Language learning styles and strategies: What every teacher should know.* Newbury House Publisher.
11. Pashler, H., & McDaniel, M. (2009). Learning styles: Concepts and evidence. *Psychological Science in the Public Interest*. https://doi.org/10.1111/j.1539-6053.2009.01038.x. PMID:26162104
12. Riener, C. & Willingham, D. (2010). The myth of learning styles. *Change the Magazine of Higher Learning,* August 2010, 33–36. https://doi.org/10.1080/00091383.2010.503139.

13. Rubin, J., & Irene, T. (1982). *How to be more successful language learner*. Heinle and Heinle; Scarcella, C. R., & Oxford, R. L. (1992). *The Tapestry of Language Learning: The Individual in the Communicative Classroom.* Heinle & Heinle.
14. Schumaker, J. B., Denton, P. H., & Deshler, D. D. (1984). *Learning strategies curriculum: The paraphrasing strategy*. University of Cansas.
15. Schumaker, J. B., Deshler, D. D., Alley, G. R., & Denton, P. H. (1982). Multipass: A learning strategy for improving reading comprehension. *Learning Disability Quarterly, 5*(3), 295–304. https://doi.org/10.2307/1510296
16. Shams, L., & Seitz, A. R. (2006). Benefits of multisensory learning. *Trends in cognitive sciences.* https://doi.org/10.1016/j.tics.2008.07.2006
17. Weinstein, C. E., & Mayer, R. E. (1983). The teaching of learning strategies. *Innovation Abstracts*, *5*(32).
18. Wenden, A. (1998). Metacognitive knowledge and language learning. *Applied Linguistics, 19*(4), 515–537. https://doi.org/10.1093/applin/19.4.515
19. Pusvyta, S. (2015). Memotivasi belajar dengan menggunakan E-Learning. *Jurnal Ummul Quro, 6*(2), 20.
20. Raheim, M. D. H. (2020). Indonesian university students' likes and dislikes about emergency remote learning during the COVID-19 pandemic. *Asian Journal of University Education (AJUE), 17*(1), 1–18.
21. Ratheeswari, K. (2018). Information communication technology in education. *Journal of Applied and Advanced Research., 3*, 45. https://doi.org/10.21839/jaar.2018.v3iS1.169
22. Lakshmi, A. (2007). Activity based learning a report on an Innovative Method in Tamil Nadu. [Online]. Available from: http://www.ssa.tn.nic.in/Docu/ABL-Report-by-Dr.Anandhalakshmi.pdf [2013, May 20].
23. NCSALL. (2006). Activity-based Instruction: Why and How. [Online]. Available from: www.ncsall.net/fileadmin/resources/teach/GED_inst.pdf [2013, May 20].
24. Kammanee, T. (2002). *To team work and learning.* Nishin Advertising Group.
25. Maneengam, N. (2004). A development of a program to promote an energy saving mind through service learning concept for prathom suksa six students. Master Thesis. Chulalongkorn University.
26. Lualamai, N. (2009). Research and development of an activity organization model to enhance moral and ethics of elementary school students. Master Thesis. Chulalongkorn University.
27. Schumaker, J. B., Walsh, L. D., & Fisher, J. B. (2021). Effects of computerized instruction on mastery and generalized use of commas strategies by students with LD. J Spec Educ Technol, 36(1):29–43. https://doi.org/10.1177/0162643419878146

Use of a Fatigue Framework to Adopt a New Normalization Strategy for Deep Learning-Based Augmentation

R. Regin, Ahmed J. Obaid, S. Suman Rajest, and M. Kalyan Chakravarthi

Abstract Current techniques for electroencephalograph (EEG) emotion recognition still train prototypes equidistant using all EEG measurements. Moreover, since a few of the source (training) samples are significantly different from the target (test) samples, they can negatively impact. As a result, rather than forcing a classification model to be trained using all of the samples, it is crucial to listen carefully to EEG samples with a high transferability. Furthermore, according to neuroscience, not all of the signalling pathways in an EEG study contain emotional information effectively conveyed to the test results. Even some data from specific brain regions would significantly negatively impact learning the emotional classification model. In the light of certain two issues, in this article, we propose a TANN for EEG speech signals that develops emotional discriminant features by emphasizing traceable EEG neural domains data and samples adaptively through locally and globally attention mechanisms. To do so, measure the outputs of different brain discriminators as well as a specific test discriminator. TANN outperforms existing state-of-the-art approaches in comprehensive EEG emotion recognition studies.

Keywords EEG emotion recognition · Sampling · Feature normalization · Brain region · Transferable attention · Normalization strategy

R. Regin (✉)
Department of Computer Science & Engineering, SRM Institute of Science & Technology, Chennai, India
e-mail: reginr@srmist.edu.in

A. J. Obaid
Faculty of Computer Science and Mathematics, University of Kufa, Kufa, Iraq
e-mail: ahmedj.aljanaby@uokufa.edu.iq

S. S. Rajest
Department of Research, Bharath Institute of Higher Education and Research, Chennai, India
e-mail: sumanrajest414@gmail.com

M. K. Chakravarthi
School of Electronics Engineering, VIT-AP University, Amaravathi, India
e-mail: kalyanchakravarthi.m@vitap.ac.in

T. D. L. Nguyen and J. Lu (eds.), *Machine Learning and Mechanics Based Soft Computing Applications*, Studies in Computational Intelligence 1068,
https://doi.org/10.1007/978-981-19-6450-3_18

1 Introduction

Due to the wide variety of application areas in areas such as sociology interaction [1], immersive narration [2], and anxiety disorders [3], emotion recognition has gained a lot of attention. Investigators are using EEG signal emotion recognition due to its low cost over such reduced options, non-intrusive technologies like as electromyogram (EMG) and electromyography (ECG), which are currently limited to multisensory emotion recognition [4], or gestures and strategies for recognizing emotions are sensitive to cognitive bias. Emotion is a necessary factor. It is a fundamental aspect of human, and it has a huge effect on people's everyday lives such as interaction, engagement, and training. It is critical to recognize those around us' mental expressions to communicate naturally [5]. Furthermore, biometric detection is an essential and complicated process in personal communication [6]. In recent years, several papers on strategy frameworks for sentiment analysis were written, and they can be classified into three types: (1) speech and facial expressions; (2) peripheral behavioural indications; and (3) central nervous system developed brain signals [7].

The playback transmitters that detect facial expression and voice achieve sentimentality with no physical touch detection in these tests. Still, they are not always reliable since people can easily hide their emotions without being detected [1]. Since users have little control over physiological signals, they have a relatively high recognition accuracy than audio-visual approaches. The peripheral nervous system (PNS) is affected by one form of structural alteration, while the nervous system (CNS) is affected by the other (CNS). Typically, functions derived from specific physiological signals like the electrocardiogram, skin conductance (SC), and heartbeat provide comprehensive and nuanced details for identifying emotional states [6]. Electroencephalogram (EEG) signals taken from the brain's cerebral cortex, compared to other distant physiological signals, can represent brain activity and get a natural affinity for specific mental responses [4]. With both the fast development of products that can be worn, versatile dry electrodes, artificial intelligence, and a wide variety of human abilities machine interface applications. Electroencephalography sentiment analysis is becoming increasingly common. Research and techniques have been proposed. Researchers used extracted features, information collection, and highly nonlinear systems are all examples of stochastic processes. Assessment to derive various EEG signals in their raw form in subsequent studies to test the association among EEG data and emotional states [8–10].

Linear discriminant analysis and principal component analysis are commonly used methods for reducing the dimension of features [11–13]. In addition, weak and redundant features were eliminated using singular value decomposition and QR factorization [10, 14]. Existing optimization maximum relevance, component analysis (PCA) and QR factorization simulating approaches such as decision tree (NB), SVMs, and random forest (RF) are often combined by mechanical uniqueness selection and procedures for choice [12, 15]. Current deep learning methods allow automated feature extraction, which greatly affects the signal and cognitive abilities [16].

The auto-encoder (AE) and co-evolutionary neural network are several computer vision frameworks effectively implemented to process physiological signals and have shown encouraging results compared to shallow models [17, 18]. Using two regular emotion recognition datasets, a multisensory deep learning approach was used to recognize different emotions.

They demonstrated that the bimodal dense vehicle (BDAE) extracted essential elevated representation features for emotion classification [2]. To help minimize overfitting, Wang et al. [19] used the region rising technique, which produces extracts from the datasets updated. They discovered that database systems might have a larger impact with the deep learning approach when evaluating PCA and Reuters systems (i.e., LeNet and Res-Net) on the SEED and MAHNOB-HCI datasets. The user's emotional states are usually viewed as different factors in many other situations. On the other hand, emotion is a complex process with a time-dependent structure that must be considered into account [9]. Deep learning approaches such as CNN and AE were unable to comprehend the temporal information provided in EEG. Recurrent neural network (RNN) is yet another classifier that uses associations between units to create a loop that allows it to handle datasets. The use of RNN in speaker identification and machine translation is popular [11].

Long-term commitments, on the other hand, are a challenge for standard RNN. Some RNNs are used to process and interpret brain measures, like long short-term memory [13], which have shown to solve this question. For multimodal signal emotion detection, a bimodal-LSTM framework was suggested by Tang et al. [20–22]. On the SEED dataset, the highly skewed model [10] utilized EEG and movement patterns characteristics as inputs, when on the DEAP dataset, it evaluated EEG and secondary sensory information. To grid-like7–15: sets the micro impulses in the DEAP file, [23] used spectral and structure walls transitions. To collect task-related attributes, investigate Bilbao association, and implement contextual data from the sets, the researchers developed a CNN-LSTM hybrid classifier. Single recurrent units (SRU), a new RNN version, has recently been proposed [24], which can simplify the calculation and reveal more parallelism, resulting in a substantial reduction in training time. We utilize SRU to build a classification model that includes temporal variations to assist EEG and computation productivity in emotion indication in this paper. In addition, community methods of instruction have combined different SRU models to achieve better outcomes than a single base model. This present study tries to analyse after another user's future emotion configuring a model tailored to the person. To check the efficacy of the proposed algorithms, we test its consistency of our method for recognizing emotions over days [25].

The above is the paper's style. Section 2 of this paper introduces the SEED dataset. Section 3 discusses DT-CWT, feature extraction methods, the SRU network, aggregate strategies, and our technique and performance. The findings are presented in Sect. 3. Section 4 examines related studies and explores the study's contributions and shortcomings. Furthermore, conclusions have been drawn in this section. It is a question of how to identify evoked emotions using EEG recordings. We quickly ran into the most difficult problem when designing brain imaging methods: low EEG activity homogeneity through participants. Figure 1 shows how the plots were made

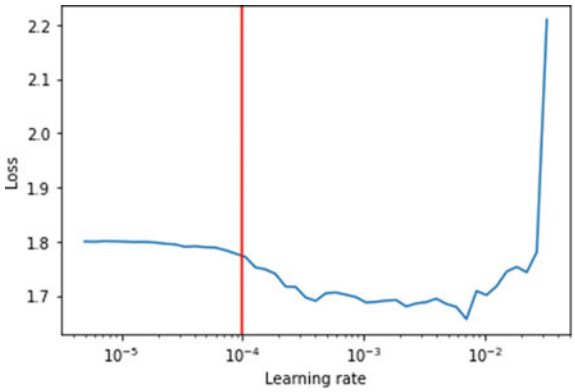

Fig. 1 Gerbing is embedded after plots were made by selecting data

by selecting data for each EEG recording for each participant and using the dimensionality reduction tool UMAP to insert the details. Colours on the left represent feelings, and colours on the right indicate who the data belongs to. As a result, if we try to infer emotions on a fifth participant using a model trained to identify emotions with four participants, the results would be bad.

The most widely used approach to this problem is to use a calibration stage to pre-train the AI model. However, since this is a time-consuming method, many researchers have been looking for alternatives. While the emphasis of this review is on brain imaging techniques, the same issue can be found in other fields such as image recognition, voice recognition, and facial expressions.

Several authors have found solutions to this problem in recent years. The majority of proposed solutions for brain imaging are focused on selecting robust features. That being said, (1) the classifier output of person involved classification techniques with all those features is still inferior to visitor models, and (2) these features are task-specific, preventing robust solutions across tasks and fields. As a result, we investigated stratified normalization, a new participant-based normalization approach for training deep neural networks.

This method's key concept is to proportionate additional information to the neural network to boost its accuracy. It is important to remember that this additional data must be distinct from the data we are attempting to infer. For example, in our dataset, we are attempting to identify emotions, so the session and participant for each data are used as additional information.

The function of cross-subject emotion classification from EEG signals is the focus of our research. The results show that networks trained by stratified normalization outperform networks trained with batch normalization.

To give a quick overview of our paper, we will concentrate on the proposed method and compare it to the well-known batch normalization method. In addition, to confirm the clarification, I will first go through the dataset we used for the study. Finally, we will present our findings and draw a brief conclusion.

2 Review of Literature

The computer vision is one of the most important study areas in sophisticated user touch, with applications in augmented reality, video game engagement, educational systems, and the diagnosis of mental diseases. For the purpose of understanding frame of mind input and its uses to emotion recognition, a diverse variety of techniques were thoroughly examined. External data, such as face features [3], speech [24], and gesture [1], were favoured in the early stages of this field, and they were easily understood and tangible cues that fit individuals' basic understanding, and they were prevalent and could be accumulated on a large scale in the laboratory or in the wild. Despite these benefits, external data has a flaw because humans have a natural inclination to hide their feelings on occasion, and their manifestations may not match their real feelings. Data base such as signals, heart rate, hypertension, and galvanic skin response [6], which are difficult to mimic, have also been attractive to the work of sentiment analysis due to the need for more reliable types of data. The widespread use of this strategy, however, has certain problems. Internal signal measurement tools used to be big and difficult to operate. Smartwatches, such as wristbands, are now convenient, and some sorts of data can be gathered by them.

Thresholding, semantic segmentation, feature engineering, and classifying are the four basic stages of a traditional EEG-based emotion identification system [16]. The accuracy of emotion recognition relies heavily on feature extraction. Areas can be examined for brain signals, but each domain has numerous related properties. Texture feature [5], Hjorth features [8], clustering algorithms [9], high frequency bridging feature [10], statistic feature [11] (mean, standard error, variability, and first and secondary difference), and so on are examples of day when features. The raw EEG data in the analysis window is first transformed into five primary bands using discrete Fourier transform or autoregressive [12] methods to obtain frequency domain characteristics. Power spectral density, divergent entropy [13], differentiated imbalance, and rational opacity [7] are common extracted properties from frequency bands. The same approach as in the time–frequency was used for the time–frequency domain characteristics, however, the signal conversion algorithm was transform [2] or wave packet compression [15]. Following the acquisition of the desired features, computer learning-based classifications were proposed to classify the feature patterns into emotions. The most commonly used classifiers in studies are the predictive model [19] and its derivatives [4]. The s n neighbour classifier, and was used in [23], is yet another good classifier.

3 Dataset

The dataset is a SEED dataset, which would be a list of EEG datasets. This dataset is one of the most significant in EEG-based affecting computing, along with the DEAP dataset.

It contains 62-channel EEG information gathered from 15 respondents in three sessions during the same 15 archive footage. Each film clip was given an emotional rating (positive, neutral, or negative) based on the results of 20 respondents who were asked to describe one of the programmes after viewing it. In overview,

- Number of participants: 15
- 3 × 15 sessions x images (45 videos for each participant).

Šlégrová et al. [23] were the first to propose batch normalization as a solution to this issue of back to a particular change, which is a shift in the allocation of neuron activations that are not needed to be caused by the learning process. It is the most widely used normalization method in neural networks, with excellent results in various applications.

We slightly modified the procedure for our purposes, as discussed further below. Our specification of the convolutional layers method is shown in Fig. 2. The normalization for this method is done per function for each batch.

In terms of the value of normalization in cross-subject classification, research by [1] and [12] provided the first glimpses into the benefits of this method after using participant-normalization of facts obtained to minimize inter-respondent variability. When they normalized the data for each individual separately, they discovered that now the difference among the clusters, where each region refers to the sole participant because the influence of respondent identity information is greater than the influence of emotion [26, 27], decreases. Later work by [11] took advantage of this finding. It introduced nonlinear collected data that smoothly incorporated individual traits into an inter-participant method while for each function and individual, the standard was used. They trained a classifier using the proposed transformation and analysed the data to a conventional Z-score standardization. Security shows that their method reduced the magnitude of this component by using PSD functionality. Their findings outperformed Z-score standardization; they concluded that different normalization methods are needed because of eliminating the specific topic. The sensor aspect is

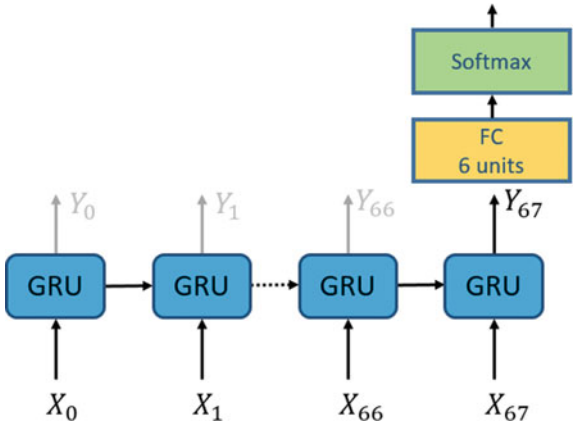

Fig. 2 Process of batch normalization. The data is processed for each function, regardless of user or event

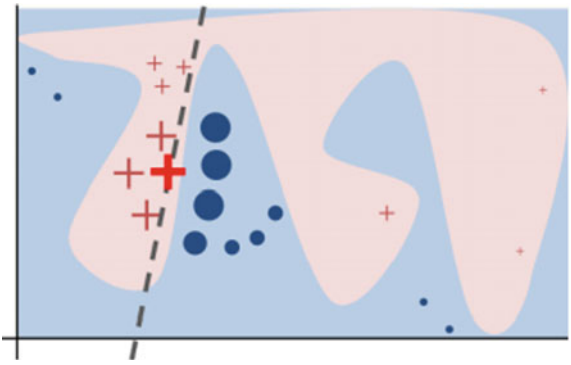

Fig. 3 Process of heterogeneous regularization

function and verbal abuse [28]. The proposed approach is stratified normalization, which entails feature normalization for each participant and session. The stratified normalization process is depicted in detail in Fig. 3. This method normalizes the data per function, participant, and session instead of the previous normalization method [29]. The key disadvantage of batch normalization is that it requires either a broad batch collection or a study of how much data is present per class in each batch [14].

4 Results

The goal of extracting features is to obtain the most important EEG features under various emotional states [15]. We analyse four distinct types of characteristics from the perspectives of time, rate, and spatial research for a detailed review. The section length should be chosen with care. The far more contextual knowledge you have, the better. A segment reflects the fewer samples we receive in the data pool. They first separated the EEG signals into 5 s segments to the frequency and length of the segments should be controlled. Every 0.5 s, four feature extraction methods were used with an interval of 0.5 s. Since each phase had a 50% duplication rate, the processing time for every section was 19. Furthermore, since 62-channel interfaces are being used in this test, each sector's source configuration was 62*19. Several iterations from each group of the three-class facial expression task were roughly equal.

Using the architecture displayed in Fig. 4, the results are displayed in Figs. 4 and 5.

Figures 5 and 6 display the predicted values' inserting at the neural net's output units. The results show that sentiment analysis reliability is better at the output nodes, and respondent detection performance is lower for trained models with strata normalization. Indeed, representations on the UMAP are more portable for stratification liberalization than average pooling this period and easily recognizable for

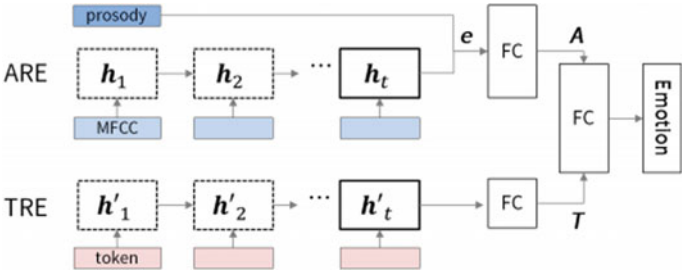

Fig. 4 Classification system's framework

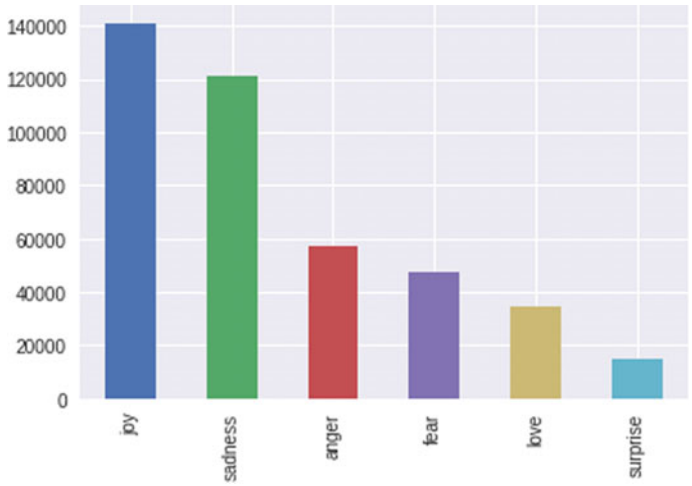

Fig. 5 Neural network's performance is embedded with regularization and three sentiment groups

attitude ratings instead of participant amounts. The variation of colours suggests that much of the brain signature is omitted.

These results indicate that segregated standardization is a powerful tool for recognizing emotions through subjects.

5 Conclusion

Strategies that allow for the construction of robust contestant systems without the necessity for each patient's prior recorded data have been extensively deployed and evaluated in studies. The main goal is to uncover characteristics that all responders have in common. Because these procedures are still less trustworthy than attending models, observers am looking at alternative ways, such as data well before. This

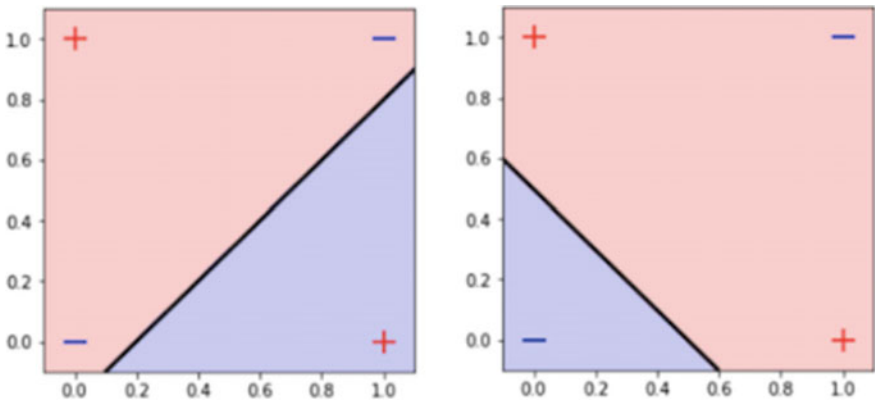

Fig. 6 Heterogeneous regularization and three sentiment divisions are used to implement the neural network's performance

post proposes and evaluates stratified normalization, a popular contestant attributes normalizing strategy for improving the inter Ferential efficiency of contestant models. It is impossible to avoid conducting research. This study looked into the inter and micro characteristics of EEGs that are linked to emotion changes. An intelligent monitoring system was created using a complex recursive units network and community learning approaches to differentiate three different mental expressions. The following are some of the basic findings: (1) higher-intensity bands, such as gamma and gamma, are better at detecting emotions than lower-frequency bands. (2) Using EEG scales, positive affect is more detectable than its other two states of mind when stimulated through auditory and visual resources in the tests. (3) Using datasets, the SRU network, as an excellent RNN performer, can comprehend the transitory changing qualities under emotional situations. (4) A well-designed Network + link prediction method for robotic emotion recognition results in a large number of invoices issued and a fair obtain accurate. (5) Our emotional network's performance reveals that neural trends are essential and rather consistent throughout and across days. These findings show that stratified standardization is effective for cross-subject sentiment analysis tasks, implying that this strategy might be used with other EEG tagging datasets and transfer classifiers.

6 Future Work

Future study should focus on the effectiveness and implementation of non-invasive brain emotion recognition. EEG can include more useful and representative elements. Numerous studies discovered that by adding power spectral and raw or before EEG signals, support vector machine got higher values of regression for classifying emotions than other features. To improve the classification performance, we

will try to mix various features. The use of spectral analysis for especially in areas sentiment analysis in space will be attempted in future. A further in-depth evaluation of approaches will be conducted, as well as the mixture of their benefits in extraction of features and avoid overfitting. Future study could include adapting the approach to data fusion and other vital signs in the analysis of brain activity.

References

1. Black, M. J., & Yacoob, Y. (1997). Recognizing facial expressions in image sequences using local parameterized models of image motion. *International Journal of Computer Vision, 25*(1), 23–48.
2. Kingsbury, N. G. (1998). The dual-tree complex wavelet transform: A new technique for shift invariance and directional filters. *IEEE Digital Signal Processing Workshop, 98*, 2–5.
3. Acharya, U. R., Sree, S. V., Peng, C. A. A., Yanti, R., & Suri, J. S. (2012). Application of non-linear and wavelet based features for the automated identification of epileptic EEG signals. *International Journal of Neural Systems, 22*(2), 565–579.
4. Li, X. W., Hu, B., Zhu, T. S., Yan, J. Z., & Zheng, F. (2009). Towards affective learning with an EEG feedback approach. In Acm International Workshop on Multimedia Technologies for Distance Learning, ACM, pp. 33–38.
5. Chen, P. (2000). References [1] R.W. Picard, Affective computing, MIT Press
6. Brosschot, J. F., & Thayer, J. F. (2003). Heart rate response is longer after negative emotions than after positive emotions. *Journal of Psychophysiology, 50*(3), 181–187.
7. Kim, K. H., Bang, S. W., & Kim, S. R. (2004). Emotion recognition system using short-term monitoring of physiological signals. *Medical and Biological Engineering and Computing, 42*(3), 419–427.
8. Chen, L. L., Zhang, J., Zou, J. Z., Zhao, C. J., & Wang, G. S. (2014). A framework on wavelet-based non-linear features and extreme learning machine for epileptic seizure detection. *Biomedical Signal Processing and Control, 10*, 1–10.
9. Chen, L. L., Zhao, Y., Ye, P. F., Zhang, J., & Zou, J. Z. (2017). Detecting driving stress in physiological signals based on multimodal feature analysis and kernel classifiers. *Expert Systems with Applications, 85*, 279–291.
10. Daimi, S. N., & Saha, G. (2014). Classification of emotions induced by music videos and correlation with participants' rating. *Expert Systems with Applications, 41*(13), 6057–6065.
11. Deng, L., Li, J. Y., Huang, J. T., Yao, K. S., Yu, D., Seide, F., Seltzer, M., Zweig, G., He, X. D., Williams, J., Gong, Y. F., Acero, A.: Recent advances in deep learning for speech research at Microsoft. In International Conference on Acoustics, Speech, and Signal Processing (ICASSP) (pp. 8604–8608), IEEE (2013)
12. Gupta, R., Laghari, K. U., & Falk, T. H. (2015). Relevance vector classifier decision fusion and EEG graph-theoretic features for automatic affective state characterization. *Neurocomputing, 174*, 875–884.
13. Hochreiter, S., & Schmidhuber, J. (1997). Long short-term memory. *Neural Computation, 9*(8), 1735–1780.
14. Majid, N. (2019). Methods of strengthening children's characters through local wisdom Mappatulung Bugis as National identity. *International Journal of Theory and Application in Elementary and Secondary School Education*, *1*(2), 10–24.
15. Koelstra, S., Muhl, C., & Soleymani, M. (2012). DEAP: A database for emotion analysis issuing physiological signals. *IEEE Transactions on Affective Computing, 3*(1), 18–31.
16. Chai, X., Wang, Q. S., Zhao, Y. P., Liu, X., Bai, O., & Li, Y. Q. (2016). Unsupervised domain adaptation techniques based on auto-encoder for non-stationary EEG-base demotion recognition. *Computers in Biology and Medicine, 79*, 205–214.

17. Muraina, K. O., S. M. G, & Kabir, Z. M. (2020). The future of guidance and counselling in the 21st century in Nigeria: Changing face-to-face counselling through cyberspace counselling. *IJRSE*, *2*(2), 91–98.
18. Utomo, K. P., & Kamal, F.: A strategy to improve the learning of political culture with debate method in vocational high school 1 Bekasi. *IJRSE*, *2*(1), 1–12
19. Li, M. Y., Chen, W. Z., & Zhang, T. (2017). Automatic epileptic EEG detection using DT-CWT-based non-linear features. *Biomedical Signal Processing and Control, 34*, 114–125.
20. Mbaya, L., Abu, G. O., Caiaphas Makadi, Y., & Umar, D.: Effect of urbanization on land use land cover in gombe metropolis. *IJRSE*, *1*(1), 22–29.
21. Abdulhamid, M., Dauda, S.: Appraisal of attitudes and utilizations of information and communication technology (ICT) among students in Nigerian universities. *IJRSE*, *1*(1), 50–61.
22. Emayavaramban, M., Kandasamy, R. K., Muthusamy, S., & M. Manickam,. (2020). India. Int. J. Theory Appl. Elem. Second. Sch. Educ., *2*(2), 121–142.
23. Šlégrová, L., Šlégr, J., & Studnička, F. (2020). Global warming: Facing confirmation bias and cognitive dissonance with hands-on activities. *IJRSE, 2*(2), 123–133.
24. Bal, U. (2012). Dual tree complex wavelet transform based de-noising of optical microscopy images. *Biomedical Optics Express, 3*(12), 3231–3239.
25. Quimson, J. M. Q. (2022). STEM students' engagement in horizontal transfer from calculus to physics and their difficulties. *IJRSE, 3*(1), 36–46.
26. Tahsildar, M. N. (2019). Investigating features related to Chinese linguistic complexities among international students learning Chinese as a foreign language. *International Journal of Theory and Application in Elementary and Secondary School Education*, *1*(1), 63–78.
27. Silalahi, M. (2019). Improving students' interest in learning english by using games. *International Journal of Theory and Application in Elementary and Secondary School Education*, *1*(1), 55–62
28. Donato, N. M. (2021). The relationship of the strategies and practices of the school heads and master teachers and teachers' competencies and skills in the new normal. *International Journal of Theory and Application in Elementary and Secondary School Education*, *3*(2), 125–139
29. Sampson, N. M., Ebong, M. S. (2019). Social media utilization and academic performance of students studying geography in public secondary schools in Nsit Atai local government area, Akwa Ibom State, Nigeria. *International Journal of Theory and Application in Elementary and Secondary School Education*, *1*(2), 25–57.

An Innovative and Smart Agriculture Platform for Improving the Coffee Value Chain and Supply Chain

Van Duy Nguyen, Tri Cong Pham, Chi Hieu Le, Thanh Trung Huynh, Tan Hung Le, and Michael Packianather

Abstract Vietnam is the world's second biggest producer of coffee and has been an exporter for several decades. However, Vietnam has been facing many well-documented issues and challenges in the whole coffee supply chain such as climate change; low productivity, poor quality and high cost; excessive use of fertilizing products and irrigations; poor collection, processing and storage solution; low sustainability and limited value-added coffee products; and low applications of smart and sustainable agriculture solutions. This paper introduces an innovative and smart agriculture (INNSA) platform for the creation and operation of a sustainable coffee value chain, with the focus on enhanced quality and added values for key elements of the coffee supply chain in Vietnam. The platform is designed based on the foundations of the key enabling digital transformation and smart agriculture technologies: Smart devices and Internet of Things, big data, artificial intelligence, blockchain and source traceability technologies, and sustainable design and manufacturing. The INNSA platform has the following key features: a smart database with real-time data inputs and updates, cost-effectiveness, and open-architectures for effective integrations of the enabling digital transformation and smart agriculture technologies. The smart platform and ecosystem of INNSA provides the information portal and open-access database for all key factors of coffee supply chain, enabling them to join and interact with each other to bring the coffee industry of Vietnam to a higher level, well-recognized in terms of values, branding and sustainability.

V. D. Nguyen (✉)
Institute of Biotechnology and Environment, Nha Trang University, Nha Trang City, Vietnam
e-mail: duynv@ntu.edu.vn

T. C. Pham
School of Computer Science and Engineering, Thuy Loi University, Hanoi 100000, Vietnam

C. H. Le
Faculty of Engineering and Science, University of Greenwich, Kent ME4 4TB, UK

T. T. Huynh · T. H. Le
SOICT, University of Science and Technology, Hanoi 100000, Vietnam

M. Packianather
School of Engineering, Cardiff University, Cardiff CF24 3AA, UK

T. D. L. Nguyen and J. Lu (eds.), *Machine Learning and Mechanics Based Soft Computing Applications*, Studies in Computational Intelligence 1068,
https://doi.org/10.1007/978-981-19-6450-3_19

Keywords Coffee value chain · Big data · Artificial intelligence · Source traceability technology · Internet of things · Vietnam

1 Introduction

The coffee production in Vietnam has developed as the world's second biggest producer of coffee production and export for several decades. However, Vietnam coffee now faces several challenges, including the following ones: (1) climate change: the coffee production is heavily affected due to tropical storms, the worst droughts, rising temperatures, and shifting rainfall patterns. 50% of the current Robusta coffee production areas in Vietnam are forecasted to be lost by 2050; (2) low productivity, poor quality and high cost: caused by ground-water loss and soil pollution in most of the coffee planting regions. About 50% of total coffee trees are between 10 and 15 years old. Aging trees, unsuitable lands and no sustainable solution for growing coffee plants will directly affect the productivity, quality of Vietnamese coffee products, and production costs; (3) excessive use of fertilizing products and irrigations: causing coffee trees to quickly become exhausted and soil to be severely polluted, with more diseases and harmful pests for coffee trees; (4) poor collection, processing, and storage solution: causing low quality and unstable productions; (5) low sustainability and limited value-added coffee products: the value-added products and types from coffee are limited, and the coffee waste and ground are mainly sent to landfill, with no recycling; and (6) low applications of smart and sustainable agriculture solutions [1–7].

Regards to the last challenge, there are limited applications of smart agriculture solutions to enhance the value streams of the coffee supply chain in Vietnam, including IoT, smart devices, unmanned aerial vehicles (UAVs), precision agriculture, hi-tech solutions for processing and recycling coffee, AI, big data, blockchain and source traceability technologies, eco-design, and sustainable manufacturing.

Compared to Brazil, the productivity of coffee in Indonesia and Vietnam is lower but the number of smallholder coffee farmers is higher. The root of the problem is the coffee farming practices in Indonesia and most small-scale farms in Vietnam are still based on traditional methods with trial and error. Therefore, in order to actually change the way of coffee farming practices in Vietnam and Indonesia, the digital transformation and the integration of smart and hi-tech agriculture for the coffee supply chain and value chain must be considered, and also include the sustainable practices that consist of continuous improvement in environmental, social, and financial aspects.

Application of the IoT through a network of wireless sensors in a coffee farm for monitoring and control of its environmental variables have currently been studied [8]. The study showed that the management of coffee cultivation is quite complex due to the large number of varieties found, the terrain and environmental conditions affecting the production process and the final grain quality. Also, the development and implementation of wireless sensor networks is possible today due to factors

such as the reduction of device costs and the use of open-source software, avoiding additional licensing values. One of the main problems with coffee plants is, however, that high humidity can, in fact, impact the activity of the sensors and their monitoring tools.

There are numerous limitations when harvesting and production processes are optimized. Vietnam has a great potential to encourage investment in agriculture. The proliferation of new technologies has enabled the enhancement and automation of industrial processes in all fields of production such as coffee. Therefore, aided by technology, an agricultural sector such as coffee production can strongly improve the country's productivity and give enormous benefits for production processes and the optimization of final products [9, 10].

Precision agriculture includes many activities such as the management of trees, flowers, crops, and plants. Pest and disease management is one of its most interesting applications. By the suitable use of sensors, parameters (such as soil temperature and relative humidity, leaf temperature and humidity, and solar radiation) can also be measured to quickly detect adverse and appropriate situations. In addition, this technology can help to manage the time-based detection and the efficiently space-based use of pesticides [2].

Hi-tech solutions for processing and recycling coffee have some great benefits and add significant values to the coffee value chain. For example, not only does it divert waste away from landfill, but the spent coffee grounds can be used to produce some value-added things like biofuels, bioactives, and anticancer drugs. It can also help businesses save money on their waste disposal [11, 12].

In this paper, the innovative and smart agriculture platform for the creation and operation of sustainable coffee value chain, with the focus on enhanced quality and added values for key elements of the coffee supply chain in Vietnam, taking into account the issues related to sustainability, well-aligned with United Nations Sustainable Goals. The platform is designed based on the foundations of the key enabling digital transformation and smart agriculture technologies: smart devices and Internet of Things, big data, artificial intelligence, blockchain and source traceability technologies, and sustainable design and manufacturing.

2 Development of an Innovative and Smart Agriculture Platform

Figure 1 presents the research method for development of an innovative and smart agriculture platform, called the INNSA platform, with the highlights of the key steps and tools. Firstly, the data types and sources are very important for development of the smart agriculture systems, in which the real-time data collection and analysis needs to be optimally implemented. Then, the latest development of the digital transformation technologies needs to be taken into account, when working on data collections and analysis, and development of the smart platform and ecosystem of INNSA, including

smart devices and Internet of Things, big data, artificial intelligence, blockchain and source traceability technologies, and sustainable design and manufacturing. Finally, value-added products and services in the value chain of the INNSA platform and its related ecosystems are developed, with the focus on the cost-effective and innovative solutions, including the hardware, software, smart devices, e-commerce platform, and innovative products from coffee trees, beans, and wastes.

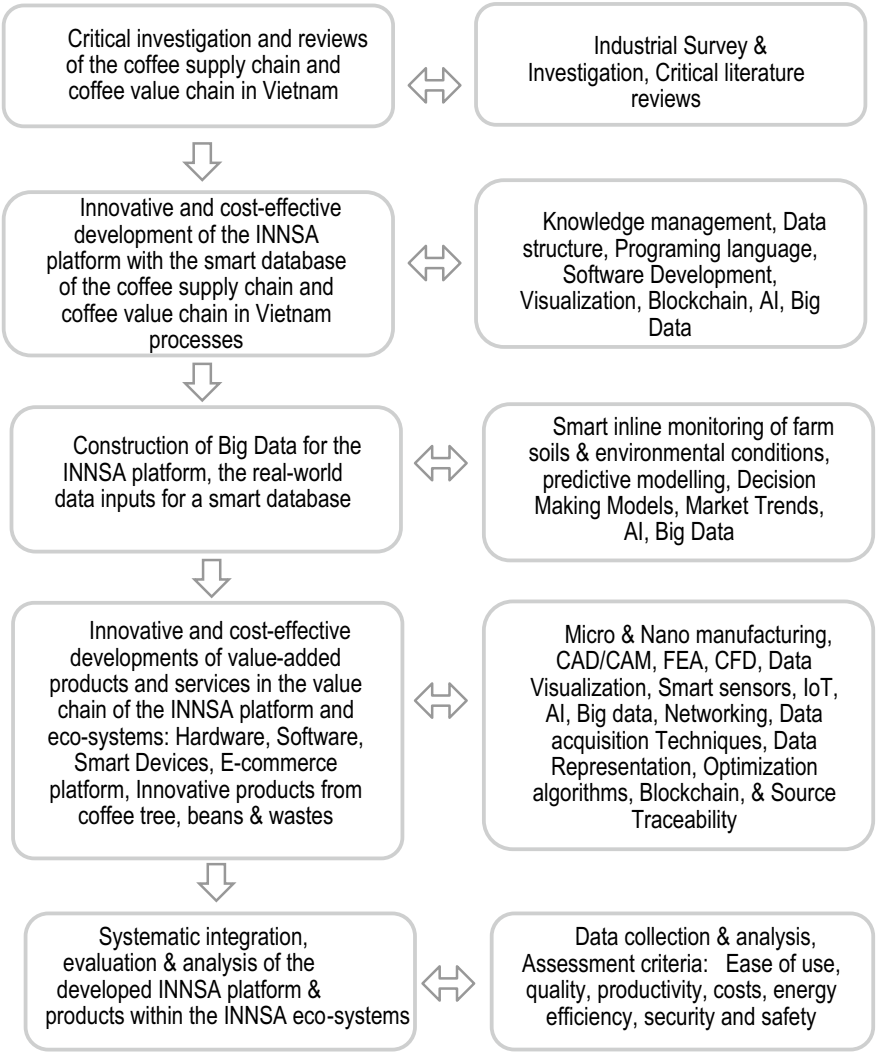

Fig. 1 Research methods for development of the INNSA platform

2.1 Data Type, Sources, and Collections for Development the INNSA Platform

A critical analysis and industrial investigations were done, with the use of both primary and secondary data, including the journal article data, open-source data about agriculture, and farming industry from both governmental and industry reports. The primary data from surveys, interviews, and sensor-based supply chain operations was also collected for value chain mapping, developing, and validating the INNSA platform.

The data sources included farm soils, environmental conditions, farm types, products from coffee farms and food wastes, and key stakeholders in the coffee supply chain and value chain. They also included the information about currently used agriculture technologies (robots, temperature and moisture sensors, aerial images, IoT, and GPS) and products such as fertilizer for growing plants and precision agriculture. The data architecture of the smart database was designed with capability of continuous update and co-creation, and automatic updates from smart devices and IoT, with options for the IP right licenses and open access.

To maximize productivity of a coffee farm, certain factors related to soil, weather, and environmental conditions must be met. The INNSA platform was designed to collect and analyze farm soil, weather, and ecosystem factors, focusing on high-yield variables of coffee plants. Based on real-time data monitored and obtained, our platform produced reports and suggestions of the best agricultural practices which the users can follow to approach the highest productivity. This is based on agronomical science and farmers' experience knowledge to produce these reports and suggestions exactly and rapidly. Besides, the INNSA platform also guided the users with farming practices to explore their resources in an efficient and effective manner. A sustainable concept was developed based on cost-effective and time-saving plans to bring to precise agricultural practices.

To set up the INNSA platform, two main components were designed: IoT devices using LoRa waves [13] and AI [7, 9]. In particular, the LoRa plays the role of continuously collecting data such as pH, oxidation reduction potential (ORP), electrical conductivity (EC), water temperature, air temperature, humidity, light intensity, and NPK. The AI is at the heart of the INNSA platform because it provides even more value to the IoT devices and enables the platform to comprehend the data it collected by IoT devices. In addition, with the use of AI, it also provides the ability to analyze market information, such as history coffee prices, to provide reports and predictive analysis for suppliers to adjust export plans. Besides, with deep learning-based technology, AI recognizes the images via camera to output advice about cultivation, harvest, pest, and disease prevention, etc. The data collected was sent back to the computer database for processing. This platform provides real-time information about the cultivating regions. Last but not least, that information, after being stored, analyzed in real time, and fed into the traceability system, helps increase transparency about the origin of the product, thereby adding the value of the product.

2.2 Data Analysis and Collections for the INNSA Platform

Big data collected by the INNSA platform was used to provide predictive insights in farming operations, drive real-time operational decisions, and redesign business processes for game-changing business models related to the coffee supply chain and value chain. Based on the quality assessment in the coffee supply chain and value chain, a standard quality certification for domestic use and export was developed to apply for the INNSA platform.

In order to make the system smarter to make food production efficiently, machine learning algorithms (e.g., neural network, random forest, support vector machine, etc.) were used to build the big data analytic models. Firstly, powered by AI, the INNSA platform is capable of analyzing the collected data to make assessments and suggestions for farmers to make decisions of fertilizing products and irrigations. For example, based on weather data, humidity, temperature, and plant care regime for each time period, AI can suggest when to water, how much water, and what fertilizer according to the growth and development of the coffee tree over time. This helps reduce costs and increase coffee production. Besides, with the use of AI to analyze and diagnose pests based on images of leaves of coffee trees collected from surveillance cameras, the platform can automatically and early detect pests, thereby helping farmers not only choosing treatment solutions but also reducing costs when pests and diseases have not been spread on a large area. In addition, the IoT system combined with an automatically controlled irrigation and care system also helps to reduce material and labor costs. Secondly, the AI-based advanced analytics of the platform is also used to improve the efficiency of coffee storage, processing, and exporting operations. With the use of IoT devices in monitoring, the warehouse environment, coffee beans quality monitoring cameras, AI-powered advanced analysis INNSA platform uses collected IoT's data to evaluate, guide, and decision support for managers. Moreover, the platform also provides predictive insights such as coffee quantity and quality based on coffee growing areas, predicts coffee price in the future, and forecasts the demand of the market. That information is analyzed and aggregated into final reports to assist suppliers in finding partners and estimating the volume of products to sign export contracts in accordance with their ability. Additionally, due to the digitization of coffee product related information, the INNSA platform is designed to be used not only as a coffee information portal but also as an advanced analysis portal of coffee beans quantity and quality of each region, each coffee growing area in Vietnam. Thereby helping the coffee industry of Vietnam to a higher level, well-recognized in terms of values, branding, and sustainability. Finally, the platform was developed based on cost-effective equipment and open-source software. This allows easy scaling and system development for responding to the actual needs of agriculture in the future.

Blockchain-based supply chain traceability systems were developed by using radio frequency identification (RFID), a non-contact automatic identification communication technology [6] to trace products with trusted information in the

entire supply chain, and by linking with IoT devices and integrating into the INNSA platform to provide digital data of production and consumption [5].

A sensor network system consisting of IoT devices and application programming interface (API) programmed by NodeJS and deployed in the server running Linux operating system (OS) were used to collect data [13]. Data transmission sensor used a communication protocol type MQTT [14]. By using this protocol, the microcontroller and computers or mobile apps were communicated wirelessly. Data collection block diagram, including array sensors, connected to IoT sensor network, API, cloud, local database, visual modeling, and computation. The sensor data from the microcontroller was sent to the LoRaWAN gateway, thus the data could be sent to the cloud and stored in a local database. Sensor data stored on a local database was used for real-time visualization. To perform computational modeling, sensor data was accessed on a local database.

2.3 The Proposed Models for the INNSA Platform

A solution architecture of the INNSA platform is designed as shown in Fig. 2, taking into account the following points: (1) critical investigation and reviews of the coffee supply chain and value chain in Vietnam; (2) innovative and cost-effective development of the platform with the smart database; (3) construction of big data for the platform, the real-world data inputs for a smart database; (4) innovative and cost-effective developments of value-added products and services in the value chain of the INNSA platform and ecosystems; and (5) systematic integration, evaluation, and analysis of the developed platform and products within the ecosystems.

First of all, the data was collected from users, video/PDF files, and IoT systems, to store it in a database, called Data Lake. From Data Lake, data was analyzed on demand to create business intelligence software, called BI tools. Then, a portal was developed to connect and integrate websites and visitors. Mobile applications were also created to control IoT devices and recommend farming care procedures. Finally, AI and machine learning technologies were used to design, optimize, and predict models, from which results are generated via an API gateway.

2.4 A General Workflow of the INNSA Platform

A general workflow of the INNSA platform was shown in Fig. 3. In the first step, a critical investigation and reviews of the coffee supply chain and coffee value chain in Vietnam is performed on the whole supply chain, including production, collection, processing, commerce—import and export, and consumption, with the focus on (1) identification of the key factors and stakeholders in the coffee supply chain and coffee value chain in Vietnam, and (2) strength, weakness, opportunity, and threat (SWOT) analysis.

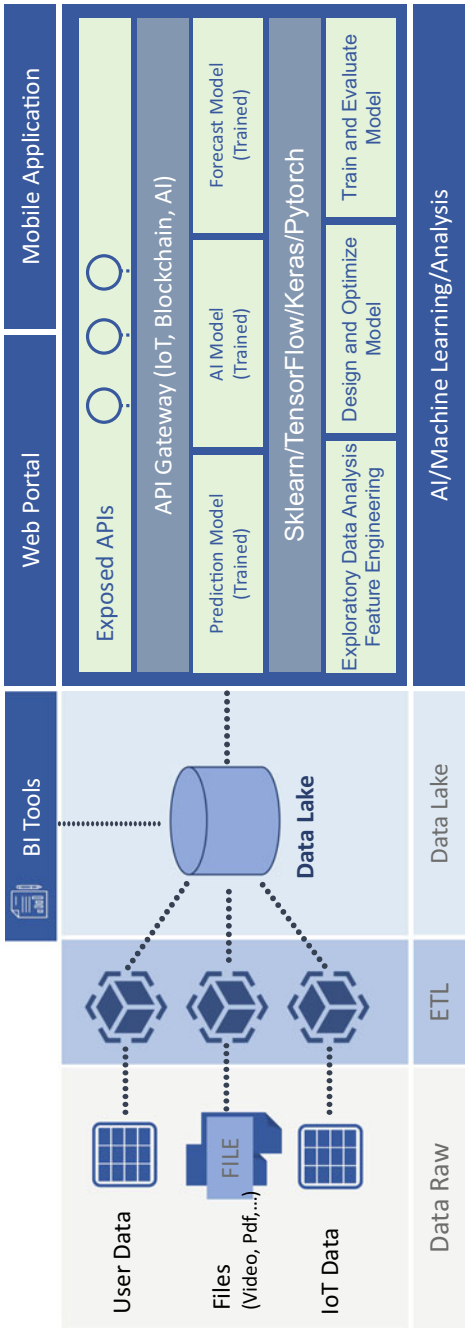

Fig. 2 Proposed models of the INNSA platform

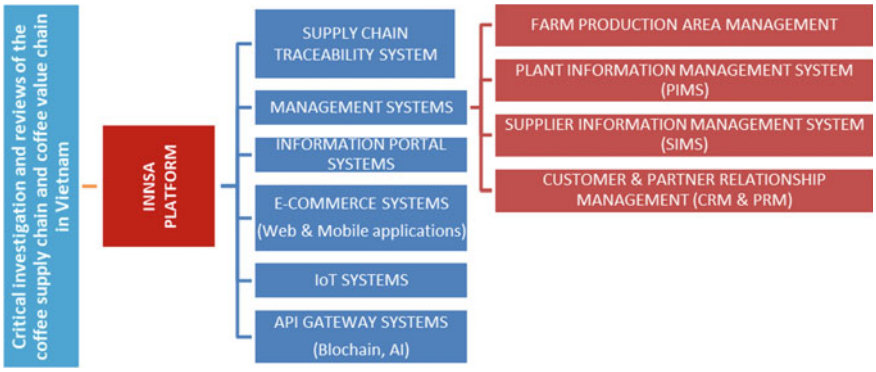

Fig. 3 General workflow of the INNSA platform

Based on the critical investigation and reviews from the first step, the INNSA platform is designed in the second step, with the focus on supply chain traceability systems, as well as management systems. The supply chain traceability system is presented in Fig. 4 with a detailed description. The management systems have key functions such as farm production area management, plant information management system (PIMS), supplier information management system (SIMS), and customer and partner relationship management (CRM and PRM). Besides, E-commerce systems (web and mobile applications), IoT devices using LoRa waves, and API Gateway systems integrated with blockchain and AI are also developed.

In the third step, the construction of big data for the INNSA platform is successfully designed and developed. The INNSA platform with the designed smart database needs the real-world data inputs, especially the ones that can be directly used for smart farming's applications: farm soils and environmental conditions (moisture levels and weather in different times of the year), as well as the latest information about the crops and market trends from all connected sources. Big data collected by the INNSA platform are being developed to provide predictive insights in farming operations, drive real-time operational decisions, and redesign business processes for game-changing business models related to the coffee supply chain and coffee value chain in Vietnam.

We seek and contract reputable partners in Vietnam and abroad to provide high quality input supply for coffee production as well as products and equipment for each key stakeholder. Information of these partners is added to the information portal systems. In addition, the platform also provides a quality assessment function of these partners. Based on this assessment, the platform will give priority to introducing reputable and quality partners to participate in the coffee supply chain and value chain. Based on the quality assessment in the coffee supply chain and value chain, a standard quality certification for domestic use and export such as UTZ and C4 assessment will be developed to apply for the platform.

In the fourth step, innovative and cost-effective developments of value-added products and services in the coffee value chain are added to the INNSA platform and its ecosystems, including: (1) products made from coffee beans and wastes,

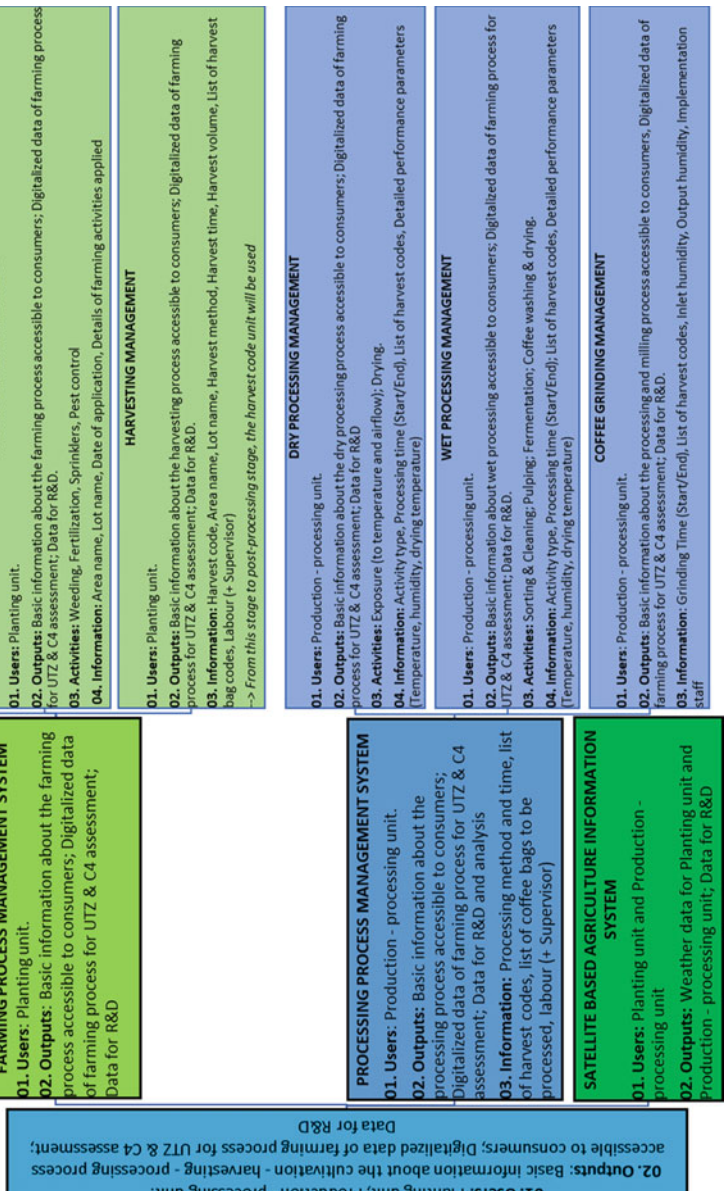

Fig. 4 Detailed workflow of the supply chain traceability system within the INNSA platform

(2) products for sustainable and precision agriculture: microbial organic fertilizer for coffee plants; (3) smart devices and IoT solutions for continuous and automatic updates of data and information to construct big data for the INNSA platform; and (4) E-commerce and commercialization of coffee beans and coffee products, with the support of AI, blockchain and supply chain traceability technologies.

Finally, systematic integration, evaluation, and analysis of the developed INNSA platform and products within the INNSA ecosystems are designed and implemented. All products, modules, and data resulting from the third and fourth steps are integrated into the INNSA platform developed in the second step for evaluation and analysis, and related risk and security assessment, quality control, and management issues. The evaluation and analysis are based on the real-world business models and data, at the laboratory scale first, and then in coffee farms and coffee storage spaces. A farm of 500 m^2 of White Lion JSC (Iced Coffee) in Mdrak district, Daklak province, Vietnam was used for demonstration, analysis, and evaluation, with the focus on how the system collect and process data to support smart farming, harvest and post-harvest processing, storage, source traceability, commercialization, as well as related issues in the coffee supply chain and value chain.

Finally, the principles of LEAN Industry 4.0 and Sustainable Developments [16] are introduced and applied in management and operations of the INNSA platform, as well as when developing value-added products and services in the value chain of the INNSA platform and its related ecosystems, including the hardware, software, smart devices, e-commerce platform, and innovative products from coffee trees, beans, and wastes. For future works, the INNSA platform can be applied to other agricultural supply chains such as marine culture and shrimp farming for a sustainable aquaculture [17, 18].

3 Summary and Conclusions

Under the impacts of Industry 4.0 and UN's sustainable development goals, it is necessary to develop an innovative and smart agriculture platform that can be effectively used for the creation and operation of a sustainable coffee value chain, to enhance the quality and create added values for key elements of the coffee supply chain. In this paper, the INNSA platform is introduced, to provide the information portal and open-access database for all key factors of coffee supply chain, enabling them to join and interact with each other effectively and systematically, with the focus on the case of the coffee industry of Vietnam, aimed at enhancement of the values, branding and sustainability of the coffee value chain and supply chain in Vietnam. The platform is designed based on the foundations of the key enabling digital transformation and smart agriculture technologies, with the following key features: A smart database with real-time data inputs and updates, cost-effectiveness, and open-architectures for effective integrations of the enabling digital transformation and smart agriculture technologies.

The successful development of the INNSA platform will potentially create the significance and impacts in the coffee supply chain, and to directly contribute to the United Nations Sustainable Goals. It also directly contributes to Vietnam's Smart Agriculture and Industry 4.0, successful development, and applications of the key enabling technologies of digital transformation and smart agriculture, including the following ones: smart devices and IoT, big data, AI, blockchain and source traceability technologies, and sustainable design and manufacturing. It is expected that, for the first time in Vietnam, there is the smart platform and ecosystem as the information portal and open-access database for farmers, traders, processing companies, import and export companies, retail shops, and coffee users, can join to obtain and share information, as well as to commercialize coffee products, to specifically meet their needs in both the coffee supply chain and coffee value chain.

Acknowledgements This work was supported by the Vingroup Innovation Foundation (VINIF) annual research support program with the research grant number VINIF.2021.DA00047.

References

1. Abideen, A. Z., Sundram, V. P. K., Pyeman, J., Othman, A. K., & Sorooshian, S. (2021). Food supply chain transformation through technology and future research directions—A systematic review. *Logistics, 5*, 83.
2. Mulla, D. J. (2013). Twenty-five years of remote sensing in precision agriculture: Key advances and remaining knowledge gaps. *Biosystems Engineering, 114*(4), 358–371.
3. Buja, I., Sabella, E., Monteduro, A. G., Chiriacò, M. S., De Bellis, L., Luvisi, A., & Maruccio, G. (2021). Advances in plant disease detection and monitoring: From traditional assays to in-field diagnostics. *Sensors, 21*, 2129.
4. Chung, S., Choi, M., Lee, K., Kim, Y., Hong, S., & Li, M. (2016). Sensing technologies for grain crop yield monitoring systems: A review. *Journal of Biosystems Engineering, 41*(4), 408–417.
5. Demestichas, K., Peppes, N., Alexakis, T., & Adamopoulou, E. (2020). Blockchain in agriculture traceability systems: A review. *Applied Sciences, 10*, 4113.
6. Deng, M., & Feng, P. (2020). A food traceability system based on blockchain and radio frequency identification technologies. *Journal of Computer and Communications, 8*, 17–27.
7. Gonzalez-de-Santos, P., Fernández, R., Sepúlveda, D., Navas, E., Emmi, L., & Armada, M. (2020). Field robots for intelligent farms—Inhering features from industry. *Agronomy, 10*, 1638.
8. Martínez, W. R., Díaz, Y., Ferro-Escobar, R., & Pallares, L. (2019). Application of the internet of things through a network of wireless sensors in a coffee crop for monitoring and control its environmental variables. *Tecno, 22*(46), 155–170.
9. Talaviya, T., Shah, D., Patel, N., Yagnik, H., & Shah, M. (2020). Implementation of artificial intelligence in agriculture for optimisation of irrigation and application of pesticides and herbicides. *Artificial Intelligence in Agriculture, 4*, 58–73.
10. Zheng, M., Zhang, S., Zhang, Y., & Hu, B. (2021). Construct food safety traceability system for people's health under the internet of things and big data. *IEEE Access, 9*, 70571–70583.
11. Hazen, B. T., Russo, I., Confente, I., & Pellathy, D. (2021). Supply chain management for circular economy: Conceptual framework and research agenda. *The International Journal of Logistics Management, 32*(2), 510–537.

12. Baghizadeh, K., Pahl, J., Hu, G. (2021). Closed-loop supply chain design with sustainability aspects and network resilience under uncertainty: Modelling and application. *Mathematical Problems in Engineering*, Article ID 9951220.
13. Lee, H., & Ke, K. (2018). Monitoring of large-area IoT sensors using a LoRa wireless mesh network system: Design and evaluation. *IEEE Transactions on Instrumentation and Measurement, 67*(9), 2177–2187.
14. Rachmad, A., Riantini, R., & Hasin, M. (2017). IoT real time data acquisition using MQTT protocol. *Journal of Physics: Conference Series, 853*, 012003.
15. Leduc, G., Kubler, S., & Georges, J. P. (2021). Innovative blockchain-based farming marketplace and smart contract performance evaluation. *Journal of Cleaner Production, 306*, 127055.
16. Arey, D., Le, C. H., & Gao, X. (2021). Lean industry 4.0: A digital value stream approach to process improvement. *Procedia Manufacturing, 54*, 19–24.
17. Pham, T. T., Ho, T. H. N., & Nguyen, V. D. (2014). Screening for bacteriocin-like antimicrobial activity against shrimp pathogenic vibrios and molecular identification of marine bacteria from otter clam *Lutraria philippinarum*. *Thai Journal of Veterinary Medicine, 44*(3), 345–353.
18. Nguyen, V. D., Le, M. H., & Trang, S. T. (2013). Application of probiotics from marine microbes for sustainable marine aquaculture development. In S.-K. Kim (Ed.), *Marine microbiology: Bioactive compounds and biotechnological applications* (pp. 307–349). Wiley.

Complex Shear Imaging Based on Signal Processing and Machine Learning Algorithms

Duc-Tan Tran and Vijender Kumar Solanki

1 Introduction

The mechanical property of the tissue can be used for medical diagnosis. In a study about shear wave elastography [1], Jeremy Bercoff et al. showed that the elasticity of the normal and abnormal tissues are different (such as in Table 1).

In [2], the authors first proposed to use shear waves to compute the elasticity and viscosity of the soft tissues. Figure 1 illustrates ultrasound images of a phantom containing a hard inclusion.

In Fig. 1, the below image was obtained by traditional ultrasound, while the above one was obtained by shear wave elastography. A tumor is detected in the above image is clearer than in the below one. The works in [3–6] also confirmed the ability of the elasticity estimation in real experiments. The work in [7] extended the estimation not only for the elasticity but also the viscosity. The noise reduction using Kalman Filter is introduced in [8]. After that, a series of studies [8, 9, 10–14, 15, 16] were focus to estimate the complex shear modulus (CSM) by using frequency-domain methods. Another approach that uses only one excitation frequency is presented in [17–19]. Not only Kalman filter was used for noise reduction in shear wave imaging, but the Extended Kalman Filter (EKF) was also used in [20], Maximum likelihood ensemble filter (MLEF) is used in [21, 22].

D.-T. Tran (✉)
Faculty of Electrical and Electronic Engineering, Phenikaa University, Hanoi 12116, Vietnam
e-mail: tan.tranduc@phenikaa-uni.edu.vn

V. K. Solanki
CMR Institute of Technology, Hyderabad, TS, India

T. D. L. Nguyen and J. Lu (eds.), *Machine Learning and Mechanics Based Soft Computing Applications*, Studies in Computational Intelligence 1068,
https://doi.org/10.1007/978-981-19-6450-3_20

Table 1 Typical elasticity values in someissues [1]

Type of soft tissue		Young's modulus (E in kPa)	Density (kg/m^3)
Breast	Normal fat	18–24	1000 ± 8% ~ water
	Normal glandular	28–66	
	Fibrous tissue	96–244	
	Carcinoma	22–560	
Prostate	Normal anterior	55–63	
	Normal posterior	62–71	
	BPH	36–41	
	Carcinoma	96–241	
Liver	Normal	0.4–6	
	Cirrhosis	15–100	

2 Working Principles

The state-of-art techniques for generating the shear wave consist of (1) using the acoustic radiation force and (2) using the vibration needle.

For using the acoustic radiation force, the shear wave is generated by ARF from a transducer (see Fig. 2). It requires a simple system whose ultrasound probe itself creates ARF impact on soft tissues. However, the disadvantage of this approach is that it is not easy to compute the amplitude of the applied force, thus significantly affecting the estimation.

For using the vibration needle, the measurement system consisted of a vibrating needle, an actuator, and a Doppler ultrasound device (see Fig. 3). The actuator generates through a needle a mechanical vibration. Doppler ultrasound device was used to measure the particle velocity at each spatial location in the region of interest [17]. In the later numerical simulation, the particle velocity propagated in tissues was modeled using the FDTD model. This particle velocity, after adding noises, simulated the measured particle velocity (from the Doppler device). Thus the measured particle velocity was the noisy particle velocity.

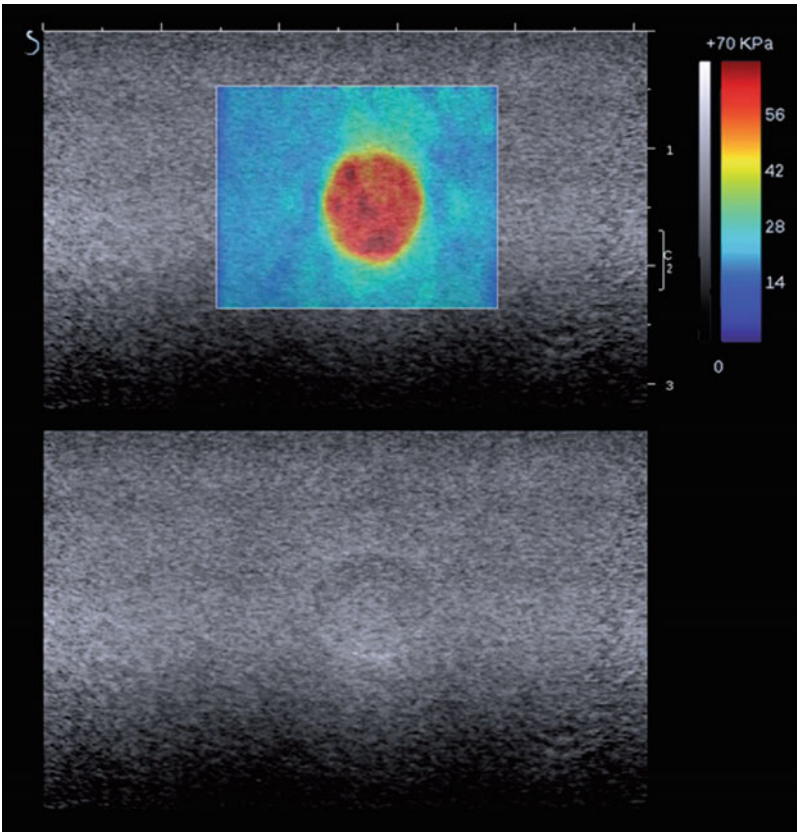

Fig. 1 Traditional ultrasound (below) and shear wave elasticity (above) images on a phantom containing a harder inclusion [1]

3 Complex Shear Wave Modulus Estimation

3.1 Kelvin–Voigt Model

Complex Shear wave Modulus (CSM) consists of two ingredients: elasticity and viscosity. However, there are several models that describe CSM, such as Maxwell, and Kelvin–Voigt. In this chapter, we calculated the elasticity μ and the viscosity η of the tissues. Figure 4 shows the Kelvin–Voigt model for CSM. In this model, CSM is defined as follows

$$G(x, y, \omega) = \mu(x, y) - i\omega\eta(x, y), \tag{1}$$

where ω is the vibration signal's angle frequency, elasticity, and viscosity at the spatial position (x, y).

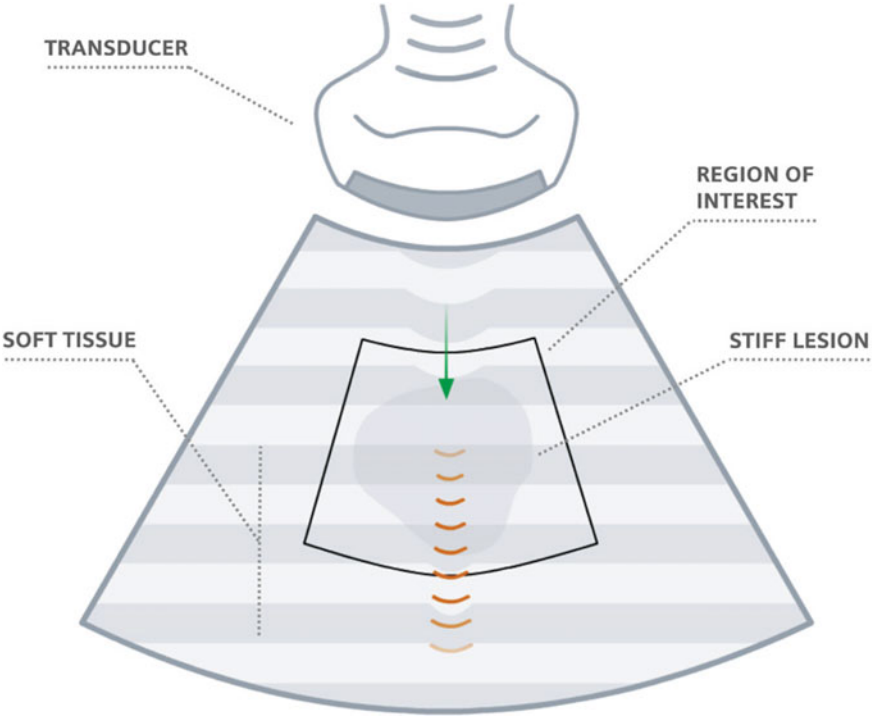

Fig. 2 Illustration of using the acoustic radiation force

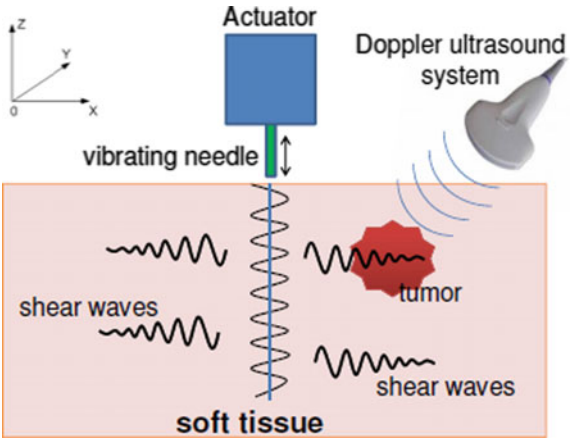

Fig. 3 Generation and measurement of the shear wave using the vibration needle

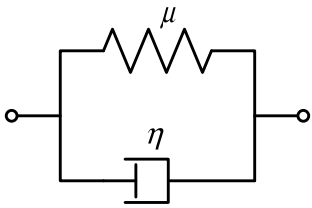

Fig. 4 Kelvin–Voigt model for tissues

3.2 *Propagation of Shear Wave*

In a 2D environment, the propagation of the shear wave is described equations [23]:

$$v_z(x, y, t) = v_z(i\Delta x, j\Delta y, n\Delta t) = v_z^n|_{i,j} \tag{2}$$

$$\sigma_{zx}(x, y, t) = \sigma_{zx}(i\Delta x, j\Delta y, n\Delta t) = \sigma_{zx}^n|_{i,j} \tag{3}$$

$$\sigma_{zy}(x, y, t) = \sigma_{zy}(i\Delta x, j\Delta y, n\Delta t) = \sigma_{zy}^n|_{i,j} \tag{4}$$

where v_z is the particle velocity vector on the plane (x, y), σ_{zx} and σ_{zy} are two elements of the stress tensor σ, ρ is the density of the tissues, Δx and Δy are the distances between continuous spatial locations following the X-axis, and Y-axis, respectively. These parameters are illustrated in Fig. 5.

By applying the FDTD method in a 2D medium, Eqs. (2), (3), and (4) are transformed into Eqs. (5), (6), and (7), respectively.

$$\begin{aligned} v_z^{n+1}|_{i,j} = v_z^n|_{i,j} &+ \frac{\Delta t}{\rho \Delta x}\left(\sigma_{zx}^{n+0.5}|_{i+0.5j} - \sigma_{zx}^{n+0.5}|_{i-0.5j}\right) \\ &+ \frac{\Delta t}{\rho \Delta y}\left(\sigma_{zy}^{n+0.5}|_{i,j+0.5} - \sigma_{zy}^{n+0.5}|_{i,j-0.5}\right) \end{aligned} \tag{5}$$

$$\begin{aligned} \sigma_{zx}^{n+0.5}|_{i+0.5j} = \sigma_{zx}^{n-0.5}|_{i+0.5j} &+ \frac{\mu \Delta t}{\Delta x}\left(v_z^{n+1}|_{i+1,j} - v_z^{n+1}|_{i,j}\right) \\ &+ \frac{\eta}{\Delta x}\left(v_z^{n+1}|_{i+1,j} - v_z^{n+1}|_{i,j}\right) - \frac{\eta}{\Delta x}\left(v_z^{n}|_{i+1,j} - v_z^{n}|_{i,j}\right) \end{aligned} \tag{6}$$

$$\begin{aligned} \sigma_{zy}^{n+0.5}|_{i+0.5j} = \sigma_{zy}^{n-0.5}|_{i+0.5j} &+ \frac{\mu \Delta t}{\Delta y}\left(v_z^{n+1}|_{i,j+1} - v_z^{n+1}|_{i,j}\right) \\ &+ \frac{\eta}{\Delta y}\left(v_z^{n+1}|_{i,j+1} - v_z^{n+1}|_{i,j}\right) - \frac{\eta}{\Delta y}\left(v_z^{n}|_{i,j+1} - v_z^{n}|_{i,j}\right) \end{aligned} \tag{7}$$

The accuracy of numerical Eqs. (5), (6), and (7) is the first order in time and space. The boundary conditions were applied by using an absorption boundary layer. It will reduce the reflections [24].

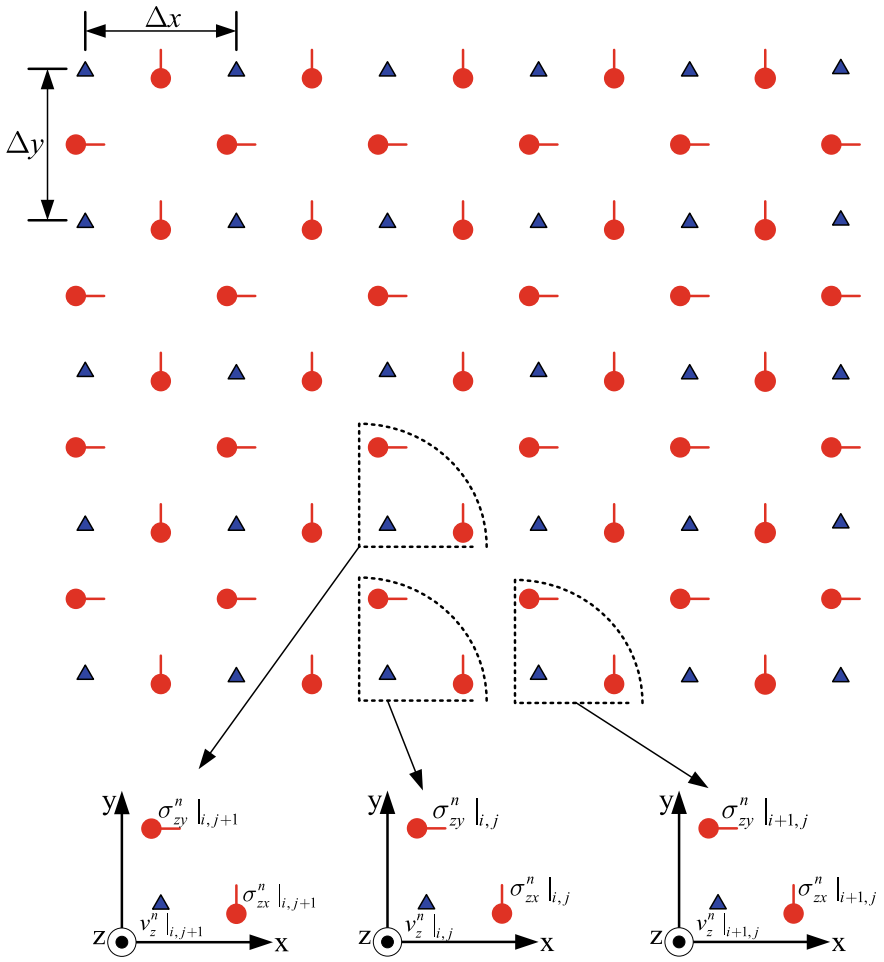

Fig. 5 Illustration of FDTD

$$\tau(i) = \tau_{\max}\left(\frac{i - i_{\text{pml}}}{N_{\text{pml}}}\right)^m \tag{8}$$

where two constants are set as $m = 2.15$ and $\tau_{\max} = 0.11$; the layer thickness in grid points $N_{\text{pml}} = 10$; and the term i-i_{pml} indicates the position within the perfectly matched absorptive layer.

3.3 Signal Improvement Using Our Proposed Approach

The FDTD method and the AHI algorithm can be used to estimate CSM at each point in the space (presented in detail in Sect. 3.4) directly. In such an approach, one important point is to minimize the propagation of error, which means that the influence of measurement noise needs to be reduced as much as before the direct estimation. In our work, we propose to use adaptive filtering [25] which was proved to give a mean error of 2.06%.

Figure 6 describes the NLMS adaptive filter we used to eliminate noise from the noisy signal. The adaptive filtering algorithm is described in Algorithm 1.

The noisy particle velocity generation can be described as follows: the Eqs. (5), (6), and (7) were used to create the ideal particle velocity $d(n)$ in each spatial location. This signal was added by a Gaussian white noise $v(n)$ to form a noisy particle velocity $v_z(n)$. The noise level that affected the particle velocities at the different observed locations was identical. Thus, the SNR is reduced from the locations near the needle to those farthest away. In our simulation scenario, the average SNR of all the spatial locations was 10.1 dB.

The reference noise generation can be described as follows: when the vibration needle stayed still, the measured signal was just the reference noise $x(n)$, as indicated

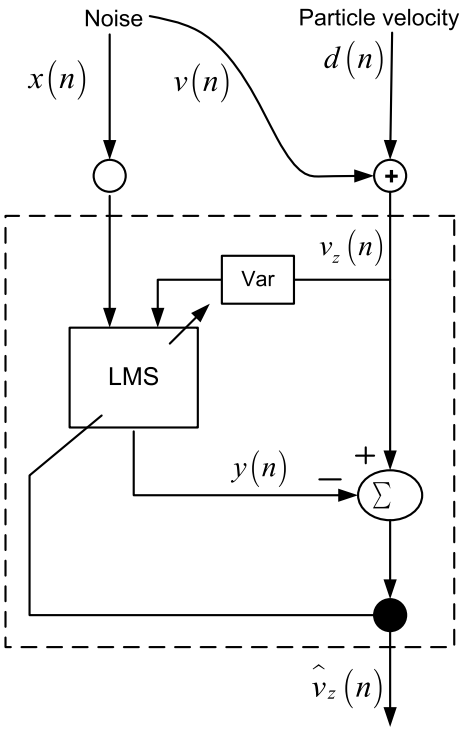

Fig. 6 Signal improvement using NLMS filter

in Fig. 6. Note that $x(n)$ was the Gaussian white noise we measured when the vibration needle stayed still, and v(n) was the Gaussian white noise we measured when the vibration needle was active. In Fig. 6, Var variable was the estimated variance of noise in $v_z(n)$. Both $x(n)$ and $v_z(n)$ were applied to a filter in [26] (Chap. 9, pp. 505–515).

In practice, the shear wave was quickly attenuated with the distance from the position of the vibration needle. Due to this fact, the SNR varied with the space points where we would like to estimate the CSM. This observation required that we use a different step size β. The complexity of this process suggested that we should use a simple structure for adaptive filtering with fast convergence [27]. We adjusted the step size at each spatial location using the formula $\beta = \beta_1(\varepsilon + \mathrm{Var})^{-1}$, where β_1 and ε are constant, and Var is the variance of $v_z(n)$ which was estimated at each spatial location as shown in Fig. 6.

3.4 Two-Dimension CSM Imaging Using NLMS/AHI Algorithm

The filtered particle velocity was brought to the AHI [28] to estimate the CSM [23]. By combining Eqs. (2), (3), and (4):

$$\rho \frac{\partial^2 v_z}{\partial t^2} = G'(x, y, t)\nabla^2 v_z, \tag{9}$$

where G'(x,y,t) is the CSM in the time domain and $\nabla^2 v_z$ is the Laplace operator of v_z, which is defined as $\nabla^2 v_z = \partial^2 v_z / \partial x^2$. We could directly estimate CSM

$$G(x, y, \omega) = \frac{-\rho\omega_0^2 V_z(x, y, \omega_0)}{\nabla^2 V_z(x, y, \omega_0)} \tag{10}$$

Following Eq. (1), $\mu(x,y)$ and $\eta(x,y)$ were real and imaginary parts of G(x,y,ω). Thus, elasticity and viscosity of the tissues at each spatial point (x, y) were calculated as

$$\mu(x, y) = \Re\left\{\frac{-\rho\omega_0^2 V_z(x, y, \omega_0)}{\nabla^2 V_z(x, y, \omega_0)}\right\} \tag{11}$$

$$\eta(x, y) = \Im\left\{\frac{-\rho\omega_0^2 V_z(x, y, \omega_0)}{\nabla^2 V_z(x, y, \omega_0)}\right\} \tag{12}$$

where $V_z(x,y,\omega_0)$ is Fourier transform of $v_z(n)$ at the specific angular frequency ω_0; $\nabla^2 V_z(x, y, \omega_0)$ is Discrete Laplacian.

Table 2 Parameters of medium and tumor

	Coordinate (mm, mm)	Radius (mm)	μ_1 (Pa)	H (Pa.s)
Medium			6000	1.2
Tumor	(40, 40)	20	9000	1.8

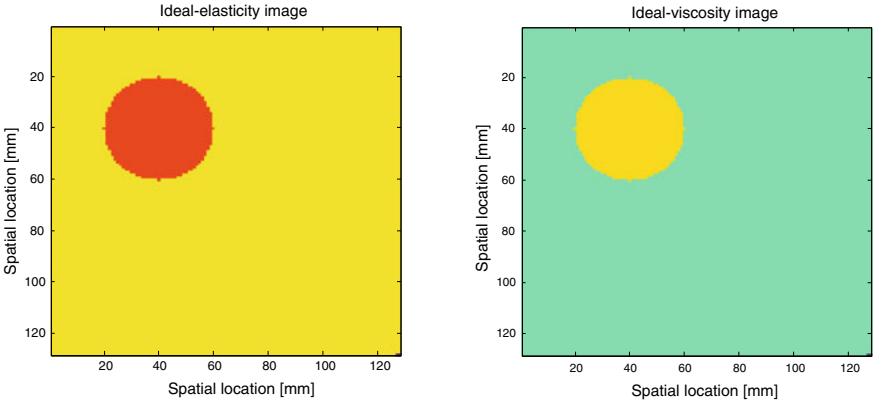

a) Ideal elasticity image b) Ideal-viscosity image

Fig. 7 A tumor exists in the simulation scenario

3.5 Simulation and Results

3.5.1 Simulation

The authors set up a scenario as summarized in Table 2.

The medium's density was $\rho = 1000$ kg/m^3. On the 2D plane of the medium (tissue), the particle velocity was measured at locations that were equally spaced 1 mm, following both the X-axis and Y-axis. Thus, the number of measured locations was $120 \times 120 = 14{,}400$. Figure 7a illustrates the ideal elasticity, and Fig. 7b shows ideal-viscosity images.

3.5.2 Results

Firstly, the ideal particle velocity at a location in tissues was modeled following the FDTD method (as shown in the above graph, Fig. 8, at the spatial location (56 mm, 56 mm)). Combining with the Gaussian noise, it simulated the measured particle velocity using the Doppler system (as shown in the between graph). The below graph in Fig. 8 shows the filtered particle velocity.

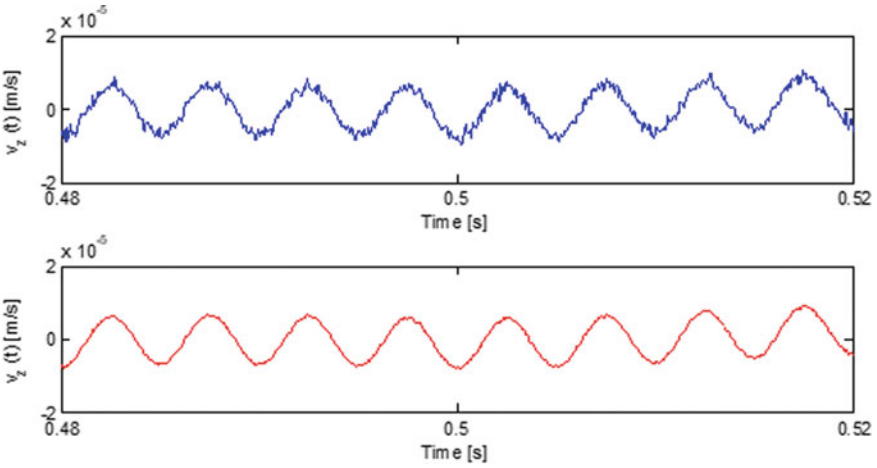

Fig. 8 The noisy and filtered particle velocities at one spatial location

Figure 9a and b show estimated-elasticity and estimated-viscosity images of tissues, respectively. In both images, tumor is seen clearly in in terms of location and shape. In fact, normal tissue and tumor elasticity are not always different.

For easy comparison between the estimated and ideal values of elasticity and viscosity, we can observe 1D data of them. Figure 10 illustrates the results of elasticity estimation on two lines (one does not exist across the tumor while the other crosses the tumor).

Figure 11 illustrates the viscosity estimation on two lines. In detail, Fig. 11b indicates the result of viscosity estimation on Line 10; Fig. 11c shows the effect of viscosity estimation on Line 40.

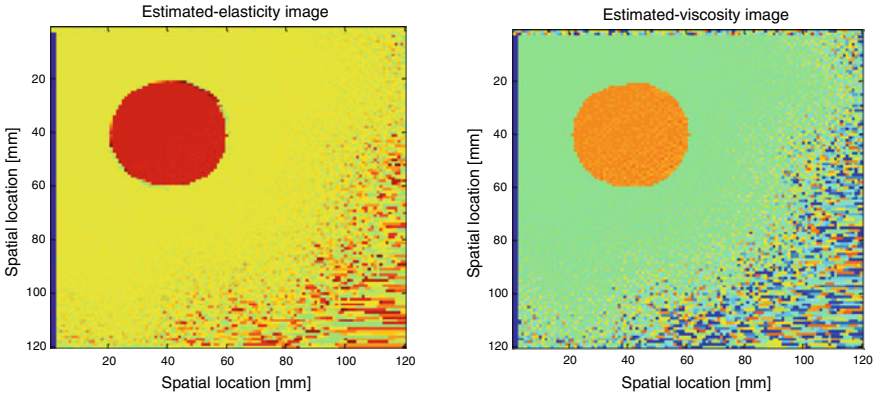

a) Estimated elasticity image b) Estimated-viscosity image

Fig. 9 Estimated 2D images

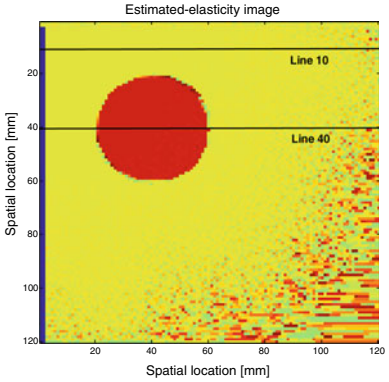

a) Locations of two lines

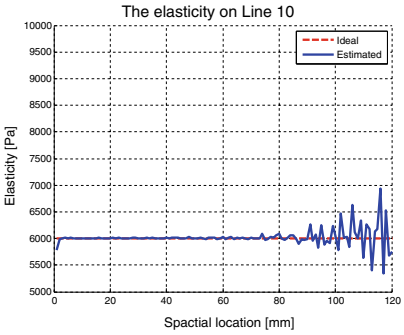

b) Estimated elasticity on Line 10

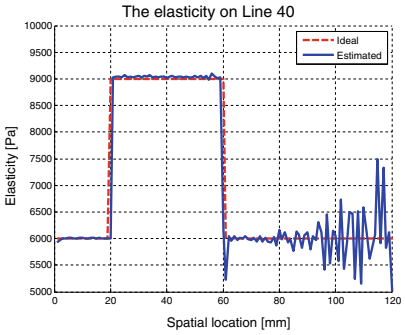

c) Estimated elasticity on Line 40

Fig. 10 Elasticity estimation on two lines

Observing Figs. 10b, c and 11b, c, it is seen that the estimation results were less accurate at locations far from the exciting source. It can explain as follows shear wave was attenuated when it propagated in the tissues, and it was a damped oscillation. At locations far from the exciting source, the velocity value was minimal. Thus, CSM estimation was less accurate. The calculated results show that the normalized error for 2D elasticity and viscosity were 1.63% and 2.49%, respectively.

4 Classification of Soft Tissues

Machine learning is a solution to categorize the data set. Classification of soft tissues based on elasticity and viscosity images is intuitive. However, a final decision about abnormal tissues depends on the elasticity and viscosity value. Machine learning comes in two distinct flavors supervised learning and unsupervised learning. Relying on each type's features, it combines with the data set's characteristics. We have

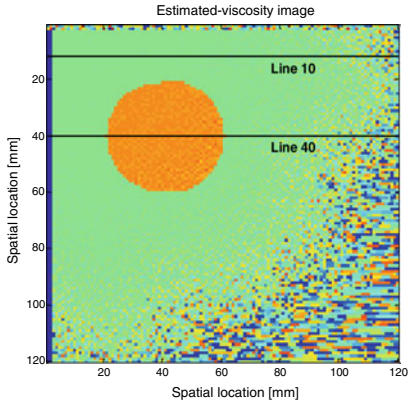

a) Locations of two lines

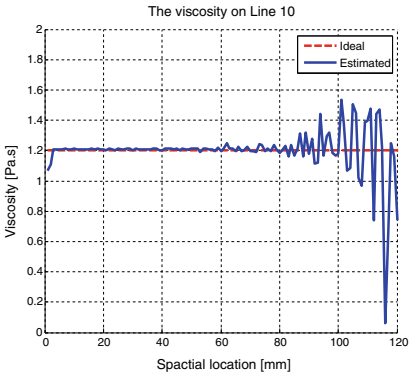

b) Estimated viscosity on Line 10

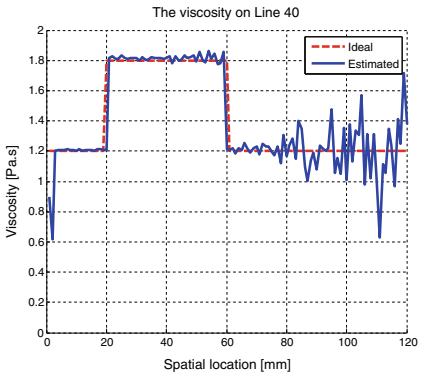

c) Estimated viscosity on Line 40

Fig. 11 Viscosity estimations on two lines

decided to choose supervised learning. After considering the advantages of the above algorithms with all the given rules in this thesis, we realize that the decision tree would be the most suitable. A decision tree has various advantages, such as handling both categorical and numerical data; performs well with large datasets. However, it has some limitations like problems in an optimal decision tree and not generalizing well with over-complex trees. To classify the status of the livers, we used two features: the value of elasticity and viscosity (Fig. 12). Figure 13 represents the classification results.

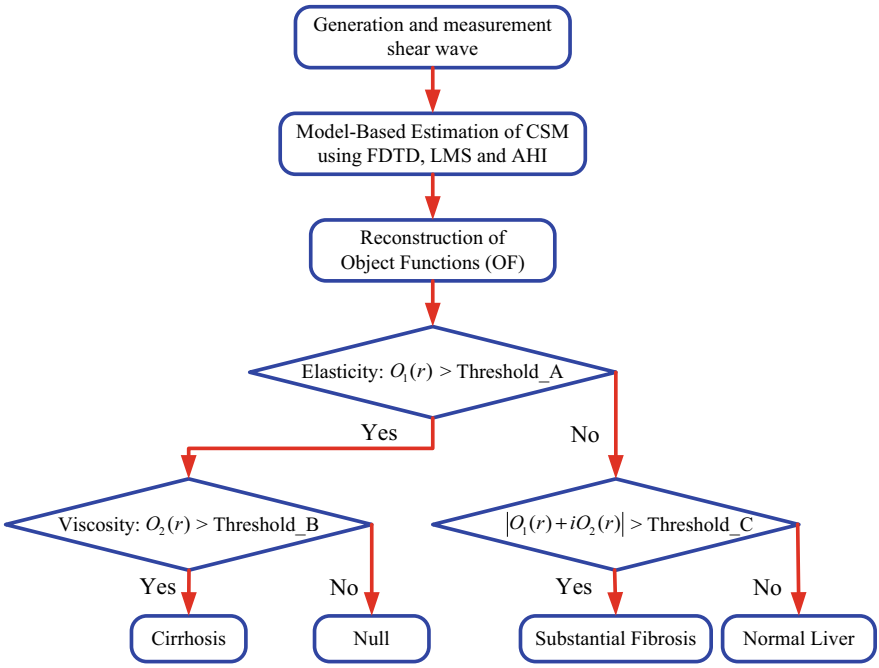

Fig. 12 Tumor detection and classification

Fig. 13 CSM image result of tumor detection and classification

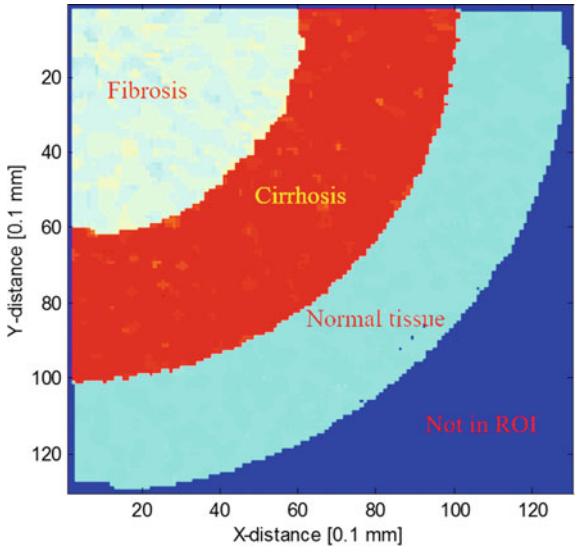

5 Conclusion

This chapter presented a method of constructing 2D CSM images using the AHI estimation method in a noisy environment. In our approach, we measured the particle velocity at only one frequency at different positions in the focused area. Noise in particle velocity measurement was eliminated by using an NLMS adaptive filter to improve the image reconstruction. The quality of image reconstruction was improved by (1) Changing the adaptive filter step size at each point of the observation space and (2) Eliminating the transient data before computing the Fourier transform of the particle velocity at the frequency of 150 Hz; this helped to improve the estimation of CSM using Eqs. (15) and (16). These estimates computed at each point in the space, as illustrated in Fig. 5, were finally used to reconstruct the CSM images.

Acknowledgements This work was supported by National Foundation for Science & Technology Development (NAFOSTED) under Grant 103.05-2020.13.

References

1. Bercoff, J., Criton, A., Bacrie, C.C., et al. (2008). ShearWave elastography a new real time imaging mode for assessing quantitatively soft tissue viscoelasticity. In Ultrasonics Symposium. IUS 2008 (pp. 321–324). IEEE.
2. Sarvazyan, A. P., Rudenko, O. V., Swanson, S. D., et al. (1998). Shear wave elasticity imaging: a new ultrasonic technology of medical diagnostics. *Ultrasound in Medicine and Biology, 24*(9), 1419–1435.
3. Gennisson, J. L., Deffieux, T., Fink, M., & Tanter, M. (2013). Ultrasound elastography: principles and techniques. *Diagnostic and Interventional Imaging, 94*(5), 487–495.
4. Ferraioli, G., Parekh, P., Levitov, A. B., & Filice, C. (2014). Shear wave elastography for evaluation of liver fibrosis. *Journal of Ultrasound in Medicine, 33*(2), 197–203.
5. John, B., Liexiang, F. (2014). Understanding ARFI and new elastography quantification technologies. *Mountain View, CA: Siemens Medical Solutions.*
6. Lee, J. E., et al. (2017). Non-invasive assessment of liver fibrosis with ElastPQ: comparison with transient elastography and serologic fibrosis marker tests, and correlation with liver pathology results. *Ultrasound in Medicine and Biology, 43*(11), 2515–2521.
7. Chen, S., Fatemi, M., & Greenleaf, J. F. (2004). Quantifying elasticity and viscosity from measurement of shear wave speed dispersion. *The Journal of the Acoustical Society of America, 115*(6), 2781–2785.
8. Zheng, Y., Chen, S., Tan, W., Kinnick, R., & Greenleaf, J. (2007). Detection of tissue harmonic motion induced by ultrasonic radiation force using pulse-echo ultrasound and Kalman filter. *Ultrasonics, Ferroelectrics, and Frequency Control, IEEE Transactions on, 54*(2), 290–300.
9. Liu, D., & Ebbini, E. S. (2008). Viscoelastic property measurement in thin tissue constructs using ultrasound. *IEEE Transactions on Ultrasonics, Ferroelectrics, and Frequency Control, 55*(2), 368–383.
10. Michael F Insana, Claire Pellot-Barakat, Mallika Sridhar, and Karen K Lindfors, "Viscoelastic imaging of breast tumor microenvironment with ultrasound," *Journal of mammary gland biology and neoplasia*, vol. 9, no. 4, pp. 393–404, 2004.
11. Yue Wang and Michael F Insana, "Viscoelastic properties of rodent mammary tumors using ultrasonic shear-wave imaging," *Ultrasonic Imaging*, vol. 35, no. 2, pp. 126–145, 2013.

12. Matthew W Urban, Shigao Chen, and James F Greenleaf, "Error Estimates in Shear Wave Speed and Tissue Material Properties in Shear Wave Dispersion Ultrasound Vibrometry," in *Ultrasonics Symposium, 2007. IEEE*, 2007, pp. 664–667.
13. Amador, C. (2015). Randall R Kinnick, Matthew W Urban, Mostafa Fatemi, and James F Greenleaf, "Viscoelastic tissue mimicking phantom validation study with shear wave elasticity imaging and viscoelastic spectroscopy," in *Ultrasonics Symposium* (*IUS*). *IEEE International, 2015*, 1–4.
14. Findley, W. N., Lai, J. S., Onaran, K., & Christensen, R. M. (1977). Creep and relaxation of nonlinear viscoelastic materials with an introduction to linear viscoelasticity. *Journal of Applied Mechanics, 44*, 364.
15. Marko Orescanin and Michael F Insana, "Shear modulus estimation with vibrating needle stimulation," *IEEE Transactions on Ultrasonics, Ferroelectrics, and Frequency Control*, vol. 57, no. 6, pp. 1358–1367, 2010.
16. Jonathan Vappou, Caroline Maleke, and Elisa E Konofagou, "Quantitative viscoelastic parameters measured by harmonic motion imaging," *Physics in medicine and biology*, vol. 54, no. 11, p. 3579, 2009.
17. Marko Orescanin and Michael F Insana, "Model-based complex shear modulus reconstruction: A Bayesian approach," in *IEEE Ultrasonics Symposium* (*IUS*), 2010, pp. 61–64.
18. Tan Tran-Duc, Yue Wang, Nguyen Linh-Trung, Minh N Do, and Michael F Insana, "Complex Shear Modulus Estimation Using Maximum Likelihood Ensemble Filters," in *4th International Conference on Biomedical Engineering in Vietnam*, 2013, pp. 313–316.
19. Nguyen Thi Hao, Tran Thuy-Nga, Vu Dinh-Long, Tran Duc-Tan, and Nguyen Linh-Trung, "2D Shear Wave Imaging Using Maximum Likelihood Ensemble Filter," in *International Conference on Green and Human Information Technology* (*ICGHIT 2013*), 2013, pp. 88–94.
20. Yo Kobayashi, Mariko Tsukune, Tomoyuki Miyashita, and Masakatsu G Fujie, "Simple empirical model for identifying rheological properties of soft biological tissues," *Physical Review E*, vol. 95, no. 2, p. 022418, 2017.
21. Arif R Albayrak, Milija Zupanski, and Dusanka Zupanski, "Maximum likelihood ensemble filter applied to multisensor systems," in *Defense and Security Symposium*, 2007, pp. 65710N-65718N.
22. Zupanski, M. (2005). Maximum likelihood ensemble filter: Theoretical aspects. *Monthly Weather Review, 133*(6), 1710–1726.
23. Marko Orescanin, Yue Wang, and Michael F Insana, "3D FDTD simulation of shear waves for evaluation of complex modulus imaging," *IEEE Transactions on Ultrasonics, Ferroelectrics, and Frequency control*, vol. 58, no. 2, pp. 389–398, 2011.
24. Christoph T Schroder and Waymond R Scott, "A finite-difference model to study the elastic-wave interactions with buried land mines," *IEEE Transactions on Geoscience and Remote Sensing*, vol. 38, no. 4, pp. 1505–1512, 2000.
25. Simon Haykin and Bernard Widrow, *Least-mean-square adaptive filters.*: John Wiley & Sons, 2003.
26. Monson H. Hayes, *Statistical digital signal processing and modeling.*: John Wiley & Sons, 2009.
27. Bismor, D. (2012). LMS algorithm step size adjustment for fast convergence. *Archives of Acoustics, 37*(1), 31–40.
28. Papazoglou, S., Hamhaber, U., Braun, J., & Sack, I. (2008). Algebraic Helmholtz inversion in planar magnetic resonance elastography. *Physics in Medicine and Biology, 53*(12), 3147.
29. Budelli, E., Brum, J., Bernal, M., et al. (2017). A diffraction correction for storage and loss moduli imaging using radiation force based elastography. *Physics in Medicine and Biology, 62*(1), 91.
30. Huwart, L., et al. (2006). Liver fibrosis: Non-invasive assessment with MR elastography. *NMR in Biomedicine: An International Journal Devoted to the Development and Application of Magnetic Resonance In vivo, 19*(2), 173–179.

Breast Cancer Detection Based on UWB Dataset and Machine Learning

Heba Mehdi and Furkan Rabee

Abstract Breast cancer is one of the worst diseases in the world and the most common cancer affected by women. Early detection of cancers allows for faster treatments. Women rarely visit a clinic or hospital for routine tests unless they are ill because of long lines, expensive tests, and life difficulties. Recent studies have focused on early breast cancer diagnosis utilizing non-invasive UWB technologies. This article presents several appropriate supervised machine learning algorithms to detect breast cancer, worked with a user-friendly microwave ultra-wideband (UWB) device within the breast tissue. Two models for compressed breast tissue were created using the CST Microwave Studio simulator. These models generated two patient datasets with differing dielectric properties similar to human tissue. These two datasets are used to train the decision tree (DT), support vector machine (SVM), and nearest neighbor (NN) in order to develop an intelligent classification model that can assist doctors in identifying malignant breast cells. KNN can classify the breast data for the first group with 78% accuracy while the SVM 93% accuracy for the second group.

Keywords UWB implemented device · Breast cancer detection · SVM · KNN · DT

1 Introduction

The most prevalent cause of death among women is breast cancer. According to the American Cancer Society, the number of female fatalities from breast cancer in the USA in 2010 was 39,840, with 207,090 new cases [1]. Researchers recommend early

H. Mehdi · F. Rabee (✉)
Faculty of Computer Science and Mathematics, University of Kufa, Najaf, Iraq
e-mail: furqan.rabee@uokufa.edu.iq

H. Mehdi
e-mail: hebam.almosawy@student.uokufa.edu.iq

T. D. L. Nguyen and J. Lu (eds.), *Machine Learning and Mechanics Based Soft Computing Applications*, Studies in Computational Intelligence 1068,
https://doi.org/10.1007/978-981-19-6450-3_21

detection and treatment because there is no way to avoid the condition. Early detection of cancers allows for faster treatments and a longer survival span for the affected women. Microwave-based breast cancer imaging is one of the most promising technologies for identifying breast cancer in its early stages. The difference in dielectric characteristics of normal breast tissues (skin, fat, fibroglandular, etc.) and malignant breast tissues (tumor) is used in this procedure [2].

Therefore, microwave imaging is expected to be an X-ray alternative. Microwaves are electromagnetic waves that use the tissue's dielectric characteristics caused by its water content. Because the malignant tumor contains much water, it has a greater dielectric constant than normal tissue, which causes much scattering when electromagnetic waves pass through it. The dielectric constant of a malignant tumor will be at least three times higher than the healthy tissue [3]. There are now a lot of "smart" devices that connect to the internet and promise better performance, convenience, efficiency, and fun for both consumers and businesses. Devices that monitor the human body, collect health and other personal data, and broadcast that data via the internet are becoming increasingly popular as part of the Internet of Things (IoT). These new technologies and their data have been referred to as the "Internet of Bodies" (IoB). This technology comes in a variety of shapes and sizes. It might be as simple as a few lines of code to set up a radio frequency identification (RFID) microchip implant, or it could be as complicated as a computer that processes artificial intelligence (AI) [4]. SRR met material antenna for RFID applications with suitable radiation characteristics used to detect the tumor. The chipless antenna, which is implementable inside the human body with non-toxic materials, is good for detecting breast tumors early in women who have previously been infected and recovered from the illness or women who have inherited a history of this disease in their family. Many suggested automated breast diagnostic systems include signal or image preprocessing, segmentation, and machine learning-based diagnosis [4]. Such systems have shown to be beneficial in assisting doctors with diagnosis. Scientists have developed a wide range of machine learning-based methods for diagnosing illnesses. According to researchers, machine-learning algorithms effectively identify problems such as heart disease, diabetes, liver disease, dengue fever, and hepatitis [5]. Microwaves with limited energy may be used to light up a breast when the patient is seated or lying down using microwave breast prototype devices. Signals resulting from backscattering are documented. The malignant tumor may be diagnosed by studying the backscattered signals and extracting the tumor signature contained within. In fact, prior research has shown that backscattered signals might vary depending on the size and location of breast cancers. In this paper, a study proposes using machine learning to identify the signals of breast cancers and make diagnoses. Non-ionizing microwave signals are sent to the breast model, and the scattering parameters (S-parameters) are read. The read signals the raw data were fed into a machine model trained to detect a tumor's existence. So, the proposed model has a good chance of being used in the future to find tumors early and save women's lives.

2 Related Work

We showed breast cancer prediction studies' work. Predicting whether a person will acquire cancer and machine learning may be useful for the medical field and individuals. Given many researchers who have used different methods or models to predict breast cancer, some are reviewed in this section. Boparai and Popović [6] have researched phantom breasts used to collect the information. Different kinds of materials have been used to create breast phantoms. Vijayasarveswari et al. [7] proposed studying the breast cancer sampling technique with dielectric properties for breast phantoms like real breasts. The feature extraction from UWB sensors employing different data normalization approaches, feature reduction algorithms, and classification stages are identified based on permittivity and conductivity. Bari et al. [8]. The authors report an artificial neural network-based "user-friendly" and cost-effective UWB technique for the early detection of breast cancer. A feedback forward propagation classification method is utilized to determine cancer's existence, size, and three-dimensional position (3D).

Ali et al. [9] examined how a woman's breast's electromagnetic properties can be used to determine if she has cancer; malignant cells are different from healthy cells in many respects. The second stage of a cancer diagnosis was determined by the size and quantity of tumors found in the breast and nearby lymph nodes. Conceição et al. [10] Researchers have categorized breast tumor models of various sizes and forms using a mono-static radar microwave imaging prototype technology and machine learning techniques for cancer detection. This paper proposed three appropriate supervised machine learning algorithms to detect breast cancer working with a microwave ultra-wideband (UWB) non-ionizing implemented device inside breast tissue. Different tissue characteristics within two breast models have been used to create two data sets. Non-ionizing microwave signals are sent to the breast model. The scattering parameter signals read by the antenna represent the raw data fed into a machine model. The implemented antennas that succeeded in detecting the tumor worked under the frequency range of Wi-Fi and IOB, which means we can use the device at home. Thus, the patient can check at home safely with no cost and early tumor detection. The results of the algorithms are tested and visualized in the R Studio.

3 Methodology and Tumor Dataset Creation

This section discusses the experimental setup for creating breasts and tumors, including an antenna. In addition, we cover the generation of the breast and tumor dataset necessary for ML processing. So the first stage of tumor detection is data creation.

Since human tissues are frequency dependent [11], the major breast components' dielectric characteristics will also differ. We will use different tissue characteristics within two types of ranges of frequencies. However, the two types fall within the

frequency of the implanted antenna. We will study the data extracted from these characteristics and train those data by machine learning, as shown in Fig. 1. The first range of characteristics we used with frequency band (1–3) GHz is provided in Table 1 [11] which will present the first group of the patient, ranging from their lowest to highest values. In contrast, the second range of characteristics is provided in Table 2 with frequency band (200 MG–5 GHz) [12] which present the second group. Using CST Microwave Studio simulator, two models were designed for the breast phantoms model. A small model design with a breast radius (2.5 cm) was designed using a hemisphere breast model with three layers according to the dielectric characteristics of breast tissues, permittivity (ε), and conductivity (σ) for each layer. The first is the skin layer with a center radius of 25 mm. The second one is the fat layer with a center radius of 23 mm placed inside the skin layer. The third layer is the fibroglandular, with a center radius of 15 mm placed inside the fat layer. In this model, 5 mm and 7 mm antennas were used. We placed the antenna inside the fat layer, which rings toward the tumor. The gland is the layer that contains cancer; if any, a spherical shape of radius (2, 3, 4, and 6) mm is used as a tumor. We put the wave source (unit cell) at a distance of 1 mm from the breast containing the antenna; the breast model is shown in Fig. 2. Large model design with a breast radius of (10 cm) was designed using a hemisphere divided into three layers according to the permittivity (ε) and conductivity (σ) of the tissues in each layer. This model employed a 10 mm antenna in the fat layer, with a center radius of 48 mm and 8 mm for the thickness. The third layer, the fibroglandular, also has a center radius of 40 mm and is placed inside the fat layer. The skin has a thickness of 2 mm and a center radius of 50 mm to cover the breast tissue completely. The spherical shape of radius (3, 4, 6, and 8) mm is used as a tumor to discover any tumors.

After extracting the breast models simulation data, data signals need to be preprocessed and converted into exile files. Two groups of data patients have been created. First group has 163 patients, and the second group has 150 patients; each group has 1001 attributes as the independent variable. In principle, a machine learning algorithm trained on a particular dataset should be able to be generalized to new, untrained datasets. The data used to train a model is typically different from the data used to test it. The training set should be as big as feasible to minimize variance in training the model. However, the unseen portion of the data should also be close to the original dataset, so the evaluation process is relevant. When dealing with ML classification, the crucial issue is not whether one learning algorithm is better than another but rather under what situations one technique might considerably outperform another on a specific application problem [13].

4 Machine-Learning Classification

The process of detecting tumors has now moved on to the second stage. The data processing step employs a variety of machine learning approaches to develop models for predicting the presence or absence of a tumor in the breast based only on

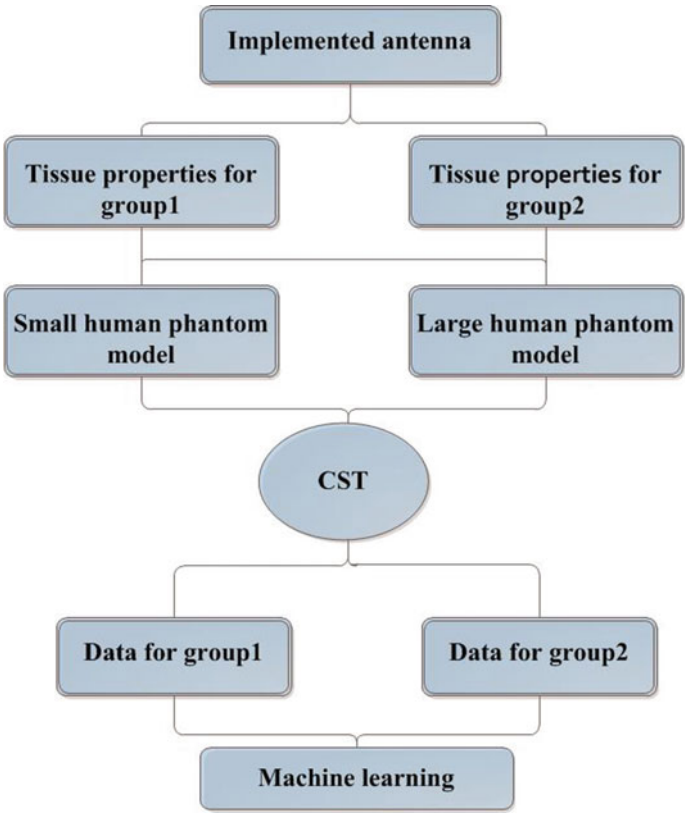

Fig. 1 Methodology for implemented antenna

Table 1 Minimum and maximum boundaries for tissue information for the first group tables

Breast phantom	Relative permittivity (ε)	Conductivity (σ)
Fat tissue	11–18	0.1–0.2
Skin tissue	33–46	0.15–3.8
Glandular tissue	28–40	0.1–3.0
Tumor	48–66	0.15–5.0

backscatter signals collected from the antennas. Developing a pattern recognition model may be separated into three stages: data preprocessing, feature selection and extraction, and algorithm classification which are all steps in the classification process [14].

Table 2 Result information for the first group

Group 1	SVM				KNN	DT
	Linear	Radial	Polynomial	Sigmoid		
Accuracy (%)	68	56	50	68	78	62
Kappa	0.3443	0.0667	-0.1228	0.3443	0.3529	0
Precision	0.833	0.777	0.666	0.833	0.958	1
Recall	0.681	0.583	0.545	0.681	0.793	0.625
F-score	0.749	0.666	0.599	0.749	0.867	0.769

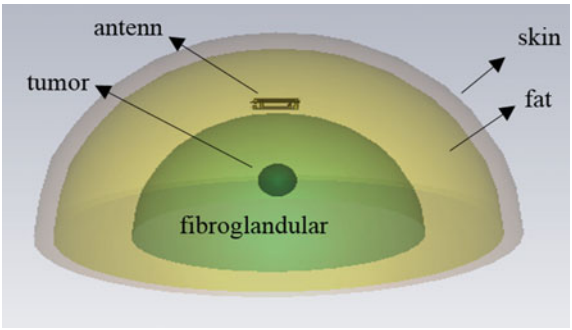

Fig. 2 Breast model with one antenna inside the fat

4.1 Data Preprocessing

Multiple uses of machine learning may be found in the healthcare industry. Healthcare data are generally large, disorganized, and complex. Before they can be utilized to train machine learning systems, data must be properly mapped and preprocessed. This is an important point in machine learning model development since the quality of the model is heavily reliant on the data's correctness in reflecting clinical reality [14]. Data must first be carefully labeled and curated because this data will be used to train a machine learning system, and the labels must correctly represent clinical reality.

Regardless matter how much work is put into enhancing the machine learning algorithm, any mistake in labeling will greatly restrict the accuracy that may be achieved. So the raw data samples for both groups labeled the category label of a tumor-contained signal which is one, and a tumor-free signal is zero. Most machine learning methods need to normalize the data [15]. Data normalization is a technique for standardizing the range of characteristics without affecting the data's dimension. Important is the data normalization procedure since it is necessary to choose the best characteristics without removing relevant information from the preprocessed data [7]. It solves two major data problems that restrict the learning process of machine learning algorithms: dominating features and outliers [16]. Several techniques have been developed for data normalization. This study uses Z-score (zs) and min–max

(mm) to standardize raw data samples. The normalized data of each group is divided into train and test datasets with a ratio of 3:1.

4.2 Feature Extraction and Selection

The algorithms for feature selection and extraction are quite important. These approaches, if used correctly, may choose the most useful, non-redundant data from electromagnetic waves, making the task of the learning classifier faster. The objective is to select or combine variables into features, which will minimize the quantity of data that must be processed (known as "dimensional reduction") while retaining the original databases' significance. The principal component analysis is the breast tumor community's most widely utilized feature extraction approach. PCA transforms the data into a new subspace in which the new orthonormal basis displays the highest variation, i.e., locates the components that can make it easier to tell if a breast tumor is present or not. Dimensional reduction is possible by selecting the most important primary components since PCA organizes them according to their relative significance, i.e., the features with the most variation [17]. When doing dimensional reduction, one of the criteria that must be considered is the number of features used (function pc from R Studio is utilized for feature extraction, reducing the dataset's dimensions from 1001 features to 131 for the first group and 121 for the second group). PCA datasets always reveal better performance than the original dataset.

4.3 Classification Algorithms

The purpose of classification algorithms is to study how to connect processed data with each class to determine the proper class when new data has to be evaluated. This study has different datasets representing different groups of patients. The first group has 163 instances; the second group has 150 instances with 1001 attributes as the independent variable and one as the dependent variable for the analysis. K-nearest neighbor (KNN), decision trees (DT), and support vector machines (SVMs) were used to train these data. SVM is a kind of supervised machine learning technology (labeled data is used). A hyper-plane is produced in SVM with a margin as broad as feasible for separating various categories of data or retaining similar data of one class on one side of the margin and similar data of another class on the other [14]. SVM can be used to make predictions and classify data. When predicting a breast tumor, disease classes can be split in a hyper-plane by the chances of developing tumor tissue on one side of the margin and normal tissue (without a tumor) on the other side.

There are two types of SVM: linear and nonlinear SVM. Data can be separated using a line in linear SVM, but nonlinear SVM is used when this is impossible. A kernel function is employed for nonlinear SVM. When using a kernel function,

various classes of data that may be separated nonlinearly are translated onto higher dimensions to be linearly separable. Equation (1) is the kernel function:

$$k(z_i, z_j) = \phi(z_i)\phi(z_j) \tag{1}$$

Polynomial, linear, radial basis function (RBF), and sigmoid kernel functions are examples of several kinds of kernel functions. Kernel functions take incoming data and turn it into a needed format. Kernel functions may transform a lower-dimensional input space into a higher-dimensional input space. [18]. When multi-collinearity and a nonlinear connection between the input and output variables, SVMs can perform very effectively. In most cases, the performance of SVMs is significantly improved when they are allowed to work with many dimensions and continuous variables [13]. KNN, as it is often known, is a supervised machine learning approach that may be used to classification and regression problems. A straightforward procedure saves all samples that are provided and separates them into new classes by applying a similarity metric (e.g., distance functions) [19]. Here is how the algorithm works. A case is put into a class by the majority vote of its neighbors. It is put into the most common class among its K closest neighbors, measured by a distance function. If $K = 1$, the case is put in the class of the case that is closest to it. It is common to employ the Euclidean, Manhattan, and Minkowski separation distances for distance calculations and computing the closest data points [19]. However, there is no assurance that a big K value is more accurate since it decreases overall noise. If a data point's target value is absent in KNN, the k-nearest data points in the training set are discovered, and the average value of the discovered data points is given. Even if the data is noisy and big, it may provide good results and predictions. According to the majority vote of KNN's K-nearest neighbors, a new data (new backscatter signal) is classified by KNN based on the knowledge of its known classes [20]. These important parameters must be selected and optimized while developing the model: K (the number of closest neighbors) and D (the distance used to measure which is the nearest neighbors) [21]. A decision tree is a method of supervised learning that can be used to classify and predict data. Figure 3 shows the basic structure of the decision tree. First, the entropy value of each feature is calculated. Then, the root is split into sub-trees or other branches based on the highest information gain [22]. With more features, the procedure recursively proceeds, and the final result is given by the last node.

$$\text{entropy}(z) = \sum_{i=1}^{m} p(z_i) \log_n p(z_i) \tag{2}$$

Class entropy is determined using Eq. (2), where m represents a set of classes in Z, Z represents the current dataset to be computed, and $p(z)$ represents the ratio of the number of items in class m to the set of items in set z.

$$\text{IN (Gain)} = \text{E (class)} - \text{E (features)} \tag{3}$$

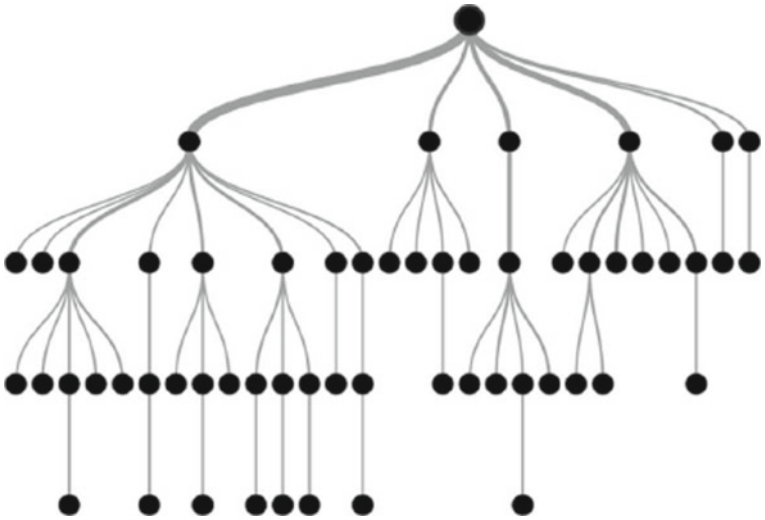

Fig. 3 Decision tree's fundamental structure

IN represents information, and E represents entropy. For information gain, each branch's entropy is subtracted from the entropy of the class in Eq. (3). Two types of data may be utilized in decision trees: continuous and categorical. The tree gave good accuracy since every characteristic was evaluated and analyzed. Models are simple to learn, and rules are simple to develop, able to replace missing values in variables with the value that has the highest probability of being correct. If a tree contains many branches, this technique might suffer from over-fitting, making it difficult to calculate and understand [23]. The overview of the system can be seen in Fig. 4.

A successful early diagnosis of breast cancer relies on accurate, specific, and sensitive measurements, which must be calculated to avoid misclassifications. A significant rate of misdiagnosis is likely when a breast is checked for lesions at an early stage. If a lesion is present but not recognized by the system, or if there is no lesion, but the classifier still diagnoses a tumor, this is known as misdiagnosis. The system's overall efficiency would be harmed if this possibility exists; hence, it must be avoided or decreased. So for the result, we calculate the flowing.

The Kappa Statistic is a performance measure that contrasts actual and expected accuracy [13]. Accuracy was calculated using a confusion matrix, which shows where the model is getting confused [24], as shown in Fig. 5.

$$\text{Accuracy} = \frac{((\text{TP} + \text{TN})}{(\text{TP} + \text{TN} + \text{FP} + \text{FN})} \tag{4}$$

Figure 5 shows the machine model's predicted class and real class where TP stands for "true positive," which denotes that cancer has been correctly categorized. FN stands for "false negative," which denotes that the prediction of not having breast

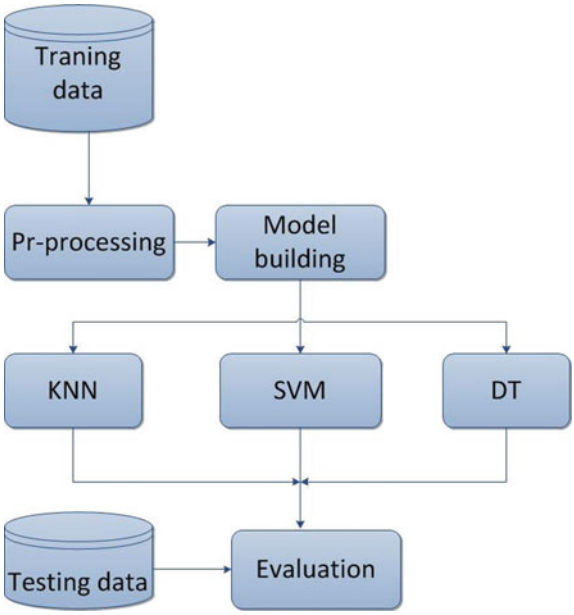

Fig. 4 Proposed system

Real \ Predicted	FREE-TUMOR	WITH TUMOR
FREE-TUMOR	TN	FP
WITH TUMOR	FN	TP

Fig. 5 Structure of the confusion matrix

cancer was wrong. At the same time, FP stands for "false positive," meaning breast cancer was misclassified. TN stands for "true negative," which shows the right way to classify cancer that does not exist. Recall (Sensitivity): Recall tells us how many true positives are correctly described. We can explain what recall is by using Eq. (5).

$$\text{Recall(Sensitivity)} = \frac{\text{TP}}{\text{TP} + \text{FN}} \tag{5}$$

Precision (Specificity): Precision tells us how many of the correctly predicted identifications there are. We can explain what precision is by using Eq. (6).

$$\text{Precision (Specificity)} = \frac{\text{TP}}{\text{TP} + \text{FP}} \tag{6}$$

O measure how accurate a model is based on a particular dataset the F-score, or F1-score, is used. A binary classification strategy that divides cases into positive and negative categories has been evaluated[25]. It is said to be the "harmonic mean" of the model's precision and recall, which is a way to mix the two Eq. (7).

$$\text{F - score} = \frac{2PR}{P + R} \tag{7}$$

5 Result and Discussion

The comparison results of the two groups are shown in Tables 2 and 3 which show an obvious variation in the accuracy between these algorithms and the two groups.

All of the algorithms have been evaluated and compared based on how well they work. We used common metrics like the confusion matrix, precision, and recall to measure accuracy and f-score. Accuracy, kappa, precision, and recall are terms used to describe the results of the three algorithms; the bold ones in these tables is the best accuracy. From the Tables, we can observe that Group 2 has the best result. This result means that the tissue properties of the second group were better because they were taken from frequencies commensurate with the frequencies used by the antenna, which made the antenna able to detect the tumor in a tissue in which it was previously implanted. For the Group 1, data signals were overlapped, and the KNN had the best result with an accuracy of 78% and an F-score of 0.867 when $k = 15$ because KNN works well in overlapping data but is still not very good. For Group 2, SVM has performed better than all the other algorithms in terms of accuracy, F-score, and other evaluations. So, according to the results obtained, we have concluded that the SVM algorithm with the three kernels (sigmoid, radial, and linear) predicts the best result. Accuracy is coming out to be 93%, F-score is 95%, and kappa is 85% for sigmoid, radial, and linear SVM, which is the best algorithm available in this research. It is known that the larger the kappa (precision), recall, and F-scores are, the better the outcome. These algorithms have the largest kappa, precision and recall, F-score, and accuracy. SVM's highest result may have been its

Table 3 Result information for the second group

Group 2	SVM				KNN	DT
	Linear	Radial	Polynomial	Sigmoid		
Accuracy (%)	93	93	70	93	63	73
Kappa	0.85	0.8421	0.129	0.85	0.046	0.4872
Precision	0.95	1	1	0.95	0.947	0.611
Recall	0.95	0.909	0.689	0.95	0.642	0.916
F-score	0.95	0.952	0.815	0.95	0.765	0.733

ability to handle high-dimensional data. The polynomial SVM classifier is less than in other cases. It can be seen that the accuracy outcome is 70%, and F-score is 81%, which means it is not very suitable for separating the data.

6 Conclusion

This research proposes an effective early breast cancer detection method. The non-ionizing implemented antennas that successfully detected the tumor worked under the frequency range of Wi-Fi and IOB, which means the device can be used at home. This method is based on a unique feature extraction technique under UWB microwave and two distinct breast model types and patient datasets. This study created acceptable data for the machine intelligence system using the UWB-implemented antenna. Many applicable supervised machine learning techniques, such as closest neighbor and support vector machines, decision trees, are trained and investigated using this data. Although the ML algorithms performed poorly in terms of accuracy for the first group (a maximum of 78 per cent), for the second group, the accuracy of the machine learning method (SVM) was as high as 93%. The second group was better because they were taken from frequencies commensurate with the antenna. SVM performing well in high-dimensionality data may have been the reason for its best performance. That implies that the antenna used to detect the tumor worked efficiently.

References

1. Cokkinides, V., et al. (2005). *American cancer society: Cancer facts and figures.* American Cancer Society.
2. Kim, T., et al. (2008). A study of dielectric properties of fatty, malignant and fibro-glandular tissues in female human breast. In *2008 Asia-Pacific symposium on electromagnetic compatibility and 19th International Zurich symposium on electromagnetic compatibility.* IEEE.
3. Nahalingam, K., & Sharma, S. K. (2011). An investigation on microwave breast cancer detection by ultra-wide bandwidth (UWB) microstrip slot antennas. In *2011 IEEE International symposium on antennas and propagation (APSURSI).* IEEE.
4. Oliveira, B. L., et al. (2018). Diagnosing breast cancer with microwave technology: Remaining challenges and potential solutions with machine learning. *Diagnostics, 8*(2), 36.
5. Fatima, M., & Pasha, M. (2017). Survey of machine learning algorithms for disease diagnostic. *Journal of Intelligent Learning Systems and Applications, 9*(01), 1.
6. Boparai, J., & Popović, M. (2022). Heterogeneous skin phantoms for experimental validation of microwave-based diagnostic tools. *Sensors, 22*(5), 1955.
7. Vijayasarveswari, V., et al. (2020). Multi-stage feature selection (MSFS) algorithm for UWB-based early breast cancer size prediction. *PLoS ONE, 15*(8), e0229367.
8. Bari, B. S., et al. (2020). Ultra wide band (UWB) based early breast cancer detection using artificial intelligence, In *ECCE2019* (pp. 505–515). Springer.
9. Ali, N., et al. (2020). Stage II cancer diagnosis using printed antenna implemented on hemispherical model for human breast. *Journal of Instrumentation, 15*(09), P09016.

10. Conceição, R. C., et al. (2020). Classification of breast tumor models with a prototype microwave imaging system. *Medical Physics, 47*(4), 1860–1870.
11. Uncu, N., & Avşar Aydin, E. (2019). The effects of dielectric values, breast and tumor size on the detection of breast tumor. *Tehnički Glasnik, 13*(3), 197–203.
12. Tiang, S. S., et al. (2013). Radar sensing featuring biconical antenna and enhanced delay and sum algorithm for early stage breast cancer detection. *Progress in Electromagnetics Research B, 46*, 299–316.
13. Osisanwo, F., et al. (2017). Supervised machine learning algorithms: Classification and comparison. *International Journal of Computer Trends and Technology (IJCTT), 48*(3), 128–138.
14. Ngiam, K. Y., & Khor, W. (2019). Big data and machine learning algorithms for health-care delivery. *The Lancet Oncology, 20*(5), e262–e273.
15. Nersisyan, S., et al. (2022). ExhauFS: Exhaustive search-based feature selection for classification and survival regression. *PeerJ, 10*, e13200.
16. Singh, D., & Singh, B. (2020). Investigating the impact of data normalization on classification performance. *Applied Soft Computing, 97*, 105524.
17. Omuya, E. O., Okeyo, G. O., & Kimwele, M. W. (2021). Feature selection for classification using principal component analysis and information gain. *Expert Systems with Applications, 174*, 114765.
18. Katarya, R., & Meena, S. K. (2021). Machine learning techniques for heart disease prediction: A comparative study and analysis. *Health and Technology, 11*(1), 87–97.
19. Nugrahaeni, R. A., & Mutijarsa, K. (2016). Comparative analysis of machine learning KNN, SVM, and random forests algorithm for facial expression classification. In *2016 International seminar on application for technology of information and communication (ISemantic).* IEEE.
20. Flach, P. (2012). *Machine learning: The art and science of algorithms that make sense of data.* Cambridge University Press.
21. Murphy, K. (2013). *Machine learning: a probabilistic perspective.* MIT Press.
22. Karthiga, A. S., Mary, M. S., & Yogasini, M. (2017). Early prediction of heart disease using decision tree algorithm. *International Journal of Advanced Research in Basic Engineering Sciences and Technology (IJARBEST), 3*(3), 1–17.
23. Ray, S. (2019). A quick review of machine learning algorithms. In *2019 International conference on machine learning, big data, cloud and parallel computing (COMITCon).* IEEE.
24. Ariza-López, F. J., Rodriguez-Avi, J., & Alba-Fernandez, M. (2018). Complete control of an observed confusion matrix. In *IGARSS 2018–2018 IEEE International geoscience and remote sensing symposium.* IEEE.
25. Mian Qaisar, S., & Hussain, S. F. (2021). An effective arrhythmia classification via ECG signal subsampling and mutual information based subbands statistical features selection. *Journal of Ambient Intelligence and Humanized Computing,* 1–15.

A Review of Mathematical Methods for Flexible Robot Dynamics Modeling and Simulation

Chu A. My, Duong X. Bien, Trinh Xuan Hiep, Nguyen Cong Dinh, Vu Minh Duc, Nguyen The Nguyen, Chi Hieu Le, and Esmail Ali Alandoli

Abstract In recent decades, lots of robots are designed and produced all over the world because of their important applications. Nowadays, using the robot is more and more popular in many different fields. In practice, the modeling and control of most of the robots are performed with an important assumption that all links of a robot are rigid bodies. This is to simplify the modeling, analysis, and control for a robot. The elastic deformation of a link always exists during a robot's operation. This elastic deformation of a flexible robot has significant effects on several characterizations and specifications of the robot such as the robot strength, the accuracy of the robot motion, the robot control, etc. In the literature, there have been many studies addressing the dynamics modeling and control of flexible robots. This paper presents an overview of the mathematical methods which have been used for the kinematic and dynamic modeling of the flexible manipulators.

Keywords Flexible robot · Dynamic modeling · FEM

1 Introduction

Modern design always aims at reducing the mass, simplifying the structure, and reducing the energy consumption of systems, especially in robotics. A priority direction in robot design is to optimize structure with longer and thinner links. However, for these structures such as flexible robots, the rigidity and motion accuracy are usually reduced because of the elastic deformation of the links. Therefore, taking into account the effects of elastic factors is necessary when investigating the dynamics and control

C. A. My (✉) · D. X. Bien · T. X. Hiep · N. C. Dinh · V. M. Duc · N. T. Nguyen
Le Quy Don Technical University, 236 Hoang Quoc Viet, Hanoi, Vietnam
e-mail: mychuanh@yahoo.com

C. H. Le
Faculty of Engineering and Science, University of Greenwich, London, UK

E. A. Alandoli
Faculty of Engineering and Technology, Multimedia University, Cyberjaya, Malaysia

T. D. L. Nguyen and J. Lu (eds.), *Machine Learning and Mechanics Based Soft Computing Applications*, Studies in Computational Intelligence 1068,
https://doi.org/10.1007/978-981-19-6450-3_22

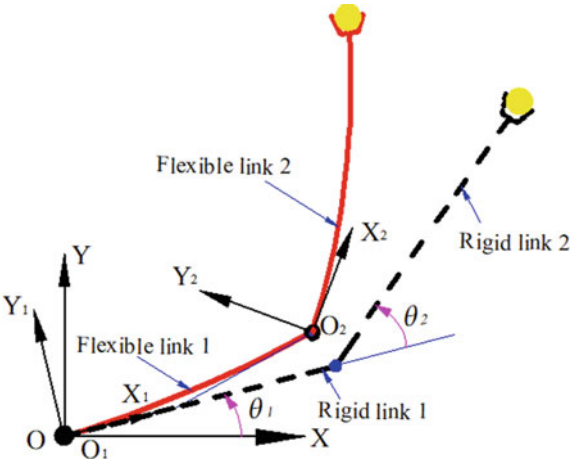

Fig. 1 Two-link manipulator with revolute joints

of flexible robots. In comparison with the traditional rigid robots, the flexible ones have potential advantages such as lower overall mass or energy consumption, small actuator, and greater payload-weight ratio. However, owing to the complex nature of such flexible systems, mathematical modeling has involved complex processes.

Since the modeling and control of the flexible robots are so complex, a simple robot structure with one or two-flexible links, connected by only rotational joints is mainly studied by most researchers. A few works consider the translational joints. Note that the use of different joint types when designing a flexible robot improves the flexibility for the robot. However, a robot model consisting of rotary and translation joints make the kinematic, dynamic modeling, and control become more complex than models which have only rotational joints. In the literature, there have been several studies focusing on the model of two-link flexible robots with all revolute joints [1–15] (Fig. 1).

Although there have been some researches considering the presence of the prismatic joint, they mainly focused on architectures of one or two links [16–20]. A few works consider the prismatic joints for multi-link manipulators [1, 13]. As for different configurations of the flexible manipulators, different modeling methods have been used. Two mainly modeling approaches, including the assumed modes method (AM method) [4, 7, 9, 20–27] and the finite elements method (FE method) [5, 6, 8, 17, 19, 28–34] have been applied to describe the motion of flexible manipulators. The governing equations for the flexible robots can be derived by using the Newton–Euler equation [3, 5, 16, 20, 35], the Lagrange-Euler equation [4, 6, 8, 9, 11, 12, 14, 17, 19, 21, 22, 30, 36–38], or the Gibbs-Appel equation [1, 13, 15, 39]. This paper presents an overview of the mathematical methods that have been exploited to model the kinematics and dynamics of flexible robots.

2 A Literature Review of Flexible Robot Modeling and Control

Due to the complexity of the formulation of the flexible robot dynamics, most of the works focus on a simplified robot mechanism consisting of one or two planar flexible links.

In recent decades, a number of researchers have made their great contributions and several approaches are now available to solve the mathematical modeling problem for the flexible robot. The surveys of the state of the art can be found out in [40–47]. The previous works in the literature, which have been focused on the modeling and analysis for different flexible robot's types, can be categorized as the follow.

One-link flexible robot [16, 17, 22, 27, 30, 36, 40, 48–51];
Two-link flexible robot [2, 5, 17, 19–21, 37, 41, 52–58], and
Multi-link flexible robot [4–9, 11–13, 59, 60].

In particular, for the multi-link flexible robot, most of the researches emphasized the robot architectures with all revolute joints. As discussed earlier in the Introduction section, some of the works [1, 13] proposed the methods to model the dynamics of the robot with the multi-flexible links, of which the links are connected one another by prismatic joints. However, the work in [1] just considered the rotating and reciprocating motion of the flexible links with the predetermined length and revolute—prismatic joints, and the authors in [13] studied the dynamics of the robot structure with multi-flexible links connected by the sliding prismatic joints, but in this research, the effects of link's time-variable length have not considered yet.

Note that there also exist some researches concerning with the flexible robot having prismatic joints. Wang and Wei [16] investigate the dynamics of a one-link flexible arm modeled by a moving slender prismatic beam. Al-Bedoor [17] addresses the dynamic modeling of one sliding link with a fixed prismatic joint. This joint in the two-link flexible robots was modeled by Ju [18] and Pan [19]. Wang [34] considers parallel robots having flexible links and sliding prismatic joints. The multi-link flexible robots with prismatic joints are considered in [1, 13]. For the kinematic and dynamic modeling, both the mentioned researches employed the assumed modes method which has proven the effectiveness to numerically simulate the single-link flexible arm [42].

Though the prismatic joint has been taken into account for the mathematical modeling, there was a little work, devoted to the flexible robot having two specific kinds of prismatic joint as shown in Fig. 2a and b.

The fixed prismatic joint can be characterized by the fixed and sliding motions between the joint and two consecutive links $(i-1)$ and link (i), respectively. The length of the link (i) varies in time (Fig. 2a), whereas when two links connecting by a sliding prismatic joint, the link $(i-1)$ is a variable length. Due to these characterizations, for a structure with the first case (Fig. 2a), the relative motion of the current link i depends on the joint's motion and the elastic deformation at the distal end of the previous link $(i-1)$. Nonetheless, this deformation does not affect the

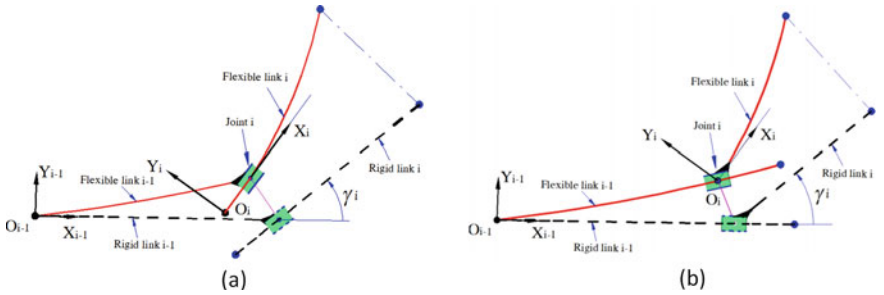

Fig. 2 Two kinds of prismatic joint

link i motion in the configuration with the sliding prismatic joint. In this case, the effect of link $(i-1)$ deformation is considered through the elastic deformation at the coincide sliding element in the connection of the link $(i-1)$ and the joint. This element moves along the link $(i-1)$, , depending on the state of the flexible robot (Fig. 2b). The dynamic model of the flexible robot with those mentioned kinds of prismatic joint is built based on the basic assumption of the element having zero elastic deformation. It is noticeable that the elasticity effects involves the variable length of such links should be taken into account to propose a model for flexible robots consisting of all the joint types as discussed.

In theory, formulating the dynamics of the multi-link flexible robot with various joint types is a difficult task. A few works have been considered this issue to generalize the dynamic modeling and control for this robot's kind [61, 62].

To formulate the flexible robot dynamics model, several analytical approaches and computational methods have been investigated. Generally, the flexible robot is investigated as continuous systems that are not confined by the number of freedom degrees, and described by nonlinear differential equations that cannot be solved exactly. To describe the dynamic motion of flexible robots, two discretized methods of the assume mode method (AM) and the finite element method (FE) are often used. Comparing the effectiveness of these methods, in [42, 43], the authors pointed out that the main disadvantage of the AM method is difficult to find the modes for non-regular cross-sections links and multi-link manipulators. Moreover, the authors in [42] also proved that the FE method is simple for the computations, resulting in suitable applications to model the multi-links flexible arms and the real-time control law computation. In practice, the FE method has been widely utilized to model the flexible robot's dynamics [5, 6, 8, 17, 19, 28–34]. In the FM method-approach, the flexible links are discretized by finite elements with the same length. The dynamic model is built based on the global mass matrixes, stiffness matrixes of the entire system. These matrixes are constructed by the assembly of the mass and stiffness matrix of each element, which is formulated through the calculation of the kinetic and potential energy in the nodal coordinates. The assembled procedure is complicated, requires expensive computational time. Especially, with the flexible robots that consist of prismatic joints, this process is even more complicated due to

the time-varying boundary conditions. Besides, there are many studies that has been focused on proposing the dynamic modeling for the flexible robots, combining the analytical approaches with the FE method or the AM method, such the approaches are:

Newton–Euler approach [3, 5, 6, 16, 20, 35, 63–65],
Approach based on Lagrange's equations [4, 6, 8, 9, 11, 12, 14, 17, 19, 21, 22, 30, 36–38],
Approach based on Hamilton's equations [18, 66],
Approach based on Gibbs–Appell equations [1, 13, 15, 39], and
Approach based on Kane's equations [10, 53].

Note that the FE method has been widely used as an efficient approach to model complex structures. In [3], Augustynek proposed the dynamic modeling for flexible robot links—like beam with rotary joint, considering the assembly errors. Based on the FM method, Naganathan [5] presented the nonlinear model to investigate the effect of elastic deformations of the flexible links, coupling with the kinematics of joints. In [6], the authors incorporated a Newton–Euler analytical model with the FM method to model the flexible robot with all revolving joins. It was shown that, in the FE method, the elastic manner of a flexible robot is assessed through the overlay of elastic deformation of a rigid body. In [8], based on the Lagrangian approach and FM method, Usoro proposed the formulations of the mathematical equations for the dynamic of lightweight flexible links. In another approach, the authors in [10] developed a recursive formulation in the matrix form for flexible multi-link systems by combining the FM method with Kane's equations. The modeling and controlling of the flexible manipulators with a prismatic joint were also developed in [17, 19]. The consideration of nonlinear behavior in the dynamic of the flexible was presented in [28] by Du. In this study, the dynamic was modeled in three-dimension by using the FM method, and the inertial of the link is consolidated at the element's nodes. Tokhi [30] developed the experiments to validate the dynamic model of the flexible system. In [34], the dynamic of flexible link in the parallel foundation was described by the finite element coupling with Lagrangian equations. By using the FE method and Kane's equations, comparing with other methods, Lochan [46] discussed the advantages of the FE method in the modeling of the flexible robot's dynamic. In this research, the main benefits of the FE method were pointed out, including the ease to handle the nonlinear conditions and complicated boundary conditions and the independence of the dynamic modeling on the link's shape.

In [61], the kinematics response of the joints and flexible links were described with a proposed transformation matrix. Also, the dynamic model was implemented by introducing a new recursive formulation. In the next developed step, the authors in [67] attempted to propose the dynamic model and its inverse analysis for a class of flexible robots, consisting of two-flexible links by using the FM-Lagrangian approach. The inverse dynamic analysis was then solved by the bisection method. Another attempt to propose new mathematical equations for flexible robot dynamics analysis, aiming at simplifying the computation process was presented in [62].

Based on the Lagrangian formulation, Tokhi [30], Al-Bedoor [31], Mahto [32] focused on one link—one rotary joint flexible robot, Karagulle [33] considered the manipulators, configured by two-links and two rotary joints, Al-Bedoor [17] and Pan [19] emphasized on the robot with one flexible link and one fixed prismatic joint. Wang [34] accounted for sliding prismatic joints in the architecture of a parallel robot, and Usoro [8] studied multi-link robot structure. In these researches, the matrix of each element was calculated based on the elastic deformation at its nodes and considering the previous joint variables and the elastic deformation of the nominal articulation. In [5, 6], the calculation of each element's matrix was derived concerning the freedom degree of nodes. Global matrices were assembled from the elemental matrices. In particular, Karagulle [33] assembled directly the global mass matrix, entry by entry. In the study by My et al. [61, 62], a recursive kinematic and dynamic formulation has been developed for the multi-link flexible robot with respect to different joint types.

It is seen that the FEM Lagrangian approach has been mostly employed in the most recent works, such as Mahto [32], Karagulle et al. [33], and My et al. [61, 62, 67], in which the modeling and controlling of the flexible robots have been investigated. In these recent FEM formulations, a flexible robot consisting of n links is usually considered.

In Fig. 3, two links of a flexible manipulator are shown. The two links are connected by a joint i which is representative of different joint types.

For every element ij, the elemental mass matrix was usually written as follows.

$$\boldsymbol{M}_{ij} = \left[m_{sp}\right]_{ij} = \int_0^{l_{ie}} m_i \boldsymbol{J}_{ij}^T \boldsymbol{J}_{ij} dx \tag{1}$$

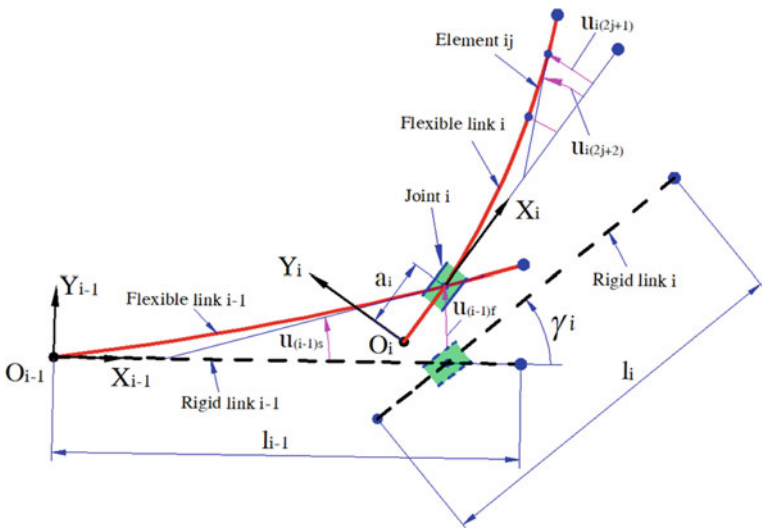

Fig. 3 General schematic of a flexible link's pair

where m_i is the mass of the element ij, and the Jacobian $\boldsymbol{J}_{ij}$ is calculated as follows

$$\boldsymbol{J}_{ij} = \frac{\partial \boldsymbol{r}_{0ij}}{\partial \boldsymbol{q}} \tag{2}$$

In Eq. (2), $\boldsymbol{r}_{0ij}$ is a point on the beam element ij, and $\boldsymbol{q}$ is the vector of the generalized coordinates. As a consequence, the mass matrix can be cumulatively calculated as follow.

$$\boldsymbol{M} = \sum_{i=1}^{n} \sum_{j=1}^{n_i} \boldsymbol{M}_{ij} \tag{3}$$

In the same approach, the global stiffness matrix for the governing equation can be calculated as follow.

$$\boldsymbol{K} = \sum_{i=1}^{n} \sum_{j=1}^{n_i} \boldsymbol{K}_{ij} \tag{4}$$

When the matrices $\boldsymbol{M}$ and $\boldsymbol{K}$ are determined in a symbolic form, the governing equation for a flexible robot is expressed as follows.

$$\boldsymbol{M}(\boldsymbol{q})\ddot{\boldsymbol{q}} + \boldsymbol{C}(\boldsymbol{q}, \dot{\boldsymbol{q}})\dot{\boldsymbol{q}} + \boldsymbol{K}\boldsymbol{q} + \boldsymbol{G}(\boldsymbol{q}) = \boldsymbol{F} \tag{5}$$

Note that $\boldsymbol{G}$ represents the gravity effects, the Coriolis and centrifugal matrix $\boldsymbol{C}$ can be determined by using Christoffel method and $\boldsymbol{F}$ is the forces/torques' vector.

Besides the FM method, to model the flexible robot arms, the AM method also has been widely exploited. In this method, the link's elasticity is modeled by a series of finite modes, in which spatial model eigenfunctions and time-varying amplitudes were truncated. Based on Lagrange's equations, several investigations were carried out for the formulation of the dynamic equations in [4, 6, 8, 9, 11, 12, 14, 17, 19, 21, 22, 30, 36–38, 68–73]. Also, with the same purpose of dynamic formulation, Gibbs–Appell's formulation was applied in the works by Korayem [1] and Khadem [13] derived, Hamilton's principle was used in [18, 66], and Newton–Euler equations were adopted in [3, 5, 6, 16, 20, 35, 63–65].

Note that the modeling of the flexible robots has been also mentioned in some investigations on control law design [74–77]. Matsuno [78] designed the laws to control the one-link flexible robot based on analyzing the AM—Lagrangian dynamic model. Bolandi [79] proposed the nonlinear controlling law for tracking the exact tip of the flexible arm. Based on Hamilton's equations, Zhang [80] formulated dynamic equations with the purpose of vibration control for one-link flexible robot. Apart from the aforementioned works, there have been many studies related to different aspects of modeling and analyzing flexible robotic systems. The inverse dynamics of the flexible arm were presented in [37, 48, 65, 81–83], the stiffness modeling

and characteristics of robot were considered in [84–86], and the experiments were implemented in [61, 87–89].

3 Conclusion

Though flexible robots have many outstanding advantages in comparison with traditional rigid robots such as energy-saving, able to operate with a small actuator, and highly efficient load carrying. The stiffness of flexible robots is a critical issue for their design and control. The flexibility of the flexible robots increases the computational complexity of the kinematic and dynamic modeling for the robots, especially when considering a multi-link flexible robot with different joint types. There has been a massive amount of research work concerning flexible robots. Various configurations of flexible robots are taken into account but mainly focus on robots with a single-flexible link or two-flexible link. A few attempts consider the multi-link flexible robots. The rotational joint is a basic joint type that is considered in most studies. A few works are interested in prismatic joints. The combination of the revolute joint and translational joint in an elastic robot configuration is still problematic to deal with. The AM method and the FE method are mainly used for the formulation of the dynamic equation. However, the AM method is suitable for configurations with less elastic stitches. The FE method has many advantages to formulate the mathematical equations of the flexible multi-link robot even with different joint types. Besides, there have been several mathematical approaches for the derivation of the flexible robot's dynamic equations. Nevertheless, the Newton–Euler method, Lagrangian formulation, Hamilton principle, and Kane equations are widely used for flexible robot modeling.

Acknowledgements This research is funded by Vietnam National Foundation for Science and Technology Development (NAFOSTED) under grant number 107.01-2020.15

References

1. Korayem, M. H., Shafei, A. M., & Dehkordi, S. F. (2014). Systematic modeling of a chain of N-flexible link manipulators connected by revolute–prismatic joints using recursive Gibbs-Appell formulation. *Archive of Applied Mechanics, 84*(2), 187–206.
2. Raouf, F., Mohamad, S., Maarouf, S., & Maamar, B. (2017). Distributed adaptive control strategy for flexible link manipulators. *Robotica, 35*(7), 1562.
3. Augustynek, K., & Adamiec-Wójcik, I. (2012). Analysis of mechanisms with flexible beam-like links, rotary joints and assembly errors. *Archive of Applied Mechanics, 82*(2), 283–295.
4. Book, W. J. (1984). Recursive Lagrangian dynamics of flexible manipulator arms. *The International Journal of Robotics Research, 3*(3), 87–101.
5. Naganathan, G., & Soni, A. H. (1987). Coupling effects of kinematics and flexibility in manipulators. *The International Journal of Robotics Research, 6*(1), 75–84.

6. Jonker, B. (1990). A finite element dynamic analysis of flexible manipulators. *The International Journal of Robotics Research, 9*(4), 59–74.
7. In, J., & Lewis, F. L. (1994). A symbolic formulation of dynamic equations for a manipulator with rigid and flexible links. *The International Journal of Robotics Research, 13*(5), 454–466.
8. Usoro, P. B., Nadira, R., & Mahil, S. S. (1986). *A finite element/Lagrange approach to modeling lightweight flexible manipulators*.
9. De Luca, A., & Siciliano, B. (1991). Closed-form dynamic model of planar multilink lightweight robots. *IEEE Transactions on Systems, Man, and Cybernetics, 21*(4), 826–839.
10. Amirouche, F. M. L., & Xie, M. (1993). An explicit matrix formulation of the dynamical equations for flexible multibody systems: A recursive approach. *Computers & Structures, 46*(2), 311–321.
11. Chen, W. (2001). Dynamic modeling of multi-link flexible robotic manipulators. *Computers & Structures, 79*(2), 183–195.
12. Subudhi, B. A. M. S., & Morris, A. S. (2002). Dynamic modelling, simulation and control of a manipulator with flexible links and joints. *Robotics and Autonomous Systems, 41*(4), 257–270.
13. Khadem, S. E., & Pirmohammadi, A. A. (2003) Analytical development of dynamic equations of motion for a three-dimensional flexible link manipulator with revolute and prismatic joints. *IEEE Transactions on Systems, Man, and Cybernetics, Part B (Cybernetics), 33*(2), 237–249.
14. Zhang, D. G. (2009). Recursive Lagrangian dynamic modeling and simulation of multi-link spatial flexible manipulator arms. *Applied Mathematics and Mechanics, 30*(10), 1283–1294.
15. Korayem, M. H., Rahimi, H. N., & Nikoobin, A. (2012). Mathematical modeling and trajectory planning of mobile manipulators with flexible links and joints. *Applied Mathematical Modelling, 36*(7), 3229–3244.
16. Wang, P. K. C., & Wei, J. D. (1987). Vibrations in a moving flexible robot arm. *Journal of Sound Vibration, 116*, 149–160.
17. Al-Bedoor, B. O., & Khulief, Y. A. (1997). General planar dynamics of a sliding flexible link. *Journal of Sound and Vibration, 206*(5), 641–661.
18. Ju, J., Li, W., Wang, Y., Fan, M., & Yang, X. (2016). Two-time scale virtual sensor design for vibration observation of a translational flexible-link manipulator based on singular perturbation and differential games. *Sensors, 16*(11), 1804.
19. Pan, Y. C., Scott, R. A., & Ulsoy, A. G. (1990). *Dynamic modeling and simulation of flexible robots with prismatic joints.*
20. Yuh, J., & Young, T. (1991). *Dynamic modeling of an axially moving beam in rotation: Simulation and experiment*.
21. Low, K. H., & Vidyasagar, M. (1988). A Lagrangian formulation of the dynamic model for flexible manipulator systems. *Journal of Dynamics Systems, Measurement, and Control, 110*(2), 175–181.
22. Wang, D., & Vidyasagar, M. (1991). Transfer functions for a single flexible link. *The International Journal of Robotics Research, 10*(5), 540–549.
23. Cetinkunt, S., & Yu, W. L. (1991). Closed-loop behavior of a feedback-controlled flexible arm: A comparative study. *The International Journal of Robotics Research, 10*(3), 263–275.
24. Koivo, A. J., & Lee, K. S. (1992). Self-tuning control of a two-link manipulator with a flexible forearm. *The International Journal of Robotics Research, 11*(4), 383–395.
25. Wang, D., & Vidyasagar, M. (1992). Modeling a class of multilink manipulators with the last link flexible. *IEEE Transactions on Robotics and Automation, 8*(1), 33–41.
26. Zuo, K., Drapeau, V., & Wang, D. (1995). Closed loop shaped-input strategies for flexible robots. *The International Journal of Robotics Research, 14*(5), 510–529.
27. Formal'sky, A. M., & Lavrovsky, E. K. (1996). Stabilization of flexible one-link arm position: Stability domains in the space of feedback gains. *The International Journal of Robotics Research, 15*(5), 492–504.
28. Du, H., Lim, M. K., & Liew, K. M. (1996). A nonlinear finite element model for dynamics of flexible manipulators. *Mechanism and Machine Theory, 31*(8), 1109–1119.
29. Płosa, J., & Wojciech, S. (2000). Dynamics of systems with changing configuration and with flexible beam-like links. *Mechanism and Machine Theory, 35*(11), 1515–1534.

30. Tokhi, M. O., & Mohammed, Z. (2001). Dynamic characterisation of a flexible manipulator system. *Robotica, 19*(5), 571–580.
31. Al-Bedoor, B. O., & Almusallam, A. A. (2000). Dynamics of flexible-link and flexible-joint manipulator carrying a payload with rotary inertia. *Mechanism and Machine Theory, 35*(6), 785–820.
32. Mahto, S. (2014). Shape optimization of revolute-jointed single link flexible manipulator for vibration suppression. *Mechanism and Machine Theory, 75*, 150–160.
33. Karagülle, H., Malgaca, L., Dirilmiş, M., Akdağ, M., & Yavuz, Ş. (2017). Vibration control of a two-link flexible manipulator. *Journal of Vibration and Control, 23*(12), 2023–2034.
34. Wang, X., & Mills, J. K. (2006). Dynamic modeling of a flexible-link planar parallel platform using a substructuring approach. *Mechanism and Machine Theory, 41*(6), 671–687.
35. Briot, S., & Khalil, W. (2014). Recursive and symbolic calculation of the elastodynamic model of flexible parallel robots. *The International Journal of Robotics Research, 33*(3), 469–483.
36. Kalker, J. J., & Olsder, G. J. (1987). On robots with flexible links: Dynamics, control and stability. *Ingenieur-Archiv, 57*(1), 16–24.
37. Asada, H., Ma, Z. D., & Tokumaru, H. (1990). Inverse dynamics of flexible robot arms: Modeling and computation for trajectory control. *Journal of Dynamics Systems, Measurement and Control, 112*(2), 177–185.
38. Meghdari, A., & Fahimi, F. (2001). On the first-order decoupling of dynamicsal equations of motion for elastic multibody systems as applied to a two-link flexible manipulator. *Multibody System Dynamics, 5*(1), 1–20.
39. Doosthoseini, M., Korayem. M. H., Shafei, & Kadkhodaei, B. (2012). An experimental interface design for a single-link elastic manipulator systems. *International Research Journal of Applied and Basic Sciences, 3*, 1726–1734.
40. Rahimi, H. N., & Nazemizadeh, M. (2014). Dynamic analysis and intelligent control techniques for flexible manipulators: A review. *Advanced Robotics, 28*(2), 63–76.
41. Kiang, C. T., Spowage, A., & Yoong, C. K. (2015). Review of control and sensor system of flexible manipulator. *Journal of Intelligent & Robotic Systems, 77*(1), 187–213.
42. Theodore, R. J., & Ghosal, A. (1995). Comparison of the AMM and FEM for flexible multi-link manipulators. *The International Journal of Robotics Research, 14*, 91–111.
43. Dwivedy, S. K., & Eberhard, P. (2006). Dynamic analysis of flexible manipulators, a literature review. *Mechanism and Machine Theory, 41*(7), 749–777.
44. Benosman, M., & Le, V. G. (2004). Control of flexible manipulators: A survey. *Robotica, 22*(5), 533–545.
45. Sayahkarajy, M., Mohamed, Z., & Mohd Faudzi, A. A. (2016). Review of modelling and control of flexible-link manipulators. *Proceedings of the Institution of Mechanical Engineers, Part I: Journal of Systems and Control Engineering, 230*(8), 861–873.
46. Lochan, K., Roy, B. K., & Subudhi, B. (2016). A review on two-link flexible manipulators. *Annual Reviews in Control, 42*, 346–367.
47. Alandoli, E. A., Sulaiman, M., Rashid, M. Z. A., & Shah, H. N. M. (2016). A review study on flexible link manipulators. *Journal of Telecommunication, Electronic and Computer Engineering, 8*(2), 93–97.
48. Kwon, D. S., & Book, W. J. (1994). A time-domain inverse dynamics tracking control of a single-link flexible manipulator. *Journal of Dynamics Systems, Measurement, and Control, 116*(2), 193–200.
49. Marghitu, D. B., & Diaconescu, C. I. (1999). Control techniques for impacting flexible systems. *Archive of Applied Mechanics, 69*(8), 555–568.
50. Pratiher, B., & Santosa. K. D. (2007). Nonlinear dynamics of a flexible single link Catersian manipulator. *International Journal of Non-Linear Mechanics, 42*, 1062–1073.
51. Tarvirdizadeh, B., & Yousefi-Koma, A. (2012). Dynamic object manipulation by a flexible robotic arm: Theory and experiment. *International Journal of Robotics and Automation, 27*(3), 263.
52. Ge, S. S., Lee, T. H., & Wang, Z. P. (2001). Adaptive robust controller design for multi-links flexible robots. *Mechatronics, 11*, 951–967.

53. Meghdari, A., & Fahimi, F. (2001). On the first-order decoupling of dynamical equations of motion for elastic multibody systems as applied to a two-link flexible manipulator. *Multibody System Dynamics, 5*(1), 1–20.
54. Green, A., & Sasiadek, J. Z. (2004). Dynamics and trajectory tracking control of a two-link robot manipulator. *Modal Analysis, 10*(10), 1415–1440.
55. Resta, F., Ripamonti, F., Cazzulani, G., & Ferrari, M.: Independent modal control for nolinear flexible structures: An experimental test rig. *Journal of Sound and Vibration, 329*, 961–972.
56. Sahab, A. R., & Modabbernia, M. R. (2011). Backstepping method for a single link flexible joint manipulator using genetic algorithm. *International Journal of Innovative Computing, Information and Control, 7*(7), 4161–4170.
57. Abdullahi, A. M., et al. (2012). Vibration and tip flection control of a single flexible link manipulator. *International Journal of Intrusmentation and Control System, 3*(4), 17–27.
58. Rone, W. S., Saab, W., & Ben-Tzvi, P.: Design, modeling, and integration of a flexible universal spatial robotic tail. *Journal of Mechanisms and Robotics, 10*(4).
59. Merabet, A., & Gu, J.: Generalized predictive control for single link flexible joint robot. *International Journal of Sciences and Techniques of Automatic Control & Computer Engineering, 3*(1), 890–899.
60. Shi, S., Wu, H., Song, Y., & Handroos, H. (2017). Mechanical design and error prediction of a flexible manipulator system applied in nuclear fusion environment. *Industrial Robot: An International Journal, 44*(6), 711–719.
61. My, C. A., Bien, D. X., Le, C. H., & Packianather, M. (2019). An efficient finite element formulation of dynamics for a flexible robot with different type of joints. *Mechanism and Machine Theory, 134*, 267–288.
62. Chu, A. M., Nguyen, C. D., Duong, X. B., Nguyen, A. V., Nguyen, T. A., Le, C. H., & Packianather, M. (2020). A novel mathematical approach for finite element formulation of flexible robot dynamics. *Mechanics Based Design of Structures and Machines,* 1–22.
63. Abbas, L. K., Zhou, Q., Bestle, D., & Rui, X. (2017). A unified approach for treating linear multibody systems involving flexible beams. *Mechanism and Machine Theory, 107*, 197–209.
64. Boyer, F., & Coiffet, P. (1996). Symbolic modeling of a flexible manipulator via assembling of its generalized Newton Euler model. *Mechanism and Machine Theory, 31*(1), 45–56.
65. Boyer, F., & Khalil, W. (1998). An efficient calculation of flexible manipulator inverse dynamics. *The International Journal of Robotics Research, 17*(3), 282–293.
66. Pratiher, B., & Dwivedy, S. K. (2007). Non-linear dynamics of a flexible single link Cartesian manipulator. *International Journal of Non-Linear Mechanics, 42*(9), 1062–1073.
67. My, C. A., Bien, D. X. (2020) New development of the dynamic modeling and the inverse dynamic analysis for the flexible robot. *International Journal of Advanced Robotic Systems,* 1–12.
68. Hewit, J. R., Morris, J. R., Sato, K., & Ackermann, F. (1997). Active force control of a flexible manipulator by distal feedback. *Mechanism and Machine Theory, 32*(5), 583–596.
69. Mehrez, M. W., & El-Badawy, A. A. (2010). Effect of the joint inertia on selection of under-actuated control algorithm for flexible-link manipulators. *Mechanism and Machine Theory, 45*(7), 967–980.
70. Choi, S. B., Lee, H. B., & Thompson, B. S. (1998). Compliant control of a two-link flexible manipulator by constraint Hamiltonian system. *Mechanism and Machine Theory, 33*(3), 293–306.
71. Abe, A. (2009). Trajectory planning for residual vibration suppression of a two-link rigid-flexible manipulator considering large deformation. *Mechanism and Machine Theory, 44*(9), 1627–1639.
72. Ata, A. A., Fares, W. F., & Saadeh, M. Y. (2012). Dynamic analysis of a two-link flexible manipulator subject to different sets of conditions. *Procedia Engineering, 41*, 1253–1260.
73. Damaren, C. J. (2000). On the dynamics and control of flexible multibody systems with closed loops. *The International Journal of Robotics Research, 19*(3), 238–253.
74. Khalil, W., Boyer, F., & Morsli, F. (2017). General dynamic algorithm for floating base tree structure robots with flexible joints and links. *Journal of Mechanisms and Robotics, 9*(3).

75. Alandoli, E. A., Lee, T. S., My, C. A., & Mohammed, M. Q. (2021). Robust PH∞ integrated controller for flexible link manipulator system in the presence of disturbance. *Journal of Applied and Computational Mechanics, 7*(2), 646–654.
76. Alandoli, E. A., & Lee, T. S. (2020). A critical review of control techniques for flexible and rigid link manipulators. *Robotica, 38*(12), 2239–2265.
77. Alandoli, E. A., Rashid, M. Z. A., & Sulaiman, M. (2017). A comparison of pid and lqr controllers for position tracking and vibration suppression of flexible link manipulator. *Journal of Theoretical & Applied Information Technology*, *95*(13).
78. Matsuno, F., Fukushima, S., Ohsawa, Y., Kiyohara, M., & Sakawa, Y. (1987). Feedback control of a flexible manipulator with a parallel drive mechanism. *The International Journal of Robotics Research, 6*(4), 76–84.
79. Bolandi, H., & Esmaeilzadeh, S. M. (2011). Exact tip trajectory tracking control of a flexible robot arm. *International Journal of Robotics and Automation, 26*(1), 100.
80. Zhang, Y., Liu, J., & He, W. (2016). Vibration control for a nonlinear three-dimensional flexible manipulator trajectory tracking. *International Journal of Control, 89*(8), 1641–1663.
81. Carrera, E., & Serna, M. A. (1996). Inverse dynamics of flexible robots. *Mathematics and Computers in Simulation, 41*(5–6), 485–508.
82. Bayo, E., Papadopoulos, P., Stubbe, J., & Serna, M.A. (1989). Inverse dynamics and kinematics of multi-link elastic robots: An iterative frequency domain approach. *The International Journal of Robotics Research, 8*(6), 49–62.
83. Zhaocai, D., & Yueqing, Y. (2008). Dynamic modeling and inverse dynamic analysis of flexible parallel robots. *International Journal of Advanced Robotic Systems, 5*(1), 13.
84. Chen, G., Zhang, Z., & Wang, H. (2018). A general approach to the large deflection problems of spatial flexible rods using principal axes decomposition of compliance matrices. *Journal of Mechanisms and Robotics, 10*(3), 031012.
85. Rone, W. S., Saab, W., & Ben-Tzvi, P. (2018). Design, modeling, and integration of a flexible universal spatial robotic tail. *Journal of Mechanisms and Robotics, 10*(4), 041001.
86. Ceccarelli, M., & Carbone, G. (2002). A stiffness analysis for CaPaMan (Cassino parallel manipulator). *Mechanism and Machine Theory, 37*(5), 427–439.
87. Cannon, R. H., & Schmitz, E. (1984). Initial experiments on the end-point control of a flexible one-link robot. *The International Journal of Robotics Research, 3*(3), 62–75.
88. Rovner, D. M., & Cannon, R. H., Jr. (1987). Experiments toward on-line identification and control of a very flexible one-link manipulator. *The International Journal of Robotics Research, 6*(4), 3–19.
89. Brogliato, B., Rey, D., Pastore, A., & Barnier, J. (1998). Experimental comparison of nonlinear controllers for flexible joint manipulators. *The International Journal of Robotics Research, 17*(3), 260–281.

Digital Twins of Robotic Systems: Increasing Capability for Industrial Applications

Tran Tuan Anh, Nguyen Thanh Tan, Dinh Than Le, Le Chi Hieu, Jamaluddin Mahmud, M. J. A. Latif, and Nguyen Ho Quang

Abstract Digital twin is one of the emerging areas of research and technology development and the enabling technologies of Smart Manufacturing and Industry 4.0. This study aims to develop and demonstrate a proof-of-concept prototype with a case study of the digital twin of a robotic system. The system has two main elements: the virtual element and the physical or the real element. The virtual element of system has been built based on the Unity platform, which is a cross-platform game engine developed by Unity Software Inc., and the physical element was built with the use of two servomotors and the NVIDIA® Jetson Nano™ Developer Kit. The virtual and the physical elements are connected and communicated via using the TCP socket protocol suite. A digital twin model of the ABB IRB 120 robot was successfully

T. T. Anh · N. T. Tan · D. T. Le · N. H. Quang (✉)
Institute of Engineering and Technology, Thu Dau Mot University, Thu Dau Mot City, Binh Duong Province, Vietnam
e-mail: quangnh@tdmu.edu.vn

D. T. Le
e-mail: than.ld@ieee.org

D. T. Le
Artificial Intelligence Laboratory, Faculty of Information Technology, Ton Duc Thang University, Ho Chi Minh City, Vietnam

L. C. Hieu
Faculty of Engineering and Science, University of Greenwich, Kent ME4 4TB, UK
e-mail: c.h.le@gre.ac.uk

J. Mahmud
School of Mechanical Engineering, College of Engineering, Universiti Teknologi MARA, Shah Alam, Malaysia
e-mail: jm@uitm.edu.my

M. J. A. Latif
Fakulti Kejuruteraan Mekanikal, Universiti Teknikal Malaysia Melaka (UTeM), Hang Tuah Jaya, 76100 Durian Tunggal, Melaka, Malaysia
e-mail: juzaila@utem.edu.my

Advanced Manufacturing Centre (AMC), Universiti Teknikal Malaysia Melaka (UTeM), Hang Tuah Jaya, 76100 Durian Tunggal, Melaka, Malaysia

T. D. L. Nguyen and J. Lu (eds.), *Machine Learning and Mechanics Based Soft Computing Applications*, Studies in Computational Intelligence 1068,
https://doi.org/10.1007/978-981-19-6450-3_23

developed and demonstrated. The collected data include the joint angle position values of the physical and virtual models, and they are stored both locally and in the cloud for the future system development, which can be used as for minimizing the errors between the physical and virtual models of digital twins of robotic systems. The successfully developed digital twin model can be considered as the cost-effective solutions for demonstrating and evaluating potential applications of digital twins in industrial practices as well as in higher educations and research.

Keywords IoT · Coffee disease · Coffee farm · Environmental factor

1 Introduction

A digital twin [1, 2] is a digital duplicate of a physical entity whose base is infrastructure and data and at its core are algorithms and models and applications software and services. This technology along with robotics has been growing rapidly in recent years and is considered by research and industry to be the main driving factors for Industry 4.0. Under the development of artificial intelligence (AI) [3–7], robotics [8–11] has made breakthrough developments in the capabilities of robots such as performing complex jobs with high danger, taking care of health, cooperation with people, and more. The combination of digital twin and robot applying new technologies and algorithms will be the foundation for building and developing smart manufacturing. The trends of using AI to analyze data and make prediction are being special care.

The Robot Operating System (ROS) platform is a collection of tool software libraries that help build robotic applications with source code [12]. The control algorithms tend to apply ML to increase performance and optimization process. In this study, ROS is used as middleware to connect the virtual and real parts and makes it possible to apply platforms like motion planning [13–16], autonomous mobile robotics [17, 18].

A digital twin provides various features such as visualization, simulation with real data, and performance monitoring. To do that, the amount of data collected must be stored. Firebase is a cloud-based database service, accompanied by an extremely powerful server system of Google. Firebase provides capabilities such as analytics, databases, activity reports, and error reporting for easy development. It has versatile services and trusted security. Therefore, the data in this project, namely the joint values and the execution time, are all stored using Firebase.

The main contribution of this paper includes data storage cloud which are the limitations of the recent research papers [19–22]. In addition, we build virtual environment, calculated the kinematics, assure real time two-way data transmission between virtual and analyze and evaluate the obtained data.

In this paper, we divide into five main sections. We first build a virtual model and a virtual environment for the robot. Second, we build the real part system for the robot. Third, we connect and transfer data between the real and the virtual models.

Fourth, we calculate the kinematics for the robot. Finally, the data will be transmitted in both directions to control, evaluate errors, and store the data on both local storage and the cloud.

2 Related Works

2.1 Proposed Framework

We have built a digital duplicate for a robot architecture. It is divided into two components: virtual and real parts. The virtual element is a software built on the Unity platform. For the real part, we use two servomotors with built-in encoder to represent the two joints of the robot. These two motors are controlled via a PID controller. In addition, we also use Jetson Nano with integrated ROS as a central processor. The virtual element and the real part are connected to each other through the TCP socket protocol suite.

Jetson Nano is a small but very powerful computer that allows to run multiple neural networks in parallel for applications such as image classification, object detection, segmentation, and speech processing. Being in one platform, it is easy to use and consumes less than 5 W. The Jetson Nano also delivers 472 GFLOPS to run modern AI algorithms quickly, with a 64-bit ARM quad-core CPU, an onboard 128-core NVIDIA GPU, as well as 4 GB of LPDDR4 memory. It is possible to run multiple neural networks in parallel and handle several high-resolution sensors simultaneously. Here, users can control from the virtual model to real model and vice versa. First, we will present the control process from virtual to real model. When the user changes the robot's joint position via the Unity controller, the matching angle data will be sent through the central processor. The central processor will calculate the forward kinematics to give the position of the end of the manipulator. Next, the matching angles will be controlled by the Virtual robot model, and the data is also given to the user interface to display the joint angle values and the coordinates of the robot's manipulator end point. After that, the data will be sent to the Physical robot to control the real model through the TCP socket protocol suite.

In this study, we take two servomotors representing two joints of the robot. The data will be sent to the central processor and then sent to the controller to control the servomotor. Then the controller will take the position value of the servomotor and send it to the central processor. The central processor will process the data through the aforementioned formula and calculate the error between the matching angles of the real and imaginary model. The data will then be stored on Cloud and sent back to Unity which calculates the delay and then saves the data including the error, the position of the real and virtual model's joints, and the delay to local storage. For the control process from real to virtual object, it will reverse the above process and start from the controller at ROS. In this process, the Unity side controller will be ignored

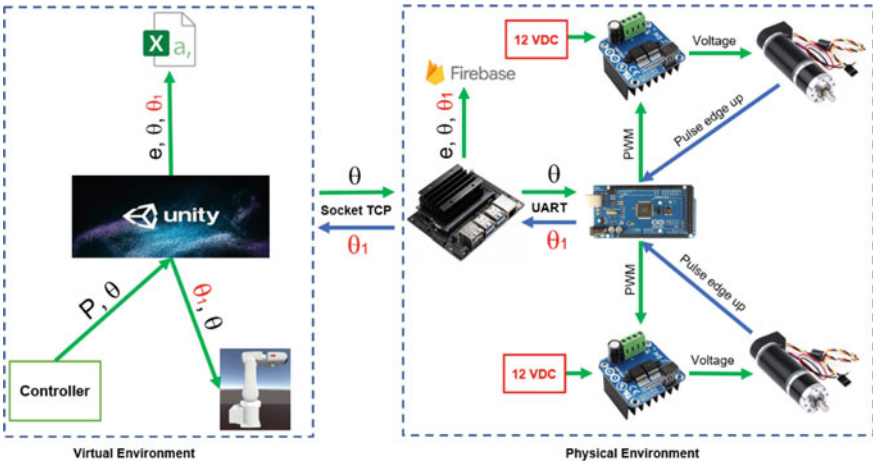

Fig. 1 System overview. The system consists of two parts: real and virtual models. On the left is a virtual element system built on the Unity platform. On the right is the real part system

and the robot's matching angle values will be fed directly into the Virtual robot model through Unity's central processor. Figure 1 is the architecture of the system.

2.2 Virtual Environment

We use the Unity platform to build and develop virtual environments. Unity is software that specializes in games, so building a virtual environment is almost easy. In addition, Unity also supports virtual reality and augmented reality for future development of the system. To build a virtual environment on Unity, we used available tools and some other graphics software like Blender. After building the objects of the virtual environment, we started to set up features such as data communication, kinematics, and rotation controller for the robot. In order to build a robot model and put it into a virtual environment, we first downloaded the details of the ABB IRB 120 robot model from the ABB homepage. Second, we edit and stitch the parts together into a robot ABB IRB 120. Third, we set the coordinate axes for each joint of the robot model. Fourth, we set the parameters of the model. Fifth, we exported the model as a URDF file and stored it in the directory where the project is located. Finally, we bring that model into the Unity virtual environment.

In the virtual environment with the Virtual robot model, the central processor will process the data, store the data in local memory, and transmit the data to the real model, meanwhile the controller helps the user to change the angles. This virtual environment allows the data visualization, monitoring, and control. Figure 2 shows the virtual environment built.

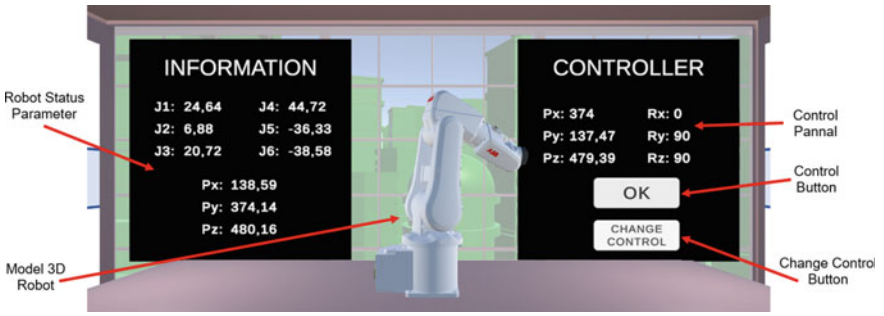

Fig. 2 Virtual environment in Unity includes robot model, robot status panel, and control panel

3 Approach: Digital Twin of Joint Angle of Robot Arm

3.1 Compare Inverse Kinematics Between the Construction Algorithm and Robot Studio

After building the inverse kinematics algorithm, we compare the inverse kinematics with Unity, MATLAB, and Robot Studio. We found that the coordinates of Unity, the algorithm we built, and Robot Studio were interchanged. The joints values have very low errors. These errors are due to the rounding process in the algorithm's calculation. The results showed that our inverse kinematic calculation is valid within very acceptable limits of error. Table 1 is the test value obtained after testing.

3.2 Build a PID Controller

A PID controller is built for the purpose of controlling the motor rotation angle. Planetary GP36 Planetary Reducer DC Servomotor with 1:27 deceleration ratio with 145 rpm integrated Optical Encoder 500 CPR (count per round) and two channels A–B has been used. From here, we get the formula to convert between pulse count to angle with angle being the current angle and p being the count of pulses, c is the number of pulses of the rising or falling edge when the motor is turn 1 revolution, and r is rate of motor reducer:

$$\alpha(x) = \frac{p}{\mathrm{c} \times \mathrm{r}} \times 360 \tag{1}$$

$$= \frac{p}{500 \times 27} \times 360 = \frac{p}{37.5} \tag{2}$$

The PID controller for the motor includes three parameters: K_p; K_i; and K_d. The above parameters are determined by the method of manual adjustment through

Table 1 Evaluation of inverse kinematics

No	Manipulator end point coordinates	Rotation angle (°)	Joint 1	Joint 2	Joint 3	Joint 4	Joint 5	Joint 6	Software
1	X: 374	R_X: 0	24.48	6.8	20.96	44.34	−36.35	−38.21	Robot Studio
	Y: 137.47	R_Y: 90	24.47	6.8	20.96	44.34	−36.35	−38.21	Unity
	Z: 479.39	R_Z: 90	24.48	6.8	20.96	44.34	−36.35	−38.21	MATLAB
2	X: 374	R_X: 0	−38.4	17.87	7.78	−61.37	−45.05	52.3	Robot Studio
	Y: −239.4	R_Y: 90	−38.4	17.87	7.78	−61.37	−45.05	52.3	Unity
	Z: 479.39	R_Z: 90	−38.4	17.87	7.78	−61.37	−45.05	52.3	MATLAB
3	X: 420.12	R_X: 0	−22.93	19.01	−26.64	72.59	24.1	−71.04	Robot Studio
	Y: −147.3	R_Y: 90	−22.93	19.01	−26.64	72.59	24.1	−71.04	Unity
	Z: 654.72	R_Z: 90	−22.93	19.01	−26.64	72.59	24.1	−71.04	MATLAB
4	X: 420.12	R_X: 0	25.41	20.95	−29.2	−73.21	26.63	71.34	Robot Studio
	Y: 165.37	R_Y: 90	25.41	20.95	−29.2	−73.21	26.63	71.34	Unity
	Z: 654.72	R_Z: 90	25.41	20.95	−29.2	−73.21	26.63	71.34	MATLAB
5	X: 535.17	R_X: 0	−14	38.4	−28.05	−54.23	−17.35	52.96	Robot Studio
	Y: −115.5	R_Y: 90	−14	38.4	−28.05	−54.23	−17.35	52.96	Unity
	Z: 516.22	R_Z: 90	−14	38.4	−28.05	−54.23	−17.35	52.96	MATLAB
6	X: 389.93	R_X: 0	26.49	22.06	−44.05	−53.08	33.91	47.84	Robot Studio
	Y: 158.43	R_Y: 90	26.49	22.06	−44.05	−53.08	33.91	47.84	Unity
	Z: 718.23	R_Z: 90	26.49	22.06	−44.05	−53.08	33.91	47.84	MATLAB
7	X: 454.39	R_X: 0	−24.88	25.73	−23.7	−85.64	−24.95	85.19	Robot Studio
	Y: −177.3	R_Y: 90	−24.88	25.73	−23.7	−85.64	−24.95	85.19	Unity
	Z: 592.51	R_Z: 90	−24.88	25.73	−23.7	−85.64	−24.95	85.19	MATLAB

experiment, respectively, $K_p = 0.01$; $K_i = 0.002$; and $K_d = 0.001$. The built-in PID controller is used to control the rotation position of the motor with the feedback signal being the number of pulses of the encoder. Through the PID algorithm, it will determine the voltage to be supplied to the motor (the desired voltage value). U(V) is the value of voltage to be supplied to the motor is shown by the formula:

$$U = K_p \times e + K_i \times \left(e_{\text{pre}} + e \times \left(t - t_{\text{pre}}\right)\right) + \frac{K_d \times \left(e - e_{\text{pre}}\right)}{t - t_{\text{pre}}} \tag{3}$$

In which, K_p, K_i, K_d, respectively, are the PID coefficients declared above. t is the current sampling time, and t_{pre} is the immediate previous sampling time. t and t_{pre} have units of seconds (s). e is the error between the desired motor angle (p) and the current motor angle (p_{cur}). e_{pre} is the number of times before.

$$e = p - p_{\text{cur}} \tag{4}$$

Since the power supply for the motor driver (U_{Pow}) is 12 V source and the microcontroller is 8-bit, the formula for converting voltage to control pulse (Pwm) is

$$\text{Pwm} = \frac{U \times 255}{U_{\text{Pow}}} = \frac{U \times 255}{12} = U \times 21.25 \tag{5}$$

3.3 Two-Way Data Transfer Between Real and Virtual Models

Here, we install ROS on a Jetson Nano and set up nodes and topics to transmit and receive data between Arduino and ROS and between ROS and Unity. ROS is an intermediary that supports sending and receiving data between Arduino and Unity. We use TCP socket protocol for two-way data transmission between ROS and Unity and UART for two-way data transmission between ROS and Arduino.

A TCP end point running as a ROS node facilitates message passing to and from Unity and ROS. The message being passed between Unity and ROS is expected to be serialized as ROS would internally serialize them.

4 Experiences and Results

4.1 Compare the Forward Kinematics Between the Construction Algorithm and Robot Studio

After building the forward kinematics algorithm, we compare the forward kinematics with Unity and Robot Studio. We found that the coordinates of Unity, the algorithm we built, and Robot Studio were interchanged. Here, Unity's X-axis is the Y-axis of our algorithm and Robot Studio's X-axis. Unity's Y-axis is the Z-axis of the algorithm we built and Robot Studio's Z-axis. Unity's Z-axis is the X-axis of the algorithm we built and the Y-axis of Robot Studio. The obtained values have very low errors. These errors are due to the rounding process in the algorithm's calculation. That proved our algorithm can accept. Table 2 is the test value obtained after testing.

4.2 Error and Latency

The error between the virtual model and the real model is calculated by the central processing unit of Physical robot. We take the value of the virtual model matching angles minus the value of the real model matching angles. Here, E_m is the value of the joint virtual model and E_n is the value of the joint physical model with m and n are from 1 to the last retrieved data stored at the system. From there, we calculate the $\Delta E(t)$ of the system using the formula:

$$\Delta \mathbb{E}(t) = \mathbb{E}_m - \mathbb{E}_n \tag{6}$$

To calculate the delay, we took the time of data sent from Virtual robot to Physical robot set as t_1 and time of data sent from Physical robot to Virtual robot set as t_2. From there, we calculate the $\Delta t(s)$ (latency) of the system using the formula:

$$\Delta t(s) = t_2 - t_1 \tag{7}$$

4.3 Data Storage

The data is stored locally, in the Firebase Cloud and Google sheet. Cloud Firestore's data transmission and reception rate is 10 Hz, and a limit of 50,000 data updates and edits in one day for the free version. We also tried storing data on Google Sheets, and it also receives and sends data at 10 Hz and is limited to 100 fetches and updates per minute. The data is divided into three parts including the collection, the directory and the file. The collection we named data contains folders inside. The name of each

Table 2 Evaluation of forward kinematics

No	Joint 1–3	Joint 4–6	P_X	P_Y	P_Z	Software
1	Joint1: 0	Joint4: 0	374	374	374	Robot Studio
	Joint2: 0	Joint5: 0	0	630	0	Unity
	Joint3: 0	Joint6: 0	630	0	630	MATLAB
2	Joint1: 10	Joint4: 100	413.94	135.34	414	Robot Studio
	Joint2: 30	Joint5: 60	135.37	413.94	135	Unity
	Joint3: 15	Joint6: 0	341.91	341.98	341	MATLAB
3	Joint1: 10.46	Joint4: 5.59	257.61	50.61	258	Robot Studio
	Joint2: −18.76	Joint5: 25.7	135.37	257.64	51	Unity
	Joint3: 6.02	Joint6: 2.86	341.91	665.05	665	MATLAB
4	Joint1: 20	Joint4: 35	315.36	143.03	315	Robot Studio
	Joint2: 25	Joint5: 40	143.01	315.35	143	Unity
	Joint3: 30	Joint6: 45	260.52	260.54	260	MATLAB
5	Joint1: 21	Joint4: 15	373.27	146.74	373	Robot Studio
	Joint2: 30	Joint5: 10	146.74	373.25	147	Unity
	Joint3: 24	Joint6: 18	256.2	256.19	255	MATLAB
6	Joint1: 26	Joint4: 18	321.37	177.03	321	Robot Studio
	Joint2: 24	Joint5: 55	176.99	321.39	177	Unity
	Joint3: 20	Joint6: 60	308.18	307.44	307	MATLAB
7	Joint1: 71	Joint4: 30	5.24	124.13	5	Robot Studio
	Joint2: 58	Joint5: 100	124.12	525	124	Unity
	Joint3: 56	Joint6: 90	165.12	165.11	165	MATLAB
8	Joint1: −131.53	Joint4: −63.18	−270.96	−255.33	−271	Robot Studio
	Joint2: 5.04	Joint5: 31.64	−255.13	−271.17	−255	Unity
	Joint3: 22.36	Joint6: −70.25	438.77	438.036	438	MATLAB
9	Joint1: −29.44	Joint4: −90.96	−130.88	21.15	−131	Robot Studio
	Joint2: −47.9	Joint5: 39.75	21.01	−131.12	21	Unity
	Joint3: −18.86	Joint6: 76.07	827.31	827.25	827	MATLAB
10	Joint1: 92.25	Joint4: −37.11	−13.8	−136.52	−14	Robot Studio
	Joint2: −3.69	Joint5: −26.07	−134.91	−13.74	−136	Unity
	Joint3: −89.73	Joint6: 70.26	919.8	919.44	919	MATLAB

folder is the time that the data inside that folder is stored in the Cloud. And the file is inside the directory. The data including the time, the matching position of the virtual model, the rotational position of the servomotor and the error between the matching position of the virtual model and the position of the virtual model, and rotation position of the servomotor at that time was collected.

We also used one more local data storage. With this local data storage, the frequency is around 165 Hz and is limited to memory on local storage only. This

is not a concern because local storage can expand memory and it also takes a long time to fill this local storage. Where the STT column is the ordinal number of the data sorted in ascending order based on the time that the data was stored, the Time column is the column that stores the data about the time that the data was stored. The Error column is the column used to represent the error between the matching position of the virtual model and the real one. The Joints Unity column is the column representing the joint position of the virtual model, and the last column is the Joints Servo column, which represents the rotation position of the servomotor.

4.4 Results

The analyzed data showed that the system takes about 2 s for the system to stabilize after booting. Here, the sampling frequency is about 165 Hz. They are shown in Fig. 3. Here, the vertical axis is the value of the number of samples taken in one second and the horizontal axis is the time the sample is taken. The system latency is about 30 ms with an error of $\pm$ 2 degrees. They are shown in Fig. 4. Figure 4 has the vertical axis being the error between the matching angle of the virtual and real model (degrees) and the horizontal axis being the time (ms).

Here, we have simulated servomotor power failure. Figure 5 shows the difference of the data when the fault occurs and when the failure occurs. When there are 3000 data stored, we have disconnected the servomotor and powered up again when 3150 data is stored, and we have also disconnected the servomotor when there is 4665 data until it stops completely system. Error is error of joint between real and virtual when the system is operating normally.

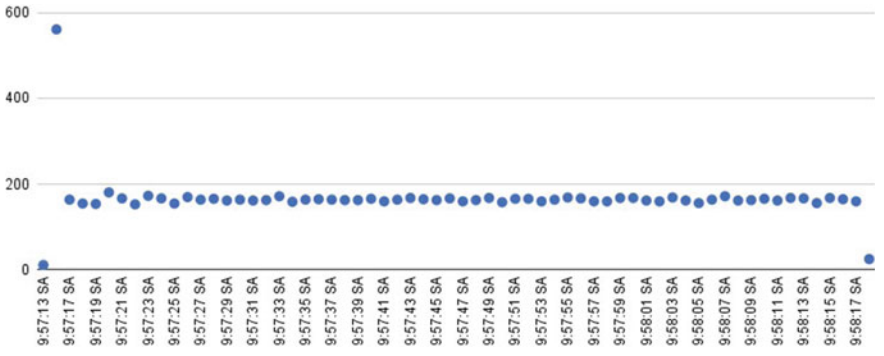

Fig. 3 Number of samples received in 1 s

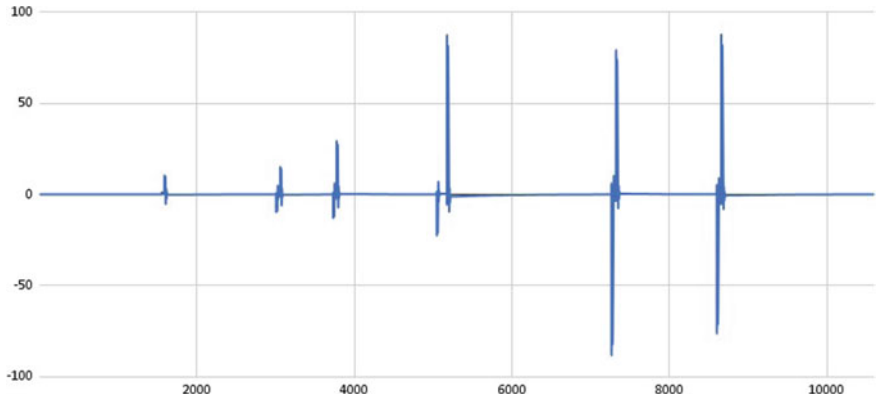

Fig. 4 Error between real and virtual model

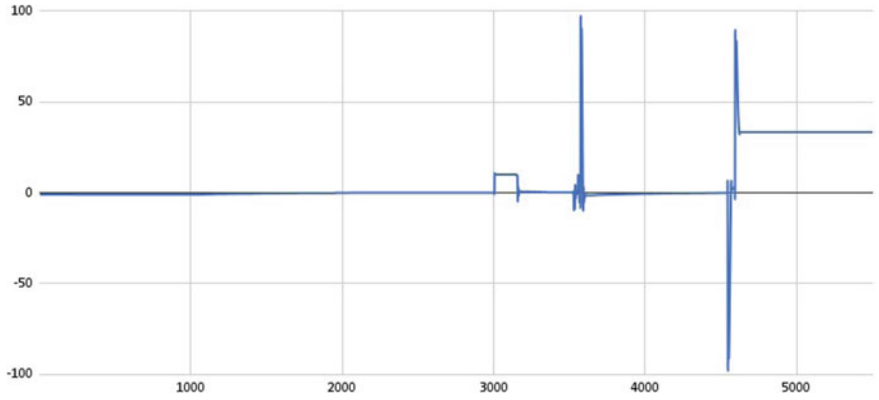

Fig. 5 Error between real and virtual model when there is a problem

5 Conclusion

In this paper, we have successfully built a digital twin model of ABB IRB 120 robot. The digital twin model has developed communication between real and virtual through the TCP socket protocol suite. We also calculated the forward kinematics of the robot and compared it with the forward kinematics of Robot Studio. In addition, we also build a PID controller for the engine and store the data on Cloud and local storage for later machine learning development.

The system operates stably with a maximum frequency of 165 Hz when not storing data and 10 Hz when putting data in the cloud. Calculation of kinematics gives results with very small error due to rounding of values in the calculation. The PID controller is stable and has been able to control the position of the motor as desired. Data is

transmitted bidirectionally with very small errors due to rounding during conversion in calculations.

In the future, we will increase the frequency of sending data to the cloud and use machine learning to analyze the collected data to help monitor and evaluate the system. We will then make digital copies of typical mobile robots like manipulator platform and rehabilitation robots that we plan to do in the near future.

Appendix

Kinematics DH

We use ABB IRB 120 robot model as a model to calculate forward and experimental kinematics. We have set representation of the coordinate positions and orientation based on the joints of the robot model as shown in Fig. 6. Figure 6 is a coordinate axis location diagram with the red axis being the X-axis, the orange axis being the Y-axis, and the blue axis is the Z-axis.

The DH parameters of the ABB IRB 120 for the specified joint frames in Fig. 6 are presented in Table 3. Here, θ_i is the relative rotation of the stitches, a_i is the length, α_i is the twist angle of the stitch, and d_i is the distance between the stitches.

According to the manufacturer's specifications, the limits of joints are shown in Table 4.

Each link can bethink as a coordinate transformation from the previous coordinate system to the next coordinate system. That transformation is described as a product of translations along and rotations about X- and Z-axes. They are expressed in formula 33:

$$
{}^{n-1}T_n = \begin{bmatrix} \cos\theta_n & -\sin\theta_n \cos\alpha_n & \sin\theta_n \sin\alpha_n & a_n \cos\theta_n \\ \sin\theta_n & \cos\theta_n \cos\alpha_n & -\cos\theta_n \sin\alpha_n & a_n \sin\theta_n \\ 0 & \sin\alpha_n & \cos\alpha_n & d_n \\ 0 & 0 & 0 & 1 \end{bmatrix} \tag{8}
$$

Table 3 DH parameters of robot ABB IRB 120

Joints	θ_i (°)	a_i (mm)	α_i (°)	d_i (mm)
1	$\theta_1(+90)$	0	−90	290
2	$\theta_2(-90)$	270	0	0
3	θ_3	70	−90	302
4	θ_4	0	90	0
5	θ_5	0	−90	0
6	θ_6	0	0	72

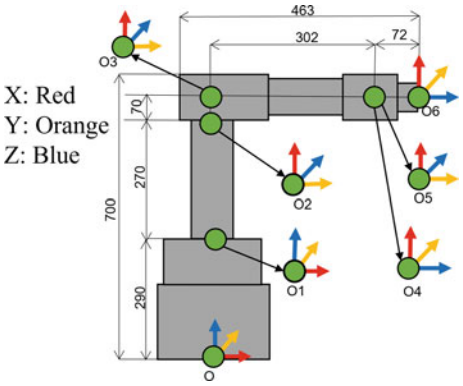

Fig. 6 Schematic and frames assignment of ABB IRB 120. ${}^{0}\mathrm{P} = [{}^{0}\mathrm{R}_1.{}^{1}\mathrm{R}_2.{}^{2}\mathrm{R}_3.{}^{3}\mathrm{R}_4.{}^{4}\mathrm{R}_5.{}^{5}\mathrm{R}_6].{}^{6}\mathrm{P} = {}^{0}\mathrm{R}_6.{}^{6}\mathrm{P}$ is the direction and coordinate location

Table 4 Table ranges of motion in every axes

Joints	Lower limit [deg]	Upper limit [deg]
1	−165	165
2	−110	110
3	−110	70
4	−160	160
5	−120	120
6	−400	400

Forward Kinematics

The purpose of this part is to find the absolute position and orientation of each frame (which is attached to each joint/servo) in reference to the global coordinate system, which is the very first frame attached to the shoulder. Apply Table 1 attributes to Eq. 33, we get transformation for each link.

Now that we have each transformation, we can calculate the position and orientation of each frame in reference to the "global coordinate system."

$$ {}^{0}T_6 = {}^{0}\,T_1^1 T_2^2 T_3^3 T_4^4 T_5^5 T_6 \tag{9} $$

$$ = \begin{bmatrix} r_{11} & r_{12} & r_{13} & p_x \\ r_{21} & r_{22} & r_{23} & p_y \\ r_{31} & r_{32} & r_{33} & p_z \\ 0 & 0 & 0 & 1 \end{bmatrix} \tag{10} $$

In matrix 35, the parameters r form the rotation matrix of the robot and the parameter P is the coordinate position of the end point of the manipulator. From that, we can derive the formula for determining the position of the manipulator's end point coordinates as follows:

$$p_x = d_5 c_1 s_{234} + d_4 s_1 - d_6 c_1 c_{234} + a_2 c_1 c_2 + d_6 c_5 s_1 + a_3 c_1 c_2 c_3 - a_3 c_1 s_2 s_3$$

$$p_y = d_5 s_1 s_{234} - d_4 c_1 - d_6 s_1 c_{234} + a_2 c_2 s_1 - d_6 c_5 c_1 + a_3 c_2 c_3 s_1 - a_3 s_1 s_2 s_3$$

$$p_z = d_1 - d_6 s_{234} s_5 + a_3 s_{23} + a_2 s_2 - d_5 c_{234}$$

Inverse Kinematics

A very large number of joints make it difficult to solve the trigonometric equation, we can divide 6 joints into two groups of joints: Group one is from joint 1 to joint 3, and group two is from joint 4 to joint 6. For joint 1 to joint 3: P_c point coordinates are shown in Fig. 7. Parameters d_1, a_2, a_3, and d_4 are taken in Table 3. Change to new end point $P_c = [P_{cx}; P_{cy}; P_{cz}]$ with the matrix a being the cosine of the three Euler angles:

$$P_c = P[x; y; z] - d_6 a[a_x; a_y; a_z] \tag{11}$$

Perform inverse matrix multiplication:

$$({}^0T_1)^{-1} \times \begin{bmatrix} r_{11} & r_{12} & r_{13} & p_x \\ r_{21} & r_{22} & r_{23} & p_y \\ r_{31} & r_{32} & r_{33} & p_z \\ 0 & 0 & 0 & 1 \end{bmatrix} = ({}^1T_2)({}^2T_3)({}^3T_4) \tag{12}$$

From 2, we have the formula

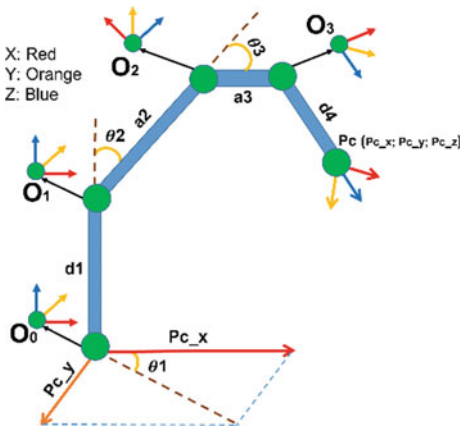

Fig. 7 Point coordinates P_c $(Pc_x; Pc_y; Pc_z)$

$$P_{cy}\cos(\theta_1) - P_{cx}\sin(\theta_1) = 0 \tag{13}$$

$$=> \theta_1 = a\tan 2\left(P_{cy}, P_{cx}\right) \tag{14}$$

$$2a_2a_3\cos(\theta_3) - 2a_2d_4\sin(\theta_3) = n_x^2 + n_y^2 - \left(a_2^2 + a_3^2 + d_4^2\right) \tag{15}$$

After simplifying, we get

$$\theta_3 = a\tan 2\left(\pm\sqrt{1 - (\frac{D}{\rho})^2}, \frac{D}{\rho}\right) - a\tan 2(d_4, a_3) \tag{16}$$

with

$$D = n_x^2 + n_y^2 - \left(a_2^2 + a_3^2 + d_4^2\right) \tag{17}$$

$$\rho = 2\sqrt{(a_2a_3)^2(a_2d_4)^2} \tag{18}$$

$$n_x = \frac{P_{cx}}{cos(\theta_1)} \tag{19}$$

$$n_y = P_{cz} - d_1 \tag{20}$$

Continuing to multiply the inverse matrix, we have

$$({}^1T_2)^{-1}({}^0T_1)^{-1} \times \begin{bmatrix} r_{11} & r_{12} & r_{13} & p_x \\ r_{21} & r_{22} & r_{23} & p_y \\ r_{31} & r_{32} & r_{33} & p_z \\ 0 & 0 & 0 & 1 \end{bmatrix} = ({}^2T_3)({}^3T_4) \tag{21}$$

We have the equation

$$d_4\cos(\theta_3) + a_3\sin(\theta_3) = \cos(\theta_2)(d_1 - P_{cz}) + P_{cy}\sin(\theta_1) + \sin(\theta_2)P_{cx}\cos(\theta_1)$$

After simplifying, we get

$$\theta_2 = \varphi - a\tan 2\left(\pm\sqrt{1 - (\frac{M}{\sigma})^2}, \frac{M}{\sigma}\right) \tag{22}$$

with

$$M = d_4\cos(\theta_3) + a_3\sin(\theta_3) \tag{23}$$

$$\sigma = \sqrt{p_x^2 + p_y^2} \tag{24}$$

$$\varphi = a\tan 2\big(p_y, p_x\big) \tag{25}$$

$$p_x = P_{cx}\cos(\theta_1) + P_{cy}\sin(\theta_1) \tag{26}$$

$$p_y = d_1 - P_{cz} \tag{27}$$

For joint 4 to joint 6: We can calculate the transformation matrix from joint 4 to joint 6

$${}^3T_6 = {}^3\ T_4^4 T_5^5 T_6 = \begin{bmatrix} c_4c_5c_6 - s_4s_6 & -c_4c_5c_6 - s_4c_6 & c_4s_5 & c_4s_5d_6 \\ s_4s_5c_6 + c_4s_6 & -s_4s_5s_6 + c_4c_6 & s_4s_5 & s_4s_5d_6 \\ -s_5c_6 & s_5s_6 & c_5 & c_5d_6 \\ 0 & 0 & 0 & 1 \end{bmatrix}$$

We get rotated matrix

$${}^3R_6 = \begin{bmatrix} c_4c_5c_6 - s_4s_6 & -c_4c_5c_6 - s_4c_6 & c_4s_5 \\ s_4s_5c_6 + c_4s_6 & -s_4s_5s_6 + c_4c_6 & s_4s_5 \\ -s_5c_6 & s_5s_6 & c_5 \end{bmatrix} \tag{28}$$

but

$${}^0R_6 = {}^0\ R_3^3 R_6 \tag{29}$$

or

$${}^3R_6 = ({}^0R_3)^T({}^0R_6) = \begin{bmatrix} r_{11} & r_{12} & r_{13} \\ r_{21} & r_{22} & r_{23} \\ r_{31} & r_{32} & r_{33} \end{bmatrix} \tag{30}$$

From matrixes 18 and 20, we have:

$$\cos(\theta_5) = r_{33} \tag{31}$$

$$\sin(\theta_5) = \pm\sqrt{1 - r_{33}^2} \tag{32}$$

$$=> \theta_5 = a\tan 2\left(\pm\sqrt{1 - r_{33}^2}, r_{33}\right) \tag{33}$$

$$\frac{\sin(\theta_5)\sin(\theta_6)}{-\sin(\theta_5)\cos(\theta_6)} = \frac{r_{32}}{r_{31}} => \theta_6 = a\tan\left(\frac{-r_{32}}{r_{31}}\right) \tag{34}$$

$$\frac{\sin(\theta_5)\sin(\theta_4)}{\sin(\theta_5)\cos(\theta_4)} = \frac{r_{23}}{r_{13}} => \theta_4 = a\tan\left(\frac{r_{23}}{r_{13}}\right) \tag{35}$$

From Eqs. (14), (16), (22), (33), (34), (35), we have obtained the formula to calculate the joint angle values to complete the inverse kinematics problem for the ABB IRB 120 robot. From here, we will build a robot controller based on this algorithm.

References

1. Wu, Y., Zhang, K., & Zhang, Y. (2021). Digital twin networks: A survey. *IEEE Internet of Things Journal, 8*(18), 13789–13804.
2. Lim, K. Y. H., Zheng, P., & Chen, C.-H. (2020). A state-of-the-art survey of digital twin: Techniques, engineering product lifecycle management and business innovation perspectives. *Journal of Intelligent Manufacturing, 31*, 1313–1337.
3. Russell, S., & Norvig, P. (2010). *Artificial intelligence: A modern approach* (3rd edn.). Prentice Hall.
4. Bishop, C. M. (2006). *Pattern recognition and machine learning (information science and statistics)*. Springer-Verlag.
5. Goodfellow, I., Bengio, Y., Courville, A. (2016). *Deep learning*. MIT Press. http://www.deeplearningbook.org
6. Le, T. D., Huynh, D. T., & Pham, H. V. (2018). Efficient human-robot interaction using deep learning with mask R-CNN: Detection, recognition, tracking and segmentation. In *2018 15th International conference on control, automation, robotics and vision (ICARCV)* (pp. 162–167).
7. Le, T. D., & Pham, H. V. 2020. *Intelligent data analysis* (Chap. 5, pp. 85–114). Wiley. [Online]. Available: https://onlinelibrary.wiley.com/doi/abs/10.1002/9781119544487.ch5
8. Siciliano, B., Sciavicco, L., Villani, L., & Oriolo, G. (2010). *Robotics: Modelling, planning and control*. Springer Publishing Company.
9. Siciliano, B., & Khatib, O. (2007). *Springer handbook of robotics*. Springer-Verlag.
10. Nguyen, H. V., Le, T. D., Huynh, D. D., Nauth, P.: Forward kinematics of a human-arm system and inverse kinematics using vector calculus. In *2016 14th International conference on control, automation, robotics and vision (ICARCV)* (pp. 1–6).
11. Than, L., & An, L. (2020). Manipulation-based skills for anthropomorphic human-arm system based on integrated anfis and vector calculus. *bioRxiv*. [Online]. Available: https://www.biorxiv.org/content/early/2020/02/10/2020.02.10.941344
12. Quigley, M., Conley, K., Gerkey, B. P., Faust, J., Foote, T., Leibs, J., Wheeler, R., & Ng, A. Y. (2009). Ros: An open-source robot operating system. In *ICRA workshop on open source software*.
13. Palmieri, L., & Arras, K. O. (2015). Distance metric learning for rrt-based motion planning with constant-time inference. In *2015 IEEE International conference on robotics and automation (ICRA)* (pp. 637–643).
14. Palmieri, L., & Arras, K. O. (2014). A novel rrt extend function for efficient and smooth mobile robot motion planning. In *2014 IEEE/RSJ International conference on intelligent robots and systems* (pp. 205–211).
15. Le, T. D., Bui, D. T., & Pham, V. H. (2018). Encoded communication based on sonar and ultrasonic sensor in motion planning. *IEEE Sensors, 2018*, 1–4.

16. Le, T., & Le, T. D. (2018). Search-based planning and replanning in robotics and autonomous systems. in R. Róka (Ed.), *Advanced path planning for mobile entities.* IntechOpen, 2018, Chap. 4. [Online]. Available: https://doi.org/10.5772/intechopen.71663
17. Le, T., Hung, B. T., Van Huy, P. (2021) *Search-Based Planning and Reinforcement Learning for Autonomous Systems and Robotics* (pp. 481–501). Springer International Publishing. [Online]. Available: https://doi.org/10.1007/978-3-030-77939-9_14
18. Le, T. D., Le, A. T., Nguyen, D. T. (2017). Model-based q-learning for humanoid robots. In *2017 18th International conference on advanced robotics (ICAR)* (pp. 608–613).
19. Garg, G., Kuts, V., & Anbarjafari, G. (2021). Digital twin for fanuc robots: Industrial robot programming and simulation using virtual reality. *Sustainability, 13*(18). [Online]. Available: https://www.mdpi.com/2071-1050/13/18/10336
20. Mengacci, R., Zambella, G., Grioli, G., Caporale, D., Catalano, M. G., & Bicchi, A. (2021). An open-source Ros-gazebo toolbox for simulating robots with compliant actuators. *Frontiers in Robotics and AI, 8.* [Online]. Available: https://www.frontiersin.org/article/10.3389/frobt.2021.713083
21. Dröder, K., Bobka, P., Germann, T., Gabriel, F., & Dietrich, F. (2018). A machine learning-enhanced digital twin approach for human-robotcollaboration. *Procedia CIRP, 76*, 187–192.
22. Wang, X., Liang, C. -J., Menassa, C., & Kamat, V. (2020) Real-time process-level digital twin for collaborative human-robot construction work. In F. H. T. K. Osumi Hisashi (Ed.), *Proceedings of the 37th International symposium on automation and robotics in construction (ISARC)*, (pp. 1528–1535). International Association for Automation and Robotics in Construction (IAARC).

Optimal Motion for Humanoid Robotic Arms Using Kinect Camera

Saif F. Abulhail and Mohammed Z. Al-Faiz

Abstract An optimal motion tracking for humanoid robotic arms (HRAs) is proposed based on Kinect sensor. HRA models are designed using inverse kinematics (IK) with aid of Denavit–Hartenberg (D-H) method for both arms. Kinect camera is used to transfer the desired position and feed the point to HRAs simulation. Next, IK is implemented to obtain the required angles for HRAs. Then, apply two optimization methods: black hole (BH) and most valuable player algorithm (MVPA) in order to minimize the computation time (CT) and root mean square error (RMSE) between the desired and actual position. After that, forward kinematics (FK) is applied to find the actual position of the obtained angles of HRAs. Finally, the simulation of graphical user interface (GUI) is designed to show the optimal motion characteristic of HRA models. Calculation and simulation results show the efficiency of the optimization methods implementation after they are compared with each other. The simulation results showed that the MVPA method is more accurate than BH method. The RMSE and CT calculated by MVPA are less than those calculated using BH.

Keywords Humanoid robotic arms · Black hole · Most valuable player algorithm · Kinetic camera · Forward kinematics · Inverse kinematics

1 Introduction

For decades, huge endeavors were spent to design and analyze HRAs that mimic the human arms [1]. HRAs are very cooperative and replace a real human worker in many places such as industry, medical and reactors [2]. The advantages of HRAs over other machines are that they are more accurate, flexible, efficient and used for multi-jobs [3, 4]. Consequently, HRAs were transplanted in a real human environment where it was expected to perform at high level [5, 6]. Therefore, an optimization methods were harnessed to make the HRAs perform accurately at high level of efficiency with optimal performance [7].

S. F. Abulhail (✉) · M. Z. Al-Faiz
College of Information Engineering, Al-Nahrain University, Baghdad, Iraq
e-mail: saifabulhail80@gmail.com

T. D. L. Nguyen and J. Lu (eds.), *Machine Learning and Mechanics Based Soft Computing Applications*, Studies in Computational Intelligence 1068,
https://doi.org/10.1007/978-981-19-6450-3_24

Many researches were viewed the influence of using optimization methods for HRAs such as using MVPA in optimal control of single link manipulator [8]. Evolutionary algorithm (EA) was applied to HRAs in order to provide optimal motion with aid of neural controller [9]. 2-norm-based optimal algorithm was implemented for HRAs mobile robot to solve multi-solution for high-redundancy IK problem [10]. A redundancy resolution algorithm was proposed to optimize the parameters of virtual joints by minimizing the cost function [11]. Particle swarm optimization (PSO) was applied to optimize the design parameters and joint velocity [12]. Topology optimization was proposed to reduce weights of the arms [13]. A nonlinear constrained optimization was implemented to encode the required motion for robotic arm [14]. Optimal numerical algorithms were presented to obtain optimal design solution for HRAs [15]. Social spider optimization was implemented to optimize the rotation matrix of IK for HRAs [16]. Generally, the mentioned researches are using optimization methods to accomplish an optimal motion by set a desired point to MATLAB GUI manually and then calculate the IK. In this paper, MVPA and BH methods are proposed to optimize the parameters of IK in order to minimize RMSE and CT. Also, the desired points are passed using Kinect sensor to the MATLAB and then take IK for HRAs with the aid of optimization methods to find the optimal rotation matrix. Consequently, the FK is implemented to obtain the actual position. Finally, the actual position is compared with the desired position to obtain the RMSE, and this operation is repeated till the optimal values are founded. The rest organization of the paper is prepared as follows. In Sect. 2, HRAs model, Kinect camera, BH and MVPA are explained. The GUI simulation results of the optimization method are presented in Sect. 3. In Sect. 4, discussion and conclusion are made on the results which are made to explain in detail the implementation of the Kinect-based optimization methods for HRAs.

2 Materials and Methods

In this section, the methodology of the paper is proposed and represented by the Kinect camera, BH optimization method and MVPA method. In addition, the procedure of the paper is explained in detail at the end of the section.

2.1 Kinetic Sensor (Camera)

Kinect camera device is one of the Microsoft product for Xbox-360 which is used for face and voice recognition as well as identify players by giving 3-D coordinate of the player (object). In this paper, the 3-D depth sensors of the device are used to assign the coordinates for the desired points. Consequently, the 3-D coordinates of the desired points are passed to the MATLAB GUI in order to be tracked by HRAs [17] (Fig. 1).

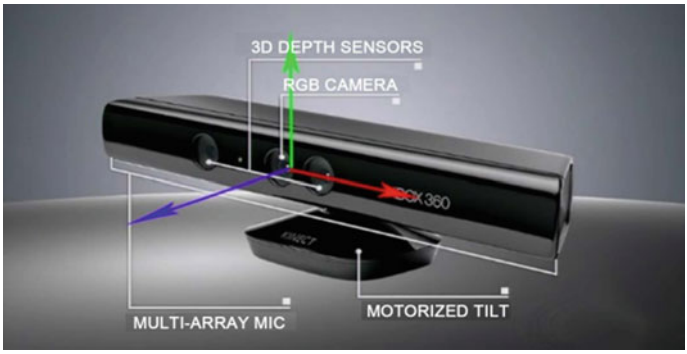

Fig. 1 Kinetic camera [17]

2.2 HRAs Derived Model

In this subsection, the FK and IK of the 5DoF HRAs are explained as in [16]. The IK is derived after Kinect sensor passed the desired points to the MATLAB file to find the joint angles. Consequently, the FK is derived to obtain the actual position of the HRAs to compare it with the desired one using RMSE cost function for the optimization methods. Figure 2 shows the 5DoF HRAs.

2.3 Black Hole Method

The BH is an optimization method that used in data clustering at first. Consequently, the BH is extended to be used for control purposes to optimize the controller and model reference parameters [18]. BH is one of the population which inspired by the black hole phenomenon of an object that has concentrated gravity in space [19]. This gravity swallows the neighborhood objects by pulling them to the center of the black hole and make them disappear from galaxy [20]. BH initials the number of population and assign a cost function that calculates the minimum error for them. A selected star represents the candidate black hole so for each iteration, the best black hole is chosen among the other stars. After the initialization method, the BH begins to absorb the close stars and new stars generated randomly and located in the search. There are some terms that should be explained before going to the next step such as *event horizon* and *Schwarzschild radius* which are the limit of the black hole in the search space and radius of the event horizon respectively. The following equation shows the Schwarzschild radius calculation [19]:

$$R = 2 \times GM/c^2 \tag{1}$$

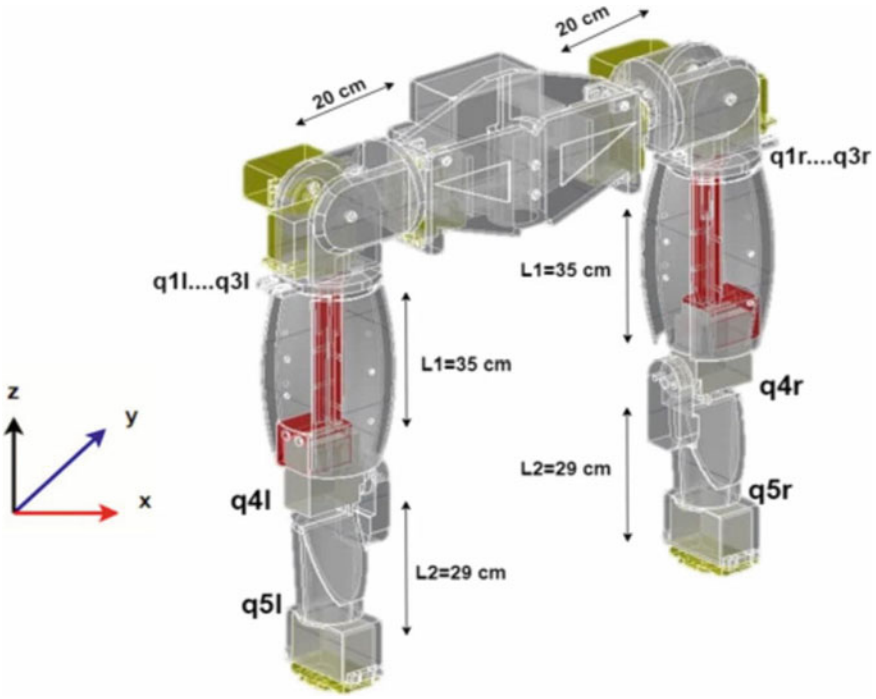

Fig. 2 5-D humanoid robotic arm [16]

where M is the representation of mass of the BH, the speed of light is represented by c, and G is the gravitational constant. The BH method starts by the BH and starts initialization. The BH absorption of stars represented as follows [21]:

$$X_i(t+1) = X_i(t) + \text{rand} \times (X_{\text{BH}} - X_i(t)), i = 1, \cdots, N \tag{2}$$

where $X_i(t+1)$ and $X_i(t)$ are the locations of the ith star at iterations $t+1$ and t, respectively and rand is a random number in the interval [0, 1], N is the number of stars, and X_{BH} is the location of the black hole in the search space. The vent horizon's radius of the BH method is obtained using the following equation [21]:

$$R = \frac{f_{\text{BH}}}{\sum_{i=1}^{N} f_i} \tag{3}$$

where f_i and f_{BH} are the cost values of the BH, N is the number of stars and the ith star. The main benefits of BH method are that it has simple structure; it is easy to implement; and it does not have the tuning issues.

2.4 Most Valuable Player Algorithm

MVPA is another optimization method inspired from sports by play multiple teams together and select the most valuable player from each team. After that, the method sure the most valuable players in an array to select the MVP of these elite players [22]. The principle of the MVPA operation is that the optimization settings are initialized such as the number of population, dimension of the problem, lower bound, upper bound and number of iterations [22]. In this method, the players and teams are presented using the following equations:

$$\text{Team}_i = \begin{bmatrix} S_{1.1} & S_{1.2} & \cdot S_{1,\text{ProblemSize}} \\ S_{2.1} & S_{2.2} & \cdot S_{1,\text{ProblemSize}} \\ \vdots & \vdots & \vdots \\ S_{\text{PlayerSize},1} & S_{\text{PlayerSize},2} & \cdot S_{\text{PlayerSize,ProblemSize}} \end{bmatrix} \tag{4}$$

$$\text{Player}_k = \begin{bmatrix} S_{k,1} & S_{k,2} & . . & S_{k,\text{ProblemSize}} \end{bmatrix} \tag{5}$$

Problem Size is the dimension of the problem, and S refers to the skills. Players Size is the players who are played in the tournament. The following represents the stages of this optimization algorithm [23]:

(a) Initialization; a population number of the player dimension; players are initialized in the search space.

(b) Team formation; the teams are titled as 'nT_1' and 'nT_2' are first and second teams, respectively. Moreover, the 'nP_1' and 'nP_2' are the players of the first and second teams, respectively. These variables are calculated as follows [23]:

$$n_{P1} = \text{ceil} \times \left(\frac{\text{Players Size}}{\text{Teams Size}} \right) \tag{6}$$

$$n_{P2} = n_{P1} + 1 \tag{7}$$

$$n_{T1} = \text{Players Size} - n_{P2} \times \text{Teams Size} \tag{8}$$

$$n_{T2} = \text{Teams Size} - n_{T1} \tag{9}$$

(c) Team competition; the player is competing each other individually to obtain which one is the optimal player with the optimal skills. This competition is computed by the following equation [23]:

$$\begin{aligned} \text{TEAM}_\text{i} = \text{TEAM}_\text{i} + \text{rand}\left(-\text{TEAM}_\text{i} + \text{FranchisePlayer}_\text{i}\right) \\ + 2\text{rand}(-\text{TEAM}_\text{i} + \text{MVP}) \end{aligned} \tag{10}$$

If $\mathrm{TEAM_i}$ is selected to play versus $\mathrm{TEAM_j}$ and $\mathrm{TEAM_i}$ wins, the player's performance is denoted as [23]:

$$\mathrm{TEAM_i} = \mathrm{TEAM_i} + \mathrm{rand}\left(\mathrm{TEAM_i} - \mathrm{FranchisePlayer_j}\right) \tag{11}$$

Otherwise, the player's performance is denoted as [18]:

$$\mathrm{TEAM_i} = \mathrm{TEAM_i} + \mathrm{rand}\left(\mathrm{FranchisePlayer_j} - \mathrm{TEAM_i}\right) \tag{12}$$

(a) Application of greediness; a new solution is selected after the comparison of the population is done. Each selection is made based on a better objective function value.
(b) Application of elitism; the best (elite) players are selected, and the other players are replaced with the best ones.
(c) Remove duplicates; if the best players have been selecting twice, then one of them is dropped.
(d) Termination condition; in this condition, the selection is done by the user himself.

The abovementioned optimization methods are applied with their phases respectively. After the desired positions have been assigned, the points are fed to the IK MATLAB file to obtain the joint angles. Next, the output of the IK MATLAB file becomes as input to MATLAB files for both optimization methods, respectively. Then, the optimal rotation matrix is obtained after certain number of iterations. After that, the parameters are passed to the FK MATLAB file to find the actual points and the RMSE that has used as a cost function. Eventually, the optimal CT, RMSE and the actual point have been found and recorded in tables in the result section. Figure 3 shows the flowchart for BH and MVPA implementation.

For the above flowchart, r_x, r_y and r_z are 3-D coordinates which represent the desired position for the right arm, and the desired position for the left arm is represented by lx, ly and lz. While $\mathrm{Rx_a}$, $\mathrm{Ry_a}$ and $\mathrm{Rz_a}$ represent the actual position for the right arm, and the actual position for the left arm is represented by $\mathrm{Lx_a}$, $\mathrm{Ly_a}$ and $\mathrm{Lz_a}$. The error between the actual and desired positions for the right and left arms is denoted as RRMSE and LRMSE, respectively.

3 Results

The simulation result has shown the desired points that passed by Kinect camera in order to feed them to the GUI. In addition, it shows the effects of using the optimization methods of the HRAs after these points have been passed to MATLAB simulation. Figure 4 shows the desired points after projected on the grid paper used by author with their numbers and 3-D coordinates.

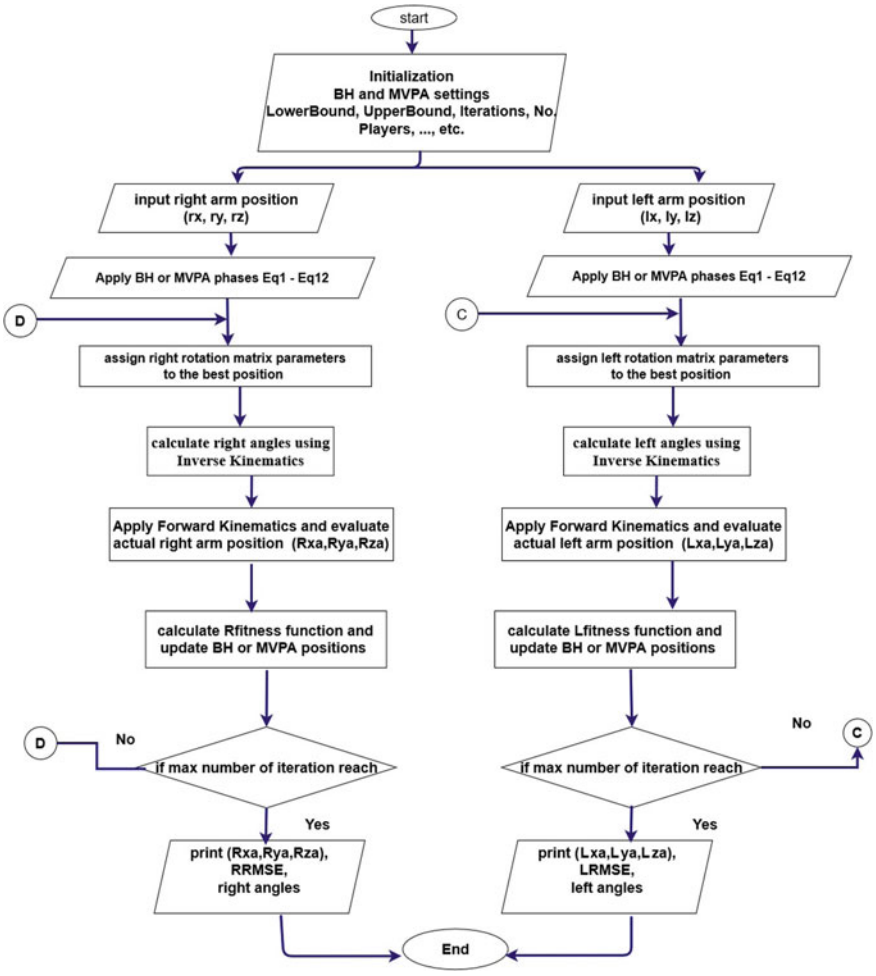

Fig. 3 BH and MVPA implementation

3.1 Right Arm Results

In this subsection, the implementation process is executed on the right arm of HRAs using both BH and MVPA methods. Table 1 shows the calculation result the BH and MVPA method on the right arm with RMSE values and CT for each point.

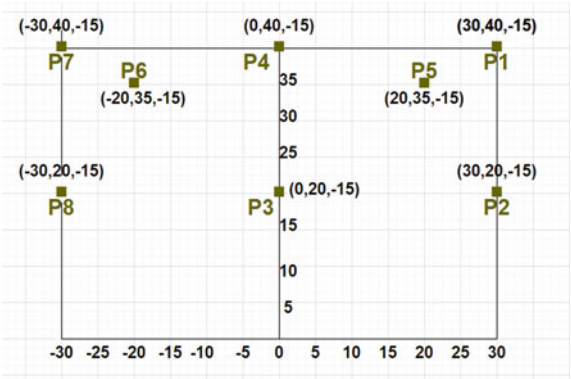

Fig. 4 Grid area with 3-D coordinates of the desired points

3.2 Left Arm Results

After implementing BH and MVPA method on the right arm of HRAs, in this subsection, the process is repeated to executed them on the left arm of HRAs. Table 2 explains results of BH and MVPA methods containing the desired points, RMSE values and CT.

3.3 GUI Results

The following sample figures of the GUI simulation results have shown the effectiveness of BH and MVPA methods, respectively. Figure 5 shows the right and left arms fetching the first point $P_1(30, 40, -15)$ after using BH method.

Figure 6 has shown the effectiveness of the MVPA after it has been applied for the sixth point $P_6(-20, 35, -15)$, and both arms are achieving the point.

4 Discussion and Conclusion

The optimal motion of HRAs has been achieved effectively by using two optimization methods BH and MVPA. Consequently, the desired positions have been transferred by using Kinect sensor instead of manual selection. In addition, the sample figures of MATLAB GUI show the effectiveness of both optimization methods. However, by comparing BH and MVPA numerically from Tables 1 and 2 for the both arms and both optimization methods, it can be seen that the CT value for each point is above $2.1e-04$s. for BH and below $0.7031e-04$s. for MVPA. Also, for the both arms RMSE values are between ($2.001e-07$ to 0.8699) for BH and between (0 to 0.3677) for MVPA method. Moreover, the sample figures taken from different

Table 1 Results of BH and MVPA method on right arm

Point	Desired position (cm)	BHO		MVPA	
		RMSE	CT (s)	RMSE	CT (s)
1	$\begin{bmatrix} 30 \\ 40 \\ -15 \end{bmatrix}$	5.7735e−06	2.7330e−04	0	0.7031e−05
2	$\begin{bmatrix} 30 \\ 20 \\ -15 \end{bmatrix}$	5.7735e−05	2.2150e−04	0	0.7001e−05
3	$\begin{bmatrix} 0 \\ 20 \\ -15 \end{bmatrix}$	5.7735e−06	2.0781e−03	5.0243×10^{-15}	0.4219e−05
4	$\begin{bmatrix} 0 \\ 40 \\ -15 \end{bmatrix}$	2.001e−07	2.0156e−03	3.5597e−09	0.6219e−05
5	$\begin{bmatrix} 20 \\ 35 \\ -15 \end{bmatrix}$	5.7735e−06	2.4156e−03	0	0.5219e−05
6	$\begin{bmatrix} -20 \\ 35 \\ -15 \end{bmatrix}$	5.7735e−04	2.4557e−03	5.7735e−11	0.5219e−05
7	$\begin{bmatrix} -30 \\ 40 \\ -15 \end{bmatrix}$	0.8699	2.1000e−03	0.3677	0.6677e−04
8	$\begin{bmatrix} -30 \\ 20 \\ -15 \end{bmatrix}$	0.5620	2.215e−03	0.1040	0.7001e−04

Table 2 Results of BH and MVPA methods on left arm

Point	Desired position (cm)	BHO		MVPA	
		RMSE	CT (sec)	RMSE	CT (sec)
1	$\begin{bmatrix} 30 \\ 40 \\ -15 \end{bmatrix}$	0.7265	2.1000e−03	0.3506	0.7031e−04
2	$\begin{bmatrix} 30 \\ 20 \\ -15 \end{bmatrix}$	0.5848	2.2150e−03	0.1451	0.7001e−04
3	$\begin{bmatrix} 0 \\ 20 \\ -15 \end{bmatrix}$	5.7735e−06	2.0781e−03	5.0243×10^{-15}	0.4219e−05
4	$\begin{bmatrix} 0 \\ 40 \\ -15 \end{bmatrix}$	2×10^{-7}	2.0156e−03	3.5597e−09	0.6219e−05
5	$\begin{bmatrix} 20 \\ 35 \\ -15 \end{bmatrix}$	5.7735e−04	2.4456e−03	5.7735e−11	0.5219e−05
6	$\begin{bmatrix} -20 \\ 35 \\ -15 \end{bmatrix}$	5.7735e−06	2.2557e−03	0	0.5219e−05
7	$\begin{bmatrix} -30 \\ 40 \\ -15 \end{bmatrix}$	5.7735e−06	2.1000e−04	0	0.7031e−05
8	$\begin{bmatrix} -30 \\ 20 \\ -15 \end{bmatrix}$	5.7735e−05	2.215e−03	0	0.7001e−05

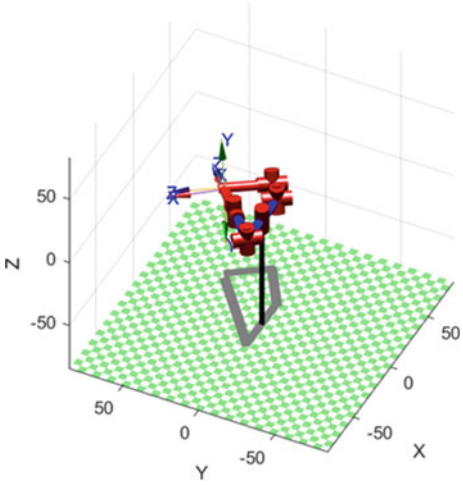

Fig. 5 HRAs at the reaching P_1 after using BH method

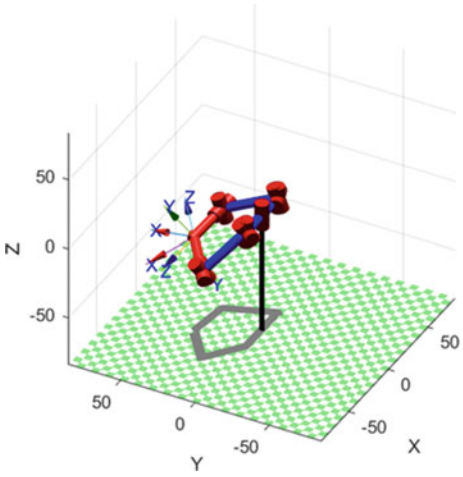

Fig. 6 HRAs at P_6 after using MVPA method

views in GUI show the ability of the HRAs to achieve the desired positions either by using BH or MVPA method which gives the HRAs the optimal performance to accomplish these motions. It can be concluded that the optimal motion of HRAs has been accomplished successively using BH and MVPA. The desired points have been transmitted using Kinect camera with the aid of MATLAB file. The simulation results show the HRAs achieving the points with high accuracy. In addition, table results show that MVPA method has the edge over BH method and proved numerically by the criteria of RMSE, CT and the actual points for both arms of the humanoid robot. Finally, this work can be extended by using a controller design to take over the motion of the HRAs.

References

1. Mick, S., et al. (2019). Reachy a 3D-printed human-like robotic arm as a testbed for human-robot control strategies. *Frontiers in Neurorobotics, 13.*
2. Zanchettin, A., Rocco, P., Bascetta, L., Symeonidis, I., & Peldschus, S. (2011). Kinematic analysis and synthesis of the human arm motion during a manipulation task. In *2011 IEEE International conference on robotics and automation.*
3. Gulletta, G., Erlhagen, W., & Bicho, E. (2020). Human-like arm motion generation: A review. *Robotics, 9*(4), 102.
4. Potkonjak, V. (2020). Is artificial man still far away: Anthropomimetic robots versus robomimetic humans. *Robotics, 9*(3), 57.
5. Schaal, S. (2007). The new robotics—towards human-centered machines. *HFSP Journal, 1*(2), 115–126.
6. Wiese, E., Metta, G., Wykowska, A. (2017). Robots as intentional agents: using neuroscientific methods to make robots appear more social. *Frontiers in Psychology, 8.*
7. Erez, T., & Todorov, E. (2012) Trajectory optimization for domains with contacts using inverse dynamics. In: *2012 IEEE/RSJ International conference on intelligent robots and systems.*
8. Hadi, M., & Ali, H. (2021). Single link manipulator trajectory tracking using nonlinear control algorithm. *Al-Nahrain Journal for Engineering Sciences, 24*(1), 30–39.
9. Mohamed, Z., Kitani, M., Kaneko, S., & Capi, G. (2014). Humanoid robot arm performance optimization using multi objective evolutionary algorithm. *International Journal of Control, Automation and Systems, 12*(4), 870–877.
10. Wang, H., Ge, L., Li, R., Gao, Y., & Cao, C. (2021). Motion optimization of humanoid mobile robot with high redundancy. *Assembly Automation, 41*(2), 155–164.
11. Maaroof, O., Dede, M., & Aydin, L. (2021). A robot arm design optimization method by using a kinematic redundancy resolution technique. *Robotics, 11*(1), 1.
12. Liu, Y., et al. (2022). Evolutionary multi-objective trajectory optimization for a redundant robot in Cartesian space considering obstacle avoidance. *Mechanical Sciences, 13*(1), 41–53.
13. Krischer, L., Sureshbabu, A., & Zimmermann, M. (2020). Modular topology optimization of a humanoid arm. In: *2020 3rd International Conference on Control and Robots (ICCR).*
14. Bodden, C., Rakita, D., Mutlu, B., & Gleicher, M. (2018). A flexible optimization-based method for synthesizing intent-expressive robot arm motion. *The International Journal of Robotics Research, 37*(11), 1376–1394.
15. Abulhail, S., & Al-Faiz, M. (2021). Design of optimal inverse kinematic solution for humanoid robotic arms. *Iraqi Journal of Information and Communications Technology, 1*(1), 11–24.
16. Abulhail, S., & Al-Faiz, M. (2021). Social spider optimization for solving inverse kinematics for both humanoid robotic arms. In *2021 IEEE International conference on automatic control & intelligent systems (I2CACIS).*
17. Al-Faiz, M., & Shanta, A. (2015). Kinect-based humanoid robotic manipulator for human upper limbs movements tracking. *Intelligent Control and Automation, 06*(01), 29–37.
18. Ali, H., & Hadi, M. (2020). Optimal nonlinear controller design for different classes of nonlinear systems using black hole optimization method. *Arabian Journal for Science and Engineering, 45*(8), 7033–7053.
19. Bouchekara, H. (2014). Optimal power flow using black-hole-based optimization approach. *Applied Soft Computing, 24*, 879–888.
20. Smail, M., Bouchekara, H., Pichon, L., Boudjefdjouf, H., Amloune, A., & Lacheheb, Z. (2016). Non-destructive diagnosis of wiring networks using time domain reflectometry and an improved black hole algorithm. *Nondestructive Testing and Evaluation, 32*(3), 286–300.
21. Hadi, M., & Ali, H. (2020). Abstract of robust control algorithm design for nonlinear MIMO", IJSR.net [Online].
22. Hadi, M., & Ali, H. (2020). Optimal model reference control scheme design for nonlinear strict-feedback systems. *Engineering and Technology Journal, 38*(9), 1342–1351.
23. Bouchekara, H. (2017). Most valuable player algorithm: A novel optimization algorithm inspired from sport. *Operational Research, 20*(1), 139–195.

6G Wireless Communication Systems and Its Applications

M. S. Swetha, M. S. Muneshwara, A. S. Murali Manohara Hegde, and Zonghyu Lu

Abstract In the coming years, additional iterations of the 5th generation (5G) of wireless communication will be introduced. However, due to the inherent constraints of 5G and the development of new applications and services with demanding specifications like latency, energy/bit, traffic capacity, and peak data rate, telecom researchers are now concentrating on conceptualizing the following generation of wireless communications, known as sixth-generation wireless communications (6G). The Internet of Things (IoT) is anticipated to transform consumer applications and services, ushering in a future of fully intelligent and autonomous systems leveraging sixth-generation networks. A collaborative effort between industry and academia has started to conceptualize the sixth generation of wireless communication systems with the aim of laying the groundwork for stratification of communication needs in the 2030s in order to meet these demanding requirements and maintain wireless networks' competitive edge. This work also goes deeply into the challenges, demands, and trends related to 6G while also providing a future vision for 6G wireless communication and its network architecture. This work includes some fresh, intriguing 6G services and use cases based on the requirements and solutions, which cannot be adequately supported by 5G. Furthermore, this study provides information on key research directions that contribute to successful 6G conceptualization and implementation.

M. S. Swetha (✉) · A. S. Murali Manohara Hegde
Department of Information, Science & Engineering, BMS Institute of Technology and Management, Bengaluru, India
e-mail: swethams_ise2014@bmsit.in

A. S. Murali Manohara Hegde
e-mail: 1by20is091@bmsit.in

M. S. Muneshwara
Department of Computer Science & Engineering, BMS Institute of Technology and Management, Bengaluru, India
e-mail: muneshwarams@bmsit.in

Z. Lu
University of Huddersfield, Huddersfield, UK
e-mail: j.lu@hud.ac.uk

T. D. L. Nguyen and J. Lu (eds.), *Machine Learning and Mechanics Based Soft Computing Applications*, Studies in Computational Intelligence 1068,
https://doi.org/10.1007/978-981-19-6450-3_25

Keywords Internet of Things (IoT) · 5G · 6G

1 Introduction

Wireless communication has grown ingrained in society and people's daily routines. Artificial intelligence (AI), robots, and automation are all rising in popularity around the world today. In the coming years, mobile phones, augmented reality glasses, virtual reality headgears, and equipment such as automobiles, robotics, home appliances, and heavy machinery will become more prevalent in our life. The need of robust networks and dependable connections is being highlighted as a result of these trends toward smarter technology and more connected devices [1]. This will usher in unparalleled wireless communication paradigm upheavals.

6G guarantees hyper-availability and a definitive encounter for both consumers and businesses. By consolidating AI applications, 6G will actually want to gather and use an immense measure of information related to many billions of associated machines and human necessities. 6G will extend and empower admittance to data, assets, and social administrations paying little heed to time or area. New high-level services in the 6G period will require a huge measure of continuous information handling, a hyper-quick information throughput, and very low idleness [2].

6G is supposed to offer an altogether new service quality and upgrade client experience in current IoT frameworks because of its better elements over past network ages, for example, ultra-low idleness communications, very high throughput, satellite-based client administrations, gigantic and independent networks. These capacities will be unmatched, supporting 6G-based IoT network applications and deployments in regions, for example, IoT information sensing, device connectivity, remote communication, and 6G network management [3].

The dependability of society's frameworks, supportability through mobile technology effectiveness, sped up automatization and digitalization reliability of society's systems, sustainability through mobile technology efficiency, accelerated automatization and digitalization to simplify and improve people's lives, and limitless connectivity to meet the demands for intensifying communication anywhere, anytime, and for anything will define the 6G era [4]. To tackle these future difficulties, 6G will need to go above the technical limitations of 5G, focusing on crucial services, immersive communication, and ubiquitous IoT. Furthermore, whole new capacity levels should be investigated by integrating compute services and providing capabilities other than communication, such as spatial and time data (Fig. 1).

5G services such as enhanced mobile broadband (eMBB), ultra-reliable and low latency communications (URLLC), and massive machine-type communications (mMTC) will continue to improve as we move closer to 6G [5]. The focus is on 6G services, which will emerge as a result of advances in communications. The solutions are offered through the hyper-connection of everyone and everything, culminating in the ideal multimedia experience [6].

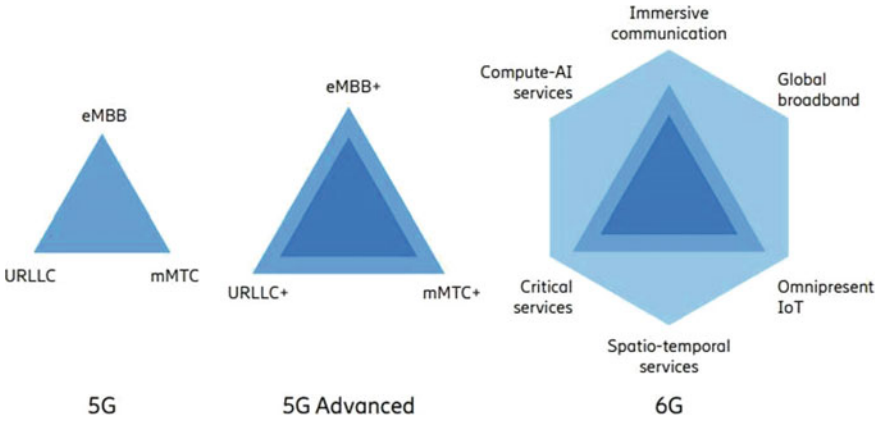

Fig. 1 Features of different cellular generations

There are five key categories of usage scenarios described, with eMBB+, URLLC+, and mMTC+ being extensions and combinations of the 5G usage scenarios, while sensing and AI being two new usage scenarios that will thrive in the 6G era.

6G is additionally connected with new business and functional models, green ICT contemplations, more agile network deployments [7] and run-time enhancements in light of ML and AI, closer RAN-Core assimilation due to start to finish virtualization and terahertz communication, paving the way for new sensing and data capacities as the new 6G era begins.

The digital, physical, and human worlds will fluidly merge in the 6G future to trigger extrasensory experiences [8]. Intelligent information systems will be integrated with powerful processing capabilities to make humans infinitely more efficient while also redefining how we live, work, and care for the environment. The role of next-generation networks is to bring our physical, digital, and human experiences together (Fig. 2).

2 Related Work

Started with the research works of:

M. Alsabah et al., The future vision for 6G networks is presented together with the key enabling technologies that will make that vision a reality. The objective of this paper is to give a complete survey of the core technologies for 6G networks, including a discussion of each technology's fundamental operating principles, potential applications, current state-of-the-art research, and associated technical challenges. This article explains how switching to higher frequency bands for 6G requires fewer scattering objects, more signal attenuation that affects transmission, and an expanded

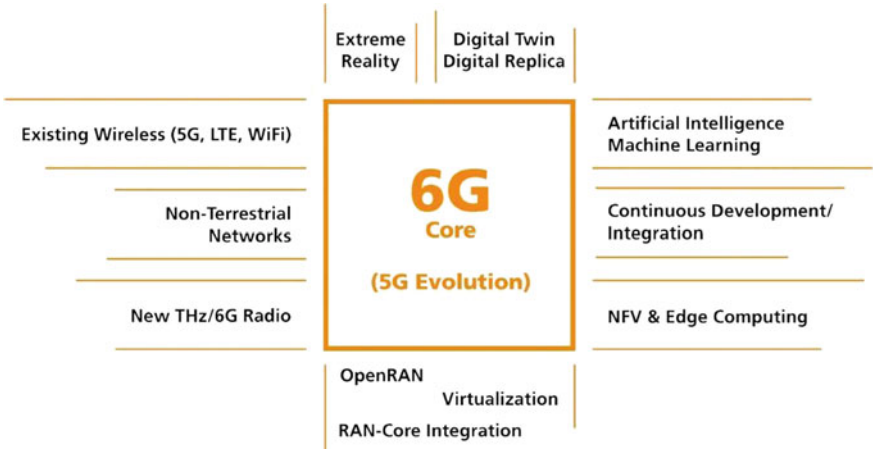

Fig. 2 Block diagram of 6G core

coverage area because of shorter-range communications. It is accomplished by the use of a reconfigurable intelligent reflecting surface (RIRS). The signal-to-noise ratio (SNR) of RIRS is lower than that of massive MIMO. Because RIRS elements are constructed around the concept of analogue beamforming, they do not support digital processing [9] (Fig. 3).

S. Elmeadawy et al., The most recent research on 6G technology and applications, as well as the related research issues, is covered in this article. According to the report, the RF band is virtually filled up completely and cannot support the rising demand for wireless communications technology. In order to achieve higher bandwidth, capacity, very high info rates, and secure transmission in 6G, the terahertz (THz) band, varies from 0.1 to 10 THz, will be essential. The main issue with the 6G wireless communication infrastructure, according to the research, is the THz band. Despite the high information rates, the high frequencies make it difficult to reduce the high path loss. Long-distance communications suffer from extremely high air

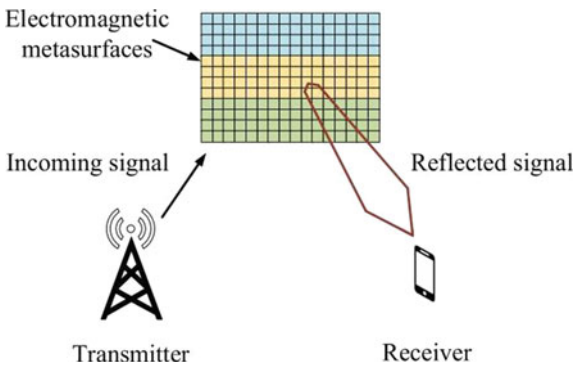

Fig. 3 RIRS-aided mobile communication

absorption and propagation loss. The result is an extremely strong attenuation of the signal [10].

E. C. Strinati et al., Beginning with gap analysis of 5G and foreseeing another combination of not so distant future tech like holographic teleportations, high-level accuracy fabricating, an unavoidable introduction of AI and mix of new advancements, for example, subterahertz or visible light correspondence, in a truly 3D inclusion situation, the paper talks about moving to a sixth generation of versatile networks. The following movement in sight and sound experience is holographic showcases, which transport three-dimensional pictures from one or various sources to one or numerous destinations, offering a vivid three-dimensional experience for the end client. The network's intuitive holographic capacity will require a blend of high information rates and extremely low inertness. At each step of multidimensional image amalgamation and gathering, the creator underlines significant constant computational issues [11].

Md. J. Piran et al., outlines some of the research avenues that helped create and successfully implement sixth generation. Satellite communication technology will be used in future sixth-generation communications to provide worldwide coverage. This paper discusses how 6G will merge satellites which are specifically used for telecommunication, earth imaging, and navigation to give cellular customers throughout the world with localization services, broadcast and Internet connectivity, and weather-related information. Each wireless communication technology has its own transceiver and antenna designs that support the technology's criteria. The development of millimeter-component devices in 5G was a problem. According to the author, 6G will be considerably more difficult because it requires mega high frequency bands in THz and spectrum and resource sharing [12].

H. Chen et al., talks about the integrated security architecture of the space–air–ground-submerged network and keeps up with the place that the 6G network is a successful reconciliation of the 5G network, satellite network, and deep ocean sea network, and that 6G will give worldwide consistent inclusion. The 6G space–air–ground–undersea network would work on submerged (seaward, subsea, and island communication gear), ground (cell mobile networks and different networks), air (a wide range of airplane), and space connects (a wide range of satellites and spacecraft). The report likewise contends that to give safe communication in a worldwide consistent network, a coordinated security architecture is constantly based on right security advancements and the executives systems to acknowledge service and information security. The heterogeneity highlight adds a lot of intricacy to the network, particularly with regards to security [13].

D. C. Nguyen et al., by leading an exhaustive evaluation on the combination of 6th generation and Internet of Things, this article examines the rising potential presented by 6th generation innovations in Internet of Things networks and applications [14].

This study additionally examines how 6G will change the Healthcare Internet of Things (HIoT) by using its supporting advancements. 6G innovations, like THz communications, are being utilized to work with very low-dormancy medical care information transmission and to accelerate clinical network associations among wearables and distant clinicians. As a matter of fact, medical services spaces like distant

wellbeing checking require low-idleness communications (under 1 ms) with an unwavering quality necessity of above 99.999% to achieve close ongoing medical services and quick and reliable remote diagnosis. The author additionally makes reference to incorporating 6G into IoT networks might open IoT to dangers like unapproved admittance to information at figuring units/servers, threats to network integrity, and denial of service (DoS) to programming and data centers, which are all connected with remote point of interface attacks.

R. S. R. Bajracharya et al., 6G communications integrate land-based, air-based, and non-terrestrial networks to deliver 3D-based connectivity and applications in three-dimensional space. Communication, computation, and caching are provided by the implementation of an aerial access network (AAN) for the UAV traffic management (UTM) ecosystem using non-terrestrial networks (NTN) like satellites, low- and high-altitude platform stations (i.e., LAPS and HAPS), in addition to heterogeneous terrestrial networking. The management of unmanned aerial vehicle (UAV) traffic and its integration with commercial aviation is one of the most urgent concerns in the UTM ecosystem in the future, according to this research. UAVs also struggle with wide-aerial network coverage, connection, and interference that extends beyond the line of sight (BVLoS) [15].

H. Tataria et al., discuss the technology requirements for enabling 6G applications and examines key problems and opportunities based on realizable system solutions across all OSI stack levels. Next-generation core network architecture, ground-breaking multiple access strategies, antenna beams, wave transmission, radio frequency, transceiver design, and signal synthesis are all addressed from a unique standpoint in this study. An extensive overview of 6G deployment is given in the article. A common application in which extremely high data rate equipment are put both inside and outside is hot spot deployment. MmWave and THz systems are best in these situations [16].

3 Proposed Work

The convergence of all previous aspects, including as network densification, greater dependability, high throughput, low latency, and huge connection, will be the major drivers of 6G. While 6G has many applications, there are some issues in the mass deployment of this technology. These problems are as follows:

1. Autonomous wireless systems

   The 6G network will fully enable automation technologies such as driverless vehicles, unmanned aerial vehicles and AI-based Industry 4.0. We need to have the convergence of many heterogeneous subsystems, such as autonomous computing, interoperable processes, machine learning and heterogeneous wireless systems, to develop autonomous wireless systems.

2. Frequency (THz) bands

   The terahertz (THz) band is the difficult part of the 6G technology. Significant frequencies enable overcoming of high route loss which is a major challenge due to the atmospheric absorption and propagation loss. To tackle the problem of frequency dispersion, new multipath channel models are required due to wide bandwidth.
3. Device capability

   Companies have just begun developing 5G devices, which should be able to support 6G as well as all other wireless communication generations. The 1Tbps information rate and high operational frequencies should be tolerated by devices supporting 6G wireless network [17]. These gadget features are both expensive and difficult to implement.
4. Spectrum and interference management

   Due to spectrum scarcity and interference concerns, it is critical to efficiently manage the 6G spectra, which includes spectrum-sharing strategies and unique spectrum management techniques. For maximum resource utilization and QoS enhancement, effective spectrum management is required.
5. Network Security

   The security approaches employed in 5G will not suffice in 6G, so new security based on creative cryptographic methods, such as physical layer security techniques and integrated network security mechanisms with low cost, low complexity, and very high security.

3.1 Objectives

The primary goals of 6G-based systems are based on past trends and forecast of future demands:

- To achieve high data rates per device

  One of the main objectives of 6th generation is to provide high data transmission rate, bit rate when compared to 5th generation.
- To attain very low latency

  6th generation will offer very low latency as the amount of time required to transfer data packages will be less than 1 ms.
- To establish global connectivity

  Unlike 5th generation, 6G will focus on global connectivity rather than local connectivity by providing a huge global coverage.

- To increase the number of connected devices

  6th generation main goal will be to incorporate and connect huge number of devices in a given area.
- To emphasize on energy efficiency

  6th generation devices will need strong batteries which are energy efficient when compared to 5th generation devices.
- To establish ultra-high reliable connectivity

  To support latency sensitive services, 6th-generation networks will need to be extremely reliable.
- To bring connected intelligence with AI capability

  AI plays a key role in enabling automation, managing complexity and scalability, and leveraging on data from distributed systems. The true potential of technologies like AI can be unleashed to its fullest effect with the help of 6th-generation networks.

4 Methodology

4.1 Holographic Communications

To convey continuous far off physical communication, 6G organizations are expected to help another kind of human remote interaction that utilizes every human sense, including hearing, vision, taste, smelling, and contact. Holographic teleportation [18] is regarded as a type of real-time virtual teleportation that is possible using mixed reality technology and a three-dimensional video (Fig. 4).

Holographic teleportation uses numerous cameras with diverse views and numerous sensing devices to enable far off communication live and produce a hologram of the actual person. This is an archetype shift from conventional video conferencing to virtual instantaneous face-to-face meetings, increasing communication experience and enabling virtual sports, concerts, and education. However, higher data rates with an order of terabytes/sec are needed for such connectivity, powered engagement, and communications, as well as a significant amount of image and video information.

The research shows that a raw hologram needs a 4.32 Tb/s data throughput in order to exhibit three-dimensional holographic teleportation. A submillisecond end-to-end latency is needed for holographic teleportation. Therefore, new semantic inference techniques are needed to enable holographic teleportation. The use of knowledge representation in communications would be made possible by such algorithms.

Fig. 4 3D hologram display

Holographic information must also be transmitted using ultra-reliable connection with extraordinarily huge bandwidth [19]. Furthermore, holographic communications may be made possible in the future by artificial intelligence and machine learning techniques. Therefore, more research into using machine learning and artificial intelligence techniques for holographic communications is needed.

The key system prerequisites for this kind of communication are as per the following:

(1) **Data rates**

The necessary data rates vary depending on the hologram's construction, the display type, and the number of synchronized images. Holograms will need enormous bandwidths even with data compression techniques, which may lower the data rates needed for transmission. When creating holograms using image-based techniques, these range from 10's of Mb/s to 4.3 Tb/s for a human-size hologram.

(2) **Latency**

Ultra-low latency is necessary for really immersive settings; otherwise, the user experiences simulator sickness. However, submillisecond latency is necessary if haptic capabilities are also provided.

(3) **Synchronization**

Holographic communications require strict synchronization in a variety of situations. The multiple sensor feeds may be supplied via various channels or flows as distinct senses may be merged, necessitating synchronization, and coordinated delivery. Precise/strict interstream synchronization is necessary to ensure the packets arrive on time when streams contain data from many sources, such as video, audio, and haptic data.

(4) **Security**

The application will determine the requirements. The integrity and security of that program are vitally crucial if remote surgery is to be performed because any flaw could endanger lives. A further difficulty is coordinating the security of numerous coflows because an assault on one flow could jeopardize all the others.

(5) **Resilience**

Resilience at the system level involves reducing packet loss, jitter, and latency. Reliability and availability are important quality-of-experience measures at the service level. An unrecovered failure occurrence could result in a severe loss of value for operators of holographic communication services. To sustain the high QoS requirements for these services, system (network) resilience is crucial.

(6) **Computation**

At every stage of hologram synthesis and reception, there are major real-time computing problems. Although compression might lower bandwidth requirements, it has a significant impact on latency. In order to do this, a trade-off between increased compression, processing bandwidth, and latency exists and needs to be optimized.

4.2 6G for Vehicular Internet of Things (VIoT) and Autonomous Driving

Intelligent transportation systems have undergone a transformation as a result of the advancements in 6G technology, which have significantly changed vehicle Internet of Things (VIoT) networks (ITSs). In VIoT networks based on 6G, the study allows vehicle-to-everything (V2X) communication for transfer of short vehicular info payloads by a large number of cars without human contact (Massive Machine-Type Communications).

ML can be a valuable method to show the reasonable way of behaving of network-assisted throughput expectation in future 6G vehicle networks by learning the past network load information in view of control channel examination. To completely understand the commitment of vehicular knowledge in VIoT, edge insight capabilities utilizing ML are associated with side of the road units (RUSs), which are liable for leading the evaluation of traffic volume and weather conditions gauge in light of the

accumulation of nearby information from vehicles. By empowering neighborhood assessment at scattered vehicles through remote information trade with nearby vehicles inside the communication range, a disseminated assessing method is proposed to additional improve the versatility of vehicular systems with regard to 6G.

The job of DL in giving knowledge to 6G-based VIoT is additionally researched by utilizing deep learning's high-layered generalization [19] abilities to display vehicular communication channels and backing network management, for example, ideal asset allotment utilizing deep reinforcement learning (DRL) algorithms, as displayed in Fig. 5.

Another area of interest is vehicular intelligence, where DL algorithms are used to automatically plan data transfer. This is enabled by using three approaches:

- **supervised learning** for data rate estimation
- **unsupervised learning** for recognizing geospatially dependent uncertainties of the estimation model
- **reinforcement learning (RL)** for autonomously coordinating data transmissions based on anticipated resource efficiency.

This linked approach shows potential for addressing multiobjective optimization in VIoT, from allocation of resources to data transmission maximization. The best classification hyperplane is built using a support vector machine, which is then used to transfer data to a high-dimensional space using a kernel function and extract the sample classes. The categories of the retrieved samples are then determined using K-neighborhood, and a decision tree is used to classify them.

5 Performance Analysis

Performance analysis of 6G can be done by comparing the existing 5G wireless communication technology with 6G technology by using some parameters listed below:

1. Data rate
2. Latency
3. Network coverage
4. Energy efficiency
5. Mobility
6. Area traffic capacity (Mbps/m^2).

The improvement of major criteria from 5 to 6G is shown in Fig. 6.

(1) **Data Rate**

6G has to offer a significantly greater data rate than 5G in order to achieve sophisticated multimedia services like totally immersive XR, mobile holographic, and digital replica. While the peak data rate for 5G was intended to be 20 Gbps, our goal for

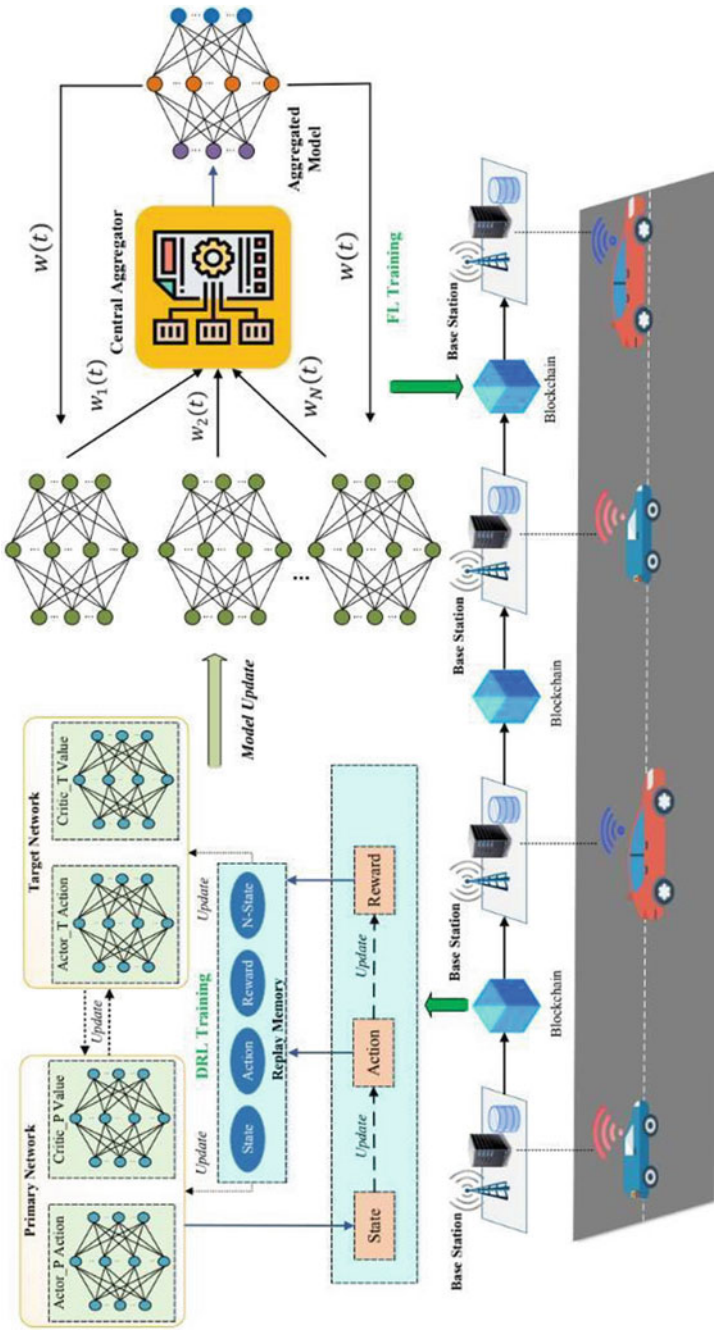

Fig. 5 DL for V2V network management

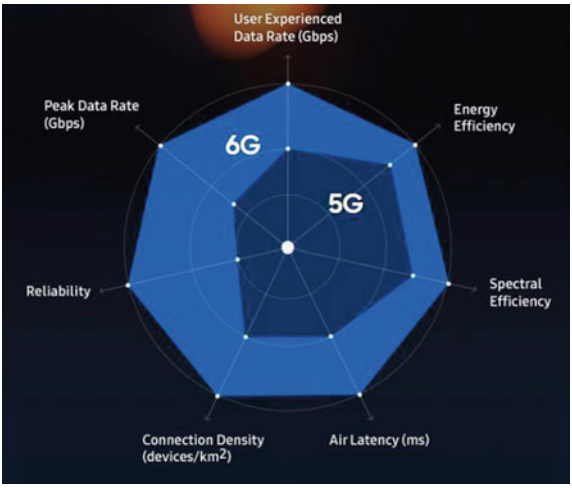

Fig. 6 Key performance requirements between 5 and 6G

6G is to deliver a peak data rate of 1000 Gbps (1 Tbps) and a user-experienced data rate of 1 Gbps. The total network performance must be enhanced in order to offer sophisticated multimedia services to a big audience, for example, by aiming for a 2 times greater spectral efficiency than 5G.

Enhanced mobile broadband (eMBB), which simply denotes high data speeds, is the reason we can quickly download HD videos in 6G [20]. Since the advent of wireless communications, customer demands for data rate have grown. The data speeds of 1G were a few kbps, and they climbed to a few Gbps in 5G as shown in Fig. 7. For certain applications, these data rates are still insufficient. As a result, we need to create certain standards and communication protocols with data speeds between 10 and 100 Gbps.

About 20 Gbps peak data rate and 100 Mbps user-experienced data rate are anticipated from 5G. However, 6G will offer a 1000 Gbps peak data rate. Additionally, it will raise the bandwidth rate that users experience to 1 Gbps.

(2) **Latency**

Low latency translates to lightning-fast communication. The packets need to be transmitted in a very swift amount of time, with minimal processing delays. In 6th generation, the maximum allowable delay is 10 μs. In the network of automation and smart handheld platforms of the future, extremely low latency will be necessary. Health care, military, monitoring, and reconnaissance are only a couple of the crucial applications which will require extreme dependability and truncated inertness.

Performance linked to latency has to be greatly enhanced in order to provide the finest constant experience for delay delicate applications like interactive tactile internet. Performance goals compromise extremely low delay jitter in the microsecond range, end-to-end (E2E) latency of less than 1 ms, and air latency of less than 100 s (Fig. 8).

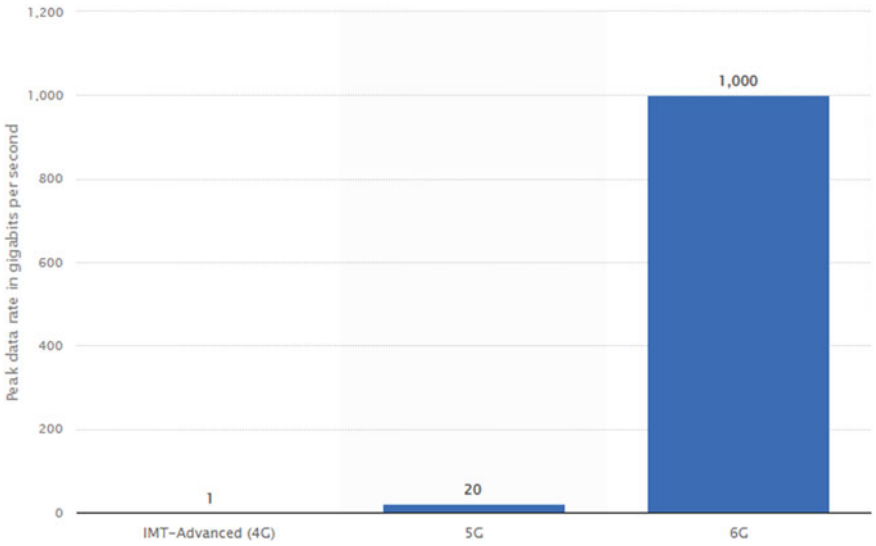

Fig. 7 Peak data rate in 4G, 5G, and 6G

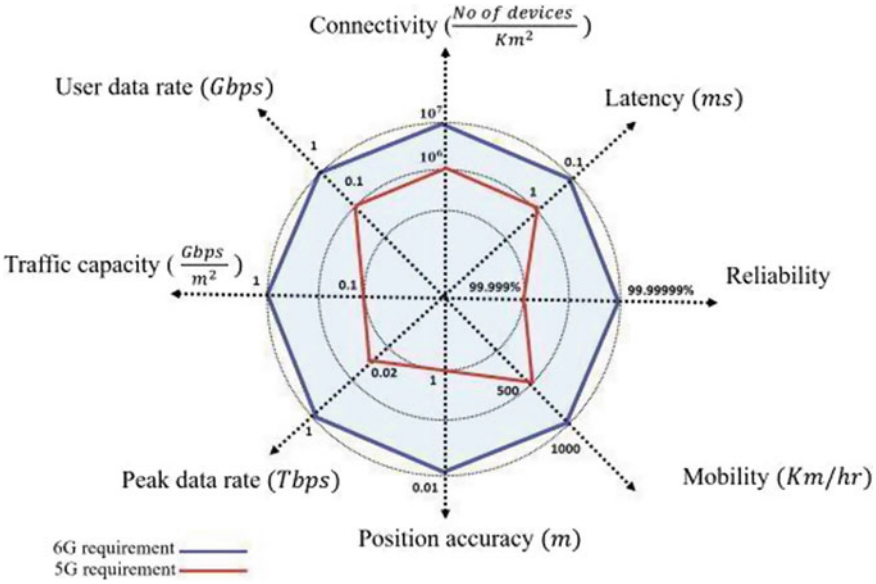

Fig. 8 Quantitative comparison between the 5G and future 6G in terms of requirements

The user-experienced latency requirement encompasses all delay components in wireless and wireline networks, as well as processing on both the client and server sides. Latency will be reduced to 1 ms thanks to 5G technology. Many real-time applications will be boosted by the ultra-low latency. However, the user experience latency will be reduced to less than 0.1 ms with 6th-generation wireless communication technology.

Many real-time applications that are delay-sensitive will benefit from the significant reduction in latency. Reduced latency will make crisis response, distant medical procedures/surgeries, and automated manufacturing easier. 6th-gen networks are 100 times more dependable than 5G networks, and delay-sensitive real-time apps will run flawlessly.

(3) **Network Coverage**

In earlier generations, network coverage was always important, and it will be important in 6G. More coverage than 5G is what 6G aims to deliver. The maximum speed that the mobile device could support rose from 350 km/h in 4G to 500 km/h in 5G. It might need to get even better in 6G, depending on how far transportation systems have come. Due to the exponential growth of connected devices, 6G will need to support 107 devices per square kilometer. In terms of connection density, this is ten times beyond what 5G calls for.

Although the infrastructure of mobile communications systems prefers lower frequency spectrum for omnipresent coverage, the increase of wireless traffic needs a broader spectrum with a higher frequency. 6G will use not just the millimeter wave (mmWave) spectrum but also the THz or perhaps visible light spectrum, possibly utilizing the entire spectrum for the first time, in order to attain the highest level of extreme connection.

(4) **Energy efficiency**

Users would anticipate seamless high-end services in their daily lives in the 6G era, hopefully with longer battery life. Given the growing concern about environmental sustainability, 6G networks' energy usage should be kept to a minimum. We want to double the energy efficiency of both devices and networks.

End-users will be able to smoothly and rapidly access a variety of high-end services through 6G. End-users, on the other hand, will require devices with powerful batteries in order to access high-end services without delay or disruption. The goal of 6G is to double the battery life of gadgets. Simultaneously, the technology will contribute to environmental sustainability by allowing the network to operate at peak efficiency without requiring more energy. In comparison to 5G, 6G intends to double the energy efficiency of the telecom network.

(5) **Mobility**

In next-generation communication systems, more mobility robustness is also necessary. In highly mobile devices, high data rates ought to be kept up. When travelling by plane or high-speed bullet train, for example, communication should not be

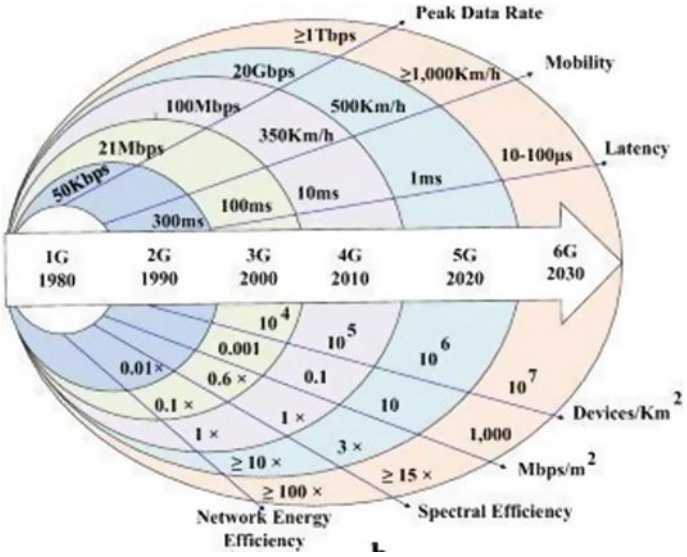

Fig. 9 Evolution of wireless communication, with timeline, from 1 to 6G based on KPIs

disrupted, and data speeds should be maintained. According to the ITU, the mobility requirements for 6G are >1000 km/h (Fig. 9).

(6) **Area traffic capacity (Mbps/m^2)**

Demand for greater capacity channels and backhauling increased expanded as the number of associated gadgets per unit region expanded. Consistently, a thickly populated network consisting of sensors makes more than terabytes worth of information. This information yield needs a high-limit backhauling line to handle the traffic.

Massive IoT connection leads to the development known as V2X (vehicle-to-infrastructure). The car must interact with other vehicles, people, and a variety of different sensors throughout the vehicle. All of this communication must be exceedingly dependable, have low latency, and be secure. 6G has a minimum area traffic throughput restriction of 1000 Mbps/m^2.

6 Conclusion

On the 2030 horizon, there will be a significant need for communication and beyond technology, with 5G setting in motion transformations and increasing societal expectations, the development of new services and use cases that will enhance people's lives is being hastened by developments in the supporting technologies.

Even though there is no 6G network yet and it is only in the research stage, businesses have begun to imagine cutting-edge use cases with 6G after a fruitful

examination of 5G and 6G network. The significant objective is to enter another time of remote innovation and present new developments that will impact the world later on years. When the most recent remote organization age, or 6G versatile organization, strikes the telecom area in a more extensive zone, profoundly thrilling possibilities concerning velocity and trustworthiness are projected to turn into a reality soon. The way we live or conduct business electronically today and in the post-Covid era will undoubtedly take on new dimensions as a result of this cutting-edge technology, making it as a hyper-connected world.

The development of capability targets for the 6G era is speeding up, as is the investigation of a variety of intriguing technology components that could become part of a 2030 network platform. Extreme radio access performance, network adaptability, and global as well as pervasive reach will be crucial aspects in this revolution. Beyond connectivity, 6G ought to develop into a dependable platform for reasoning, computing, and spatial data, encouraging innovation and acting as the skeleton of information for the community.

7 Future Enhancement

As per the 6G organization's vision and the requirements for the cutting-edge organization, the 6G organization will perform obviously better than the 5G organization because of its capacity to fulfill the high needs of next gen use cases like independent vehicles, medical services, industry computerization, and the development of a few verticals. The expected utilizations of 6th-gen networks innovations incorporate AI, intelligent surfaces, cell-free architecture, digital twins, and quantum computing. In any case, these advances are not yet ready for the market. Global business and scholastic joint efforts for research, mechanical turn of events, and commercialization are vital for the genesis of the 6th gen networks.

End-clients will actually want to without a hitch and quickly access an assortment of very good quality administrations through 6G. However, in order for end consumers to enjoy premium services without delay or interruption, they will need devices with strong batteries. The 6G network is designed to double-device battery life.

References

1. Bariah, L., Mohjazi, L., Muhaidat, S., Sofotasios, P. C., Kurt, G. K., Yanikomeroglu, H., & Dobre, O. A. (2020). A prospective look: key enabling technologies, applications and open research topics in 6G networks. *IEEE Access, 8*, 174792–174820.
2. Mao, B., Kawamoto, Y., & Kato, N. (2020). AI-based joint optimization of QoS and security for 6G energy harvesting internet of things. *IEEE Internet of Things Journal*.
3. Zhang, S., Xiang, C., & Xu, S. (2020). 6G: Connecting everything by 1000 times price reduction. *IEEE Open Journal of Vehicular Technology*.

4. Gui, G., Liu, M., Tang, F., Kato, N., & Adachi, F. (2020). 6G: Opening new horizons for integration of comfort, security and intelligence. *IEEE Wireless Communications.*
5. Zhang, L., Liang, Y., & Niyato, D. (2019). 6G visions: Mobile ultrabroadband, super internet-of-things, and artificial intelligence. *China Communications, 16*(8), 1–14.
6. Tomkos, I., Klonidis, D., Pikasis, E., & Theodoridis, S. (2020). Toward the 6G network era: Opportunities and challenges. *IT Professional, 22*(1), 34–38.
7. Yaacoub, E., & Alouini, M. (2020). A key 6G challenge and opportunity—Connecting the base of the pyramid: A survey on rural connectivity. *Proceedings of the IEEE, 108*(4), 533–582.
8. Zhang, Z., et al. (2019). 6G wireless networks: Vision, requirements, architecture, and key technologies. *IEEE Vehicular Technology Magazine.*
9. Alsabah, M., Naser M. A., Mahmmod, B. M., Abdulhus. S. H. "6G Wireless Communications Networks: A Comprehensive Survey." *In IEEE Access, 9*
10. Elmeadawy. S., Shubair. R. M. (2019). "6G Wireless Communications: Future Technologies and Research Challenges." *In 2019 International Conference on Electrical and Computing Technologies and Applications (ICECTA).*
11. Strinati. E. C., Barbarossa. S., Jimenez. J. L. G., Ktenas. D. (2019). "6G: The Next Frontier: From Holographic Messaging to Artificial Intelligence Using Subterahertz and Visible Light Communication." *In IEEE Vehicular Technology Magazine, 14,* pp. 42–50.
12. Piran, M. J., & Suh, D. Y. (2019). "Learning-Driven Wireless Communications, towards 6G." *In 2019 International Conference on Computing, Electronics & Communications Engineering (iCCECE).*
13. Chen, H., Tu, K., Li, J., Tang, S., Li, T., & Qing, Z. (2020). "6G Wireless Communications: Security Technologies and Research Challenges." *In 2020 International Conference on Urban Engineering and Management Science (ICUEMS)*
14. Nguyen, D. C., Ding, M., Pathirana, P. N., Seneviratne, A., Li, J., Niyato, D. (2022). "6G Internet of Things: A Comprehensive Survey." *In IEEE Internet of Things Journal, 9*, pp. 359–383.
15. Bajracharya, R. S. R., and Kim. S. (2021) "6G Enabled Unmanned Aerial Vehicle Traffic Management: A Perspective." In IEEE Access, vol. 9, pp. 91119 – 91136, https://doi.org/10.1109/ACCESS.2021.3092039
16. Tataria, H., Shafi, M., Molisch, A. F., Dohler, M., Sjöland, H. (2021). "6G Wireless Systems: Vision, Requirements, Challenges, Insights, and Opportunities." *In Proceeding of the IEEE, 109*, pp. 1166–1199.
17. Mahmood, N. H., Alves, H., López, O. A., Shehab, M., Osorio, D. P. M., & Latva-Aho, M. (2020). Six key enablers for machine type communication in 6G. In: Proceedings of 2nd 6G Wireless Summit (6G SUMMIT), Levi, Finland, March 2020 (pp. 1–5).
18. Zhao, Y., Yu, G., & Xu, H. (2019). 6G mobile communication networks: Vision, challenges, and key technologies. *Scientia Sinica Informationis, 49*(8), 963–987.
19. Zong, B., Fan, C., Wang, X., Duan, X., Wang, B., & Wang, J. (2019). 6G technologies: Key drivers, core requirements, system architectures, and enabling technologies. *IEEE Vehicular Technology Magazine, 14*(3), 18–27.
20. Nawaz, F., Ibrahim, J., Awais, M., Junaid, M., Kousar, S., & Parveen, T. (2020). A review of vision and challenges of 6G technology. *International Journal of Advanced Computer Science and Applications, 11*(2), 1–7.

Compensation Techniques for Nonlinear Effects Using NG-RoF-DSP: A Review

Ahmed Jasim Obaid, Hassan K. Al-Musawi, and Mohammed Ahmed Abdl-Nibe

Abstract In a radio over fiber (RoF) transmission, the light wave transmitted through an optical fiber is modulated by the radio signal. This technique provides a better path for the transmission of wireless signals over optical media in broadband wireless networks. RoF has developed over the past three decades along with a plethora of studies in the field. However, RoF still encounters several challenges, many of which have already been overcome, yet many still need to be addressed. In newly evolving networks such as 5G and what follows, bandwidth demands, response time, jitter, and fidelity on front-end networks cause significant challenges to RoF systems. Moreover, the movement from the lower microwave scope to the microwave scope was of direct advantage to wireless operations in terms of bandwidth. However, this movement poses more challenges to RoF expansion because combining wired and a wireless (fiber) network into one basic structure is a task of considerable challenge. Therefore, this paper provides an overview of RoF technology with a specific focus on linear and nonlinear effects, mitigation methods, and a discussion of future challenges.

Keywords Radio over fiber · Linear and nonlinear effects · Networks 5G

1 Introduction

Over the last decades, the Internet traffic has been growing rapidly. Researchers have been endeavoring to service providers such as HD video downloading, online gaming, cloud computing, and Internet of Things (IOT) [1–3]. Radio over fiber (RoF) plays an

A. J. Obaid (✉) · H. K. Al-Musawi · M. A. Abdl-Nibe
Department of Electronics and Communication Engineering, Faculty of Engineering, University of Kufa, Kufa, Iraq
e-mail: najafahmed32@gmail.com

H. K. Al-Musawi
e-mail: hasank.baqir@uokufa.edu.iq

M. A. Abdl-Nibe
e-mail: Mohammeda.khaleel@uokufa.edu.iq

T. D. L. Nguyen and J. Lu (eds.), *Machine Learning and Mechanics Based Soft Computing Applications*, Studies in Computational Intelligence 1068,
https://doi.org/10.1007/978-981-19-6450-3_26

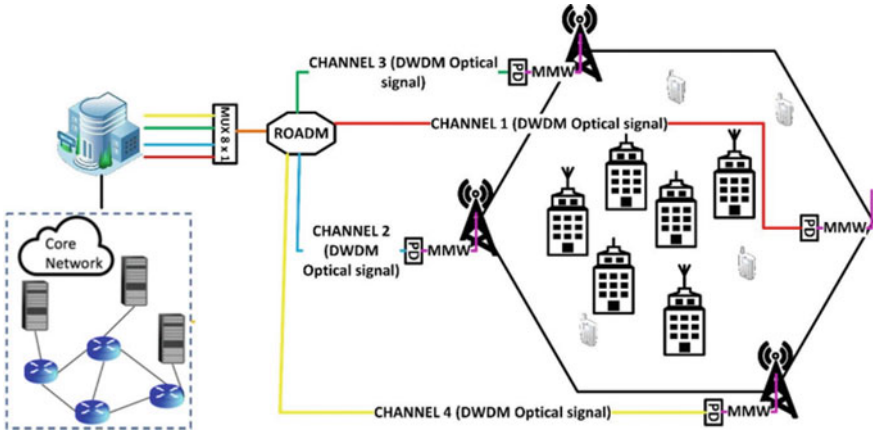

Fig. 1 NG-RoF from central station [11]

essential role in addressing such issues related to wireless devices and applications that are rich in content. Moreover, single-band Internet of Things (IoT) access is more effective when it is implemented with radio [4]. Radio over fiber (RoF) technology is promising to move to the next generation networks, and it is a potential solution for providing high bit rates. It also reduces power consumption, especially in the base station, where the radio signal depends on optical fibers, which have an impact on the optical system performance leading to linear and nonlinear distortions [5].

It has a very high capacity to be compatible with large data rates over very over long transmission distances [6]. The combination of Wi-Fi, wireless, optical fibers, and wires, resulted in radio over fiber technology. It is considered an innovative solution to provide maintenance-effective as well as cost-effective bandwidth [7]. Multi-density DWDM technology is implemented for short vertical distances between channels. Typically, its bandwidth ranges from 0.1 to 0.8 nm; hence, DWDM has the possibility of connecting dozens of optical channels using a single fiber. This possibility increases the delivery of optical fibers [8], which increases the number of stations in telecommunication networks [9]. Base station (BS) can be retrieved and used mainly as transmission [10, 11]. In many cases, disconnections during signal transmission could occur mainly because of nonlinear effects and note that the refractive index changes when the optical power density also changes [12]. The generated optical pulse suffers from nonlinear effects [13, 14] (Fig. 1).

2 Radio over Fiber Transmission

The main idea in radio optical fiber transmission systems is to use the numerous advantages of optical fibers as transmission lines compared to other cables or transmission through space in order to transmit a high number of bits, taking into account

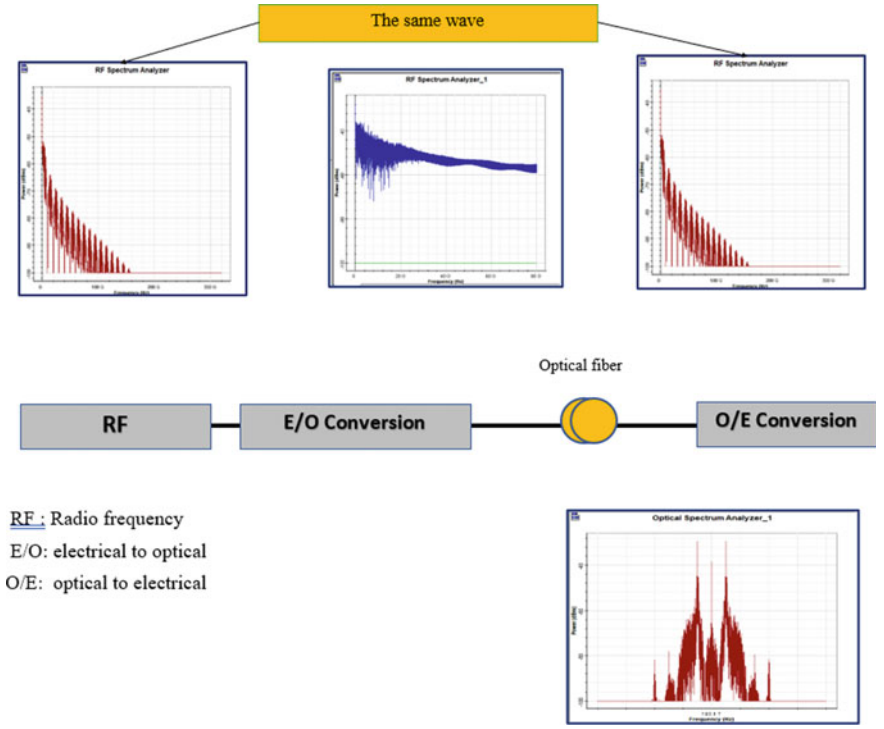

Fig. 2 Basic concept of a RoF system

the low cost. The information is transmitted by the following mechanism [15, 16]. The information is modified in the proper modulation pattern to be loaded onto an optical frequency (or transmission wavelength) from a laser source, i.e., modulating the optical intensity of the laser source with the information signal. This is accomplished by injecting the semi-carrier laser feed input directly with the electrical signal carrying the information (direct modulation usually used for relatively low transmission rates of less than 2.5 Gbps) or by using a continuous laser source with an external photoelectric rate fed by an information signal so that it gives an output optical power proportional to the electrical input signal (up-conversion). This signal is injected into the optical fiber, which will deliver it to the receiver side. There, the signal is detected using a down-conversion photodetector, and then the information sent by the demodulator is extracted [17–19] (Fig. 2).

2.1 Light Source

Since the beginning of optical fiber communication, semiconductors have been selected to be light sources because of their small dimensions and the relative

simplicity of modulating the emitted light directly. Moreover, the optical spectrum is relatively narrow and the power consumption is low. The laser diode (LD) source is the most convenient transmitter for optical communications because it is highly effective in terms of optical coherence in the propagation of light through optical fibers. Below are the most important sources of light used in optical communications [20]. Laser diode (LD) is an acronym for Light Amplification by Stimulated Emission of Radiation, which means light amplification by emitting stimulated radiation compared to other light sources. This allows the laser to emit a high-power beam of monochromatic light, (spatial) coherent and collimated, with a very limited expansion or diffraction rate. This allows the laser light beam to travel a longer distances and focused within a very small spot parallel to the laser with high level. [21]. Light-emitting diode (LED), in its simplest form, consists of a junction between two different semiconductors, one is called (n-type) and the other is (p-type). When a voltage is applied to their ends, an electric current will travel through them, releasing quanta of electromagnetic energy as light photons. The light-emitting semiconductor chip is placed in a frame structure to protect it from direct exposure to the surrounding environmental factors and to secure the wires conducting to the chip practically. This frame structure should be designed to increase the efficiency of the light energy emitted by the diode [22].

2.2 Amplification

The data transmitted over long distances, starting from the source to the furthest point in the network, are exposed to many undesirable effects, causing weakness in the transmitted signal. In any optical communication system, it is necessary to provide repeater points to expand the optical packet to ensure accuracy and of data delivery. These points are known as amplifiers. There are types of amplifiers [23] which are semiconductor optical amplifiers (SOAS) and erbium-doped fiber amplifier (EDFA). According to the current study, there are significant differences between EDFA and SOA. In EDFA, the gain is twice as high as double SOA gain, allowing for great signal amplification. Also, EDFA transmits signal with less noise [24].

2.3 Light Detectors

Light detectors convert an optical signal to an electrical signal, where the current is proportional to the intensity of the incident light. Many light detectors are used in optical communication, the most famous of which is the photodiode [25–27].

3 Nonlinear Effects

The fact that optical communication systems operate in a linear manner (i.e., the mean refraction index, dielectric constant, and propagation are unchanging factors) is appropriate to understand how these systems work at average values of transmission power (multiple mill watts). When the transmission rate does not exceed 2.5 Gb/s but with high transmission power or transmission rate to 10 Gb/s or more, then these systems become nonlinear [28, 29]. The nonlinear effects are classified into two parts. The first occurs due to the interaction between light and photons (molecule vibration) within the silica material resulting in multiple types of scattering, including Raman scattering and Brillion scattering. The second type of nonlinear effects depends on the applied electric field, which is proportional to the square of the field amplitude, the most important of which are self-phase modulations (SPM), cross-phase modulation (CPM), and four-wave mixing (FWM), which is the most important in optical communication systems. The nonlinear effects are [26, 28–32] Stimulated Brillion Scattering (SBS), Stimulated Raman Scattering (SRS), Self-phase Modulation (SPM), Cross-phase Modulation (CPM), and Four-Wave Mixing (FWM).

3.1 Stimulated Brillion Scattering (SBS)

The stimulated Brillion scattering (SBS) results in weakening the energy of the transmitted wave within a single channel. It occurs due to the interaction between the incoming signal and photons in the propagation medium for a specific wavelength of 1.55 μm and within a narrow range of frequencies (ΔfB) ranging from 20 to 100 MHz only. SBS does not lead to an interaction between the different waves when the channel space is greater than 100 MHz. SBS generates an opposite gain to the direction of propagation, i.e., opposite to the source. The increase of this interaction significantly weakens the signal strength with time and exhausts its energy. As a result of the interaction between the incoming waves and the propagation medium, two waves are produced. The first is called the pump wave and the second is called stokes. The pump wave loses part of its energy which the stokes wave gains, produced by SBS scattering [33] (Fig. 3).

3.2 Stimulated Raman Scattering (SRS)

Stimulated Raman scattering is the transference of power from a short-wavelength signal to a long-wavelength signal. The interaction between the light-wave signal and the molecule vibrations (optical photons) in the silica fiber causes the SRS-catalyzed Raman scattering which in turn scatters the light in all directions. The maximum

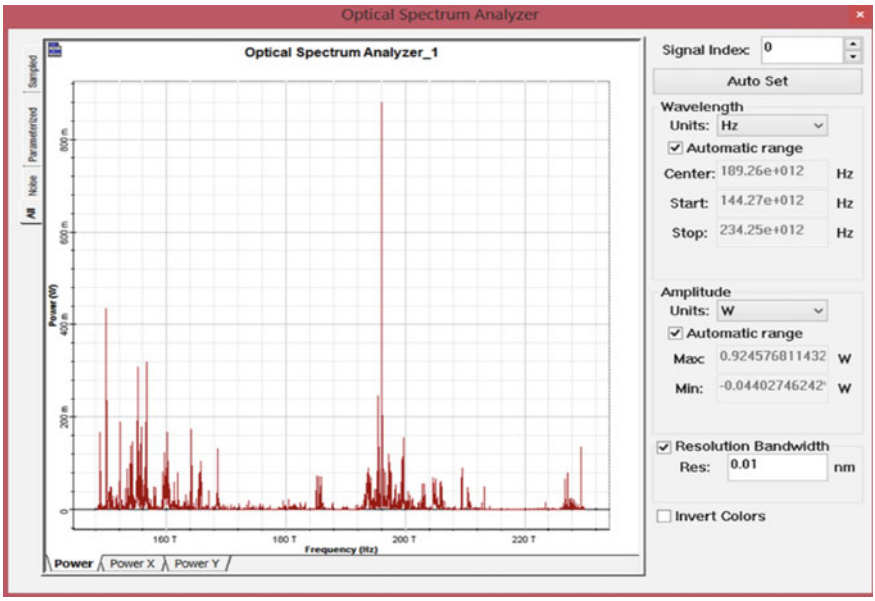

Fig. 3 Stimulated Brillion scattering

effect of SRS occurs at the difference in wavelengths between two signals about 100 nm (132.2 THz) for example 1550–1650 nm [34] (Fig. 4).

3.3 Self-Phase Modulation (SPM)

It is the effect of a signal with the same phase as the propagation signal, which leads to high-intensity signal. Also, the light itself leads to changes in the refractive index in the fibers. This phenomenon is known as Kerr effect. They are produced in different time phases in the same channel. In time, the varying refractive index regulates the transmitted wavelength phase and increases the wavelength range of the transmitted light pulse [35].

$$\Delta\varphi = 2.\pi/\Lambda \times L/S.P$$

where L is the path length, S is the fiber part, and P is the optical power.

This results in a shift toward shorter wavelengths at the trailing edge of the signal (blue shift) as well as a shift toward longer wavelengths at the leading edge of the signal (red shift). Self-phase modulation (SPM) causes wavelength shifts opposite to that caused by positive chromatic dispersion. SPM can be used in advanced designs

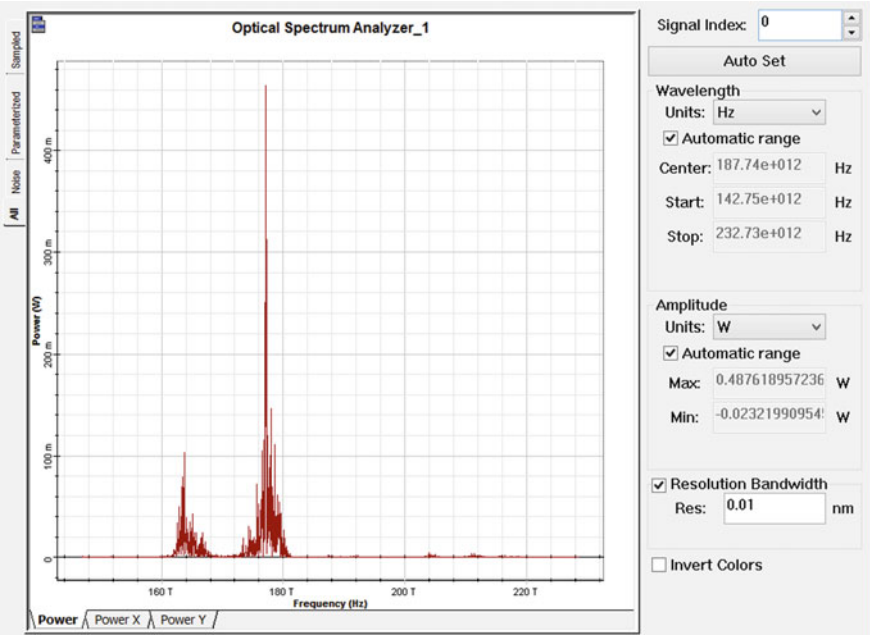

Fig. 4 Stimulated Raman scattering

of networks to partially compensate for the excitation of chromatic dispersion [36] (Fig. 5).

3.4 Cross-Phase Modulation (CPM)

Cross-phase modulation is the effect of signal on the same phase with another signal in the same channel as in SPM. Cross-phase modulation, XPM, occurs as a result of Kerr effect, although the effects of XPM only appear when multiple channels are sent to the same fiber. XPM makes shifts in frequency at the signal edges in the modulation channel, as in SPM, causing spectral expansion of the signal pulse [37] (Fig. 6).

3.5 Four-Wave Mixing (FWM)

This is the phenomenon of unwanted overlap which produces three signals of frequencies ($\lambda 123 = \lambda 1 + \lambda 2\_3\lambda$) known as ghosting channels where three different channels produce a fourth channel. A number of ways lead to different group speeds on

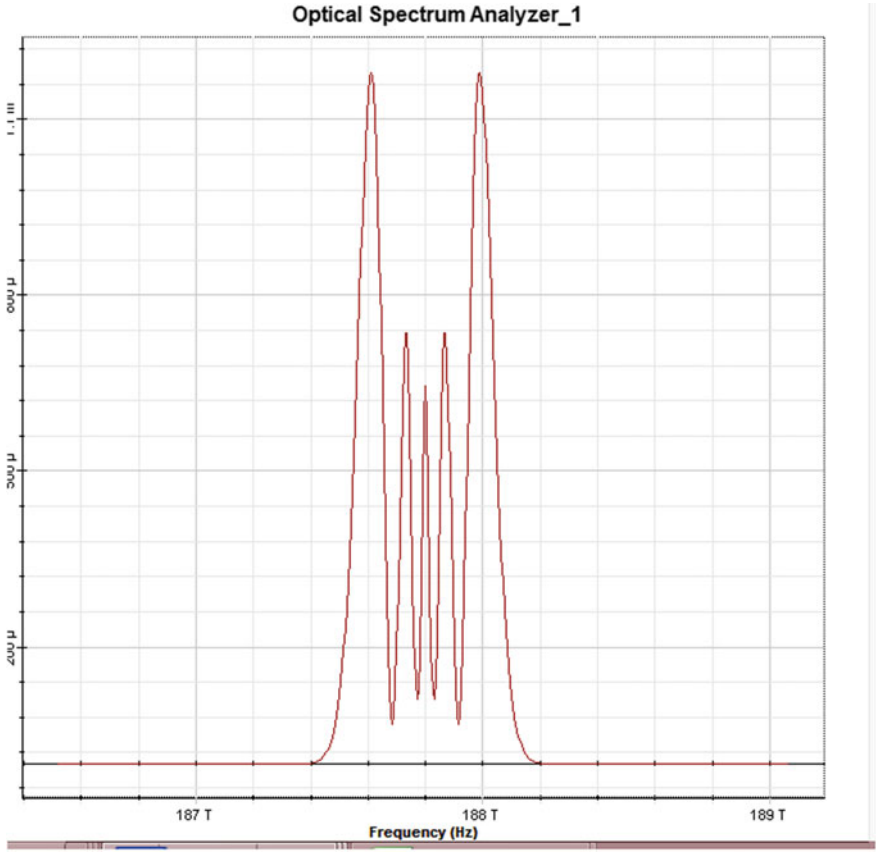

Fig. 5 Self-phase modulation

some waves and mitigate the effect of FWM. Using channels at irregular distances reduces the effects of FWM [38] (Fig. 7).

4 Data Modulation in Optical Communication Systems

In modern communication system, data are stored and transmitted digitally, represented by selected symbols of a limited alphabet. The digital data are modulated by linking each value to a specific reference signal. In this modulation, the data are stored in the transmitted signal phase. The most significant advantages of this mode are the high tolerance of noise at the receiver and greater tolerance of scattering compared to the on–off keying. However, this tolerance decreases with increasing modulation levels. When using more than one bit of the input signal a multi-level phase shift modulation M-PSK is obtained, where M is the number of levels $M =$

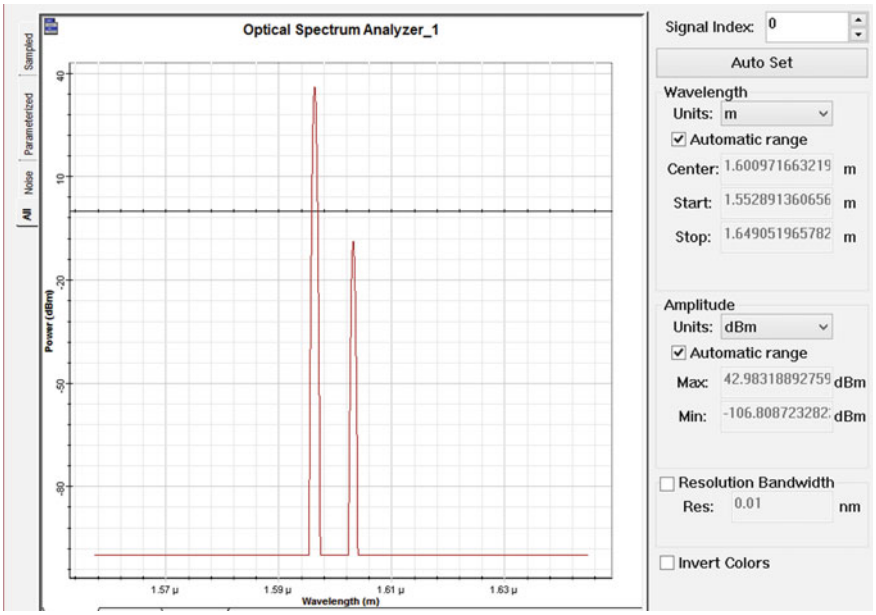

Fig. 6 Cross-phase modulation

2^m and m is the number of bits used to encode each sample of the input signal [39]. In this modulation, the amplitude and phase can take more than one value, allowing for the largest possible number of levels or values. Given that the number of possible amplitudes is KA and the number of possible phases is KP, the number of possible levels: $M = \mathrm{KA} \times \mathrm{KP}$. N which requires a number of bits [40].

$$N = \mathrm{Log2}M = \mathrm{Log2}(\mathrm{KA} \times \mathrm{KP})$$

5 DSP (Digital Signal Processing)

DSP is applied by using ADC with DSP circuits to eliminate noise. The transmitted data are recovered by DSP, and security links of signals and optical communications are enhanced by organizing the channels in terms of spacing and equal data distribution. Hence, DSP eliminates the effects of CD, BMD, and noise when the DSP is coupled with coherent detection. Then, the entire data of the incoming signal will be stored. Therefore, the receptor sensitivity will increase [41].

The Viterbi–Viterbi (VV) is implemented in the DSP circuit, which regulates the threshold level responsible for decoding the signals and converting them into sequence of bit streams at the output. Hence, the researcher in the current study

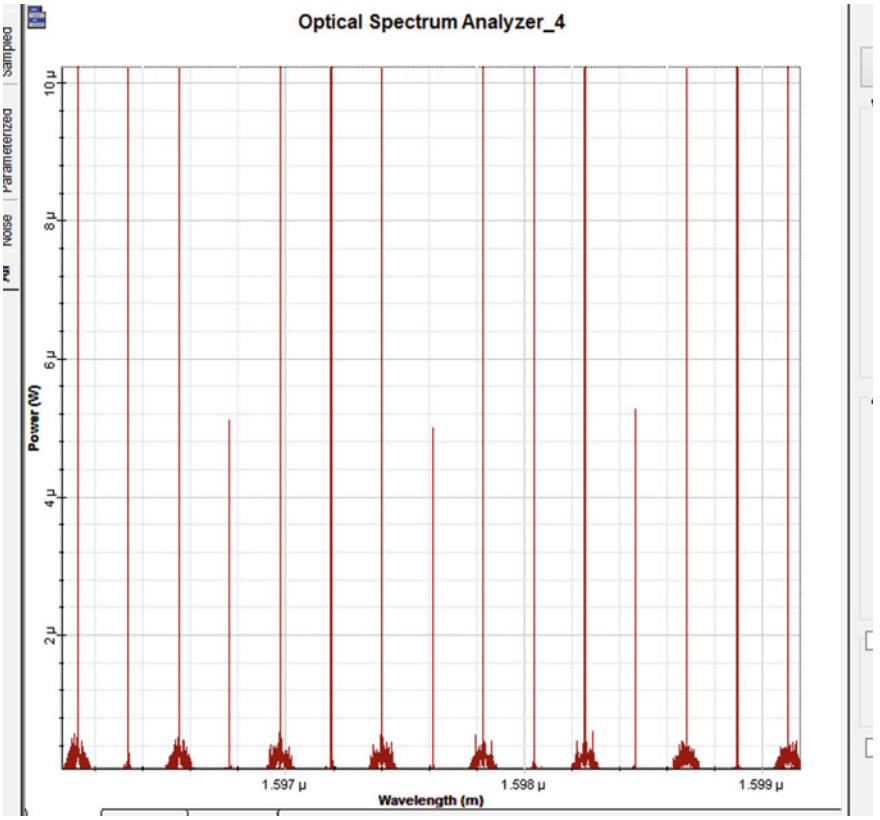

Fig. 7 Four-wave mixing (FWM)

applies DSP for optical modulation of radio frequency (RF) signal producing electro-optic modulation. This electro-optic modulation is responsible for phase distortions and nonlinear effects. The DSP is the most effective method to boost the signals and control the polarization status. Therefore, when controlling the polarization of the transmitted data, the DSP facilitates the process of maintaining polarization. It is worth mentioning that the DSP has different phases to recover the polarized optical signal. After processing, the signals are passed through filters. Then, the filtered signals are reconstructed by interpolation. In turn, the signals are passed through compensation of quadratic imbalance (QI), causing the amplitude and phase imbalances in the phase as well as the quadratic signals (Q) to diminish [42, 43].

6 Architecture of the DSP Optical System

In general, the structure of the DSP optical system is responsible for retrieving signals when they are weak. DSP systems provide significant enhancements for signal processing especially regarding the transceivers performance. To cope with high data rates, these enhancements of SDP systems provide new solutions for many technological problems as shown in Figs. 8 and 9.

After processing, the input bits in the transmitter are converted into four waveforms compatible with the components of phase (I), quadratic (Q), and X and Y polarizations. Branches I and Q belong to the components of orthogonal polarization which in turn belong to a quadratic-channel optical modulator. At this point, they create multi-level modulations, (I) and (Q), are [44]: TX DSP ADCMOD ADCRX DSP ADCSSMF EDFE. The PN was structured by electrical signals, which should be multi-level generated in the DACs. After this optical modulation, two modulations are passed to the polarizing beam combiner (PBC) to combine the orthogonal polarizations. Then, the optical signal will be launched through the channel and amplifiers. Channels consist of various distances of standard single-mode fiber (SSMF). DSP power can be applied in a transmitter, receiver, or both.

In the transmitter, DSPs and DACs are combined to achieve extra flexibility, to compensate for the optical signal that was previously modulated. In this process, the bone mineral density (BMD), compact disk (CD), inelastic scattering, and nonlinear disabilities will be compensated. In addition, DCPs and DACs can perform efficient

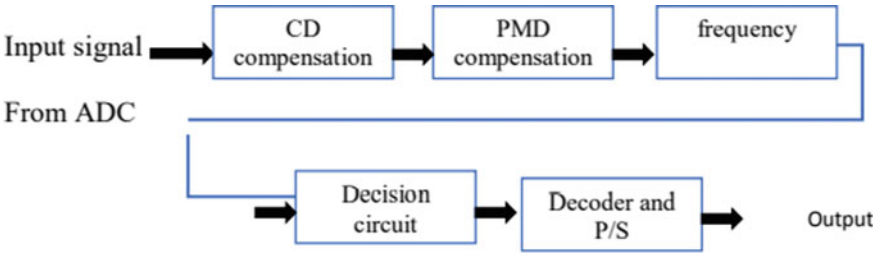

Fig. 8 DSP block diagram

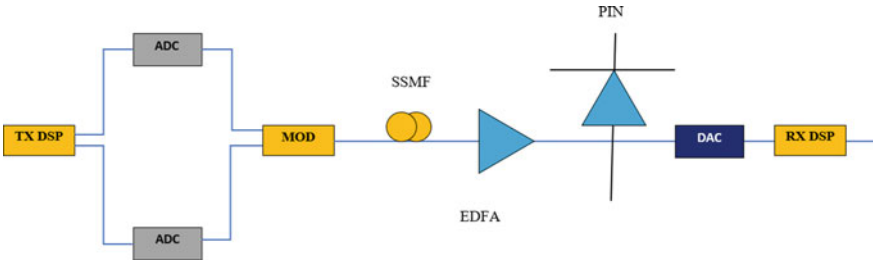

Fig. 9 System architecture Tx and Rx DSP

spectral transmission by tuning a multi-level electrical signal and by modulating a fitting signal pulse at the output of the DACs [45].

7 Types of Filters

A Bessel filter provides the maximum flat transmission delay or group delay across the frequency spectrum. However, the rolling rate from pass band to stop band is slow compared to other filters of the same order. It is the most commonly used filter due to its linear phase properties. For the square wave input, this filter does not produce any bypass because all frequencies are delayed by the same value [46]. These are considered ideal filters. They have a smooth transfer function with no scattering. Moreover, it has a landing time and an attenuated rise time. The rectangle filter has no pass band attenuation. Also, it has a random attenuation that exceeds the bandwidth. It is an ideal filter with phase response and flat volume [47]. Rectangle optical filter is an ideal optical filter for time domain. It is considered the least delayed filter. Rectangle optical filters reduce noise in signals with minimal time spent falling and rising without any gaps. These filters offer to adjust the frequency domain from 50 MHz to 4 GHz with an accuracy of less than 15 MHz. The completely rectangular shape of this filter is realized by using digital control in spectral line feedback of the comb-like pump. The pass band of the filter is suppressed to ~1 dB by reducing the nonlinear effects of the spectral lines in the comb-like pump. These spectrum lines are created in electrical expansions and optical fibers [48].

8 Performance Evaluation Parameters

These parameters are the basis of evaluating the performance of system. Three of them were used in the current study. Q-factor is the parameter which defines the minimum signal-to-noise ratio determining the bit error rate of a given any given [49]. Bit error rate (BER) determines the amount of bit errors of the total bits transmitted. The bit error rate defines the relationship between bit errors and the total of bits transmitted in terms of rate. Hence, a low bit error means that the system is functioning well.

There are various factors that could influence the bit error rate (BER) such as noise, attenuation, scattering, nonlinearity, neighboring channel interference, jitter as well as bit synchronization problems. The (BER) performance can be promoted when a strong signal is released into the transmission system. But, if the release of a strong signal causes problems such as crosstalk, then alternative methods should be used. These methods could be channel coding or strong modulation scheme. The bit error rate is calculated according to the following equation [50]: BER = NE/NT. Eye diagram is a graphical representation that shows the quality of the signal in a visual method. It shows the signals as overlapping circles. According to the eye diagram, the inter-symbol interference (ISI), noise ratio, and signal periodicity can

be evaluated. Power budget is used to measure the power that determines the total values of allowable attenuation between transmitting power and sensitivity power. Basically, the power budget evaluates the losses of the system at each stage such as distance attenuation, total losses of conductors, fusion splice losses, and losses of coexistence element (CE). The power budget is determined by the optical path losses (OPL). On the other hand, OPL is specified by the standards ITU-T for XG-PON and NG-PON2 systems. Error vector magnitude (EVM) or *error vector size* shows the inconsistency between the perfectly modulated reference signals. The EVM also measures the ratio of the size change to phase errors, which correspond directly to the volume and phase change between the measured and reference signals.

9 Results

Most researchers of RoF nonlinear effects used various compensation techniques, including the digital signal processing technology. They used nonlinear filters and improved them by MATLAB software, in particular, Yu-Han Hun who used MATLAB, resulting in a well operating proposed system at (BER = 1.9 * 10^-6 and 7.8 EVM). However, the researcher of the current study establishes that most of these studies in the last five years (2017–2021) had experienced problems with optical fibers, especially the nonlinear effects due to the development of future generations such as the third generation, which was established in 2015, and the fifth generation, which handles data rate of greater than 80 Gb/s. Most researchers studied the flexible effects (XPM SPM FWM) within different transmission distances from 100 to 300 km, except for the Mohamed Ahmed (2020), who studied all the elastic and inelastic effects. However, he studied them within very short distances (100 km) at a transmission data rate of (40 Gb/s). Therefore, more research is required to study all the elastic and inelastic effects at long transmission distances for users of the next generation of optical communications, in addition to fulfilling the requirements of the current era, which is the Internet of Things, by finding and improving new filters.

References

1. Jiang, D., & Liu, G. (2017). An overview of 5G requirements. *5G Mobile Communications*, 3–26.
2. Akyildiz, I. F., Nie, S., Lin, S.-C., & Chandrasekaran, M. (2016). 5G roadmap: 10 key enabling technologies. *Computer Networks, 106*, 17–48.
3. Deng, Y., Li, Y., Seet, R., Tang, X., & Cai, W. (2017). The server allocation problem for session-based multiplayer cloud gaming. *IEEE Transactions of Multimedia, 20*(5), 1233–1245.
4. Kamalinejad, P., Mahapatra, C., Sheng, Z., Mirabbasi, S., Leung, V. C. M., & Guan, Y. L. (2015). Wireless energy harvesting for the Internet of Things. *IEEE Communications Magazine, 53*(6), 102–108.

5. Hilario-Tacuri, A., Maldonado, J., Revollo, M., & Chambi, H. (2021). Bit error rate analysis of NOMA-OFDM in 5G systems with nonlinear HPA with memory. *IEEE Access, 9*, 83709–83717.
6. Alimi, I. A., Teixeira, A. L., & Monteiro, P. P. (2017). Toward an efficient C-RAN optical fronthaul for the future networks: A tutorial on technologies, requirements, challenges, and solutions. *IEEE Communications Surveys & Tutorials, 20*(1), 708–769.
7. König, L. (2019). *Analysis of a robot welding system and possible concepts for improvement for a Norwegian SME*. NTNU.
8. Benner, A. F., Ignatowski, M., Kash, J. A., Kuchta, D. M., & Ritter, M. B. (2005). Exploitation of optical interconnects in future server architectures. *IBM Journal of Research and Developments, 49*(4.5), 755–775.
9. Kalfas, G., et al. (2019). Next generation fiber-wireless fronthaul for 5G mmWave networks. *IEEE Communications Magazine, 57*(3), 138–144.
10. Brackett, C. A., et al. (1993). A scalable multiwavelength multihop optical network: A proposal for research on all-optical networks. *Journal of Lightwave Technology, 11*(5/6), 736–753.
11. Musumeci, F., et al. (2018). An overview on application of machine learning techniques in optical networks. *IEEE Communications Surveys & Tutorials, 21*(2), 1383–1408.
12. Ganeev, R. A., et al. (2004). Nonlinear refraction in CS2. *Applied Physics B, 78*(3), 433–438.
13. Imran, M., Anandarajah, P. M., Kaszubowska-Anandarajah, A., Sambo, N., & Potí, L. (2017). A survey of optical carrier generation techniques for terabit capacity elastic optical networks. *IEEE Communications Surveys & Tutorials, 20*(1), 211–263.
14. Menber, T. (2020). Performance evaluation and comparison of optical amplifiers in non-linear effects for long-haul transmission system.
15. Asha, D. S. (2021). A comprehensive review of Millimeter wave based radio over fiber for 5G front haul transmissions. *Indian Journal of Science and Technology, 14*(1), 86–100.
16. Dat, P. T., Kanno, A., Umezawa, T., Yamamoto, N., Kawanishi, T. (2017). Millimeter- and terahertz-wave radio-over-fiber for 5G and beyond. In *2017 IEEE Photonics Society Summer Topical Meeting Series (SUM)* (pp. 165–166).
17. Garg, D., & Nain, A. (2021). Next generation optical wireless communication: A comprehensive review. *Journal of Optical Communications*.
18. Kebe, M., Gadhafi, R., Mohammad, B., Sanduleanu, M., Saleh, H., & Al-Qutayri, M. (2020). Human vital signs detection methods and potential using radars: A review. *Sensors, 20*(5), 1454.
19. Lin, C.-T., Chen, J., Shih, P.-T., Jiang, W.-J., & Chi, S. (2010). Ultra-high data-rate 60 GHz radio-over-fiber systems employing optical frequency multiplication and OFDM formats. *Journal of Lightwave Technology, 28*(16), 2296–2306.
20. Gaydos, C. A., & Quinn, T. C. (2005). Urine nucleic acid amplification tests for the diagnosis of sexually transmitted infections in clinical practice. *Current Opinion in Infectious Diseases, 18*(1), 55–66.
21. Zhang, X., Bian, Z., Yuan, X., Chen, X., & Lu, C. (2020). A review on the effects of light-emitting diode (LED) light on the nutrients of sprouts and microgreens. *Trends in Food Science & Technology, 99*, 203–216.
22. Zhong, H., Duan, T., Lan, H., Zhou, M., & Gao, F. (2018). Review of low-cost photoacoustic sensing and imaging based on laser diode and light-emitting diode. *Sensors, 18*(7), 2264.
23. Alsos, I. G., et al. (2007). Frequent long-distance plant colonization in the changing Arctic. *Science, 316*(5831), 1606–1609.
24. Wen, J., Arakawa, T., & Philo, J. S. (1996). Size-exclusion chromatography with on-line light-scattering, absorbance, and refractive index detectors for studying proteins and their interactions. *Analytical Biochemistry, 240*(2), 155–166.
25. Baeg, K., Binda, M., Natali, D., Caironi, M., & Noh, Y. (2013). Organic light detectors: Photodiodes and phototransistors. *Advanced Materials, 25*(31), 4267–4295.
26. Li, Y., Jiang, X., Zhao, G., &Yang, L. (2018) Whispering gallery mode microresonator for nonlinear optics. arXiv Prepr. arXiv1809.04878.

27. Xiong, W.-W., Chen, J.-Q., Wu, X.-C., & Zhu, J.-J. (2015). Visible light detectors based on individual $ZrSe_3$ and $HfSe_3$ nanobelts. *Journal of Material Chemistry C, 3*(9), 1929–1934.
28. Sasikala, V., & Chitra, K. (2018). All optical switching and associated technologies: A review. *Journal of Optics, 47*(3), 307–317.
29. Jack, M. W., Collett, M. J., & Walls, D. F. (1995). Enhanced squeezing due to the influence of two instabilities. *Physical Review A, 51*(4), 3318.
30. Sirleto, L., & Ferrara, M. A. (2020). Fiber amplifiers and fiber lasers based on stimulated Raman scattering: A review. *Micromachines, 11*(3), 247.
31. Marhic, M. E., Andrekson, P. A., Petropoulos, P., Radic, S., Peucheret, C., & Jazayerifar, M. (2015). Fiber optical parametric amplifiers in optical communication systems. *Laser & Photonic Review, 9*(1), 50–74.
32. Davoodi, F., & Granpayeh, N. (2012). All optical logic gates: A tutorial. *International Journal of Information and Communication Technology Research, 4*(3), 65–98.
33. Cotter, D. (1983). Stimulated Brillouin scattering in monomode optical fiber. *Journal of Optical Communication, 4*(1), 10–19.
34. Ajmani, M., & Singh, P. (2015). FWM in WDM system, effects and techniques to minimize: A review. In *2015 Fifth International Conference on Advanced Computing & Communication Technologies* (pp. 385–389).
35. Liao, Y., Song, C., Xiang, Y., & Dai, X. (2020). Recent advances in spatial self-phase modulation with 2D materials and its applications. *Annalen der Physik, 532*(12), 2000322.
36. Tantawy, M., & Abdel-Gawad, H. I. (2020). On multi-geometric structures optical waves propagation in self-phase modulation medium: Sasa-Satsuma equation. *The European Physical Journal Plus, 135*(11), 1–10.
37. Folick, A., Min, W., & Wang, M. C. (2011). Label-free imaging of lipid dynamics using Coherent Anti-stokes Raman Scattering (CARS) and Stimulated Raman Scattering (SRS) microscopy. *Current Opinion in Genetics & Development, 21*(5), 585–590.
38. Abed, H. J., Din, N. M., Al-Mansoori, M. H., Fadhil, H. A., & Abdullah, F. (2013). Recent four-wave mixing suppression methods. *Optik (Stuttg), 124*(15), 2214–2218.
39. Tsividis, Y. (2010). Event-driven data acquisition and digital signal processing—A tutorial, IEEE Trans. *IEEE Transactions on Circuits Systems II: Express Briefs, 57*(8), 577–581.
40. El-Nahal, F. (2018). Coherent 16 quadrature amplitude modulation (16QAM) optical communication systems. *Photonics Letters of Poland, 10*(2), 57–59.
41. Agrell, E., et al. (2016). Roadmap of optical communications. *Journal of Optics, 18*(6), 63002.
42. Bennett, G., Wu, K.-T., Malik, A., Roy, S., & Awadalla, A. (2014). A review of high-speed coherent transmission technologies for long-haul DWDM transmission at 100G and beyond. *IEEE Communications Magazine, 52*(10), 102–110.
43. Zhao, J., Liu, Y., & Xu, T. (2019). Advanced DSP for coherent optical fiber communication. *Applied Sciences, 9*(19), 4192.
44. Liu, X., Chandrasekhar, S., & Winzer, P. J. (2014). Digital signal processing techniques enabling multi-Tb\/s superchannel transmission: An overview of recent advances in DSP-enabled superchannels. *IEEE Signal Processing Magazine, 31*(2), 16–24.
45. Bower, P., & Dedic, I. (2011). High speed converters and DSP for 100G and beyond. *Optical Fiber Technology, 17*(5), 464–471.
46. Ip, E., Lau, A. P. T., Barros, D. J. F., & Kahn, J. M. (2008). Coherent detection in optical fiber systems. *Optics Express, 16*(2), 753–791.
47. Liu, Y., Choudhary, A., Marpaung, D., & Eggleton, B. J. (2020). Integrated microwave photonic filters. *Advances in Optics and Photonics, 12*(2), 485–555.
48. Afshari, H. H., Gadsden, S. A., & Habibi, S. (2017). Gaussian filters for parameter and state estimation: A general review of theory and recent trends. *Signal Processing, 135*, 218–238.
49. Matzik, A., & Anwar, S. (2016). Review of electrical filters. *International Journal of Innovative Science Engineering and Technology, 3*(4), 543–556.
50. Anwarsha, A., & Narendiranath Babu, T. (2022). A review on the role of tunable Q-factor wavelet transform in fault diagnosis of rolling element bearings. *Journal of Vibration Engineering & Technologies*, 1–16.

An IoT Solution Designed for Remote Automatic Control and Supervisor Systems to Key Environmental Factors and Diseases in Coffee Farms in Vietnam

Thang Long Vu and Van Duy Nguyen

Abstract Growth and development of the coffee plant depend on many environmental and management factors that must be continuously supervised and controlled. However, most of the coffee farms in Vietnam do not have any remote automatic control and supervisor systems for them. The care of coffee plants fully depends on weather and farmer experience, which have caused many issues and challenges such as low quantity, poor quality, and common pests. The present study describes the design of local network architecture of data acquisition controllers from the environmental sensors and cameras used for measuring, monitoring, and recording environmental parameters such as temperature and humidity as well as image of coffee leaves damaged due to disease. The slave controllers collect data and transfer them to a master controller through the Lora network, so that the master can send data to server using Internet. The slave controller also controls the actuator such as water pump and electrical fan to keep the environmental parameters within a suitable range. This design is the base to fabricate the real systems and experiments in coffee farms in Western Highlands of Vietnam later.

Keywords IoT · Coffee disease · Coffee farm · Environmental factor

1 Introduction

The coffee plays an important role in the agriculture economy in Vietnam. Currently, Vietnam is the world's second-largest coffee exporter, behind only Brazil. In 2021, the export value for Vietnam's coffee reached US$3.1 billion. However, Vietnam has been facing many challenges in the whole coffee supply chain such as climate change, low productivity, and quality, as well as the excessive use of fertilizing products and

T. L. Vu (✉)
Faculty of Transportation Engineering, Nha Trang University, Nha Trang City, Vietnam
e-mail: longvt@ntu.edu.vn

V. D. Nguyen
Insititute of Biotechnology and Environment, Nha Trang University, Nha Trang City, Vietnam
e-mail: duynv@ntu.edu.vn

T. D. L. Nguyen and J. Lu (eds.), *Machine Learning and Mechanics Based Soft Computing Applications*, Studies in Computational Intelligence 1068,
https://doi.org/10.1007/978-981-19-6450-3_27

irrigations. Especially, most of the farmers in coffee farms have not been supported by automatic control technology.

The coffee yield, supply chain traceability, and quality control can be increased by using IoT systems to make the agriculture more intelligent. Until now, many authors focus on low range-based IoT devices such as Bluetooth [1], IEEE 802.11 and IEEE 802.15.4 [2, 3], and long range-based IoT devices such as LTE [4, 5], narrowband (NB) [6–9], and Sigfox [6–8]. Some others [10–12] use a small number of industrial or laboratory sensors to measure environmental parameters such as temperature, humidity, and pH level, and these systems cannot satisfy the real requirements or cannot deploy in the field [13, 14].

However, in recent years, the researchers have applied Lora devices into IoT [15–17]. The important advantage of LoRa in comparison with NB IoT or Sigfox is the cost, NB IoT, and Sigfox require a monthly fee, but a LoRaWAN is free if it is set up at the unlicensed band. So, LoRa is an excellent selection for the wireless interface to the Internet for remote automatic agriculture supervisor and control system. Besides, most areas of Western Highlands of Vietnam do not have reasonable speed in Internet connectivity and low Internet coverage, so the low-range communication modules are not suitable. Therefore, the present study focuses on the design of local network architecture of data acquisition controllers from the environmental sensors and cameras used for measuring, monitoring, and recording environmental parameters by using LoRa communication module that assists in long-range free-of-cost communication.

2 Design Methodology

To set up the digital transformation platform for coffee supply chain, two main components were designed: IoT devices using LoRa waves [18] and AI. In particular, the LoRa plays the role of continuously collecting data such as potential of hydrogen (pH), oxidation–reduction potential (ORP), electrical conductivity (EC), water temperature, air temperature, humidity, light intensity, and NPK. AI recognizes the images via camera in order to output advice about cultivation, harvest, pest and disease prevention, etc. The data collected are sent back to the computer database for processing. This platform provides real-time information about the cultivating regions.

In the present research, IoT devices using LoRa waves were designed based on the step-by-step approach with key steps as follows:

Step 1: Purpose and Requirements Specification

The system purpose, behavior, and requirements were captured.

Step 2: Process Specification

The use cases of the IoT system were formally described based on and derived from the purpose and requirement specifications.

Step 3: Domain Model Specification

The domain model was defined to describe the main concepts, entities, and objects in the domain of IoT system to be designed.

Step 4: Information Model Specification

Information Model Specification was described with the structure of all the information in the IoT system.

Step 5: Service Specifications

Service specifications were defined as the services in the IoT system, service types, service inputs/output, service endpoints, service schedules, service preconditions, and service effects.

Step 6: IoT Level Specification

IoT Level Specification was defined as the IoT level for the system.

Step 7: Functional View Specification

The Functional View was described with the functions of the IoT systems grouped into various Functional Groups. Each Functional Group either provides functionalities for interacting with instances of concepts defined in the Domain Model or provides information related to these concepts.

Step 8: Operational View Specification

Many options pertaining to the IoT system deployment and operation were defined, including service hosting options, storage options, device options, and application hosting options.

Step 9: Device and Component Integration

The devices and components were integrated in this step.

Step 10: Application Development in a coffee farm

The final step in the IoT design methodology is to develop the IoT application. We deployed 5 LoRa mesh networking devices over a 70 m $\times$ 70 m area of a coffee farm in Western Highlands, Vietnam, and installed a gateway that collected data at 15-min intervals through LoRa waves.

3 Results and Discussion

The present study focuses on the design of IoT modules deployed in the coffee farm using LoRa devices in Western Highlands of Vietnam. In order to satisfy many different requirements, the IoT systems include three kinds of modules such as Water Quality Monitoring Module, Environmental Parameter Monitoring Module, and Water Flow Monitoring and Pump Control Module.

3.1 Water Quality Monitoring Module

This module is equipped a potential of hydrogen (pH) sensor, an oxidation–reduction potential (ORP) sensor, an electrical conductivity (EC) sensor, and a water temperature sensor. The industrial sensors are chosen based on the real conditions in Vietnam. Their specifications are shown in Table 1.

This module is powered by a solar energy electricity and a battery shown in Fig. 2. On the sunny day, the solar energy will supply for the module and charge to the battery, and in the evening and on the rainy day, the battery will provide the current for it.

Based on the specifications of all devices in Table 1, the interface between these devices and MCU (ESP32) is described in Fig. 3.

3.2 Environmental Parameter Monitoring Module

This module is used to monitor environmental parameters including water temperature, air temperature, air and soil humidity, light intensity, and NPK. Similarly, the industrial sensors are also chosen based on the real conditions in Vietnam. Their specifications are shown in Table 2.

Based on the specifications of all devices in Table 2, the interface between these devices and MCU (ESP32) is described in Fig. 4.

3.3 Water Flow Monitoring and Pump Control Module

This module controls two pump motors and three magnetic valves and measures water flow and the level of water in the water reservoir. The pump motor is controlled by a magnetic contactor through a relay module. The first motor is used to extract underground water from the reservoir, and the second is used to deliver water to the coffee tree. The flow sensor is used to measure water flow. The ultra-sonic sensor is used to measure the water level in the reservoir. The specifications of devices are shown in Table 3.

Based on the specifications of all devices in Table 3, the interface between these devices and MCU (ESP32) is described in Figs. 5 and 6.

Table 1 Water quality monitoring module devices

Name	Function	Specifications
SX 1278	Ultra-Low Power Long-Range Transceiver	168 dB maximum link budget + 20 dBm - 100 mW constant RF output vs. V supply Programmable bit rate up to 300 kbps High sensitivity: down to -146.5 dBm Low RX current of 10 mA, 200 nA register retention FSK, GFSK, MSK, GMSK, LORA, and OOK modulations
SEN0169-V2	Measuring potential of hydrogen	**Signal conversion board** Supply voltage: 3.3–5.5 V Output voltage: 0–3.0 V Signal connector: PH2.0-3P Measurement accuracy: ±0.1@25 °C Dimension: 42 mm * 32 mm/1.66 * 1.26 in Analog signal **pH probe** Probe type: Industrial Grade Detection range: 0–14 Temperature range: 0–60 °C Accuracy: ±0.1pH (25 °C) Response time: <1 min
SEN0464	Measuring oxidation–reduction potential	**ORP signal converter** Input voltage: 5 V Input signal: 0.5 V–4.5 V Measuring range: −2000 mV to + 2000 mV Output interface: PH2.0–3Pin **Industrial ORP probe** Indicator electrode: Platinum Reference electrode: silver-silver chloride Suitable temperature: 5–70 °C Electrode potential: 245–270 mV Reference electrode internal resistance: ≤ 10KΩ Electrode stability: ±8 mV/24 h
DFR0300	Measuring electrical conductivity	**Signal conversion board (transmitter) V2** Supply voltage: 3.0–5.0 V Output voltage: 0–3.4 V Signal connector: PH2.0–3Pin Measurement accuracy: ±5% F.S **Electrical conductivity probe** Probe type: Laboratory Grade Cell constant: 1.0 Support detection range: 0–20 ms/cm Recommended detection range: 1–15 ms/cm Temperature range: 0–40 °C

(continued)

Table 1 (continued)

Name	Function	Specifications
DS18B20	Measuring water temperature	Working voltage: 3–5.5 V Measuring temperature range: −10 to + 85 °C Operating temperature range: −55 to + 125 °C (−67 to 257 °F) Wire temperature resistance: −55 to + 125 °C Resolution: 9–12 bits Single-wire Interface: only one digital interface is needed for communication A 64-bit ID embedded in the chip Query time: ≤ 750 ms Wiring Instructions: red—VCC, black—GND, blue—DATA

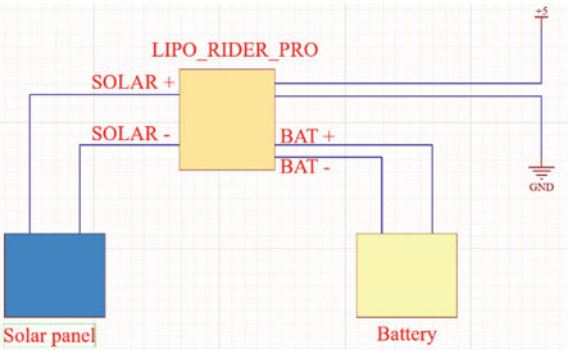

Fig. 2 The power supply

3.4 The Gateway (Central Module)

The gateway includes a LattePanda single board computer connected with Lora SX1278 in order to enable LoRaWAN communications. The gateway is also connected to Internet through Wi-Fi.

In order to collect images of coffee leaf, an industrial camera is mounted near a coffee tree and connected to the LattePanda to send image to cloud servers. An AI program is installed in cloud servers to analyze the image to predict coffee disease.

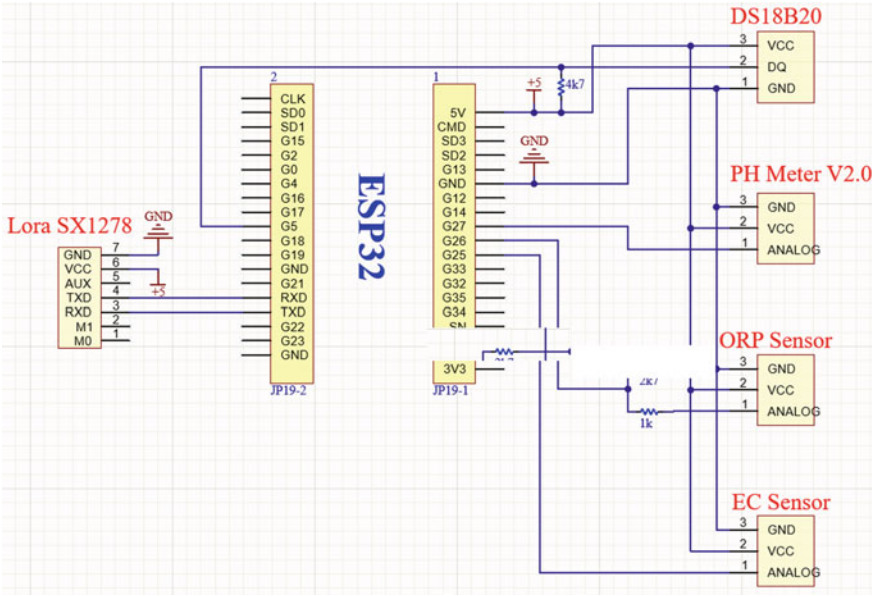

Fig. 3 The schematic of water quality monitoring module

3.5 The Complete Local Network Architecture Deployed in a Coffee Farm

By combining sensor nodes (Water quality monitoring module and Environmental parameter monitoring module), actuator nodes (Pump control module), and the gateway, the complete local network architecture is shown in Fig. 7.

3.6 Deployment Configuration in a Coffee Farm in Vietnam

To evaluate the results, an experimental area of 70 m × 70 m in a coffee farm in Western Highlands, Vietnam, was divided into 3 regions to test with 3 different farming care conditions. The deployment configuration of IoT system is shown in Fig. 8.

The yellow circle is the well, and the white polygon is the reservoir. Water is pumped by a Submersible Pump to the reservoir. At the reservoir, manure will be mixed in a certain ratio. The water level at the reservoir is determined through the level sensor SEN0246 to calculate the current volume of water in the reservoir as a basis for mixing manure.

After mixing, the water continues to be pumped by the 2nd Pump to the crop areas. On 3 water pipes, there are 3 solenoid valves to open and close water to the

Table 2 Environmental parameter monitoring module devices

Name	Function	Specifications
SHT35	Measuring air temperature and humidity	Wide supply voltage range, from 2.4 to 5.5 V 10–90% ratiometric analog voltage output Typical accuracy of ±2%RH and ±0.3 °C
Soil moisture sensor	Measuring soil moisture	Operating Voltage: 3.3V to 5V DC Operating Current: 15mA Output Digital - 0V to 5V, Adjustable trigger level from preset Output Analog - 0V to 5V based on infrared radiation from fire flame falling on the sensor
S-Light-02	Measuring light intensity	RS485 Modbus-RTU and analog voltage 0–2 V output interface 3.9–30 V DC power supply 7 mA @ 24VDC power consumption −40 to 85 °C operating temperature range Operating Temperature: −40 to 85 °C
DS18B20	Measuring water temperature	Shown in Table 1
Soil NPK Sensor	Measuring nitrogen, phosphorus, potassium	Model: RS-NPK-*-TR Power supply: 5-30VDC Maximum power consumption: ≤ 0.15 W Operating temperature: −40 to 80 °C Range: 0–1999 mg/kg(mg/L) Resolution: 1 mg/kg(mg/L) Precision: ±2%FS Response time: ≤1S Output signal: RS485/4-20ma/0-5v/0-10v

corresponding area. The volume of irrigation water is measured by the G5/4 inch Water Flow sensor located right behind the 2nd Pump.

System operation: The signals from the water quality sensor are sent to the Water Quality Monitoring Module (ESP32) at each region, and the environmental parameter sensors are sent to the Environmental Parameter Monitoring Module (ESP32). These two sets will be sent to the Central Module (Gateway) through Lora. Gateways perform 2 tasks:

- Transfer the received value to Cloud Servers to display on user system via Web Server or App on smart device (Smartphone).

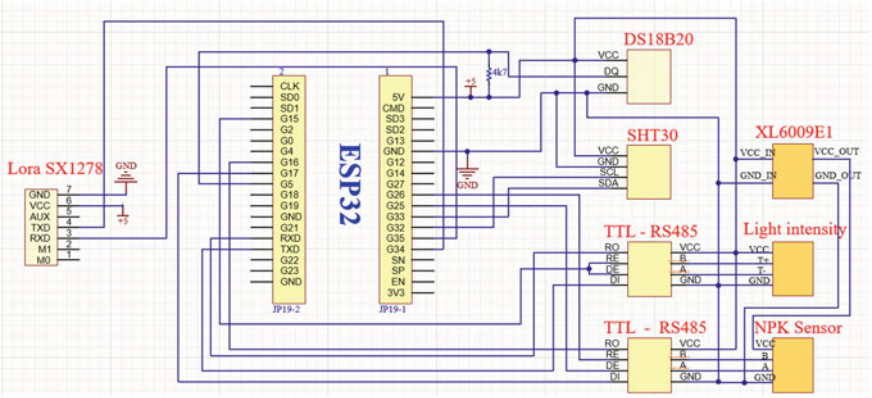

Fig. 4 The schematic of environmental parameter monitoring module

Table 3 Water flow monitoring and pump control module devices

Name	Function	Specifications
SEN0246	Measuring water level in the tank	Power supply: 9–24VDC Rated power: 4.8 W Operating temperature range: − 10 to +70 °C Effective detection range: 70 to 1500 cm Resolution: 1 cm Accuracy: 1% Communication interface: RS485
G5/4 inch water flow sensor	Measuring water flow	Mini. working voltage: DC 4.5 V Max. working current: 15 mA (DC 5 V) Working voltage: 5–24 V Flow rate range: 1–120 L/min Load capacity: ≤10 mA (DC 5 V) Operating temperature: ≤80 °C Operating humidity: 35–90%RH Water pressure: ≤ 2.0 MPa Storage temperature: −25 to + 80 °C Storage humidity: 25–95%RH

- Calculate, process signals, and determine the irrigation area and the amount of water, and then send control commands to the Water Flow Monitoring and Pump Control Module through Lora waves.

After receiving commands from Central Module (Gateway), Water Flow Monitoring and Pump Control Module will check the amount of water in the reservoir. If

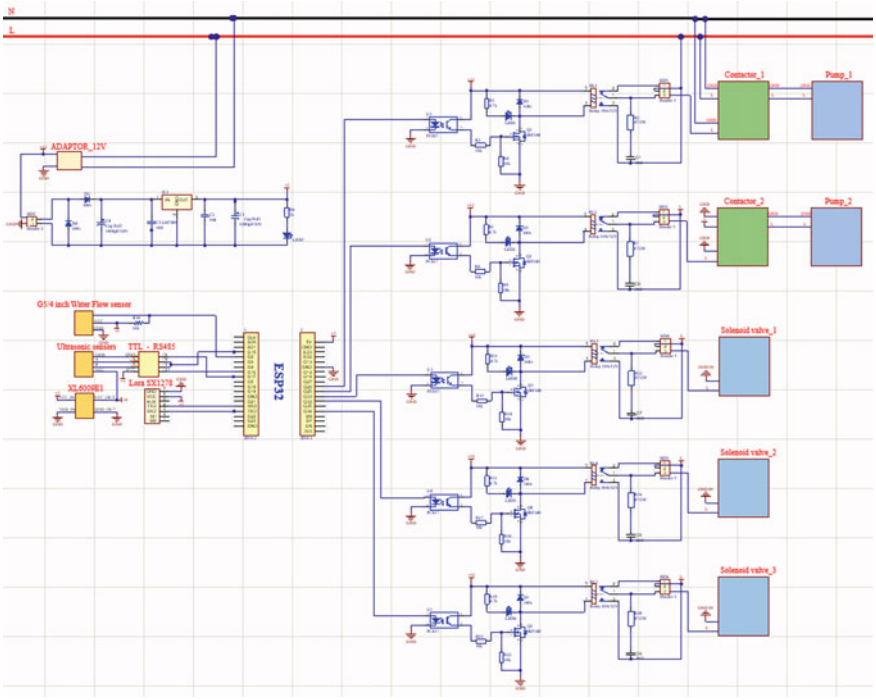

Fig. 5 The complete schematic of water flow monitoring and pump control module

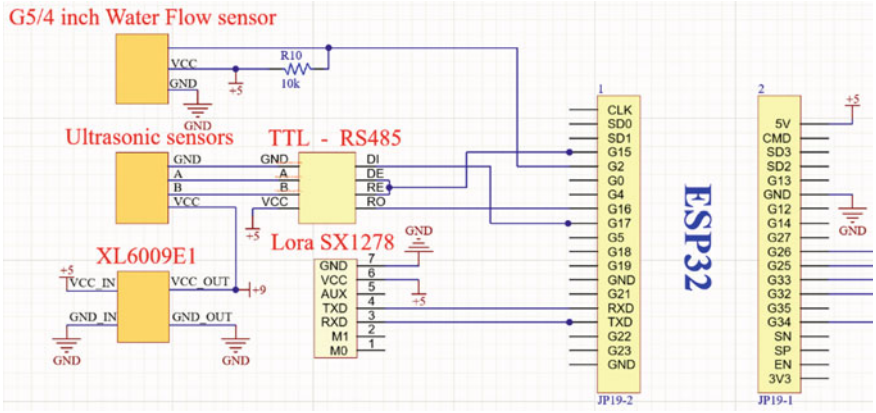

Fig. 6 The sensor node schematic of water flow monitoring and pump control module

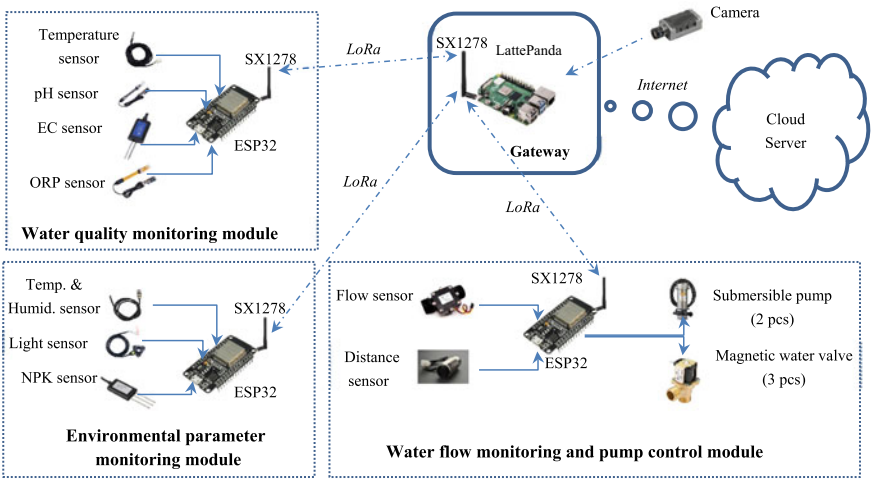

Fig. 7 The complete local network architecture

Fig. 8 Deployment configuration in a coffee farm in Western Highlands of Vietnam

the amount of water is still within the allowable range, it will open the 2nd Pump and the corresponding solenoid valves to the areas to be irrigated according to the Gateway's command. The G5/4 inch Water Flow sensor will measure the amount of water that has actually been irrigated, when there is enough water, the Water Flow Monitoring and Pump Control Module will disconnect the solenoid valve in that area

and continue to open the irrigation valve to the next zone. This process continues until all zones are irrigated according to the command from Gateway.

4 Conclusions and Future Work

The present research has shown a full IoT solution designed for remote automatic control and supervisor systems to key environmental factors and diseases in coffee farms in Vietnam. By using LoRa devices, the sensor nodes and actuator nodes can transfer and receive data to the gateway/master from very far distance in comparison with low range-based IoT system. In addition, it saves electric energy powered by solar energy electricity. This is very suitable for the real conditions in Western Highlands of Vietnam. This design has integrated the most numbers of sensors and used industrial sensors in comparison with other researches [10–12, 14]; thus, most of necessary parameters of water and environment are monitored. Because it can be deployed in the real coffee farm conditions, it can help the farmers give the right decisions for their farms. The irrigation and nutrient are controlled automatically to save water and make growing conditions suitable for the coffee plant.

Acknowledgements The present research is funded by Vingroup Innovation Foundation (VINIF) under Research Grant No. VINIF.2021.DA00047 to VDN.

References

1. Ilapakurti, A., & Vuppalapati, C. (2015). Building an IoT framework for connected dairy. In *Proceedings of the 2015 IEEE First International Conference on Big Data Computing Service and Applications*, Redwood City, CA, USA (pp. 275–285).
2. Liao, M. S., Chen, S. F., Chou, C. Y., Chen, H. Y., Yeh, S. H., Chang, Y. C., & Jiang, J. A. (2017). On precisely relating the growth of phalaenopsis leaves to greenhouse environmental factors by using an IoT-based monitoring system. *Computers and Electronics in Agriculture*, 125–139.
3. Truong, T., Dinh, A., & Wahid, K. (2017). An IoT environmental data collection system for fungal detection in crop fields. In *Proceedings of the 2017 IEEE 30th Canadian Conference on Electrical and Computer Engineering (CCECE)*, Windsor, ON, Canada (pp. 1–4).
4. Trilles, S., Torres-Sospedra, J., Belmonte, A., Zarazaga-Soria, F. J., Gonzalez-Perez, A., & Huerta, J. (2019). Development of an open sensorized platform in a smart agriculture context: A vineyard support system for monitoring mildew disease. *Sustainable Computing: Informatics and Systems*.
5. Edwards-Murphy, F., Magno, M., Whelan, P. M., OHalloran, J., & Popovici, E. M. (2016). b+WSN: Smart beehive with preliminary decision tree analysis for agriculture and honey bee health monitoring. *Computers and Electronics in Agriculture*, 211–219.
6. Aldahdouh, K. A., Darabkh, K. A., & Al-Sit, W. (2019). A survey of 5G emerging wireless technologies featuring LoRaWAN, Sigfox, NB-IoT and LTE-M. In *Proceedings of the IEEE International Conference on Wireless Communications Signal Processing and Networking (WiSPNET)*, Chennai, India (pp. 561–566).

7. Olatinwo, S. O., & Joubert, T.-H. (2019). Enabling communication networks for water quality monitoring applications: A survey. *IEEE Access, 7*, 100332–100362.
8. Popli, S., Jha, R. K., & Jain, S. (2018). A survey on energy efficient narrowband internet of things (NBIoT): Architecture, application and challenges. *IEEE Access, 7*, 16739–16776.
9. Martinez, B., Adelantado, F., Bartoli, A., & Vilajosana, X. (2019). Exploring the performance boundaries of NB-IoT. *IEEE Internet of Things Journal, 6*, 5702–5712.
10. Navarro-Hellín, H., Martinez-del Rincon, J., Domingo-Miguel, R., Soto-Valles, F., & Torres-Sánchez, R. (2016). A decision support system for managing irrigation in agriculture. *Computers and Electronics in Agriculture, 124*, 121–131.
11. Hoogenboom, G., Jones, J., Wilkens, P., Porter, C., Batchelor, W., Hunt, L., Boote, K., Singh, U., Uryasev, O., Bowen, W., et al. (2022). *Decision support system for agrotechnology transfer version 4.0*; University of Hawaii: Honolulu, HI, USA, 2004; *Sustainability*, *14*, 827 19 of 20.
12. Tahri, M., Maanan, M., Tahri, H., Kašpar, J., Purwestri, R. C., Mohammadi, Z., & Marušák, R. (2021). New Fuzzy-AHP Matlab based graphical user interface (GUI) for a broad range of users: Sample applications in the environmental field. *Computers & Geosciences, 158*, 104951.
13. Kökten, E., Çalıskan, B. C., Karamzadeh, S., & Soyak, E. G. (2020). Low-powered agriculture IoT systems with LoRa. In *Proceedings of the IEEE Microwave Theory and Techniques in Wireless Communications (MTTW)*, Riga, Latvia, 1–2 October (pp. 178–183).
14. Kodali, R. K., Yerroju, S., & Sahu, S. (2018). *Smart farm monitoring using LoRa enabled IoT*. IEEE. 978-1-5386-5657-0/18.
15. Boonyopakom, P., & Thongna, T. (2020). Environment monitoring system through LoRaWAN for smart agriculture. In *Proceedings of the IEEE 5th International Conference on Information Technology (InCIT)*, Chonburi, Thailand (pp. 12–16).
16. Mya, K. T., Sein, M. M., Nyunt, T. T. S., Lewlompaisarl, U., & Owada, Y. (2020). A Design for IoT Based Smart Watering System Using LoRa. In *Proceedings of the IEEE 9th Global Conference on Consumer Electronics (GCCE)*, Kobe, Japan (pp. 278–279).
17. Siregar, B., Tanjung, K., & Nurmayadi, F. (2020). Remotely controlled water flow monitoring system with mechanical control on the faucet using LoRa communication. In *Proceedings of the IEEE International Conference on ICT for Smart Society (ICISS)*, Bandung, Indonesia (pp. 1–5).
18. Lee, H., & Ke, K. (2018). Monitoring of large-area IoT sensors using a LoRa wireless mesh network system: Design and evaluation. *IEEE Transactions on Instrumentation and Measurement, 67*(9), 2177–2187.

Artificial Intelligence as a Strategic Partner to HRM 4.0

Shivani Agarwal, Thi Dieu Linh Nguyen, and Gloria Jeanette Rincón Aponte

Abstract New age automation technologies that are digital and disruptive in nature are penetrating all spheres and processes of the modern economy and corporate world with a profound impact and at a global level. The function of human resources too has definitely undergone a paradigm shift in tune with the pace of technologies changes, in contrast to what it was several years ago. In this context, a set of challenges and opportunities await the profession. Artificial intelligence stimulated and transforming job roles, in terms of redefined work roles and enacting newer skills and tools and preparing the workforce for newer challenges. Artificial intelligence will make our employees work easier; monotonous task can be further automated, and relevant information from a huge volume of data will be more identifiable. The HR department must take proactive steps to adopt these technologies and update itself in terms of necessary skill. The chapter shows the strategic partner role of human resource management and artificial intelligence. The chapter shows how AI impacts the role of HRM practices in changing economy.

Keywords Industry 4.0 · Artificial intelligence · Disruptive economy · Smart HR 4.0

1 Introduction

The first predominant variable which is responsible for modifying the working of service and manufacturing processes is "globalization." It refers to the boundaryless

S. Agarwal (✉)
KIET School of Management, KIET Group of Institutions, Delhi-NCR, Ghaziabad 201206, India
e-mail: jindal.shivani24@gmail.com; shivani.agarwal@kiet.edu

T. D. L. Nguyen
Hanoi University of Industry, Hanoi, Vietnam
e-mail: nguyenlinh79.haui@gmail.com

G. J. R. Aponte
Facultad de Ingeniería, Universidad Cooperativa de Colombia, Bogotá, Colombia
e-mail: gloriaj.rincon@campusucc.edu.co

T. D. L. Nguyen and J. Lu (eds.), *Machine Learning and Mechanics Based Soft Computing Applications*, Studies in Computational Intelligence 1068,
https://doi.org/10.1007/978-981-19-6450-3_28

organization which makes organizations interdependent and helps in increasingly integrated worldwide. With globalization, the other variable comes into the picture is artificial intelligence which is in its developing stage and helps the economy across globe to change the scenario of working in all the departments (production, marketing, finance, IT, quality, and HR).The seven ways of reinventing ***human resource management via artificial intelligence*** are HR Reporting Confidence in AI Integration, Candidate Resumes on Smart Digital Forms, Understanding Employee Referrals, Data-Backed Resources and Insights, AI-Backed Chatbots Keep Engagement Conversation Going, Boosting Learning and Development Programs, Leveraging Transactional Workforce Data, and Powering Workforce Analytics (Dom Nicastro, 2020).

2 AI as the Future of HR

- AI is considered as the future of HR as it is working as a backbone for the HR functions by using several tools like turbohire especially for recruitment on different connected platforms such as LinkedIn, Naukri.com, Career builder, etc.
- AI helps in clustering of data via different links across different job titles, skills, knowledge, etc.
- AI helps in proving orientation via video calls, different software, etc [1, 2].
- AI helps in selecting the employees from a pool of candidates [3].
- AI helps in providing digital training to the employees.
- AI helps in creating and handing different compensation packages for the employees.
- AI helps in reducing the brain load to utilize in different directions for the benefits of the organization [4].
- AI can also help in finding the employees referral.
- AI also helps in shift swap data at run time.
- AI helps in handling the changing environment and adapting new techniques easily.

The chapter discusses three major domains which are shown in Fig. 1. Figure 1 depicts the interrelationship between artificial intelligence, Smart HR, and the strategic partner role between both the variables.

- **Artificial Intelligence**

  AI is one of the oldest fields of study in technical domain, and it has started evolving since the mid-1950s. The term artificial intelligence evolves in the year 1956 at the Dartmouth Summer Research Project on Artificial Intelligence conducted in a workshop by John McCarthy. It would not be prudent enough to frame any absolute definition of AI. AI generally correlated as "thinking machines." The concept of artificial intelligence is defined ***as "machines that***

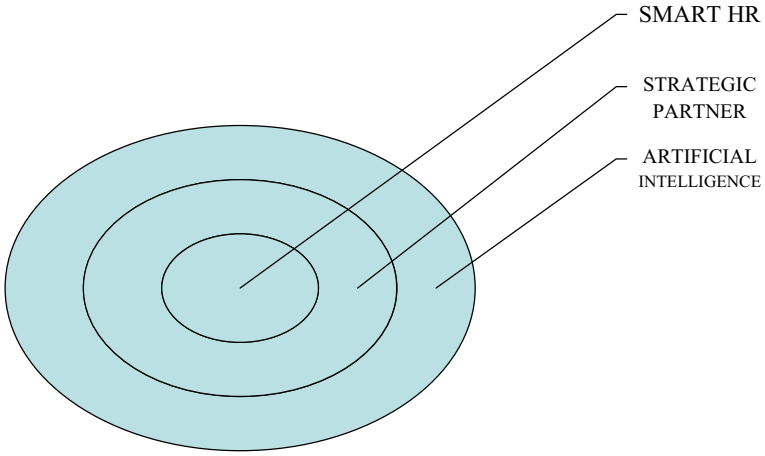

Fig. 1 Relationship between HRM and AI. *Source* Author's Own Work

simulate the thinking capabilities of human being" [5]. *Nowadays, AI is omnipresent in almost all the areas.*

- **Smart HRM**

  The first variable is the HRM professional's primary role as indicated by the HRM professionals themselves. This variable is measured on a nominal scale: (1) directing/supervising (i.e., HRM director, HRM manager, HRM supervisor), (2) HRM policy-making (i.e., HRM policy advisor, HRD specialist, or compensation and benefits specialist), (3) general HRM advising roles (i.e., HR advisor), (4) specialist (i.e., career advisor, recruitment, or outplacement advisor), and (5) administrative or operational (i.e., HR assistant, HR administrator). The focus is on the "administrative/operational" role as the development of this role may reflect the shift from "administrative" to "strategic."

- **Strategic Partner**

  The term strategic partner means mutual relationship between two entities, commodity, variables, and organizations. Nowadays, organizations are creating partners to implement their budding strategies for the successful outcome. Strategic partners generally help each other to create a niche for themselves. It helps in developing the employees to take strategic decision and develop their entity as successful bonding between the two.

- **Role of Strategic Partner in AI and HRM**

  Human resource is responsible for enlargement. It has the capacity to enhance synergy and convert the lifeless products into useful products. *HRM is defined as "the art of procuring, developing and maintaining competent workforce to achieve the goals of an organization in an effective and efficient manner*." The

evolution of HR starts with the commodity concept and now till the time it is considered as strategic partner for the organizations.

Majorly HR functions were divided into two parts

a. Managerial functions
b. Operative functions
c. **Managerial Functions**: The managerial functions consist of PODC model which means planning, organizing, directing, and controlling.
d. **Operative Functions**: The operative functions consist of procurement, development, motivation and compensation, maintenance, integration, and emerging issues.

To discuss in detail the strategic role of HRM at managerial level and AI, author describes all the subsets one by one mentioned below (Fig. 2):

AI Planning: The term planning means choking out the whole idea in black and white to describe the tasks. It includes 5W + 1H which indicates the What, Why, Where, When and by Whom + 1 How. So, in traditional method planning was executed by the humans as per their decision-making capabilities which sometimes results in human error and human biasing.

With the introduction of artificial intelligence into planning process, the data was imported into abundance and helps in identifying the trends and patterns which create different models for decision making. Further, applying the optimization techniques, AI helps in conducting proper planning, ***for example,*** Deloitte.

AI-Organizing: AI creates and helps in changing organizing structures of the organizations. With the help of AI, organizations can easily find out the reporting

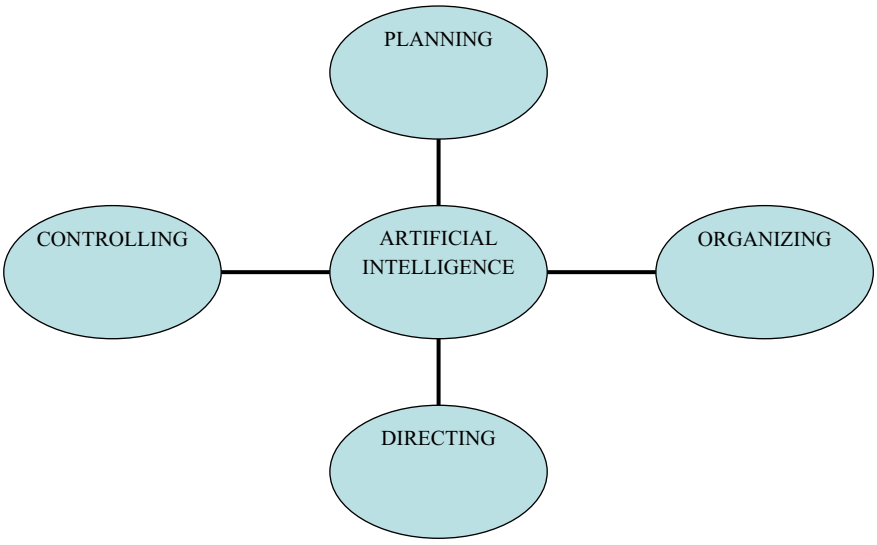

Fig. 2 Relationship between AI and managerial functions of HRM. *Source* Author's Own Work

and subordinating authority. In case there is flat structure, AI will help in utilizing the employees in an optimized manner. Where the structure is hybrid, AI helps in finding the duplicate resources and helps in reducing the headcount by automating various functions and processes, ***for example,*** IBM.

AI-Directing: The process of directing and guiding the employees to achieve their assigned tasks and duties is known as directing. The implementation of AI helps in giving proper guidance and direction to the employees to complete their tasks. AI helps in performing administrative duties which engage the managers most in the organizations. Further, with the help of AI, manager's time will be saved, efficiency will be enhanced, and helps in minimizing the cost as well***, for example,*** Layne Thompson.

AI-Controlling: The process of checking the actual performance with the planned performance is known as controlling. With the involvement of AI, the gap between the actual performance and the planned performance is reduced to minimum. So, with the inclusion of AI, the controlling needs minimum investigation which again helps in saving time and money of the organization. Further, it helps in avoiding the doing and redoing approach within the organization, *for example, Infosys.*

Table 1 shows the variables utility with respect to traditional method and contemporary method.

b. Operative Functions: The operative functions consist of procurement, development, motivation and compensation, maintenance, integration, and emerging issues.

- **AI Procurement Function**: The term procurement is predominantly capturing the whole functions of human resource management. It consists of various subfunctions, namely job analysis, human resource planning, recruitment, selection, placement, induction and orientation, internal mobility.

The foundation of human resource management is **job analysis**. Job analysis is a combination of job description and job specification. AI-powered job analysis helps employers to identify the useful skill set and competencies for the prementioned job description. AI completes the task of analyzing the job in couple of seconds, whereas traditional method took months to match the required skill set.

The second part of human resource management is **human resource planning** which consists of demand and supply of human beings. To reduce the gap between demand and supply, AI plays the major role. With the help of AI, the gap between

Table 1 Traditional method versus AI method in terms of Management Functions

S. No.	Variables	Traditional method	AI-enabled method
1	Planning	More chances of error	Less chances of error
2	Controlling	In bigger organization, controlling is difficult	Streamline controlling
3	Directing	Chances of human error are more	Less chances of error
4	Controlling	Biased controlling	Rational controlling

the two is minimized and the cost in terms of monetary and non-monetary will be earned for the organization.

The third part of human resource management is **recruitment.** There are lot of software available in the market for the purpose of hiring the right candidate for the organization, namely Turbohire (applicant tracking system). With the help of these software, you can shortlist the CVs, select the relevant ones, and schedule the interview automatically.

The fourth part of human resource management is **selection**. To select the best candidate from the pool of recruited individuals, AI software automatically gives you the best candidature on the basis of summation of all the steps of selection within no time.

The fifth part of human resource management is **placement**. AI helps in placing the right person at the right place within no time. It gives a complete information and the best suitability of candidature within the organization.

The sixth part of human resource management is **induction and orientation**. Nowadays, organization is doing orientation in an online mode with the help of chatbots. Chatbot helps in reducing monotonous human efforts. In human, monotonous behavior creates lethargy in the behavior of the person responsible for orientation, but this is not the case of chatbots.

The seventh part of human resource management is **internal mobility**. Internal mobility is basically movement of human being within the organization be it horizontal movement and vertical movement. AI helps in finding the right candidate for the internal movement after analyzing the job, skillset of individual.

- **AI Development Function**: After procuring the employees, it is the moral duty for the employer to train and develop their employees. The development function consists of training,executive development, career planning and development, and human resource development.

The **training** function is defined as to increase the knowledge, skill, and abilities of employees. AI helps in identifying the training needs and the individuals for the organization who required the training.

Secondly, AI-powered **executive development** also helps at the senior level to find them and create value for the organization.

Thirdly, there are software which helps in developing the **career path and development** for the employees so that they feel secured within the organization and believe that they have a long way to go.

Lastly, **human resource development** can take place with the help of AI as they provide precise information about the individuals.

- **AI Motivation and Compensation**: When the employee feels that they have the opportunity to develop within the premises and their urge of motivation and perception about compensation becomes prominent. It consists of job design,work scheduling, motivation, job evaluation, performance appraisal, compensation administration, and incentives and benefits [6].

The first way is **work scheduling** which can be easily done with the help of AI. Employees can easily schedule their work, tasks, duties with the help of software's like email, Excel, data analytics tool. It helps in prioritizing the job and earned the time and cost for the organization.

There are chatbots which talk with human being and as per their coding helps in answering the questions of human being. **Motivation** chatbots are available in the market which helps in counselling and guidance for the employees. The information shared with chatbots is kept secured within the privacy guidelines of the organization.

Third and the most important shift in handling the concept is **performance appraisal, compensation administration, and incentives and benefits**. Traditionally, all the above-mentioned parameters were suffered from the human bias. With the introduction of AI in appraisals, all the tasks are rationalized and equal remuneration for equal performance without any judgment biasness will be given to the employees.

- **AI Maintenance Function**: The booming area of human resource management is maintenance function which consists of health and safety, employee welfare (housing, transportation, recreation), social security. AI enabled all the functions online and easy identification of health insurance, medical benefits, terms and conditions for welfare and security of employees [7].
- **AI Integration Function**: The major role of human resource management is to integrate all the ends to create an intact and strong system of organizations. The integration function consists of grievance redressal, discipline, teams and teamwork, collective bargaining, employee participation and empowerment, trade unions and employers' associations, industrial relations**.** AI-enabled system provides helps in maintaining the discipline, resolving grievances timely, making the teams and handling diverse teams, virtual teams [8].
- **AI Emerging Issues**: To create a strategic role in HRM, there are emerging issues which are namely mentioned as personnel records, human resource audit, human resources research, human resource accounting, human resource information system, stress and counselling, international human resource management. To maintain the personnel records, access them, and take decisions, AI helps in getting and providing information to take relevant decisions.

Table 2 shows the variables utility with respect to traditional method and contemporary method.

3 Benefits of AI in HRM

- AI improves various internal processes of the organization [9].
- AI reduces the human errors.
- AI helps in taking decision with time effective method.
- AI saves cost of finding a best suitable person of the organization.

Table 2 Traditional method versus AI method in terms of HRM functions

S. No.	Variables	Traditional method	AI-enabled method
1	Procurement	Human supply is limited	Human supply is huge
2	Development	Development requirements are limited	Abrupt technological change
3	Motivation and compensation	People were self-motivated	People required motivation
4	Maintenance	Health and safety requirements were not required much	Health and safety were required as there are environmental changes
5	Integration	People were integrated strongly	People were not integrated with the organization
6	Emerging issues	Personnel records were easily maintained	Personnel records were hard to maintain

4 Conclusion

With the invent of artificial intelligence, it helps to the core of the organization. Steve Meier (2019) Artificial intelligence shows a lot of benefits to the organization in terms of enhancing the features, functions, performance of the products and services, to make and take better decisions, create new products, optimize internal business operations, help in automation of tasks, and process which ultimately free up the employees. Those employees can further utilize their time and brain in more creative and innovative learnings. Further, AI also helps in pursue new markets, capture and apply scarce knowledge wherever needed, reduce headcount through automation, etc.

To conclude, AI is the boon for businesses. AI is considered as the backbone for the organizations in the current scenario. Usage of AI especially in the domain of HRM is a ray of hope for the HR managers [10]. The subdomains of HRM are HRIS, HRP, and HR analytics coming up in big way as a way of growth for businesses. Artificial intelligence is supporting in making the processes easy (Shurlly Tiwari). AI in business is not to replace human being but considered as a spouse to human beings [11].

References

1. Agarwal S., Linh N., & Aponte G. (2022) Student perception regarding chatbot for counselling in higher education. In: V. E. Balas, V. K.Solanki, & R. Kumar (Eds.), *Recent advances in internet of things and machine learning*. Intelligent Systems Reference Library (Vol. 215). Springer, Cham. https://doi.org/10.1007/978-3-030-90119-6_22 (Scopus Indexed)
2. Agarwal, S. (2021). Trust or no trust in chat bots: A dilemma of millennial. In: Cognitive Computing for human-robot interaction: Principles and practices. Elsevier. ISBN-9780323857697. https://www.elsevier.com/books/cognitive-computing-for-human-robot-int

eraction/mittal/978-0-323-85769-7 (Scopus Indexed)
3. Agarwal, S., & Teotia, P. (2021). Cold calling as a strategic tool to improve recruitment and selection process. In: *Using strategy analytics to measure corporate performance and business value creation*. IGI Global. https://www.igi-global.com/chapter/cold-calling-as-a-strategic-tool-to-improve-the-recruitment-and-selection-processes/285843. ISBN 9781799877165 (Scopus Indexed)
4. Rana, G., & Agarwal, S. (2021). Techno innovative tools for employer branding in Industry 4.0. In: *Employer branding for competitive advantage: Models and implementation strategies*. CRC, USA. https://www.routledge.com/Employer-Branding-for-Competitive-Advantage-Models-and-Implementation-Strategies/Rana-Agarwal-Sharma/p/book/9780367650964. ISBN-9781003127826
5. Prikshat, V., Malik, A., & Budhwar, P. (2021). AI-augmented HRM: Antecedents, assimilation and multilevel consequences. *Human Resource Management Review*, 100860.
6. Malik, A., Srikanth, N. R., & Budhwar, P. (2020). *Digitization, artificial intelligence (AI) and HRM* (pp. 88–111). Sage.
7. Hossin, M. S., Ulfy, M. A., & Karim, M. W. (2021). Challenges in adopting artificial intelligence (AI) in HRM practices: A study on Bangladesh perspective. *International Fellowship Journal of Interdisciplinary Research, 1*.
8. Arslan, A., Cooper, C., Khan, Z., Golgeci, I., & Ali, I. (2021). Artificial intelligence and human workers interaction at team level: a conceptual assessment of the challenges and potential HRM strategies. *International Journal of Manpower*.
9. Budhwar, P., Malik, A., De Silva, M. T., & Thevisuthan, P. (2022). Artificial intelligence–challenges and opportunities for international HRM: A review and research agenda. *The International Journal of Human Resource Management, 33*(6), 1065–1097.
10. Pan, Y., & Froese, F. J. (2022). An interdisciplinary review of AI and HRM: Challenges and future directions. *Human Resource Management Review*, 100924.
11. Agarwal, S. (2022). Human leaders and artificial intelligent leaders: Workplace spouses. In: *Handbook of Research on Innovative Management Using AI in Industry 5.0* (pp. 257–264). IGI Global.